

https://dspace.org/

Improving open pit mine economics through ultimate pit slope optimization: case study of Pickstone Peerless mine

Nyamande, Pardon

2021
https://hdl.handle.net/10539/33371

Downloaded from a DSpace repository. https://dspace.org/

School of Mining Engineering



UNIVERSITY OF THE
WITWATERSRAND,
JOHANNESBURG

IMPROVING OPEN PIT MINE ECONOMICS THROUGH ULTIMATE PIT SLOPE OPTIMIZATION: CASE STUDY OF PICKSTONE - PEERLESS MINE.

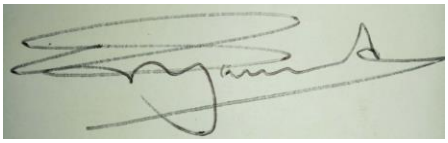
Pardon Nyamande

A research report submitted to the Faculty of Engineering and the Built Environment, University of the Witwatersrand, Johannesburg, in partial fulfilment of the requirements for the degree of Master of Science in Engineering.

Johannesburg, 2021

DECLARATION

I declare that this report is my own, unaided work. I have read the University Policy on Plagiarism and hereby confirm that no plagiarism exists in this report. I also confirm that there is no copying nor is there any copyright infringement. I willingly submit to any investigation in this regard by the School of Mining Engineering and I undertake to abide by the decision of any such investigation.



1st July 2021

Signature of Candidate Date

ABSTRACT

In most open pit mining operations the need to create stable pit slopes and the influence of the overall pit slope on the economics of such an operation is highly appreciated. Despite such knowledge many open pit mines are designed with little or no geotechnical investigations being carried out so as to come up with an optimized pit slope in line with site specific conditions. This can lead to under or over estimating pit slope angles. Conservative (too gentle) slopes result in high stripping ratios therefore a high operating cost. Slopes too steep may result in slope failures, which may lead to high operating costs or premature mine closure. This project emphasises the importance of geotechnical investigations not only for safety reasons but for economic reasons as well. A case study of Pickstone Peerless mine was used. Geotechnical data was gathered through core logging and face mapping of the existing pit. The data gathered was then used for stability analysis employing empirical, kinematics, limit equilibrium and numerical modelling. Rocscience software packages were used for numerical based analysis. From the results obtained it was concluded that it is possible to steepen the current 52^{o} overall pit slope angle of the Peerless pit by 1^{o} without compromising stability at both bench and regional scales. This will be possible provided adequate slope management practices are put in place and adhered to. The steeper slope would have saved the mine more than 2,681,110 m^3 of waste stripping, translating to in excess of $12,064,995.00 (USD) in financial savings for the existing pit. The steeper angle applicable to the current pit may not be appropriate to the pit extensions. Further geotechnical evaluations should be done on suitably positioned and spaced boreholes in the area of the extension, to verify the

stability of steeper slopes in that area. The analysis done as part of this project was used to show that the current pit can be deepened by 5 m without a push back.

DEDICATION

To my loving wife Buhle and beautiful daughters Princess and Precious, you were a source of encouragement and your love gave me the much required impetus especially when the going seemed like an uphill climb. To my parents Kennard and Dorothy Nyamande, I say hats off to you for you are always there for me even now when I have grown into a parent as well.

ACKNOWLEDGEMENTS

I would like to acknowledge the guidance and assistance of my supervisor Professor Bryan Watson. His vast knowledge and expertise in the subject matter together with his tolerance resulted in this work seeing the light of day.

Mr Japhet Makwasha, General Manager, and the rest of the management team at Breckridge Investments (Pickstone Peerless Gold Mine) for granting me the golden opportunity to use their operation as a case study.

I sincerely appreciate the support given by the technical team on site at Pickstone Peerless Gold mine, George Rusike, Martin Mateveke, Nicholas Coetsee, Charles Duma, Gilbert Zengeya, Chris Musa and Collette Ngulube.

Table of Contents

DECLARATION ii
ABSTRACT iii
DEDICATION v
ACKNOWLEDGEMENTS vi
LIST OF FIGURES x
LIST OF TABLES xxii
1. INTRODUCTION 1
1.1 Background Of The Study Area 4
1.2 Geological Setting 6
1.3 Seismicity 6
1.4 Problem Statement 7
1.5 Research Objectives 7
1.6 Key Questions To Be Addressed 8
1.7 Research Methods 8
1.8 Structure of The Research Report 8
2. LITERATURE REVIEW 10
2.1 Introduction 10
2.2 Basic Geometric Design Components Of An Ultimate Pit Slope 11
2.3 Influence Of Overall Pit Slope Angle On Pit Optimization 19
2.4 Factors Affecting Slope Stability 22
2.5 Slope Failure Modes 36
2.6 Rock Mass Characterization 43
2.7 Acceptability Criteria For Open Pit Slope Design 55
2.7.1 Factor of safety (FOS) criteria 55
2.7.2 Probability analysis criteria 56

2.7.3 Risk analysis criteria 57
2.8 Open Pit Slope Stability Analysis And Design 59
2.8.1 Conventional Analysis Methods 61
2.9 Numerical Stability Analysis 74
2.9.1 Continuum models 75
2.9.2 Discontinuum models 77
2.9.3 Comparison between numerical and limit equilibrium analysis techniques 78
2.9.4 Benefits of numerical modelling to rock engineering 80
2.10 Open Pit Mine Slope Management 81
2.10.1 Slope stability monitoring 82
2.10.2 Slope stabilization 82
2.11 Slope Failure Preparedness 82
2.12 Literature Discussion 83
3. METHODOLOGY 85
3.1 Introduction 85
3.2 Geotechnical Data Gathering 85
3.2.1 Oriented diamond core drilling 85
3.2.2 Oriented core logging 95
3.2.3 Face mapping 99
3.3 Rock Mechanical Properties 100
3.4 Slope Stability Analysis 117
3.4.1 Empirical slope stability analysis and design 120
3.4.2 Kinematic analysis 124
3.4.4 Limit equilibrium analysis 130
3.4.5 Numerical analysis 133

4. RESULTS AND ANALYSIS 139
4.1 Introduction 139
4.1.1 Circular charts analysis results 139
4.1.2 Mining rock mass rating (MRMR) system analysis results 140
4.1.3 Kinematic analysis results 140
4.1.4 Limit equilibrium analysis results 144
4.1.5 Numerical analysis results 148
4.2 Comparison between existing and optimized pit slopes 154
5. CONCLUSION AND RECOMMENDATIONS 156
5.1 Conclusion 156
5.2 Recommendations 157
References 160
Appendix A 169
Geotechnical Core Log Sheets 169
Appendix B 176
Face mapping log sheets for the southern and northern walls 176
Appendix C 179
Failure codes for compression test of core samples. 179
..... 179
Appendix D 180
Kinematic analysis at bench scale level 180
Kinematic analysis at inter-ramp scale level 186
Kinematic analysis at overall pit slope scale level 195

LIST OF FIGURES

Figure 1-1 location of Pickstone-Peerless Mine (Bosman, 2013). 4

Figure 1-2 Satellite image of the PE03 pit. (Google, 2019) 5

Figure 2-1 Bench geometry (Hustrulid & Kuchta, 1998) 13

Figure 2-2 Safety bench with berm constructed along the crest (Hustrulid & Kuchta, 1998). 13

Figure 2-3 Geometrical parameters for a bench; inter ramp slope and overall slope (Wyllie & Mah, 2004). 15

Figure 2-4 Effect of ramp on the final pit slope angle. (Hustrulid & Kuchta, 1998) 16

Figure 2-5 Elements and equation to calculate the overall pit slope angle (Alegre, et al., 2019). 17

Figure 2-6 Reduction in the waste, maintaining ore recovery (Madowe, 2016) 21

Figure 2-7 Increase in ore recovered while maintaining same amount of waste stripped (Madowe, 2016). 21

Figure 2-8 Increase in both ore and waste (Madowe, 2016). 22

Figure 2-9 Schematic of the primary geometrical properties of discontinuities in rock. (Hudson 1989) 24

Figure 2-10 Terminology defining discontinuity orientation: (a) isometric view of plane (dip and dip direction); (b) plan view of plane (Wyllie & Mah, 2004) 25

Figure 2-11 Variation of joint frequency as the scanline is moved from being perpendicular to the joint plane to being parallel to it (Hudson & Harrison, 1997). 26

Figure 2-12 Joint persistence (Piyal & Konietzky, 2016) 28

Figure 2-13 Two-dimensional representation of the redistribution of horizontal stress around a long open pit (large dimension perpendicular to this plane). (Sjoberg, 1996) 35

Figure 2-14 Simplified illustrations of most common slope failure modes. (Hoek, 2009) 37

Figure 2-15 Relationship between dip of slope face, dip of discontinuity plane and friction angle of discontinuity for sliding to take place (Wyllie & Mah, 2004). 38

Figure 2-16 release surfaces at ends of plane failure (Wyllie & Mah, 2004). 39

Figure 2-17 Geometric conditions for wedge failure: (a) pictorial view of wedge failure; (b) view of slope at right angles to the line of intersection (Wyllie & Mah, 2004). 40

Figure 2-18 Common classes of toppling failures: (a) block toppling of columns of rock containing widely spaced orthogonal joints; (b) flexural toppling of slabs of rock dipping steeply into face; (c) block flexure toppling characterized by pseudo-continuous flexure of long columns through accumulated motions along numerous cross-joints (Goodman and Bray 1976)..... 41

Figure 2-19 Procedure for measurement and calculation of *RQD* (After Deere, 1989). 44

Figure 2-20 the scale effect on the use of the *GSI* system. (Hoek, 1983) 52

Figure 2-21 Geological strength index for jointed rock masses (After Hoek & Marinos, 2000) 54

Figure 2-22 Definition of POF and Relationship with FOS according to uncertainty magnitude (after Tapia *et al.*, 2007) 57

Figure 2-23 Stability and design chart for soil and weathered rock slopes (Stacey & Swart, 2001). 62

Figure 2-24 Sequence of steps involved in using circular failure charts to find the factor of safety of a slope (Wyllie, 2018). 64

Figure 2-25 Stereographic representation of plane and line on lower hemisphere of reference sphere: (a) plane projected as great circle; (b) isometric view of line (plunge and trend) (Wyllie, 2018). 65

Figure 2-26 Equal area projections of plane and line: (a) plane projected as great circle and corresponding pole; (b) line projected as pole. (Wyllie, 2018) 66

Figure 2-27 Main types of block failures in slopes, and structural geology conditions likely to cause these failures 68

Figure 2-28 (a) Kinematic analysis of blocks of rock in slope: (a) discontinuity sets in slope;..... 69

Figure 2-29 Kinematic analysis of blocks of rock in slope: envelopes on equal area stereonet. (Wyllie, 2018) 70

Figure 2-30 Down dip directions of discontinuities 1, 2, 3 and 4 with respect to a rock slope..... 71

Figure 2-31 Manual construction of the daylight..... 72

Figure 2-32 Empirical slope design chart based on rock mass classification (Stacey & Swart, 2001)..... 74

Figure 2-33 Illustration of FEM (Differential Method) and BEM (Integral Method) (Hoek, et al., 1991). 77

Figure 3-1 Plan view of the PE03 pit showing location of the pure geotechnical holes (PE03DDGT)..... 86

Figure 3-2 Satellite image of the PE03 pit. (Google, 2019) 87

Figure 3-3 Total number of planned boreholes as shown on the table that was used by the drillers..... 87

Figure 3-4 Core trays with depth recorded on plastic core blocks separating the drill runs for one of the drilled boreholes (Courtesy of Pickstone-Peerless Mine). 89

Figure 3-5 Determining the driller's datum against which to measure the stick-up for borehole depth calculation (Orpen, 2014). 90

Figure 3-6 Determining the in situ core orientation with a Reflex ACT III orientation tool connected to the upper end of the core barrel whilst the core is inside the core barrel (Courtesy of Pickstone-Peerless Mine). 91

Figure 3-7 Marking the bottom of core with a Reflex marking jig whilst the core is still in the core barrel and the Reflex Orientation tool is still attached on the upper end of the core (Courtesy of Pickstone-Peerless Mine). 92

Figure 3-8 Drilled core just after removed from the core barrel and cleaned lying on the angled iron core stand (Courtesy of Pickstone-Peerless Mine). 93

Figure 3-9 Drawing the orientation line along the entire length of the drill core extending it from the bottom of core mark (Courtesy of Pickstone-Peerless Mine)..... 94

Figure 3-10 Measuring the Total Core Recovery (TRC) for a particular drill run using a steel measuring tape (Courtesy of Pickstone-Peerless Mine). 95

Figure 3-11 A goniometer for measuring alpha and beta angles (Westernex, 2018) 97

Figure 3-12 Definition of the alpha (α) and the beta (β) angles (HolcombeCoughlinOliver, 2010) 98

Figure 3-13 Brunton geological compass that was used to measure dip and dip direction during face mapping. 99

Figure 3-14 Sigma 1 versus Sigma 3 (Bosman, 2013). 103

Figure 3-15 Failure envelopes obtained from RockLab software for Weathered Rock, GSI 41 (Bosman, 2013). 110

Figure 3-16 Failure envelopes obtained from RockLab software for Weathered Rock, GSI 29 (Bosman, 2013). 111

Figure 3-17 Failure envelopes obtained from RockLab software for Weathered Rock, GSI 52 (Bosman, 2013). 112

Figure 3-18 Failure envelopes obtained from RockLab software for Fresh Rock, GSI 59 (Bosman, 2013). 113

Figure 3-19 Failure envelopes obtained from RockLab software for Fresh Rock, GSI 64 (Bosman, 2013). 114

Figure 3-20 Failure envelopes obtained from RockLab software for Fresh Rock, GSI 54 (Bosman, 2013). 115

Figure 3-21 The best-fit Mohr-Coulomb envelope (Blue line) on a normal and shear stress plot (Rocscience, 2002). 117

Figure 3-22 Determination of the value of $\tan\phi F$ for a 60.4 º slope in weathered rock 121

Figure 3-23 Haines and Terbrugge design chart for overall stope angles 124

Figure 3-24 Mean joint sets for PE03 southern wall. 125

Figure 3-25 Mean joint sets for PE03 northern wall. 126

Figure 3-26 Planar failure for PE03 Southern Wall at 52º final pit slope angle. 128

Figure 3-27 Wedge failure for PE03 Southern Wall at 52º final pit slope angle. 129

Figure 3-28 Toppling failure for PE03 Southern Wall at 52º final pit slope angle. 130

Figure 3-29 Location of the slip surfaces using the grid search method. (Rocscience, 2018) 132

Figure 3-30 Model for overall slope with 90º bench slopes and alternating 10 m and 5 m berms. 133

Figure 3-31 Typical recommendations for locations of artificial far-field boundaries in slope stability analyses. (Wyllie & Mah, 2004) 134

Figure 3-32 Finite element model for a slope with alternating 10 m and 6 m benches at 90º bench slope angle and 51.75º overall slope angle. 137

Figure 4-1 Limit equilibrium analysis results for a slope with alternating 10 m and 6 m benches at 90 º bench slope angle and 52 º overall slope angle (Current design)..... 145

Figure 4-2 Limit equilibrium analysis results for a slope with alternating 10 m and 5 m benches at 90 º bench slope angle and 54 º overall slope angle (OD1). 145

Figure 4-3 Limit equilibrium analysis results for a slope with alternating 7 m and 5 m benches at 85º bench slope angle and 54º overall slope angle (OD5). 146

Figure 4-4 Factor of safety (FoS), Relative Frequency curve for OD4. 148

Figure 4-5 Finite element model for a slope with alternating 10 m and 6 m benches at 90 º bench slope angle and 52 º overall slope angle (Current design). 149

Figure 4-6 Finite element model for a slope with alternating 10 m and 5 m benches at 90 º bench slope angle and 54 º overall slope angle (OD1). 149

Figure 4-7 Finite element model for a slope with alternating 7 m and 5 m benches at 89 º bench slope angle and 57 º overall slope angle. 150

Figure 4-8 Finite element model for a slope with alternating 7 m and 5 m benches with different slope angles in weathered and fresh rock. 152

Figure 4-9 Geometry of the optimized final pit slope. 154

Figure 4-10 Additional overburden material (shaded area) to be mined when using the current design as compared to the optimized design. 155

Figure 5-1 Geometry of the optimized final pit slope. 158

Figure C-1 Failure codes for compression test (Bosman, 2013) 179

Figure D-1 Planar failure for PE03 Southern Wall at 90º bench slope angle (Current design and OD1). 180

Figure D-2 Planar failure for PE03 Southern Wall at 89º bench slope angle (OD5). ... 181

Figure D-3 Wedge failure for PE03 Southern Wall at 90º bench slope angle (Current design and OD1). 181

Figure D-4 Wedge failure for PE03 Southern Wall at 89º bench slope angle (OD5)… 182

Figure D-5 Toppling failure for PE03 Southern Wall at 90º bench slope angle (Current design and OD1). 182

Figure D-6 Toppling failure for PE03 Southern Wall at 89º bench slope angle (OD5). 183

Figure D-7 Planar failure for PE03 Northern Wall at 90º bench slope angle (Current design and OD1)..... 183

Figure D-8 Planar failure for PE03 Northern Wall at 89º bench slope angle (OD5). ... 184

Figure D-9 Wedge failure for PE03 Northern Wall at 90º bench slope angle (Current design and OD1). 184

Figure D-10 Wedge failure for PE03 Northern Wall at 89º bench slope angle (OD5).. 185

Figure D-11 Toppling failure for PE03 Northern Wall at 90º bench slope angle (Current design and OD1). 185

Figure D-12 Toppling failure for PE03 Northern Wall at 89º bench slope angle (OD5). 186

Figure D-13 Planar failure for PE03 Southern Wall at 61º inter-ramp slope angle (Current design). 186

Figure D-14 Wedge failure for PE03 Southern Wall at 61º inter-ramp slope angle (Current design). 187

Figure D-15 Toppling failure for PE03 Southern Wall at 61º inter-ramp slope angle (Current design). 187

Figure D-16 Planar failure for PE03 Southern Wall at 63º inter-ramp slope angle (OD1). 188

Figure D-17 Wedge failure for PE03 Southern Wall at 63º inter-ramp slope angle (OD1). 188

Figure D-18 Toppling failure for PE03 Southern Wall at 63º inter-ramp slope angle (OD1). 189

Figure D-19 Planar failure for PE03 Southern Wall at 67º inter-ramp slope angle (OD5). 189

Figure D-20 Wedge failure for PE03 Southern Wall at 67º inter-ramp slope angle (OD5). 190

Figure D-21 Toppling failure for PE03 Southern Wall at 67º inter-ramp slope angle (OD5). 190

Figure D-22 Planar failure for PE03 Northern Wall at 61º inter-ramp slope angle (Current design). 191

Figure D-23 Wedge failure for PE03 Northern Wall at 61º inter-ramp slope angle (Current design). 191

Figure D-24 Toppling failure for PE03 Northern Wall at 61º inter-ramp slope angle (Current design). 192

Figure D-25 Planar failure for PE03 Northern Wall at 63º inter-ramp slope angle (OD1). 192

Figure D-26 Wedge failure for PE03 Northern Wall at 63º inter-ramp slope angle (OD1). 193

Figure D-27 Toppling failure for PE03 Northern Wall at 63º inter-ramp slope angle (OD1). 193

Figure D-28 Planar failure for PE03 Northern Wall at 67º inter-ramp slope angle (OD5). 194

Figure D-29 Wedge failure for PE03 Northern Wall at 67º inter-ramp slope angle (OD5). 194

Figure D-30 Toppling failure for PE03 Northern Wall at 67º inter-ramp slope angle (OD5). 195

Figure D-31 Planar failure for PE03 Southern Wall at 52º overall slope angle (Current design). 195

Figure D-32 Wedge failure for PE03 Southern Wall at 52º overall slope angle (Current design). 196

Figure D-33 Toppling failure for PE03 Southern Wall at 52º overall slope angle (Current design). 196

Figure D-34 Planar failure for PE03 Southern Wall at 54º overall slope angle (OD1). 197

Figure D-35 Wedge failure for PE03 Southern Wall at 54º overall slope angle (OD1). 197

Figure D-36 Toppling failure for PE03 Southern Wall at 54º overall slope angle (OD1). 198

Figure D-37 Planar failure for PE03 Southern Wall at 57º overall slope angle (OD5). 198

Figure D-38 Wedge failure for PE03 Southern Wall at 57º overall slope angle (OD5). 199

Figure D-39 Toppling failure for PE03 Southern Wall at 57º overall slope angle (OD5). 199

Figure D-40 Planar failure for PE03 Northern Wall at 52º overall slope angle (Current design). 200

Figure D-41 Wedge failure for PE03 Northern Wall at 52º overall slope angle (Current design). 201

Figure D-42 Toppling failure for PE03 Northern Wall at 52º overall slope angle (Current design). 201

Figure D-43 Planar failure for PE03 Northern Wall at 54º overall slope angle (OD1).. 202

Figure D-44 Wedge failure for PE03 Northern Wall at 54º overall slope angle (OD1). 202

Figure D-45 Toppling failure for PE03 Northern Wall at 54º overall slope angle (OD1). 203

Figure D-46 Planar failure for PE03 Northern Wall at 57º overall slope angle (OD5).. 203

Figure D-47 Wedge failure for PE03 Northern Wall at 57º overall slope angle (OD5). 204

Figure D-48 Toppling failure for PE03 Northern Wall at 57º overall slope angle (OD5). 204

LIST OF TABLES

Table 2-1 Summary of the design components of an open pit mine and their associated risk areas. (Sullivan, 2006) 18

Table 2-2 Classification of joint apertures (Bieniawski, 1984). 30

Table 2-3 Deere's classification of rock quality (Deere, 1989) 45

Table 2-4 Classification of rock quality based on RMR (Bieniawski, 1989). 47

Table 2-5 Adjustment to MRMR for weathering (Stacey & Swart, 2001) 48

Table 2-6 Adjustment to MRMR due to joint orientation (Stacey & Swart, 2001) 49

Table 2-7 Adjustment to MRMR for blasting effects (Stacey & Swart, 2001) 49

Table 2-8 Typical FoS and PoF acceptance criteria values (Wesseloo & Read, 2009) 59

Table 2-9 Adjusted MRMR values and recommended overall rock slope angles (Stacey & Swart, 2001) 73

Table 2-10 Comparison of numerical and limit equilibrium analysis methods (Wyllie, 2018). 79

Table 3-1 Geotechnical core logging data sheet used for PE03 logging exercise. 96

Table 3-2 Face mapping data log sheet used for PE03 mapping exercise. 100

Table 3-3 Uniaxial Compressive Strength test results with elastic constants for fresh rock (Bosman, 2013). 101

Table 3-4 Results of Triaxial Compressive Strength tests (Bosman, 2013). 101

Table 3-5 Brazilian Tensile Strength test (Bosman, 2013) 102

Table 3-6 Determination of RMR..... 104

Table 3-7 Rock Mass Rating System (After Bieniawski, 1989) 105

Table 3-8 Mean RMR values of the core samples used (Bosman, 2013). 106

Table 3-9 Mechanical properties for weathered rock, from surface to 25 m below surface. 108

Table 3-10 Mechanical properties for fresh rock, below 25 m from surface. 109

Table 3-11 Geometrical parameters for the current and optimized overall pit slope designs in the unweathered rock, below 25 m. 118

Table 3-12 Average MRMR value for fresh rock 123

Table 3-14 Mean joint sets for PE03 southern wall. 126

Table 3-15 Mean joint sets for PE03 northern wall. 127

Table 3-16 Mechanical properties used as model input parameters. 138

Table 4-1 circular charts analysis results summary. 139

Table 4-2 MRMR and Haines and Terbrugge design chart analysis results summary 140

Table 4-3 Kinematic analysis at bench slope scale. 141

Table 4-4 Kinematic analysis at Inter-ramp slope scale. 142

Table 4-5 Kinematic analysis at Overall Pit slope scale. 143

Table 4-6 Limit equilibrium analysis results summary. 147

Table 4-7 Finite element modelling results summary. 151

Table 4-8 Design parameters of the resultant optimum ultimate pit slope. 152

Table A-1 Geotechnical core logging data sheet for PE03DDGC8_01. 169

Table A-2 Geotechnical core logging data sheet for PE03DDGC8_02. 170

Table A-3 Geotechnical core logging data sheet for PE03DDGC8_03. 171

Table A-4 Geotechnical core logging data sheet for PE03DDGC8_04P. 172

Table A-5 Geotechnical core logging data sheet for PE03DDGT_01. 173

Table A-6 Geotechnical core logging data sheet for PE03DDGT_03. 174

Table A-7 Geotechnical core logging data sheet for PE03DDGT_06. 175

Table B-1 Northern wall face mapping. 176

Table B-2 Northern wall face mapping (continued) 177

Table B-3 Southern wall face mapping. 178

1. INTRODUCTION

Mining is a unique industry that is characterized by certain economic factors which are not found in other sectors of the economy (Runge, 2012). Some of the unique characteristics associated with the sector include (Runge, 2012):

- Capital intensiveness accompanied by long preproduction periods. Though other sectors of the industry might also be capital intensive, the difference comes in the percentage of the capital which is sunk. Mining is characterized by high sunk cost. In economics a sunk cost is defined as a part of a fixed expense that has been incurred and cannot be reclaimed and does not affect future decisions of the project.
- The initial plans and designs of a mine are based on limited data due to the high cost of data gathering through drilling hence it's difficulty to optimize the plans and designs during the feasibility phase of the project.
- Ore deposits are naturally occurring and they come with their inherent features such as grade distribution, geology, geometry, geotechnical properties etc., which cannot be controlled by the mine planner and designer thus the mine plans and designs must suit the natural characteristics of the ore deposit and its surrounding country rock. This also results in every mine being unique since different mines have different ore bodies.

In addition, the following are also characteristics exceptional to this sector:

- There is limited choice in terms of location as mines are located where the deposit is. Thus, the investor may incur the cost of developing the area as some areas might not have the basic infrastructure such as electricity, roads, water, accommodation for workers etc., which are needed for the smooth operation of the mine.
- Due to the fungible nature of minerals, (that is minerals of the same type once mined and processed will be identical irrespective of where and how they were mined and processed) they are traded on the international market and the sellers will be price takers. So, the selling price is independent of the production cost. Thus, for the sellers to make profit and remain in business they must minimize the production cost as much as they can.
- Minerals are non-renewable resources and there is an uncertainty associated with future exploration as a result a mine has got a life span which is dependent on the amount of ore reserves. Thus, the amount of reserves available for mining must match the amount of capital invested.
- There are a number of interested parties with different views such as: Politicians who are concerned about ownership of mineral properties, repatriation of profits, minerals policies etc. Environmentalists who are concerned with the control of negative environmental impacts brought about by mining as well as sustainable development. Thus policies, terms and conditions of the business environment are prone to change at any point in time during the life of mine and this might have a negative impact on the economics of the business. The investors are concerned with profit maximization.

These characteristics make the industry high risk in terms of investment and act as barriers to entry for investors. Therefore, if an investor has decided to undertake a mining project, wise investment decisions need to be made for both capital expenditure as well as operating expenditure. Thus, there is need to optimize the mine plans and designs as much as possible in order to reduce the risks associated with mining investments. The ultimate pit slope is one of the major design parameters that must be optimized for an open pit operation, as it has a direct influence on safety, amount of ore reserves available for extraction and the profitability of the operation (Stacey, 2009). A slope with a shallow angle results in high stripping ratios thus high mining cost per ton of ore and the steeper the slope the lower the stripping ratio and the lower the mining cost per ton of ore. But on the other hand, the shallower the slope the more stable the pit slope and the steeper the slope the less stable it is. Thus, the slope angle used must strike a balance between safety and cost. The stripping ratio is directly proportional to pit depth and it increases with depth up to a breakeven point where the cost of producing and selling minerals from a ton of ore equals the revenue from the minerals. The stripping ratio at this point is called the breakeven stripping ratio. For a shallow slope angle the breakeven stripping ratio is reached at a shallow depth thus disabling mining, since mining beyond the breakeven point will result in the operation realizing a loss. Thus, any mineralized zone beyond the breakeven point will not be part of the ore reserves as it is uneconomic to extract and in turn the life of mine will be cut short. On the other hand, the steeper the slope angle the deeper the pit can be mined since the breakeven point will be reached at a deeper level. In this case a greater portion of the mineralized zone will be available for mining and the more the reserves the longer the Life of Mine (LOM) and the returns on investment will

be high as well. Thus, there is always a need to optimize the ultimate pit slope angle as it reduces the amount of waste stripped and maximizes the ore reserves thereby reducing cost and maximizing the life of mine. Thus, justifying the huge investment associated with mining by maximizing the return on investment.

1.1 Background Of The Study Area

Pickstone-Peerless gold mine is equally owned by Vast Resources Zimbabwe Private Limited and Grayfox Investments Private Limited. It is located in Chegutu, 120 km south west of Harare, Zimbabwe Figure 1-1.

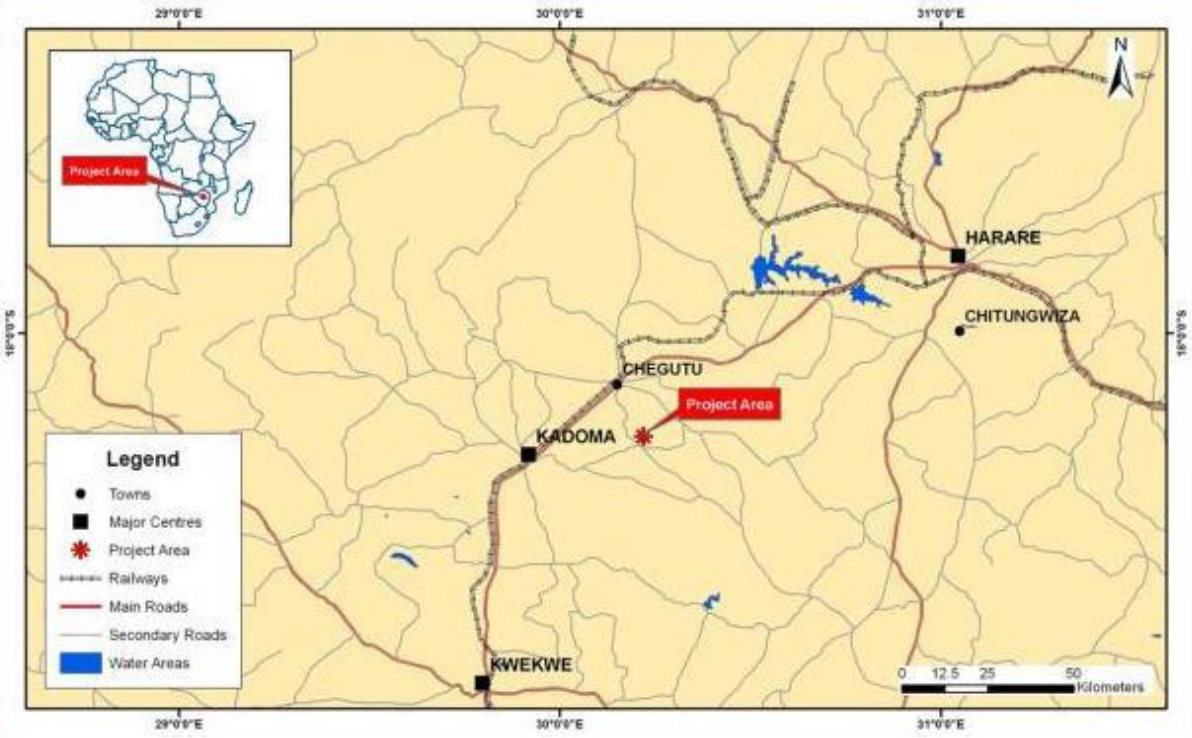


Figure 1-1 location of Pickstone-Peerless Mine (Bosman, 2013).

Development work started in July 2014 with production commencing in September 2015. The operation is an open pit mine with an expected life estimated at 18 years, at a milling

capacity of 50 kilotons per month (ktpm). The property is made up of two separate ore bodies, Pickstone and Peerless ore bodies which are almost parallel to each other. These ore bodies are being mined separately. For Pickstone ore body the pit currently being mined is the PK01and for the Peerless ore body the PE03 pit is being mined. The maximum pit depth was projected to be 175 m for the Pickstone pit and 165 m for the Peerless pit, after which there are plans to convert from open pit mining to underground operations (Vast-Resources, 2015). The current overall pit slope for the Peerless pit was designed at 52^{o}. The mine wanted to deepen the PE03 pit (Figure 1-2) by a further 5 m to 170 m. The research conducted in this investigation was to understand if the pit-wall slope angles could be further optimized to allow for the additional extraction without a cutback, i.e by steepening the slopes. The site was therefore used as the case study.



Figure 1-2 Satellite image of the PE03 pit. (Google, 2019)

It is currently made up of 10 m high, vertical benches, with alternating 10 m and 6 m wide safety benches. The pit is serviced by two 12 m wide ramps which are positioned one on

the northern and the other one on the southern side of the pit. The inter-ramp stack height is 40 m. At the time of study, the pit was 1.03 km long along strike with a width of around 210 m.

1.2 Geological Setting

The Pickstone-Peerless gold mineralisation is hosted by a sedimentary succession associated with mafic and ultramafic volcanic lithologies of the Sebakwian Group, within the Archaean Chegutu Greenstone Belt. The mineralised trends are located on the southern limb of an easterly-trending synform, which contains a number of subsidiary folds. The Pickstone-Peerless ore body outcrop forms a substantial ridge, pronounced from the surrounding topography (Bosman, 2013). The orebody is oriented at a dip and dip direction of 80/010.

1.3 Seismicity

According to (Bosman, 2013), Pickstone-Peerless gold mine is located in a tectonically stable region since the African continent is not a tectonically active region. Therefore, there is no need to worry about exposure to natural seismic activity. There is also little risk of mining induced seismicity since mining operations will be conducted at shallow depths, less than 1 000 m below surface. Under such conditions there will not be significant changes to the stress field to cause mining induced seismicity. There are also no surrounding mines that are likely to cause seismicity.

1.4 Problem Statement

In mining, initial designs are generally not fully optimized as there is limited information about the deposit and the surrounding country rock in the initial stages of the project. This is due to the cost and impracticality of gathering all the necessary data before any mining excavations are created. Thus, there is always need to update assumptions used in the initial designs when the deposit and the country rock are exposed by mining excavations. In the case of pit slopes it is common that the initial designs will be too conservative, resulting in:

- High stripping ratios:
- Shallow pit depth:
- Under estimation of reserves; and
- A shorter LOM with a lower net present value than the optimum for the project.

Often the slope design is re-visited during the open-pit life resulting in the improvement of the aforementioned factors and improving project economics.

1.5 Research Objectives

The objectives of the research are as follows:

1. To determine the optimum ultimate pit slope angle that will maximize ore recovery in a safe and economic way.
2. To determine the bench geometrical parameters compatible with the optimum ultimate pit slope and discontinuity orientations.
3. To determine slope management practices that will ensure safety of operations.

4. Compare the calculated slope angle to the existing slope angle.

1.6 Key Questions To Be Addressed

The following are the key questions to be answered by the research:

1. What is the steepest overall pit slope angle that will result in a safe and most economic operation for the mine?
2. What are the potential geotechnical risks associated with this maximum overall pit slope angle?
3. What are the control measures and monitoring systems that can be put in place in order to eliminate or reduce the potential risks?

1.7 Research Methods

Data was collected through geotechnical core logging, face mapping and literature review of previous work done on the project site. This data was then used as input in stability analysis. Empirical, kinematic, limit equilibrium and numerical modelling techniques were used in the analysis. A number of slope angles were analysed by determining their Factor of Safety (FOS) and Probability of Failure and comparing these to acceptable industry limits.

1.8 Structure of The Research Report

Chapter 2 presents the literature review of the following aspects:

- basic geometrical design components of an open pit mine;
- influence of overall pit slope angle on pit optimization;

- factors affecting slope stability;
- slope failure modes,
- rock mass characterization;
- acceptability criteria for open pit slope design;
- slope stability analysis and design;
- open pit mine slope management and slope failure preparedness.

This was then used as basis for the work presented in chapter 3, the methodology. The results obtained from the methodology were then presented and analysed in chapter 4. Finally, chapter 5 presents the conclusions and recommendations made based on the results of the research.

2. LITERATURE REVIEW

2.1 Introduction

Mining differs from other engineering disciplines in that the engineer has no control over the properties of the rock material. Mines are geotechnical structures constructed in rock, with *in situ* rock mass being used as the construction material. The *in situ* rock mass is unlike most engineering materials, in that it is made up of solid intact rock material which is separated by discontinuities. It is usually heterogeneous and anisotropic in character (Brady & Brown, 2005). Hence the designing engineer generally cannot directly assign laboratory determined rock mass properties or loading conditions (Hudson & Harrison, 1997). Instead one must account for the existing geotechnical properties of the rock material. In open pit mining or quarrying operations, the slope geometry must suit the geotechnical setting in which it is going to be excavated (Stacey & Swart, 2001). Considering all this it can be deduced that each mine design is unique as different mines are located in different geotechnical settings. Thus, each case must have its own specific design that will meet the requirements for safety, production and cost with respect to its specific geotechnical setting.

The focus of this chapter is on summarizing the current state of knowledge about the impact of slope design and optimization on the overall economics of an open pit mine and the principles governing the practices and techniques used in open pit mine slope design and optimization. This will then be used as a basis for the pit slope design and optimization of the mine in question.

2.2 Basic Geometric Design Components Of An Ultimate Pit Slope

An open pit mine is an excavation made in the earth's crust for the purpose of extracting ore and will remain open to the outside environment for the duration of the mine's life. For ore to be extracted in an open pit mine there is need to remove or strip all the waste rock above it. An economic mining operation minimizes the amount of waste stripped per every ton of ore mined and this is of paramount importance to the success of the operation. This can only be achieved through understanding the influence of the geotechnical parameters on the safety and economic performance of the mine. This section outlines the basic geometric design components of the ultimate pit slope and their impact on the safety and economics of the open pit mine. According to Sullivan (2006) there are three basic components of an open pit mine slope and these are:

- Bench,
- Inter-ramp slope,
- Overall slope.

2.2.1 Bench

The bench is the smallest building element of an open pit mine slope. There are two types of benches, the working bench and the catch bench or safety bench. A safety bench prevents boulders falling from benches above to proceed down to the benches below or to the pit bottom. The final pit slope is an accumulation of safety benches that will improve the stability of the ultimate pit slope. The bench geometry is described by the following:

Bench height (H), which is the vertical distance from the lowest point of the bench, known as the toe, to the highest point of the bench, known as the crest. The bench height is a

function of the capacity and reach of the loading equipment, selective mining requirements, statutory requirements and safety. Sometimes a double bench system is employed whereby the height of safety benches forming the ultimate pit slope is double the height of the working benches. This will result in a much steeper ultimate pit slope and thus reduced stripping ratio and improved pit economics.

The bench face or bench slope angle is defined as the angle formed by an imaginary line joining the crest and the toe of a bench and the horizontal. The bench slope angle is defined by the need to minimize scaling of rocks from the bench face posing harm to personnel and equipment working below. The bench face being the exposed inclined surface of a bench. The scaling of rocks is a function of the rock mass characteristics, and in some geotechnical settings, environmental conditions such as rain and snow will also contribute. The blasting practices employed also have an effect on the resulting bench slope angle as in some cases blasting leads to back breaks and damage of the remaining rock mass (Hustrulid & Kuchta, 1998). The general bench geometry is shown in Figure 2-1. The width of the safety bench (S_B) can be determined using the Modified Ritchie Criteria (Ryan & Pryor, 2001), which is shown in Equation 2-1.

$$\boldsymbol{Bench\ width\ (m) = 0.2 \times bench\ height + 4.5\ m} \qquad \text{Equation 2-1}$$

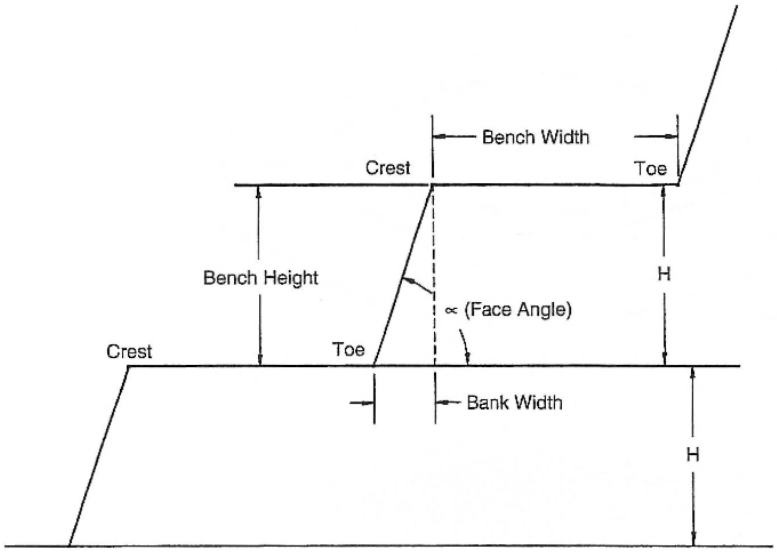


Figure 2-1 Bench geometry (Hustrulid & Kuchta, 1998)

The width of the safety bench is designed to catch the fallen material if the higher bench fails. The catching capacity of the safety benches can be increased by building a ridge of blasted waste rock called a berm along the crest of the safety bench to create a ditch between the berm and the toe of the safety bench above, Figure 2-2.

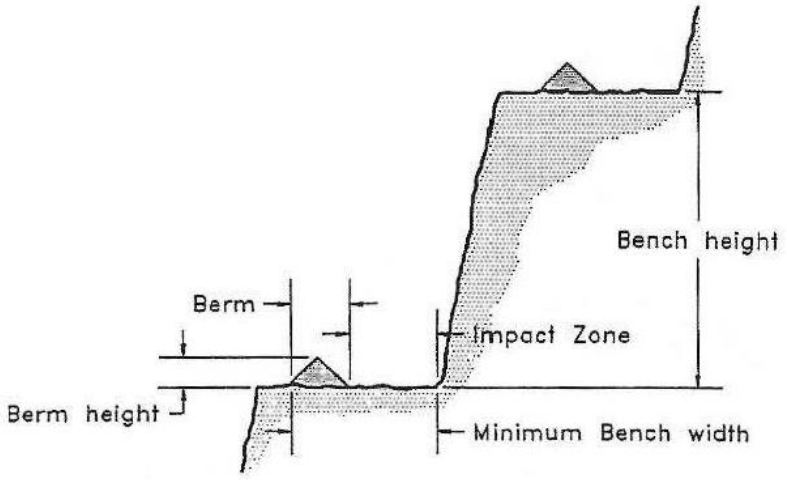


Figure 2-2 Safety bench with berm constructed along the crest (Hustrulid & Kuchta, 1998).

2.2.2 Inter-Ramp Slope

The final pit slope will be comprised of a number of safety benches arranged in stacks. A stack is usually made up of two to six benches and the bench width at the bottom of the stack will be wide enough to contain fallen material if the stack fails. The safety benches on the final pit slope will sometimes be intersected by a ramp or haul road that will be used for gaining access from surface down to the pit bottom or from the pit bottom up to the surface. The width of the safety benches will be narrow as compared to the width of the ramp. In this case the ramp will replace the wider safety bench at the bottom of the stack and it will catch fallen material if the stack fails. The inter-ramp slope is defined as the slope formed by a number of safety benches between the crest of the uppermost bench of an open pit mine and the immediate ramp section or wider safety bench or between two successive portions of a ramp or wider safety bench or between a ramp or wider safety bench and the pit bottom (Mathis, 2009), (Figure 2-3).

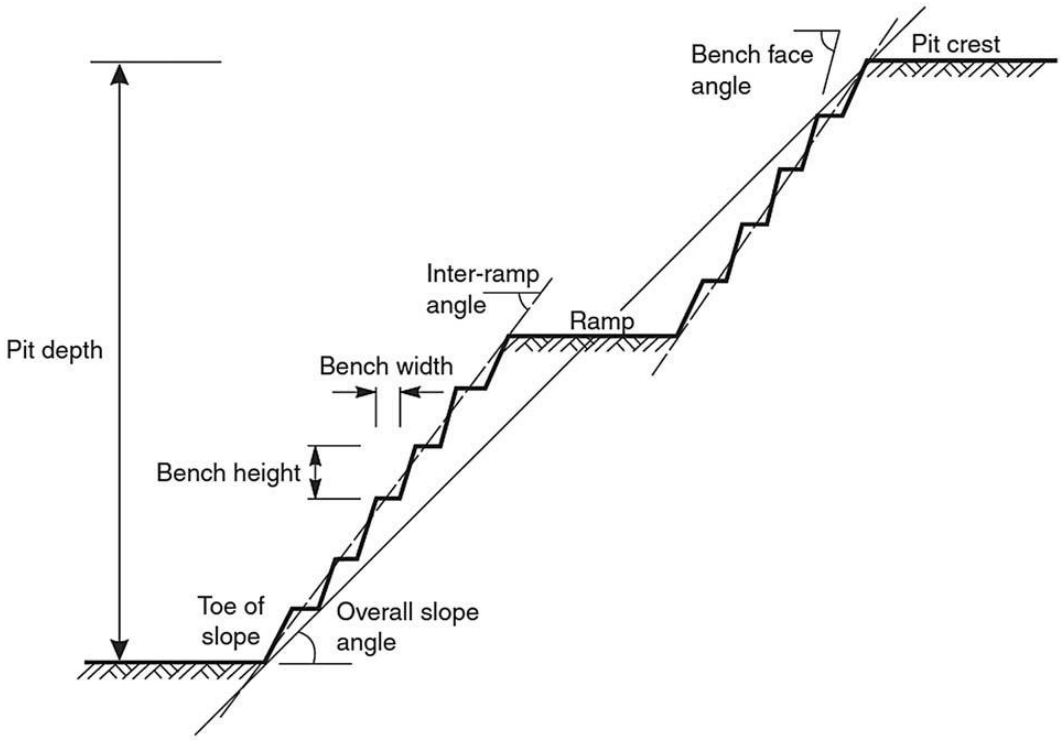


Figure 2-3 Geometrical parameters for a bench; inter ramp slope and overall slope (Wyllie & Mah, 2004).

The geometry of an inter-ramp slope is described by inter-ramp slope height or stack height which is defined as the vertical extent of a stack of safety benches that will remain stable under the prevailing geotechnical conditions and design parameters. The other parameter used to describe the geometry is the inter-ramp angle which is the angle between a line joining the toe of the lower safety bench and the crest of the upper safety bench of the inter-ramp slope and the horizontal. The greatest possible inter-ramp slope angle is influenced by the safety bench geometry which in turn is a function of the structural properties of the rock mass in which the benches are constructed. Inter-ramp slope failure does not only pose safety risk but also economic risk as it can significantly

affect the ramp that provides access to and from the pit thus resulting in major disruptions to production.

2.2.3 Overall Slope

The overall slope is also known as the final pit slope or the ultimate pit slope and will be made up of safety benches that will improve the stability of the ultimate pit slope. Since the final pit slope is comprised of safety benches arranged in stacks with a wider safety bench or a haul road or ramp at the bottom of the stack, this will result in the overall slope being shallow as compared to the inter ramp slope. The effect of a ramp on the final pit slope is illustrated by Figure 2-4 **.**

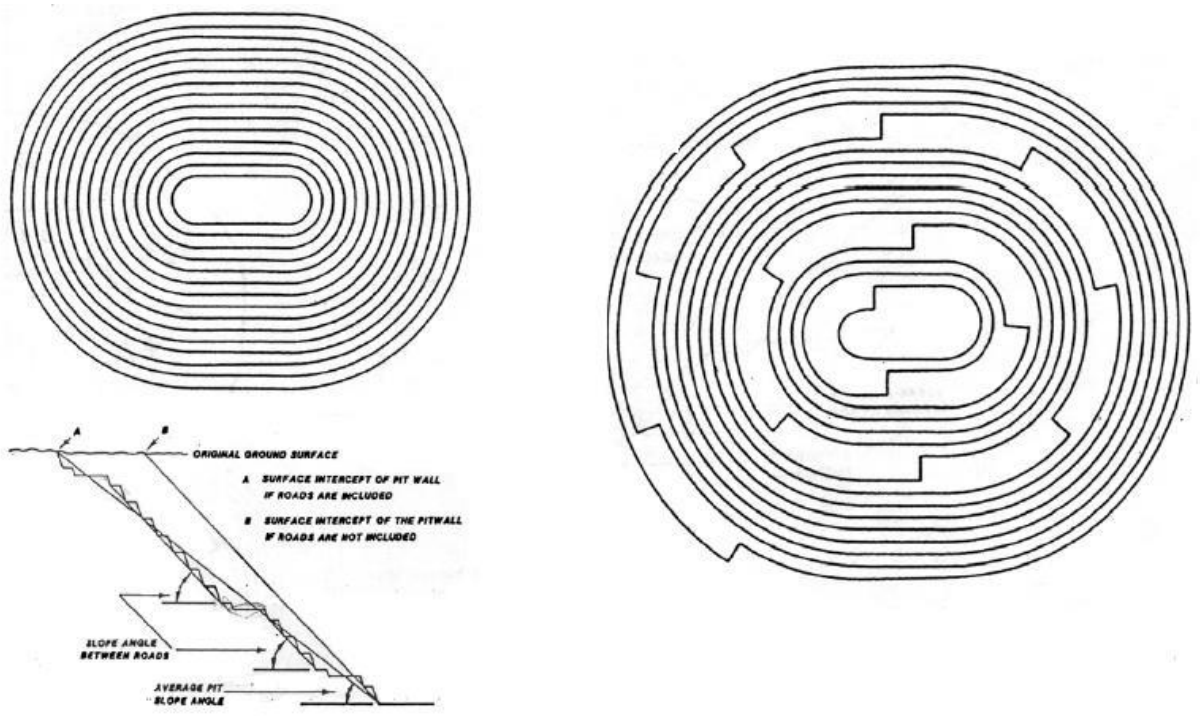


Figure 2-4 Effect of ramp on the final pit slope angle. (Hustrulid & Kuchta, 1998)

The overall slope is geometrically described by the overall slope height and the overall slope angle. The overall pit slope angle is defined as the inclination to the horizontal of the line joining the crest of the uppermost bench of the pit to the toe of the lowermost bench Figure 2-5.

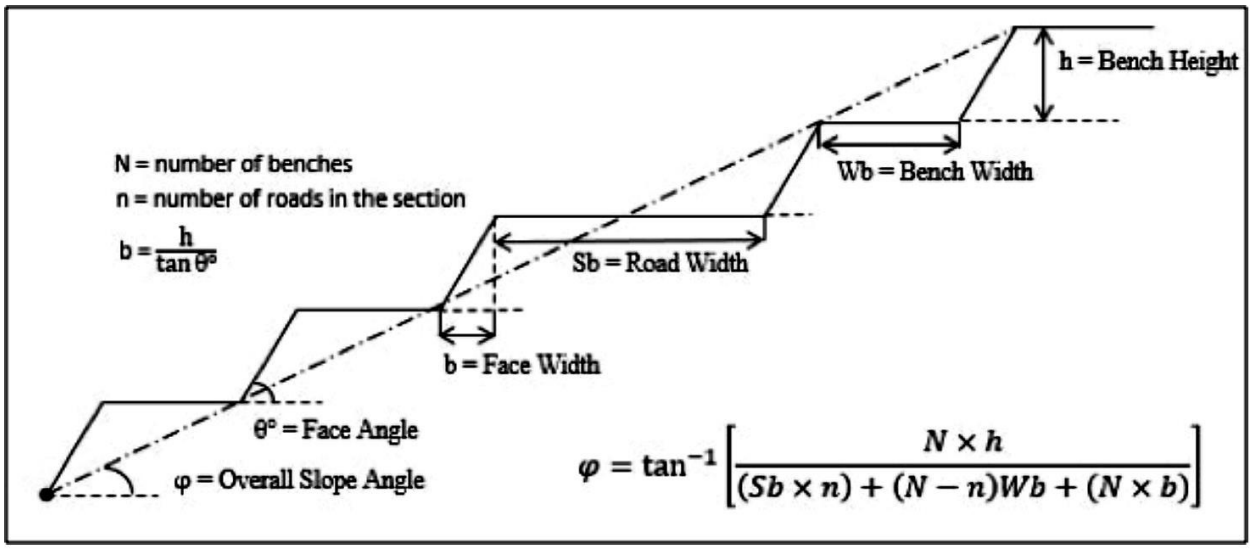


Figure 2-5 Elements and equation to calculate the overall pit slope angle (Alegre, et al., 2019).

The overall pit slope angle is controlled by structural geology, intact rock strength, rock mass strength, geohydrological conditions, *in situ* stress conditions, blast induced vibrations, mining equipment requirements and so on.

The author noticed an error in the overall slope angle equation presented in Figure 2-5, the coefficient for ***Wb*** is supposed to be ***(N -n - 1)*** as shown in Equation 2-2

$$\varphi = \tan^{-1}\left[\frac{\mathrm{N} \times \mathrm{h}}{(\mathrm{Sb} \times \mathrm{n}) + (\mathrm{N} - \mathrm{n} - 1)\mathrm{Wb} + (\mathrm{N} \times \mathrm{b})}\right] \qquad \text{Equation 2-2}$$

Summary of the design components of an open pit mine and their associated risk areas is provided in Table 2-1.

Table 2-1 Summary of the design components of an open pit mine and their associated risk areas. (Sullivan, 2006)

Slope design element	component	MAIN CONTROLLING OR INFLUENCING FACTOR			RISK AREA	
		Geotechnical Issues	Mining Systems	Environmental Factors	Safety	Economics
Bench geometry	Angle	•	•	✓	•	•
	Height	•	•	✓	•	✓
	Berm width	•	•	✓	•	✓
Inter ramp	Angle	•	✓		[1]	•
	Height	•			[1]	•
overall	Angle	•	✓		[1]	•
	Height	•			[1]	•

[1] Assuming that good pit slope management procedures and practices are being followed

Key:

- • Major factor
- ✓ Minor factor

Table 2-1shows two basic risk elements in an open pit mining operation, safety and economics (Sullivan, 2006). Bench geometry affects both elements but the main area of concern is safety whereas the design of the inter ramp and the overall slopes is mainly concerned about economics assuming that good pit slope management procedures and practices are being followed.

2.3 Influence Of Overall Pit Slope Angle On Pit Optimization

Defining ultimate pit limits is the first step in planning an open pit mine. The pit limits are defined as the lateral and vertical extent to which mining can be economically carried out. Within the ultimate pit shell lies the total material to be mined during the LOM and this material is comprised of both waste and ore. The major contributing factor to the size and shape of the final pit shell is the pit slope angle. Thus the overall pit slope angle will in turn influence the amount of waste and ore to be handled from the pit as well as to what extent the pit can be economically operated (Kennedy, 1990). According to (Stacey, 2009), a 1° increase in pit slope angle of a 500 m high slope inclined at 50° to the horizontal will minimize waste stripping by approximately 9000 tonnes per metre of face length. This indicates that the first step in pit optimization is slope optimization. According

to (Hajdasinski, 1988), mine optimization can be done in different forms and at any phase of the project, i.e planning or exploitation stages:

Planning stage:

- *Maximizing NPV by pit optimization.*
- *Maximizing the recovery.*
- *Minimizing environmental impact by pit optimization.*

Exploitation stage:

- *Extend mine life by pit optimization.*
- *Improve discounted cash flows (DCF) by pit optimization.*
- *Extend the recovery.*
- *Decrease operating expenditure (Opex)*

The effect of a steeper ultimate pit slope on the shape and size of the pit depends on the way the steep slope is implemented. In most cases steepening the overall slope angle results in decreased stripping ratios, but this does not necessarily mean a decrease in the total waste to be mined. In some instances it can give room to the expansion of the pit limits or overall size of the pit increasing both ore and waste amounts, maintaining the stripping ratio (Golestanifar, et al., 2018). Figure 2-6 shows the common scenario in which the resultant effect is reduction in the amount of waste whilst the same amount of ore will be recovered as compared with the flatter slope.

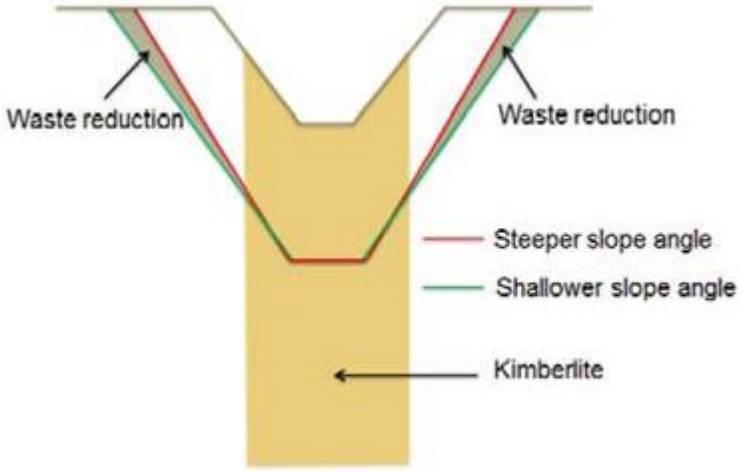


Figure 2-6 Reduction in the waste, maintaining ore recovery (Madowe, 2016) .

Figure 2-7 shows a scenario in which the amount of ore recovered increases whilst the amount of waste stripped remains the same as before.

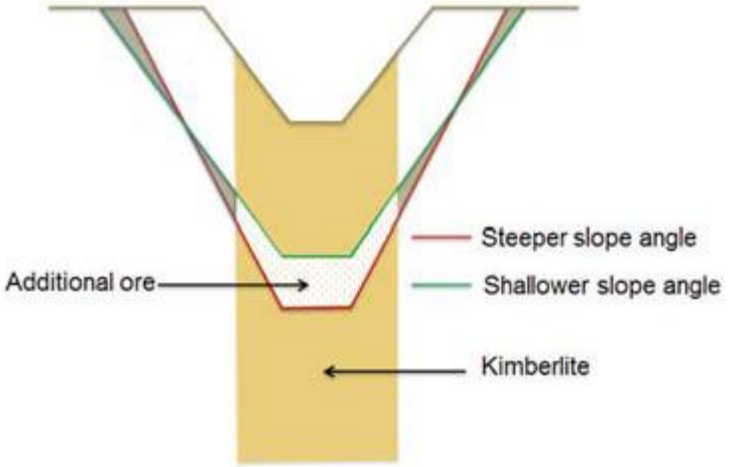


Figure 2-7 Increase in ore recovered while maintaining same amount of waste stripped (Madowe, 2016).

Figure 2-8 shows a scenario in which the amount of both ore and waste are increased with stripping ratio remaining the same or slightly decreased.

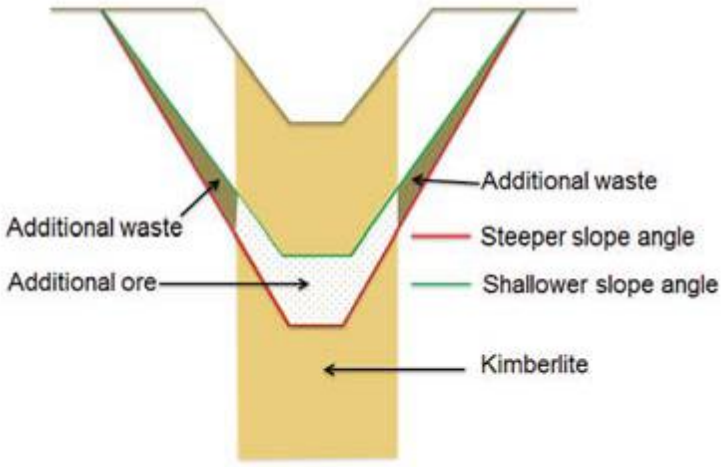


Figure 2-8 Increase in both ore and waste (Madowe, 2016).

The third scenario has an advantage over the first two scenarios in that there is more value realized in mining more tons of ore than saving cost by reducing waste mined whilst maintaining the same amount of ore or having a small increase in ore while maintaining the same amount of waste, as the net value from a ton of ore is much more as compared to the cost of extracting a ton of waste.

2.4 Factors Affecting Slope Stability

The safety and economic risks associated with open pit mine slopes are due to the potential instability of the slopes. In order to reduce these risks, one must understand the different factors that trigger instability of these slopes, both at bench scale as well as global scale. A list of some of the factors that control pit slope stability is shown below (Stacey, 1968):

- Geological structures,
- Rock stresses,

- Groundwater conditions,
- Strength of discontinuities and intact rock,
- Pit geometry, including both slope angles and slope curvature,
- Vibration from blasting or seismic events,
- Climatic conditions, and,
- Time.

2.4.1 Geological structures

A rock mass consists of solid intact blocks of rocks that are separated by naturally occurring geological discontinuities or structures. These discontinuities form planes of weakness within the rock mass as they have lower shear or tensile strength as compared to the intact rock blocks. These discontinuities have a major impact on the strength of the rock mass as they provide the weak path along which sliding or separation of blocks can occur. They also accommodate and enable water to flow through the rock mass further weakening it (Singhal & Gupta, 2010). Geological structures come in a number of forms and some of these are described below.

2.4.1.1 Bedding planes

These are planes of weakness found in sedimentary and certain other rocks, generally formed when different layers of sediments are deposited on top of each other. Bedding planes are usually highly persistent and cover a wider area as compared to other types of discontinuities.

2.4.1.2 Joints

Joints are planar fractures resulting from brittle failure of the rock along which no visible shear movement has occurred (Schultz & Fossen, 2008). They are a common feature in most rocks. According to (Hudson & Harrison, 1997) joints are described by a number of geometrical attributes which are shown in Figure 2-9.

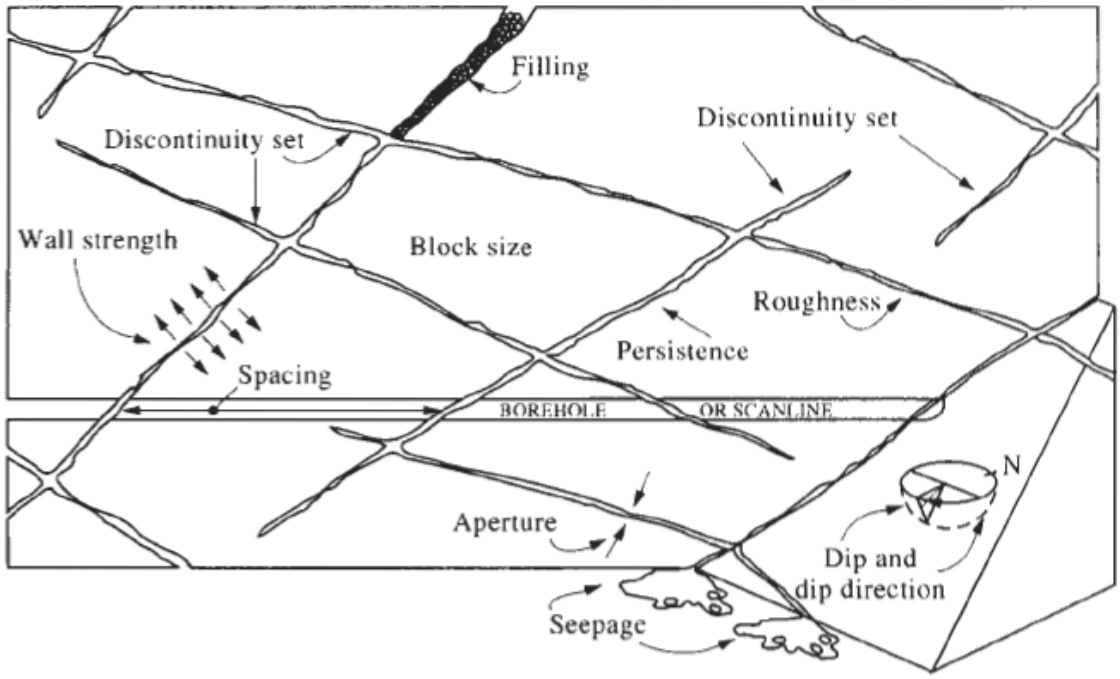


Figure 2-9 Schematic of the primary geometrical properties of discontinuities in rock. (Hudson & Harrison, 1997)

Orientation: Joint orientation is uniquely defined by the dip and dip direction of a joint plane (Hudson & Harrison, 1997). Since a joint is assumed to be a planar feature its dip is defined as the angle between the horizontal plane and the steepest line along the joint plane. The dip direction is then taken as the compass bearing of the horizontal projection of this steepest line. Figure 2-10 is a schematic diagram showing dip (ψ) and dip direction

(α) of a joint (Wyllie & Mah, 2004). The strike is another parameter which can be used to define the orientation of a joint and is defined as the horizontal line formed when the inclined joint plane intersects with the horizontal plane.

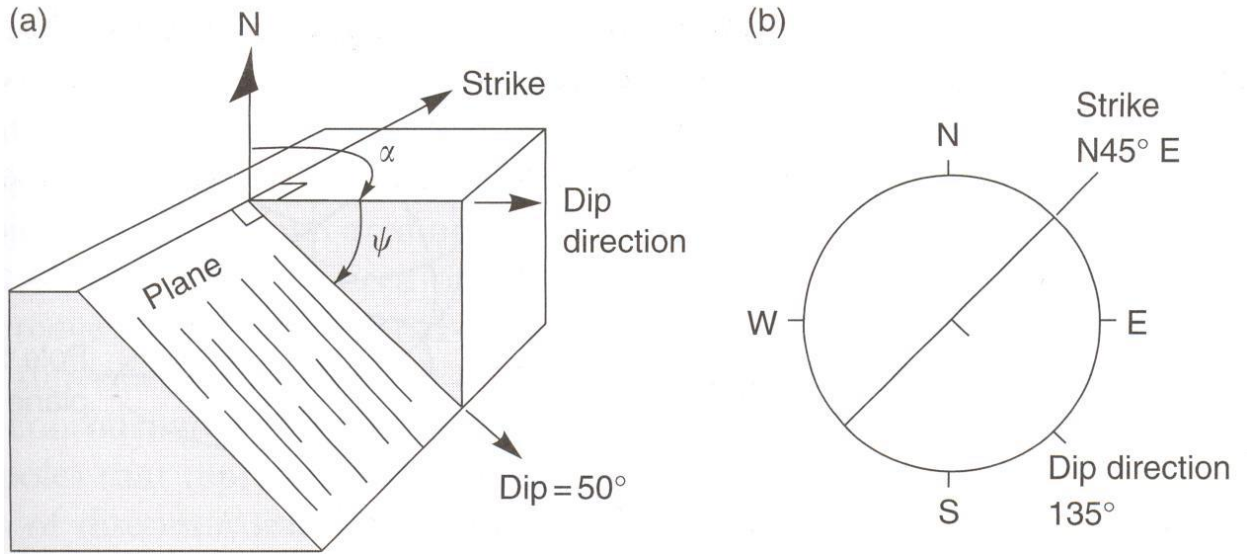


Figure 2-10 Terminology defining discontinuity orientation: (a) isometric view of plane (dip and dip direction); (b) plan view of plane (Wyllie & Mah, 2004)

Spacing and frequency: Joint spacing is defined as the distance that separates two adjacent joints or discontinuities intersected by a scanline or diamond drill hole, with the scanline oriented perpendicular to the joint plane. Joint frequency defines the number of joints that are intersected per metre length of the scanline or diamond drill hole. Thus, joint frequency is the inverse of the joint spacing. Joint spacing determines the block size distribution associated with a potentially unstable rock mass. That is failure can take the form of very large blocks sliding down the slope face or small blocks unravelling from the slope face depending on the spacing of joints. For a scanline L metres long intersecting

N number of joints, spaced at X m, with the scanline oriented perpendicular to the joint plane, the Joint frequency (λ) will be given by Equation 2-3:

$$\lambda = N/L\ m^{-1}$$ Equation 2-3

It can be noted that as the orientation of the scanline to the normal of the joint plane is varied so is λ (Figure 2-11). An increase in the angle between the scanline and the normal to the joint plane, (θ), will see the joint spacing increasing to (X/cos θ) (Hudson & Harrison, 1997). This will result in λ decreasing from its maximum to zero as θ increases from 0° to 90°. If θ is further increased beyond 90°, λ will start to increase up to its maximum at the point where θ equals 180°. The new spacing and frequency is referred to as apparent spacing ad apparent frequency but the actual spacing ad frequency do not change.

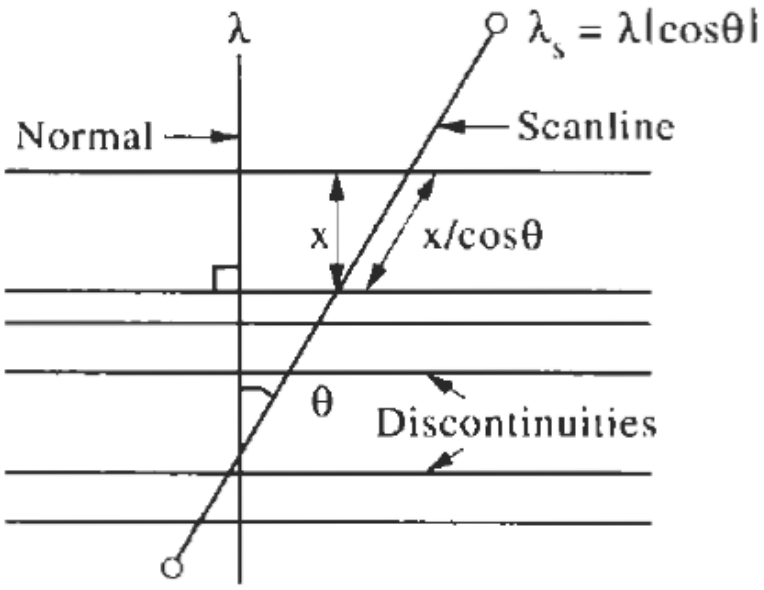


Figure 2-11 Variation of joint frequency as the scanline is moved from being perpendicular to the joint plane to being parallel to it (Hudson & Harrison, 1997).

The length of the scanline intersecting N number of joints with scanline oriented at an angle θ to the normal of the joint plane is given by $L/\cos\theta$. The joint frequency for this case is denoted by, λ_s, given by Equation 2-4.

$$\lambda_s = \frac{N}{L}\cos\theta, \text{ or } \lambda_s = \lambda\cos\theta \qquad \text{Equation 2-4}$$

Since joint frequency is always positive Equation 2-4. is used in the form of Equation 2-5.

$$\lambda_s = \lambda|\cos\theta| \qquad \text{Equation 2-5}$$

Equation 2-5 is thus used when estimating the actual frequency when a scanline has been set not perpendicular to the plane of the joint set.

Persistence: Refers to the total extent of a joint in terms of area or length covered by the joint. It describes the continuity of a joint. According to (Piyal & Konietzky, 2016) discontinuities form the weakest path in a rock mass along which failure can easily occur as compared to intact rock blocks. The less persistent discontinuities are, the greater the percentage of the rock mass consisting of intact rock material. Rock “bridges” often exist between parallel non-persistent joints, which need to be broken before sliding or failure can take place. Figure 2-12 illustrates the difference between persistent and non-persistent joints as defined by (Kim, et al., 2007).

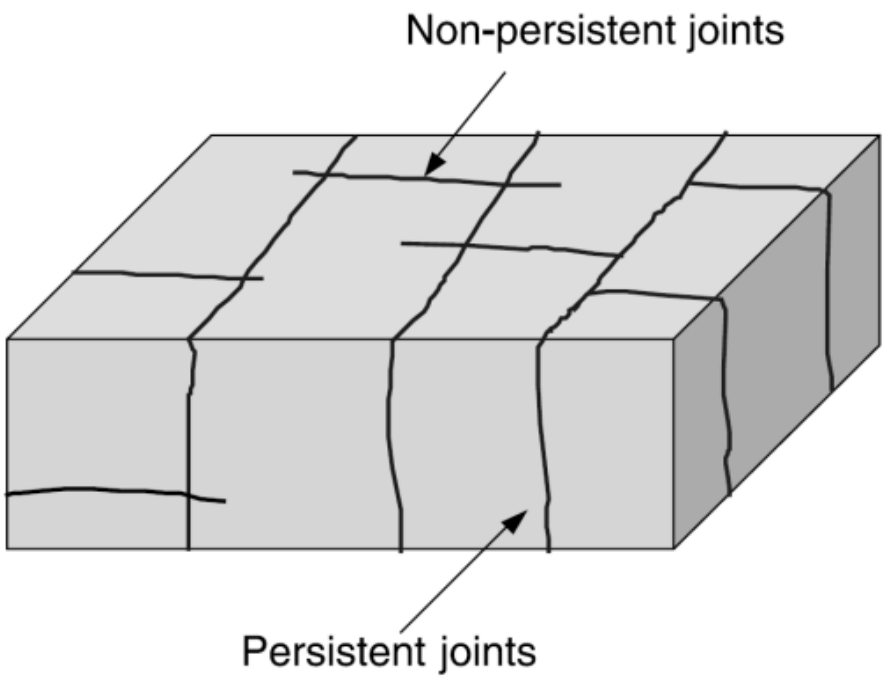


Figure 2-12 Joint persistence (Piyal & Konietzky, 2016)

In conjunction with joint spacing, joint persistence influences the size of rock blocks that can detach and slide from the pit wall. The greater the persistence of the joints the greater the chances of different joint sets interconnecting with each other forming loose unstable rock blocks that can detach from the slope face. However, it is not always possible to determine the persistency of a joint when it is not parallel to the face. The following formula is generally accepted for estimating persistency (Priest & Hudson, 1981).

$$N''_{\delta j \vartheta j} = N'_{\delta j \vartheta j} L_s / L$$ Equation 2-6

Where:

$N'_{\delta j \vartheta j}$	Number of joints that would have been mapped
L_s	Standard length
L	Actual sampling length
$N''_{\delta j \vartheta j}$	Is the number of joints in a given class interval that would have been sampled had the exposure been long enough to measure the standard length of the joint L_s

Joint roughness: Joints can be described as being made up of two rock blocks in contact and the contact surfaces of these blocks are not normally flat but wavy in nature. This waviness is the one defined as the joint roughness. The degree of roughness of a joint has got influence on the joint strength as it affects the amount of friction between the two contacting blocks. The rougher the joint the greater the friction between the two blocks resulting in greater shear resistance of the joint against sliding. According to (Goodman, 1976) the roughness angle of the joint surfaces will have an effect on the joint shear strength at low normal stresses but as the normal stress increases the saw teeth (asperities) of the joint surfaces tend to lock tightly together such that the strength of the asperities will be the main influence on the joint shear strength as sliding will only occur after these asperities have been broken.

Aperture and filling: Aperture is a measure of how widely the two blocks forming the joint are separated from each other. This gap is usually filled with a soft material and

measured in a direction normal to the two surfaces forming the joint. Joint aperture varies across the joint plane with the degree of roughness of the joint. Table 2-2 shows classification of joint apertures (Bieniawski, 1984).

Table 2-2 Classification of joint apertures (Bieniawski, 1984).

TERM	**SEPARATION**
Very tight	< 0.1 mm
Tight	0.1- 0.5 mm
Moderately open	0.5- 2.5 mm
Open	2.5-10 mm
Very open	10-25 mm

Joints can be classified according to the material occupying the joint aperture. Thus, a joint can be said to be open in which case the joint opening will be filled with air and/or water. A joint can also be termed filled in which case the joint opening will be filled with material other than air or water only. Joints can be filled with materials of different types and origins. Filling material can originate from crushed country rock resulting from shearing during fracture or discontinuity creation, it can be a result of *in situ* weathering or alteration of the joint wall surface or it can be a result of foreign material being deposited into the joint opening (for example calcite) and also igneous intrusion into the joint opening. The type of fill material and fill thickness has an impact on the shear strength of the joint and thus on the stability of rock slopes. The aperture size and type of fill material

also influences the hydraulic conductivity characteristics of the rock mass. For planar smooth joint surfaces a thin layer of clay filling will greatly reduce the joint shear strength whilst for rough undulating joint surfaces the fill thickness needs to be greater than the amplitude of the asperities in order for the joint shear strength to be purely equal to the shear strength of the fill material (Hoek, 2006).

Joint or discontinuity set: Usually joints are formed as a group and this group will have a common orientation related to the stress orientation which resulted in the formation of these joints. Thus, a joint set is defined as a number of joints which are parallel or sub-parallel to each other. A rock mass can be subjected to a number of different stress regimes thus resulting in the formation of a number of different joint sets within the rock mass. This group of joint sets is defined as a joint system. The greater the number of joint sets and systems within a rock mass the weaker the rock mass will be.

Block size: As mentioned earlier discontinuities within rock mass give rise to detached rock blocks. The average block size and the block size distribution within a rock mass are critical inputs in the design of stable excavations and excavation support and thus need to be known. The block size is a function of the extent of jointing within a rock mass. The dimensions of the blocks are influenced by the joint spacing, joint persistence and the number of joint sets within the rock mass. A rock mass can also contain random and individual joints that do not belong to any joint set and these can also have an influence on the size and shape of the rock blocks (Palmström, 1995). For well-defined blocks to be created at least three joint sets must exist within the rock mass. However, in some cases the presence of the random individual joints will assist in the formation of well-

defined rock blocks. In cases where most of the joints are non-persistent or irregular it will be a challenge to identify the actual size and shape of individual rock blocks.

2.4.2 Groundwater

According to (Wyllie & Mah, 2004) groundwater has the following negative impacts on pit slope stability:

Water pressure: This reduces the shear strength of rock discontinuities since the pressure exerted by the water on the walls of the rock blocks forming the joint plane is the same in all directions, therefore it tends to open up the joint reducing the frictional resistance of the joint plane. Water pressure tends to reduce the normal stress acting on the discontinuity plane thus reducing the shear resistance of the discontinuity. In tension cracks and near vertical fissures water pressure tends to act in favour of slope destabilizing forces thus increasing the chances of slope failure. This is the major effect of ground water on slope stability.

Weathering: Some rock formations can be easily weathered if they are subjected to frequent changes in moisture content and this will result in cohesion loss and thus reduction in rock shear strength.

Freezing: If water in discontinuities freezes this will result in further widening of the discontinuity aperture since water expands when frozen. Thereby further weakening the discontinuity. If surface water freezes it will block drainage ways thus locking water inside the rock mass resulting in water pressure build up within the rock mass giving rise to slope instability.

Erosion: Surface water can wash away loose weathered material and groundwater can wash away loose infill material or dissolve infill material which is not chemically stable in water resulting in local instability as the toe of the slope can be undercut or a block of rock loosened.

2.4.3 Rock mass stresses

In mining the rock mass is subjected to two types of stress loads and these are *in situ* stresses (also known as virgin or primitive stresses) and induced stresses.

In situ stress is defined as the stress state of the rock mass in its natural state before being disturbed by human activities in this case mining. According to (Sjoberg, 1996) it is almost always the case that *in situ* rock mass stresses are compressive in nature and are a result of or the combination of the following:

Gravitational stresses due to the weight of the rock above the point in question.

Tectonic stresses resulting from external tectonic forces.

Stresses caused by previous glaciations.

Residual stresses.

The gravitational and tectonic factors are regarded as the key contributors to the final *in situ* stress state. The vertical stress component is usually assumed to be a result of the gravitational factor and thus is estimated from the weight of the overlying rock mass, Equation 2-7.

$$\sigma_v = \gamma z$$ **Equation 2-7**

Where: σ_v Vertical stress (MPa)

γ Unit weight of the overlying rock (MN/m^3)

z Depth below surface (m)

The horizontal stress component is however very difficult to estimate due to the influence of the tectonic factor which varies greatly from place to place across the world (Sjoberg, 1996). The ratio between the average horizontal stress (σ_h) and the vertical stress has been found to be a constant and is denoted by the letter *k* known as the *k* ratio, Equation 2-8, (Hoek, 2006).

$$\sigma_h = k\sigma_v = k\gamma z$$ **Equation 2-8**

Measurements taken around the world from mining and civil engineering cases indicate that the *k* ratio is higher at shallow depth and decreases as the depth increases (Brown & Hoek, 1978). This means that at shallow depths horizontal stresses tend to be higher than vertical stresses and the opposite at great depth.

Induced stress state is created when an excavation is made in the rock mass, disturbing the initial stress field by redistributing the stresses in the rock mass surrounding the excavation, resulting in a new stress field in this rock mass. The excavation of an open pit mine results in some areas of the slope losing some of the initial stress and this stress will be directed to other areas of the slope creating higher stress concentrations in these areas. The resultant is that some areas will be relieved of stress whilst others will gain

additional stress (Hoek, et al., 2009). As the open pit mine slope is excavated the rock mass immediately behind the slope face deforms and is relieved of stress, this results in the formation of a weak zone in this rock mass which can later on fail under the influence of gravity. According to (Sjoberg, 1996) the horizontal stress relieved from the upper part of the slope face is redirected and squeezed under the pit bottom giving rise to high stresses at the toe of the pit (Figure 2-13) resulting in stress driven failure at the toe, stress relief (destressing) at the upper part of the slope face will result in the opening of pre-existing discontinuities resulting in gravity driven failure along these planes of weakness. Stress related slope failures are usually of great concern in large scale slopes as opposed to small scale slopes (Sjoberg, 1996).

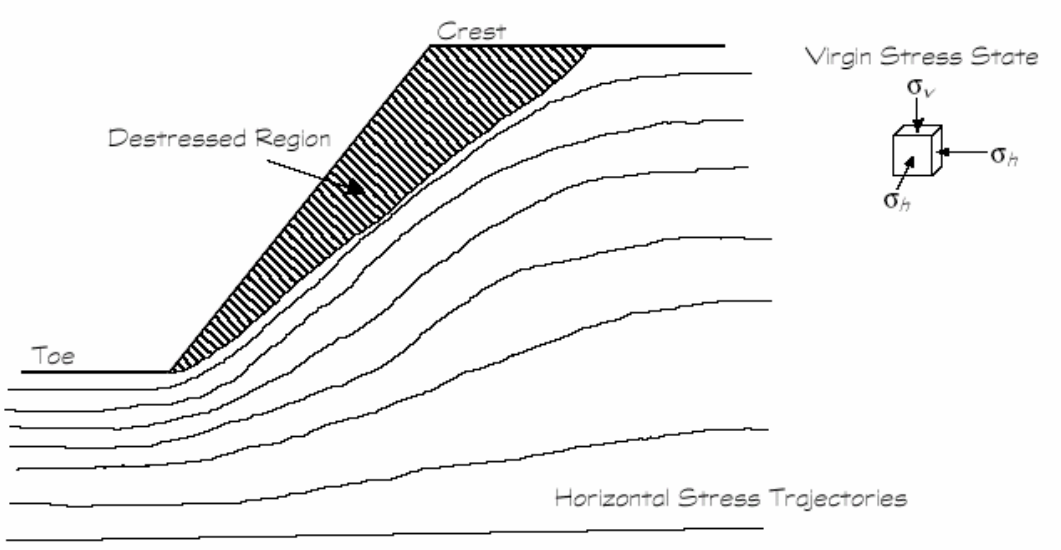


Figure 2-13 Two-dimensional representation of the redistribution of horizontal stress around a long open pit (large dimension perpendicular to this plane). (Sjoberg, 1996)

2.4.1 Seismicity and blast induced vibrations

In the regions of the world where seismic activity is a problem rock slope design must take into consideration the impacts of earthquake-induced slope instabilities (Wyllie & Mah, 2004). Blast induced vibrations from a poorly designed blast have the potential of causing rock mass failure especially for small scale slopes, that is at bench scale level (Sjoberg, 1996).

2.5 Slope Failure Modes

(Hoek & Pentz, 1968) defined open pit slope failure as follows: "*slope failure in an open pit mine maybe defined as that rate of displacement of the rock mass surrounding the open pit which would render the recovery of ore uneconomic if the pit was being actively mined".*

Slope failure mode is defined as follows (Sjoberg, 1996): "*A macroscopic description of the manner in which failure occurs, for example the shape and appearance of the resulting failure surface. The mode can be regarded as the geometric description of the failure development".*

The most common slope failure modes in open pit mines are plane, wedge, circular and toppling failure (Figure 2-14).

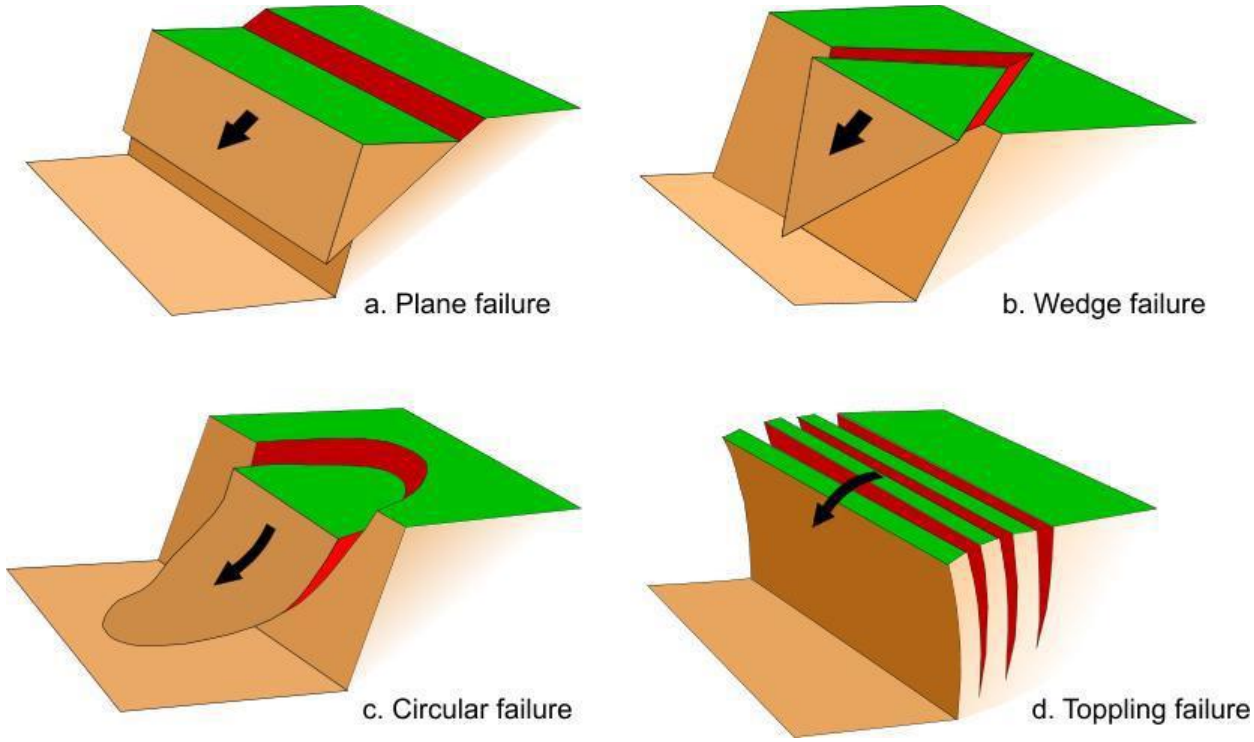


Figure 2-14 Simplified illustrations of most common slope failure modes. (Hoek, 2009)

These failure modes can be experienced at bench scale level as well as overall pit slope level. With the exception of toppling failure the other three failure modes involve gravity driven sliding along discontinuity planes in the rock mass whereas toppling involves rotational detaching of blocks as a result of in-dipping discontinuities along the slope face (Hoek, 2009). Each of these failure modes is briefly described below.

Plane Failure

A plane failure is the simplest mode of failure to understand and analyse. It occurs when a block detaches from a rock mass and slides along a pre-existing discontinuity that dips out of a rock slope. For a plane failure to occur the following conditions need to be satisfied (Wyllie & Mah, 2004):

- The discontinuity plane along which the block will slide must strike parallel or almost parallel to the slope face (ranging between +/-20^{o}).
- The discontinuity plane along which the block will slide must "daylight" on the slope face, that is, its dip must be flatter than the dip of the slope face ($\psi_p < \psi_f$) (Figure 2-15).
- The dip of the discontinuity plane along which the block will slide must be steeper than its friction angle ($\psi_p > \phi$) (Figure 2-15).

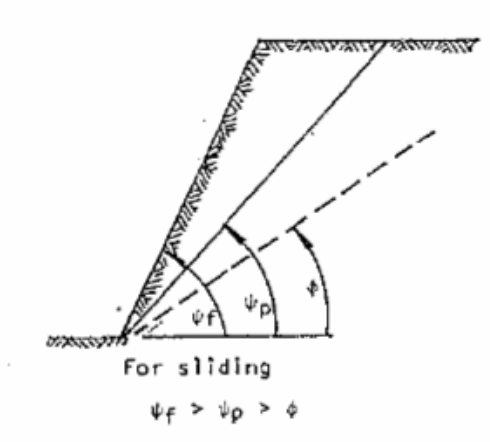


Figure 2-15 Relationship between dip of slope face, dip of discontinuity plane and friction angle of discontinuity for sliding to take place (Wyllie & Mah, 2004).

- The discontinuity plane must intersect the upper surface of the slope or terminate in a tension crack.
- There must be release surfaces of almost zero resistance bounding the sliding block (Figure 2-16)

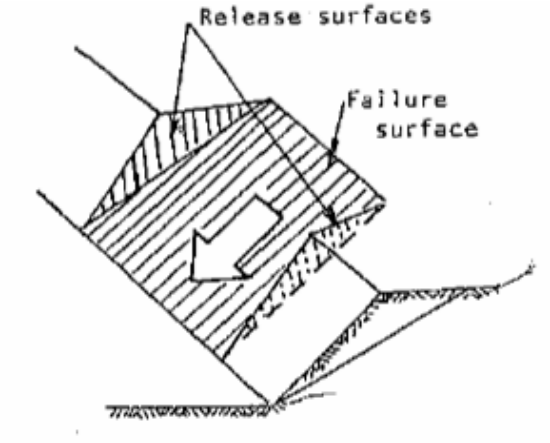


Figure 2-16 release surfaces at ends of plane failure (Wyllie & Mah, 2004).

A structure is said to daylight if it dips shallower than the slope face and dips towards the slope face, resulting in the possibility of a rock mass sliding along the structure and detaching from the slope face if frictionally unstable.

Wedge Failure

Wedge failure takes place when two planes of weakness striking oblique to the strike of the slope face intersect. Wedge failure is more common than plane failure since it can occur in a variety of geological conditions and geometrical configurations. According to (Wyllie & Mah, 2004) wedge failure takes place under the following conditions:

- The line of intersection between the two planes of weakness along which sliding will take place must "daylight" on the slope face, that is, its plunge must be shallower than the dip of the slope face ($\psi_i < \psi_{fi}$) (Figure 2-17).
- The plunge of the line of intersection along which the block will slide must be steeper than the average friction angle of the two planes of weakness ($\psi_i > \phi$) (Figure 2-17)

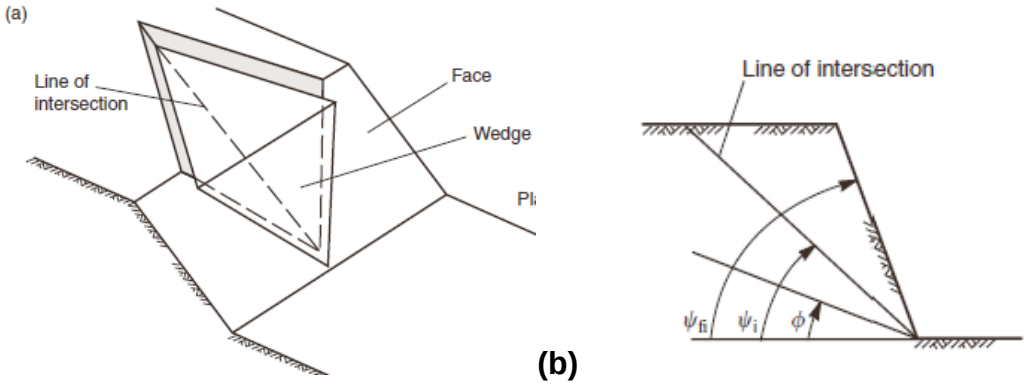


Figure 2-17 Geometric conditions for wedge failure: (a) pictorial view of wedge failure; (b) view of slope at right angles to the line of intersection (Wyllie & Mah, 2004).

Circular Failure

Circular failure takes place in weak material such as soils, highly weathered or closely fractured rock masses, and rock fills. The failure surface assumes a circular shape though the shape will not be a perfect circle and is not controlled by any one specific plane of weakness, it just follows a path of minimum resistance within the rock mass (Wyllie & Mah, 2004). For circular failure to take place the discrete soil particles or the rock blocks within the rock mass must be very small in comparison to the slope dimensions.

Toppling Failure

According to (Wyllie & Mah, 2004) toppling failure involves rotation of columns or blocks of rocks about a fixed base as opposed to the other failure modes described earlier which

involve sliding of rock blocks along discontinuity planes. As indicated by (Goodma & Bray, 1976) in (Wyllie & Mah, 2004) toppling failure comes in a number of different ways (Figure 2-18) and these are described below:

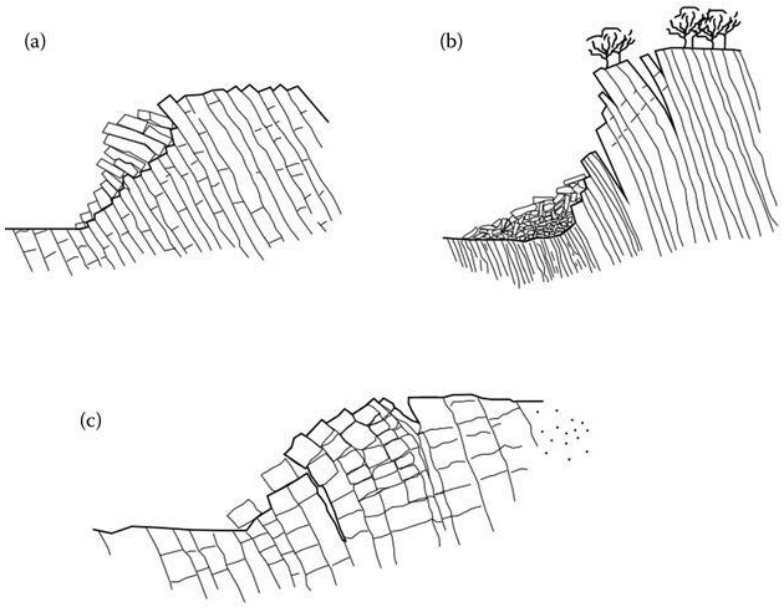


Figure 2-18 Common classes of toppling failures: (a) block toppling of columns of rock containing widely spaced orthogonal joints; (b) flexural toppling of slabs of rock dipping steeply into face; (c) block flexure toppling characterized by pseudo-continuous flexure of long columns through accumulated motions along numerous cross-joints (Goodman and Bray 1976).

- Block toppling, in which discrete columns are formed in strong rock as a result of the presence of two joint sets in the rock mass, one that dips steeply into the slope face and another perpendicular to the first one and widely spaced, defining the height of the columns or blocks of rocks. The short columns forming the toe of the slope are pushed forward by the loads from the longer overturning columns behind,

and this sliding of the toe allows further toppling to develop higher up the slope. The base of the failure generally consists of a stepped surface rising from one cross joint to the next. Typical geological conditions in which toppling failure is likely to take place are bedded sandstone and columnar basalt in which perpendicular jointing is well developed.

- Flexural toppling, in which continuous columns or rock blocks are formed as a result of two joint sets, one well developed steeply dipping set and another poorly developed set perpendicular to the first one. This leads to the long rock columns failing in flexure as they bend forward. Such type of jointing and failure is common in bedded shale and slate.
- Block-Flexural toppling, in which pseudo-continuous flexure takes place along long columns that are divided by numerous cross joints. Instead of the flexural failure of continuous columns resulting in flexural toppling, toppling of columns in this case results from accumulated displacements on the cross-joints.
- Secondary toppling, in which failure is initiated by the undercutting of the toe of slopes either by natural means such as weathering or human activities.

Combination Of Failure Modes

For large scale slope failure it is common that several failure modes are involved, for instance failure might involve a combination of movement along discontinuous planes and rupture of intact rock bridges (Azzuhry, 2016).

2.6 Rock Mass Characterization

Rock mass characterization systems are used to divide the rock mass into different geotechnical domains, each domain having similar geotechnical properties. These geotechnical properties include geological, structural, stress and hydrogeological in situ rock mass characteristics which when combined will define the overall rock mass behaviour. In the case of open pit slope design, geotechnical domains are used in slope stability analysis and selection of appropriate design parameters that will improve safety and economics of an open pit mine. Following are some of the rock mass classification systems currently in use (Moser, et al., 2017):

- *RQD value after* (Deere & Deere, 1988) *(employs one parameter only).*
- *RMR after* (Bieniawski, 1989) *(sum of single parameters).*
- *MRMR after Laubscher (1990) (sum of single parameters).*
- *Q-system after Barton (1990) (product of different factors).*
- *GSI after Hoek and Brown (2002) (on the basis of a chart).*

2.6.1 Rock quality designation (RQD)

RQD was developed by Deere in the 1960s (Hoek, 2006), as means to quantify the quality of rocks from samples obtained through diamond core drilling. RQD is defined as the ratio between the total lengths of intact drill core samples of NX size, at least 100 mm long, and the total length of the core run, expressed as percentage. Mechanical breaks as result of core drilling and handling are ignored in the determination of RQD and only natural breaks must be considered. RQD is affected by direction of drilling for example poor RQD values can be obtained when drilling across bedding as compared to the values

that can be obtained along bedding in the same rock for sedimentary rock formations. Figure 2-19 illustrates the correct way of measuring core samples and determining RQD as proposed by Deere (1989) as indicated in (Hoek, 2006).

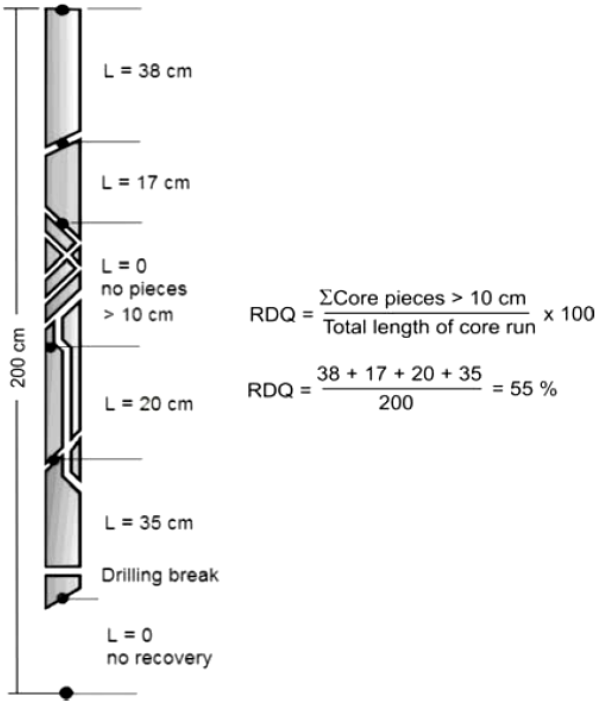


Figure 2-19 Procedure for measurement and calculation of *RQD* (After Deere, 1989).

Currently RQD is rarely used as a classification system on own its but as an input parameter in other rock mass classification systems such the Norwegian Geotechnical Institute's Q system and the Rock Mass Rating (RMR).

According to Palmstrom (1982) as indicated in (Hoek, 2006) , in the absence of drill core samples, RQD can be estimated from rock exposures such as rock outcrops, cut slopes and exploration adits by using Equation 2-9:

$$RQD = 115 - 3.3J_v$$ Equation 2-9

Where J_v is the volumetric joint count, defined as the total number of joints per unit volume of rock mass for all joint sets present, mathematically expressed as follows Equation 2-10:

$$J_v = \sum_{i=1}^{n} \frac{1}{S_i}$$ Equation 2-10

Where: *S* is the joint spacing in metres for the actual joint set.

i is the actual joint set.

Deere suggested a description that can be used to classify rock masses based on their RQD values. Table 2-3 below outlines these descriptions.

Table 2-3 Deere's classification of rock quality (Deere, 1989)

RQD (%)	**DESCRIPTION OF ROCK QUALITY**
0-25	Very poor
25-50	Poor
50-75	Fair
75-90	Good
90-100	Excellent

2.6.2 Geomechanics classification

The Geomechanics Classification system quantifies the quality of a rock mass by determining a rock mass rating (RMR) value which is obtained by adding five (5) parameter values (Bieniawski, 1989). The parameters summed up by the system are:

- Uniaxial Compressive strength (UCS) of intact rock material.
- RQD
- Joint spacing
- Joint condition
- Ground water conditions.

Each of the parameters is rated according to conditions of the rock mass obtained through field observations and laboratory testing. These rating values are added to give an RMR value which varies from 0 to 100. Table 2-4 gives a description used to classify rock masses based on RMR values.

Table 2-4 Classification of rock quality based on RMR **(Bieniawski, 1989)**.

RMR	ROCK QUALITY
0-20	Very poor
21-40	Poor
41-60	Fair
61-80	Good
81-100	Very good

2.6.3 Mining rock mass rating (MRMR)

Bieniawski's RMR system was developed based on civil engineering environments, so Laubscher modified that system to suit mining environments. The modified system is known as Mining Rock Mass Rating (MRMR). MRMR takes into consideration the same parameters as the RMR system except that it combines two of the parameters which are the joint condition and the groundwater conditions, resulting in four parameters remaining. The rating values of the four parameters are added and then adjusted for weathering, mining-induced stresses, joint orientation and blasting effects. Table 2-5 through to Table 2-7 show adjustment factors of these parameters for different conditions.

Table 2-5 Adjustment to MRMR for weathering (Stacey & Swart, 2001)

Rate of weathering and adjustments (%)					
Description of weathering extent	**6 months**	**1 year**	**2 years**	**3 years**	**4 + years**
Fresh	100	100	100	100	100
Slightly	88	90	92	94	96
Moderately	82	84	86	88	90
Highly	70	72	76	78	80
Completely	54	56	58	60	62
Residual soil	30	32	34	36	38

Table 2-6 Adjustment to MRMR due to joint orientation (Stacey & Swart, 2001)

Number of joints defining the block	**Adjustments (%)** **Number of faces inclined away from the vertical**				
	70	75	80	85	90
3	3	-	2	-	-
4	4	3	-	2	-
5	5	4	3	2	1
6	6	5	4	3	2 or 1

Table 2-7 Adjustment to MRMR for blasting effects (Stacey & Swart, 2001)

Excavation technique	**Adjustment (%)**
Boring	100
Smooth wall blasting	97
Good conventional blasting	94
Poor blasting	80

Adjustments of MRMR to consider mining induced stresses are based on the fact that good confinement improves stability and maximum positive adjustment factor is 120 % and poor confinement in closely jointed rock masses results in poor stability and the maximum negative adjustment is 60 % (Stacey & Swart, 2001).

The adjusted RMR is obtained by multiplying the Laubscher's RMR value by the adjustment factors and it varies between 0 and 100 (LAUBSCHER, 1990).

2.6.4 Q-System

The Q-system also known as the Norwegian Geotechnical Institute (*NGI*) system takes into account six parameters as indicated by Equation 2-11 (Hoek, 2006).

$$Q = \frac{RQD}{J_n} \times \frac{J_r}{J_a} \times \frac{J_w}{SRF} \qquad \text{Equation 2-11}$$

Where: *RQD* is the rock quality designation

J_n is the joint set number

J_r is the joint roughness number

J_a is the joint alteration number

J_w is the joint water reduction factor

SRF is the stress reduction factor

The three ratios in the system result in the system being controlled by only three factors which are:

- Rock block size (RQD/J_n)
- Joint shear strength (J_r/J_a)
- Confining stress (J_w/SRF)

The six parameters are assigned a certain value using tables already prepared for this depending on the observed or estimated rock mass conditions and these values are substituted into Equation 2-11 to calculate the rock quality index *Q*. The value of *Q* ranges from 0.001 to 1000 on a logarithmic scale.

The rock quality index *Q* is linked to the *RMR* value by Equation 2-12.

$$RMR = 9lnQ + 44 \qquad \text{Equation 2-12}$$

2.6.5 Geological strength index (*GSI*)

The *GSI* is a simple system that can be applied to estimate the strength of rock masses for different geological conditions. It is based upon the extent of fracturing of the rock mass and the ease with which individual blocks can slide or rotate under different stress conditions (Hoek, 2006). It assumes isotropic rock and rock mass behaviour and must be used for rock masses with sufficient closely spaced fractures such that the behaviour of the rock mass is not influenced by any one individual discontinuity. The average block size in the rock mass must be very small as compared to the size of the structure under consideration. Figure 2-20 illustrates the scale effect on the use of the *GSI* system.

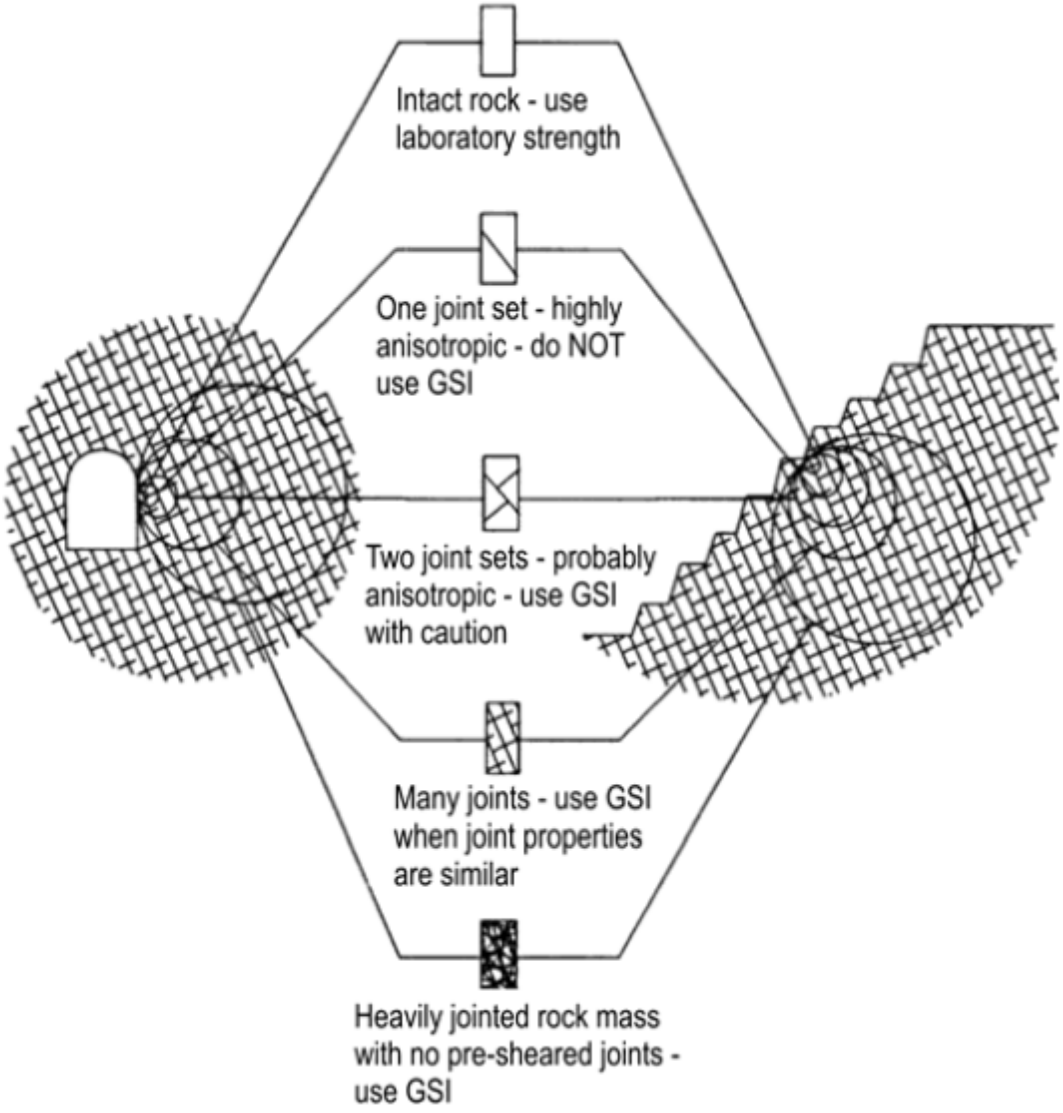


Figure 2-20 The scale effect on the use of the *GSI* system. (Hoek, et al., 2013)

The system works well for poor quality rock masses like the jointed rock mass and a rock mass with several discontinuities as shown in Figure 2-21. *GSI* must be used with caution for rock masses with two discontinuities and does not apply for the remaining rock mass conditions (Hoek, et al., 2013). *GSI* values range from 0 to 100 and are determined based

on observations made on the rock mass in conjunction with the chart shown in Figure 2-21 (Hoek, 2006).

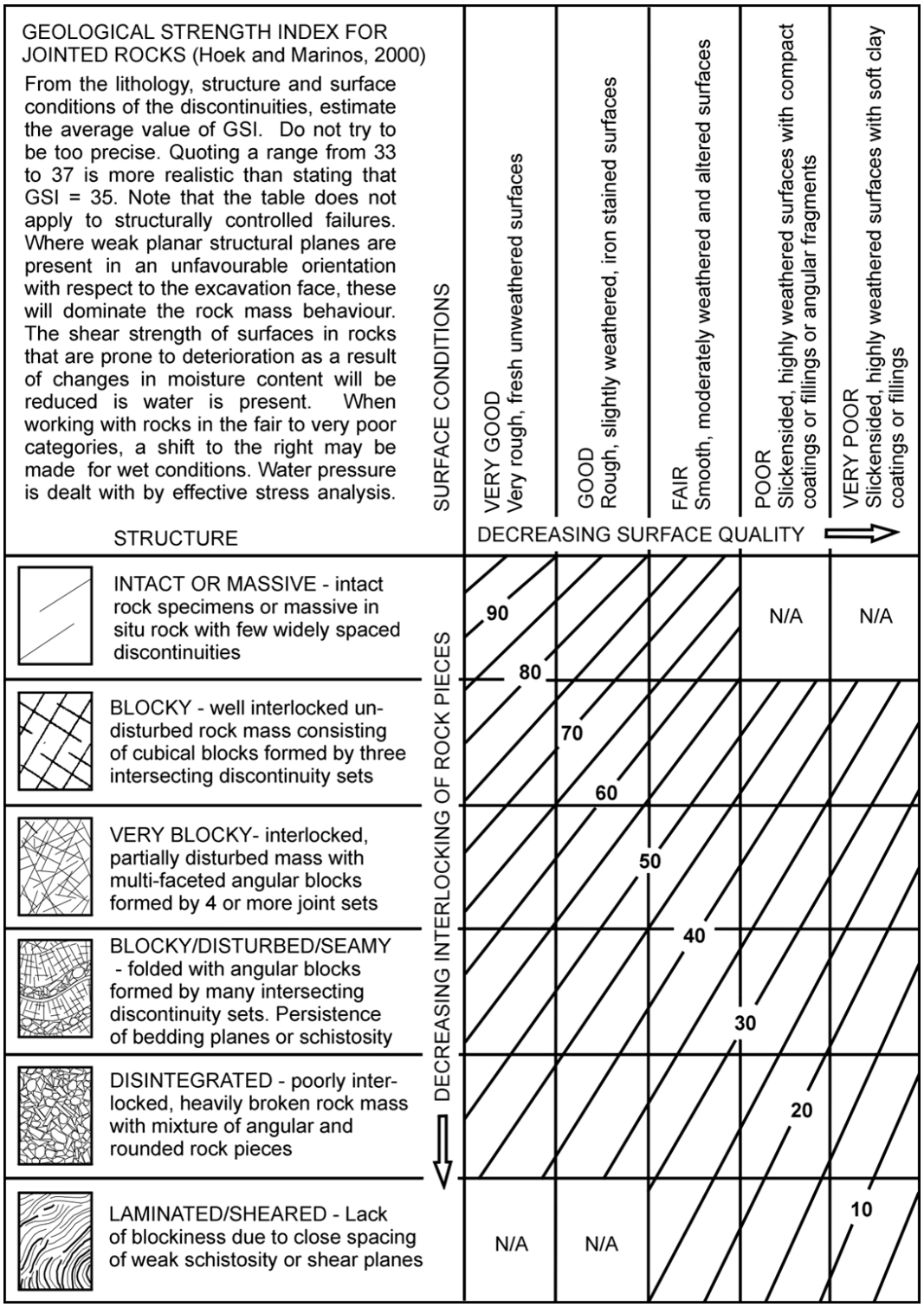


Figure 2-21 Geological strength index for jointed rock masses (Marinos & Hoek, 2000).

2.7 Acceptability Criteria For Open Pit Slope Design

As indicated earlier on, pit slope steepening despite resulting in improved economics of the open pit mining operations also brings with it risk as a result of reduced pit wall stability. Therefore, a balance must be made between the positive and negative impacts brought about by the steeper pit slope. In order to account for uncertainties related to pit slope design some design criteria are used as a basis of accepting the suitability of the design. The commonly used acceptance criteria for open pit slope design are factor of safety, probability of failure and risk analysis (Contreras, 2015).

2.7.1 Factor of safety (FOS) criterion

The factor of safety is interpreted as the proportion between capacity of the slope to withstand failure and the demand on the slope along a plane of weakness. The rationale behind this approach is that when capacity is equal to demand then the slope is in limit equilibrium state and in such case the FOS will be equal to one. When FOS is greater than one it means capacity is greater than demand and in such a case the slope will be stable. Therefore for a design to be stable and acceptable it must have a FOS greater than one and in mining operations the acceptable range of FOS is 1.2 to 2 as stated by Priest and Brown (1983) as shown in (Contreras, 2015). But considering the nature of rock masses it is not possible to have constant strength and loading conditions over the entire potential failure plane hence the FOS criterion is said to be deterministic as it assigns a single value to represent these parameters which in reality vary over the entire plane. Another shortcoming associated with the FOS approach is that it is based on experience, thus it is empirical and therefore the conditions under which the acceptable

range was determined might not be the same as those to which it will be applied when designing a certain pit slope (Chiwaye & Stacey, 2010).

2.7.2 Probability analysis criterion

The criterion involves the determination of the probability of slope failure (POF). It depends on a deterministic model but differs from the factor of safety approach in that the input parameters are not considered as point estimates of the values but rather as probability distributions, thereby taking into consideration the variable nature of the rock mass properties. The probability of slope failure is determined by combining these distributions in the deterministic model. The distributions are combined using the Monte Carlo simulation. This involves random sampling of the input parameter values and then calculating the FOS for the sampled values. This exercise is repeated several times resulting in the generation of a FOS distribution. The ratio between the total number of samples with FOS less than unity to the total number of samples used will give the POF for the slope. The POF offers an advantage over the FOS criterion as a stability analysis method in that the POF values are directly proportional to the possibility of failure whereas this does not apply for FOS. For example, the stability of a slope with a POF equal to 5% will be double that of a slope with POF equal to 10%, whereas this is not the case for a slope with FOS equal to 3 compared with another with FOS of 1.5. Figure 2-22, shows a comparison of POF and FOS for two cases, **A** and **B**.

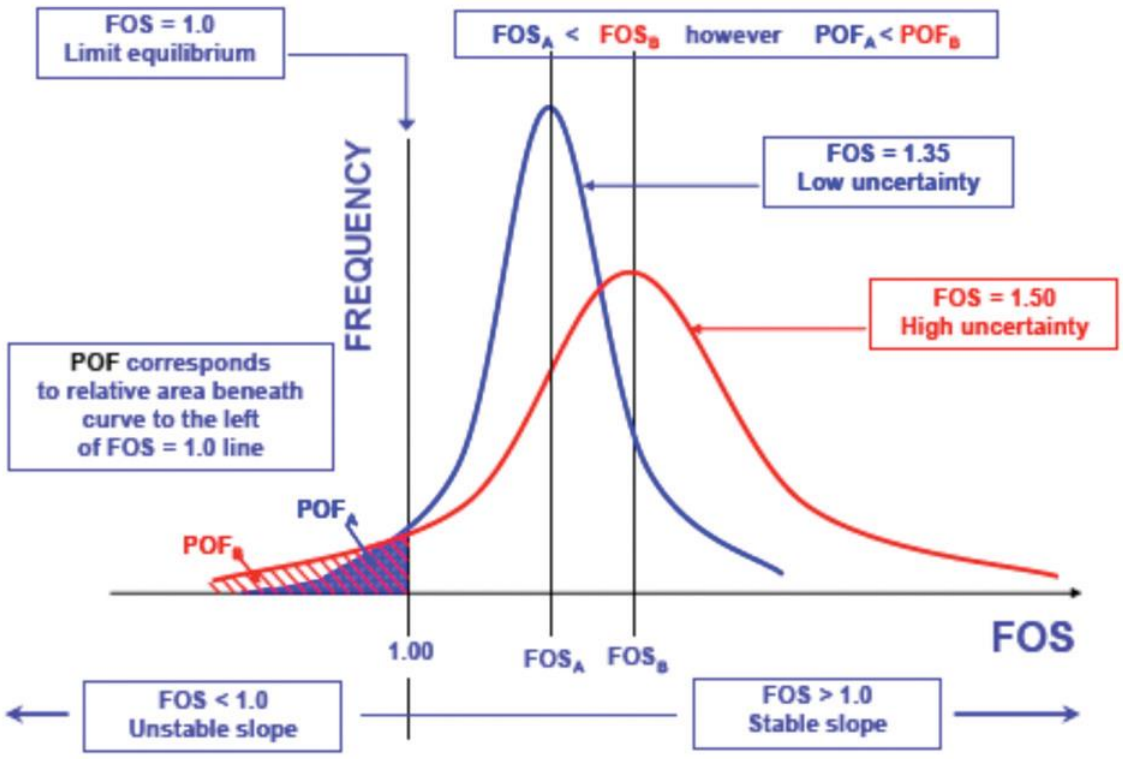


Figure 2-22 Definition of POF and Relationship with FOS according to uncertainty magnitude (Tapia, et al., 2007).

Case **A** has a lower FOS than case **B** indicating that **B** is more stable than **A**, however case **A** has a lower POF than **B** indicating that **B** is more likely to fail than **A**. The differences in these results illustrate the advantage of POF approach's ability to take into account the variability in the rock mass conditions.

2.7.3 Risk analysis criteria

Unlike the previous methods risk criteria are not based only on the possibility of slope failure but also incorporate the consequences of potential failure. It therefore requires the owners of the mine to define an acceptable risk level and this will be used by the design engineer to determine the maximum slope angle that will meet the required level of risk.

The acceptable risk is defined taking into consideration the benefits associated with steeper slope angles as well as the accompanying consequences resulting from the potential slope failure. Risk can be defined as a measure of the likelihood of a hazardous event to occur and cause harm or loss combined with the severity of the harm or loss. Mathematically it can be expressed as shown by Equation 2-13:

$$Risk = P_{event} \times Consequence\ of\ the\ event. \qquad \text{Equation 2-13}$$

In this case, event refers to slope failure and the consequences associated with such an event include the following: injury to personnel, equipment damage, economic impact on production, force Majeure (a major economic impact), industrial action, public relations, such as stakeholder resistance, environmental impact, etc. (Steffen, et al., 2008). However, the owners of the operation can only define risk levels for the economic consequences and not for the safety consequences as they are guided by regulatory authorities with regard to safety. The risk approach combines the other two approaches as it requires that POF be determined first before factoring in the consequence of failure. But to determine the POF a distribution of FOS must be generated first. The other convenience of the risk criterion is that it enables the engineer designing the slopes to define the specific extent of geotechnical drilling and testing necessary to provide adequate data for the design exercise.

Table 2-8 is a summary of commonly used values for FOS and POF for designing open pit mine slopes. The consequence of failure is described as either low, medium or high

and this will control the values of FOS or POF to be used for design depending on what component of the pit is being designed.

Table 2-8 Typical FoS and PoF acceptance criteria values (Wesseloo & Read, 2009)

Slope scale	Consequences of failure	Acceptance criteria		
		FOS (min) (static)	FOS (min) (dynamic)	POF (max) P[FOS≥1]
Bench	Low-high	1.1	NA	25-50%
Inter-ramp	Low	1.15-1.2	1.0	25%
	Medium	1.2	1.0	20%
	High	1.2-1.3	1.1	10%
Overall	Low	1.2-1.3	1.0	15-20%
	Medium	1.3	1.05	5-10%
	high	1.3-1.5	1.1	≤ 5%

2.8 Open Pit Slope Stability Analysis And Design

After the rock mass in which the open pit mine slopes are going to be created has been characterized and the design acceptability criteria selected, slope stability analysis for the different geotechnical domains of the pit is carried out and the slopes are designed according to the stability conditions of each domain. According to (Hoek, 2009), a good

open pit mine slope design is one that takes into account all the geotechnical properties of the rock mass to strike a balanced compromise between safety and economics, two factors which are difficult to satisfy simulteneously.

Following are the main reasons why slope stability analysis is necessary:

- To determine the rock slope stability conditions.
- To investigate the potential failure mechanisms.
- To determine the slope's sensitivity or susceptibility to various triggering mechanisms.
- To determine appropriate support and stabilisation systems.
- To design optimum slopes with regard to safety, reliability and economics.

Open pit slope design requires that stability analysis be carried out, the analysis involves comparison between the destabilising forces and stabilising forces. Destabilising forces are due to gravity and water pressure whereas the stabilizing forces are due to the rock mass shear strength (Hoek, et al., 2000). Slope stability analysis methods can be grouped into conventional and numerical analysis methods (Stead, et al., 2006).

Conventional analysis methods include:

- Limit equilibrium analysis
- Stereographic and kinematic analysis
- Rock fall simulators

Whereas numerical analysis includes:

- Continuum modelling
- Discontinuum modelling
- Hybrid modelling

2.8.1 Conventional analysis methods

Limit equilibrium analysis

Limit equilibrium techniques have been in use for a long period of time over 25 years and during this period they have proved to be a reliable technique for slope stability analysis and design (Hoek, et al., 2000). They are applicable for analysing structurally driven instabilities such as plane and wedge failures as well as circular or near circular instabilities in soil or heavily weathered rocks which are almost homogeneous in character. The technique is based on the factor of safety criterion. As mentioned in section 2.7.1 stability is achieved when the destabilizing forces are less than the stabilizing forces, which is to say when the *FOS* is greater than unit.

Simple circular stability analysis and slope design charts

The charts were created by carrying out many circular analyses which gave rise to a number of dimensionless parameters which link the *FOS* to the following material properties (Wyllie, 2018):

- Unit weight, γ, (kN/m^3)
- Friction angle, ϕ, (^{o})
- Cohesion, *c*, (kPa)
- Slope height, *H*, (m)

- Slope face angle, ψ_f, (º)

The charts are used in conjunction with the groundwater conditions classified as dry, saturated and partially saturated conditions, corresponding to the slope being analysed. Figure 2-23 illustrates the chart together with corresponding water conditions.

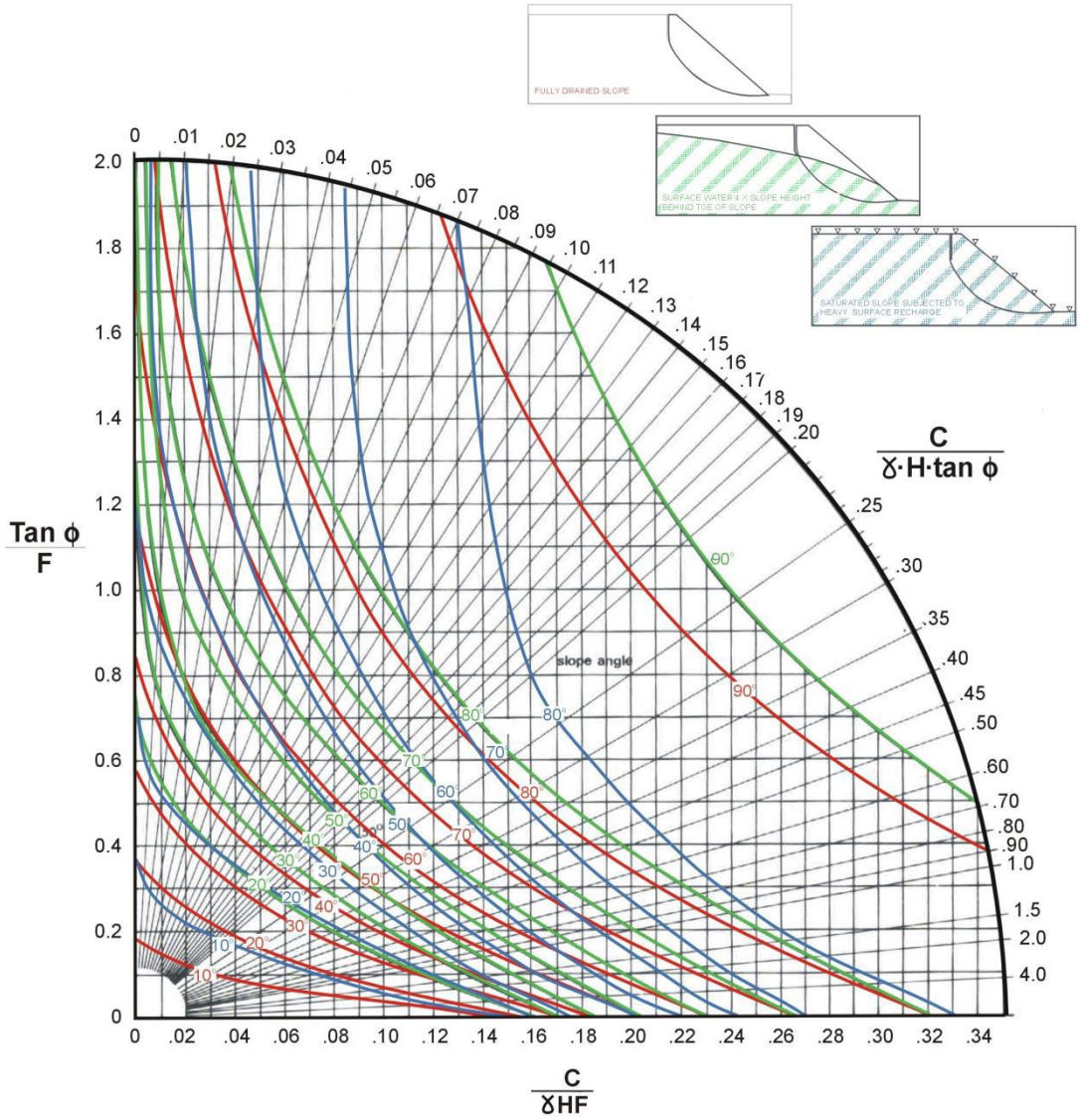


Figure 2-23 Stability and design chart for soil and weathered rock slopes (Stacey & Swart, 2001).

Steps in using the circular failure charts

The following steps are followed when calculating the *FOS* using the charts (Wyllie, 2018). These are also illustrated in Figure 2-24.

1. Estimate the ground water conditions of the slope in question and use this to select the appropriate chart to use.
2. Compute the value of $c/\gamma H.\tan\phi$ and locate this value on the outer curved scale of the chart.
3. Move inwards along a line from this value to a point of intersection with the curve corresponding to the slope face angle.
4. Read the value of $\tan\phi/F$ or $c/\gamma HF$ and calculate the value *FOS* represented by *F* in these two expressions.

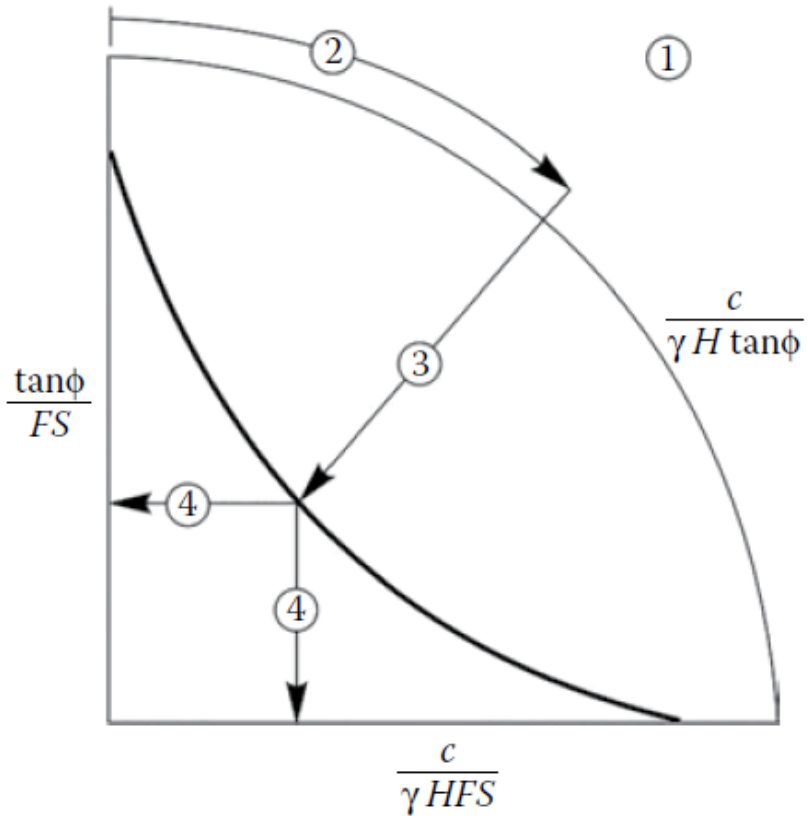
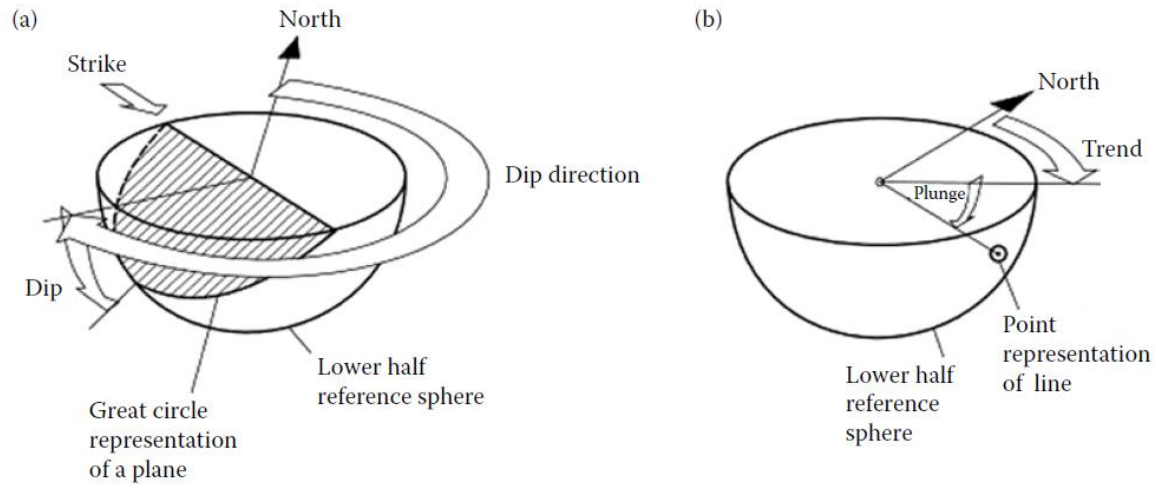


Figure 2-24 Sequence of steps involved in using circular failure charts to find the factor of safety of a slope (Wyllie, 2018).

Stereographic and kinematic analysis

Stereographic projections provide a way of representing the orientation data of structural geological features in two dimensions. Planes of weakness can be represented by lines or points and lines of intersection between the planes are represented by points, Figure 2-25 (Wyllie, 2018).



.

Figure 2-25 Stereographic representation of plane and line on lower hemisphere of reference sphere: (a) plane projected as great circle; (b) isometric view of line (plunge and trend) (Wyllie, 2018).

The major disadvantage of this way is that it only takes into account the angular link between planes and lines without considering the physical location or extent of the feature.

Planes are represented by lines called great circles or points called poles, Figure 2-26.

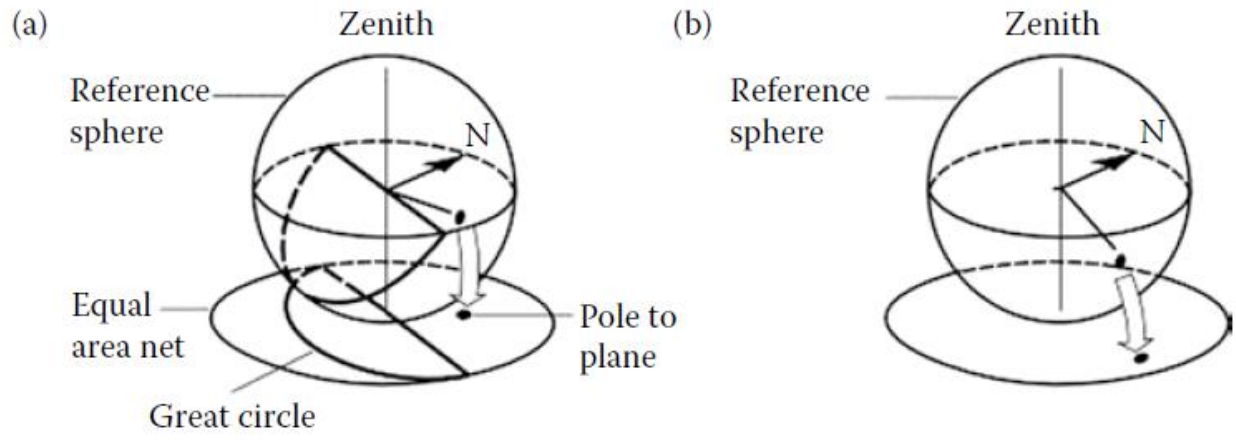


Figure 2-26 Equal area projections of plane and line: (a) plane projected as great circle and corresponding pole; (b) line projected as pole. (Wyllie, 2018)

A great circle is a characteristic line formed by the intersection of the structural plane and the bottom half of a reference sphere. A Stereographic projection is produced when these lines are projected downwards onto a horizontal plane below the reference sphere. A pole is another way of showing the orientation of a plane. It is a point on the bottom half of the reference sphere intersected by a line perpendicular to the plane passing through the centre of the sphere. It is a very convenient way since the orientation of the whole plane can simply be represented by a single point. The projected pole on the stereonet will appear as a point as well. The projected great circles or poles will represent a characteristic orientation, dip and dip direction of the plane.

The main advantage of poles compared to great circles is that with poles it is easy to analyse a larger number of planes.

Great circles of planes of weakness such as joint sets and faults plotted on the same stereonet with the great circle of slope face are used to assess if there is potential of

unstable blocks forming which can slide off the slope. The great circle of the slope is necessary since movement of loose blocks can only happen towards an open space created by the slope face. Stereoplots of great circles and poles can be used to detect the different failure modes (Figure 2-27) that can be experienced in certain geological conditions for a particular slope face.

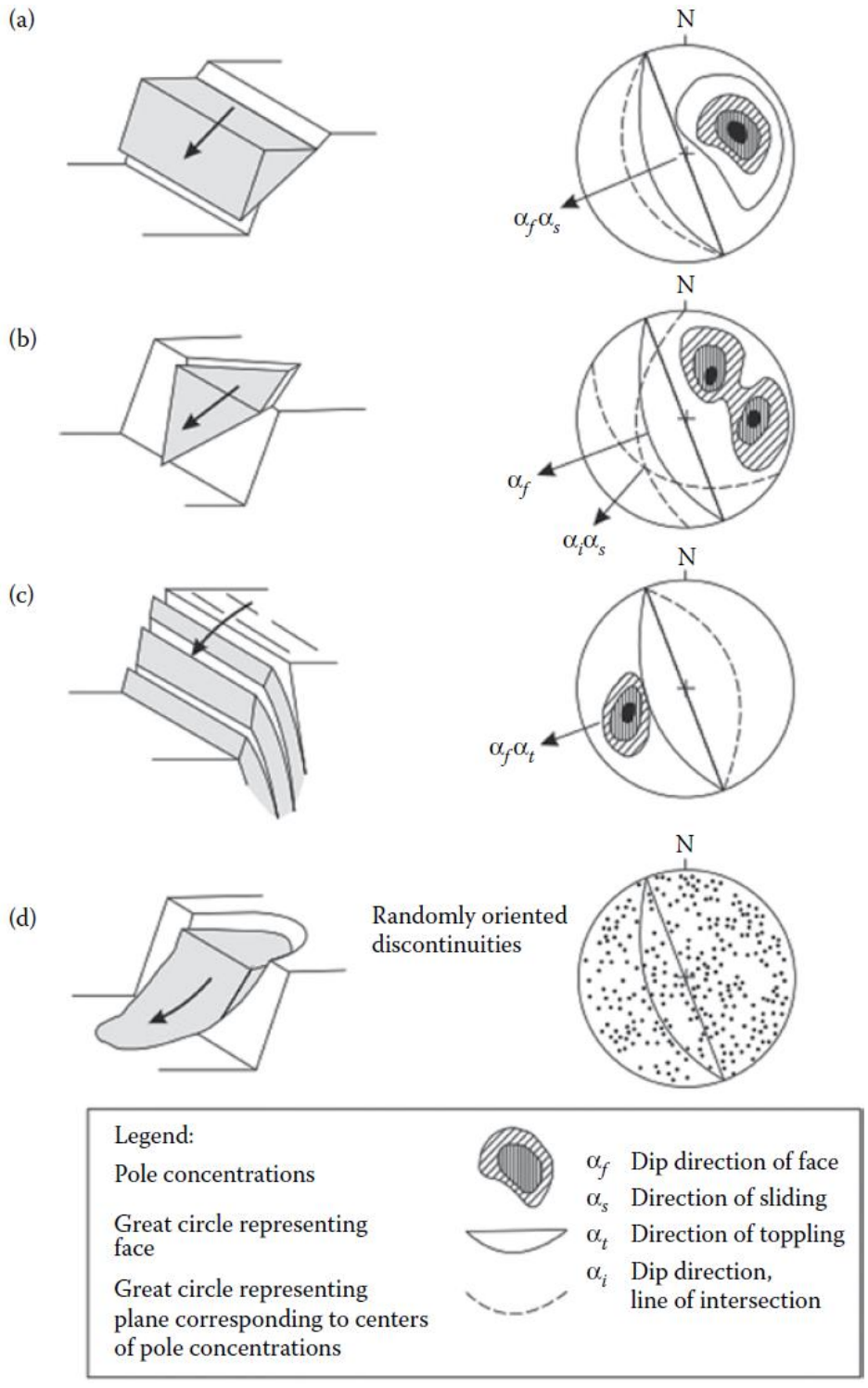


Figure 2-27 Main types of block failures in slopes, and structural geology conditions likely to cause these failures (Wyllie, 2018)

In Figure 2-27, (a) represents plane failure in rock containing persistent joints dipping out of the slope face, and striking parallel to the face; (b) wedge failure on two intersecting discontinuities; (c) toppling failure in strong rock containing discontinuities dipping steeply into the face; and (d) circular failure in rock fill, very weak rock or closely fractured rock with randomly oriented discontinuities. (Wyllie, 2018)

Besides providing a way of identifying different types of slope failure, a stereonet also helps in providing a way of determining the direction in which rock blocks will slide, thereby indicating slope stability conditions. The use of stereonets in assessing stability is referred to as kinematic analysis. Kinematic analysis only takes in account the direction of block movement without considering other factors like water pressure and weight of the sliding mass (Wyllie & Mah, 2004). Failure potential depends on dip and dip direction of the planes of weakness or lines of intersection between planes of weakness. Kinematic analysis of different modes of failure is outlined below using Figure 2-28 and Figure 2-29.

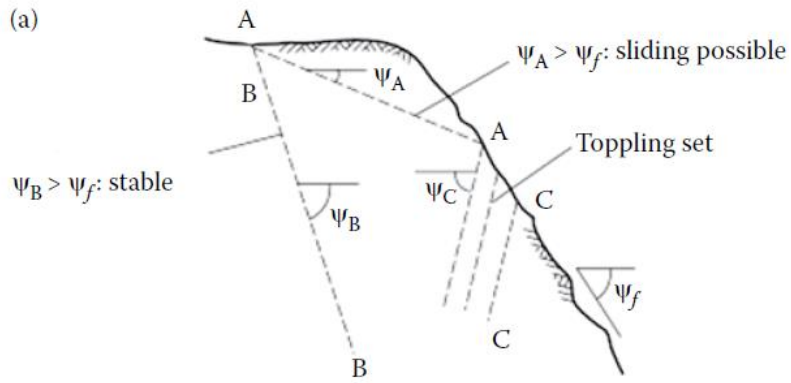


Figure 2-28 Kinematic analysis of blocks of rock in slope: (a) discontinuity sets in slope;

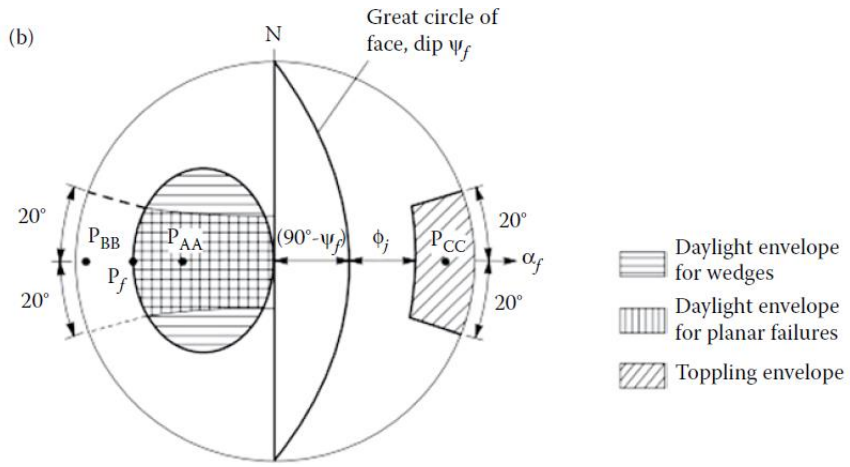


Figure 2-29 Kinematic analysis of blocks of rock in slope: envelopes on equal area stereonet. (Wyllie, 2018)

Kinematic analysis of plane failure

In Figure 2-28, plane AA daylights into the face as it dips shallower than the slope face and dips towards the slope face, resulting in the possibility of a rock mass sliding along the structure detaching from the slope face if frictionally unstable. However, plane BB is stable as it does not daylight into the face since its dip angle is greater than that of the face. Plane CC, dips away from the slope face and thus it is impossible for the block to slide off the face (Wyllie, 2018). On the stereonet, Figure 2-29, the poles of the face and those of the planes of weakness are plotted. The pole of plane AA is inside the pole of the face which is the case for all planes that daylight and have a potential of forming unstable blocks. This region is called the daylight envelope and can be used to locate unstable blocks rapidly. The daylight envelope is a curve drawn joining the poles of discontinuities whose down dip lines lie on the plane of the excavated slope, e.g lines 3

and 4 in Figure 2-30. These planes are said to be marginal in terms of daylighting conditions. A slight increase in dip angle will result in the discontinuity being steeper than the slope and a slight decrease in dip angle will result in it being shallower than the slope and therefore the slope might be unstable.

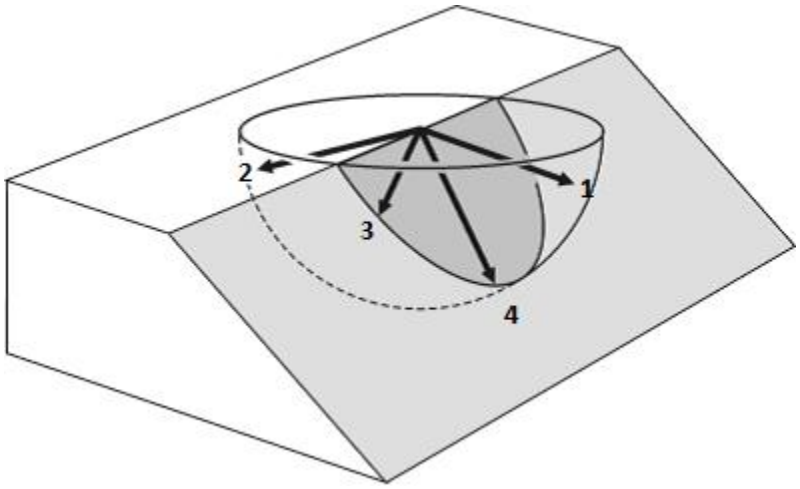


Figure 2-30 Down dip directions of discontinuities 1, 2, 3 and 4 with respect to a rock slope (Wyllie, 2018).

The daylight envelope of the slope shown in Figure 2-30 can be drawn manually on a stereonet as shown in Figure 2-31, as follows (Lisle, 2004): The great circle of the slope is first drawn on the stereonet. Points are then selected from the great circle e.g points 3 and 4 (Figure 2-31). For each selected point the corresponding pole is plotted on the stereonet. At least twenty such points are required. The poles of these points are then joined together to produce a curve which will be the daylight envelope. Any discontinuity with its pole enclosed within this daylight envelope will be shallower than the slope face and will have the potential to slide. This manual construction is time consuming and

computer programs such as Rocscience's DIPs software have built-in equations, which automatically calculate and construct the envelope when the kinematic analysis is run.

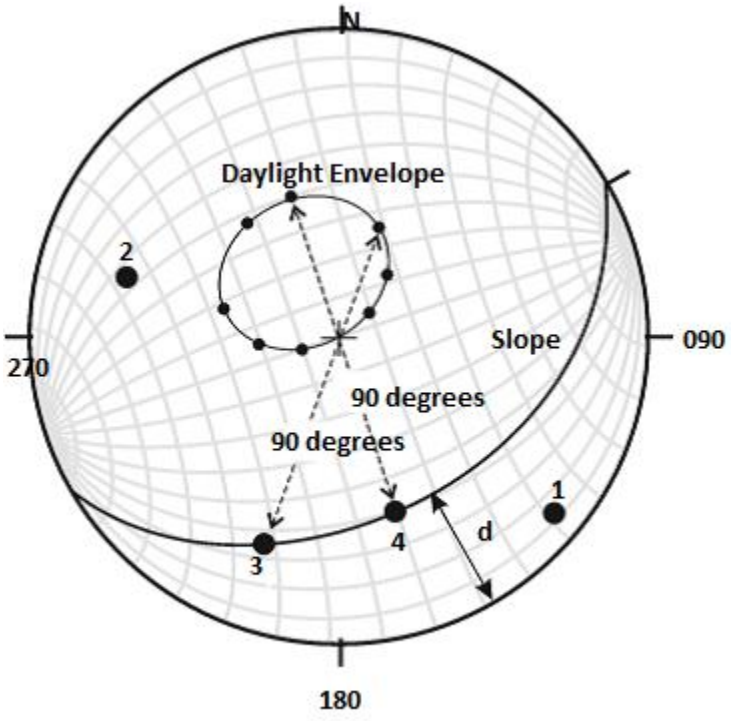


Figure 2-31 Manual construction of the daylight (Lisle, 2004).

To completely analyse planar failure a pole friction cone and lateral limits are also required in addition to the daylight envelope. The pole friction cone indicates the average friction angle of all the planar structures in the slope. It is represented on a stereonet by a circle measured from the centre of the stereonet (Figure 3-26). Pole vectors are used with a pole friction cone and, the angle of friction is measured from the centre of the stereonet (Rocscience, 2019). All pole vectors located outside the friction cone represent discontinuities which dip steeper than the friction angle, and will be unstable, if kinematically possible (adversely oriented).

For sliding to take place, the dip direction of the planar structure must be the same as that of the slope face or it must lie within the range of plus or minus 20^{o} of the slope face dip direction. This is represented on the stereonet by two lines of dip direction equal to slope dip direction plus or minus 20^{o} (Figure 2-29). These lines are called lateral limits. Poles outside this range have a low risk of sliding, thus the slope is considered stable.

Empirical slope design based on rock mass classification

This design approach is most appropriate under conditions in which overall stability is not governed by major geological structures. Table 2-9 was developed to relate MRMR values to overall slope angles according to Haines and Terbrugge (1991), as indicated in (Stacey & Swart, 2001)..

Table 2-9 Adjusted MRMR values and recommended overall rock slope angles (Stacey & Swart, 2001)

Adjusted MRMR rating	100	90	80	70	60	50	40	30	20	10	0
Overall slope angle	>75^{o}	75^{o}	70^{o}	65^{o}	60^{o}	55^{o}	50^{o}	45^{o}	40^{o}	35^{o}	<35^{o}

The Table 2-9 is mostly used when determining slope angles during the initial stages of open pit mine design.

According to Haines and Terbrugge (1991), as indicated in (Stacey & Swart, 2001), a chart (Figure 2-32) was also developed to incorporate slope height in the determination of the overall slope angle.

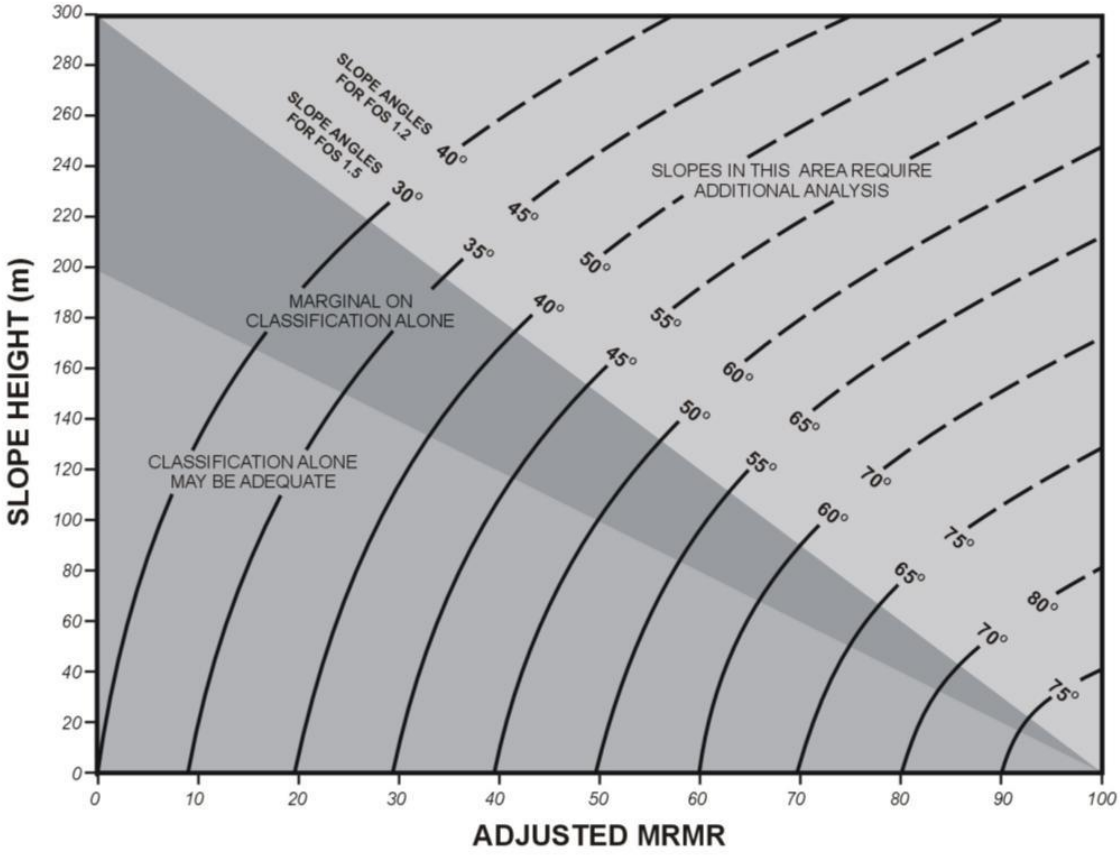


Figure 2-32 Empirical slope design chart based on rock mass classification **(Stacey & Swart, 2001)**

2.9 Numerical Stability Analysis

Numerical modelling or analysis is the use of computer programs to simulate the mechanical behaviour of rocks and rock masses when subjected to certain boundary conditions such as in situ stresses and/or water pressure (Wyllie, 2018). In numerical

modelling techniques the rock mass is divided into regions with certain material properties and sets of differential equations are formed and solved for each region. The equations will represent the mechanical response of each region to external loading. The overall response of the rock mass will be the sum of the responses of the individual regions. Numerical solutions are thus said to be an estimate of the exact solution (Bobet, 2010). The model will indicate whether the rock mass is stable or unstable. If the outcome indicates a stable rock mass, then a comparison can be done between the stresses or displacements shown by the model to the actual values measured from the field. If the outcome indicates that the rock mass is unstable then the expected mode of failure can be demonstrated. By carrying out a number of simulations using different properties the minimum factor of safety relating to the point of failure can be determined (Wyllie, 2018). Numerical models fall into two classes, continuum and discontinuum models. These models differ in the way they take into consideration the discontinuous nature of rock masses. The choice between continuum and discontinuum models depends on the size of the discontinuities in comparison with the size of the excavation (Bobet, 2010).

2.9.1 Continuum models

In its simplest form the continuum model assumes that the material of the structure under consideration cannot be broken down and separated. The material particles will remain intact and cannot be split apart during loading and deformation. With continuum models the discontinuities in the rock mass are considered implicitly that is to say the model is assumed to behave exactly the same way as the fractured rock mass which is being simulated (Wyllie, 2018). The most commonly used continuum models are:

- Finite element method (FEM),
- Finite difference method (FDM),
- Boundary element method (BEM)

The finite element method (FEM) involves partitioning the model material representing the rock mass surrounding the excavation being modelled into smaller elements Figure 2-33. These elements will be joined together at particular points called nodes (Scheldt, 2002). The number of elements and nodes to be used will depend on the required accuracy from the model. The smaller the elements the closer the solution will be to the exact solution, that is the closer it will be to the actual behaviour of the rock mass in question.

The disadvantage of using small and many elements is the longer computing time required and the time required to prepare data for each element as each element will be assigned its own material properties thus resulting in the whole process being expensive. *RS2* is one FEM used for open pit mine slope analysis.

Finite difference methods (FDM), make use of points arranged in a grid pattern to compute displacements, velocities and accelerations at these points. Compared to FEM, FDM methods are simpler to use but approximations of space between points in the grid might be a challenge. *FLAC* (Fast Langrangian Analysis of Continua) is one FDM used for open pit mine slope analysis.

The Boundary element method (BEM) only partitions the surface of the excavation instead of the entire rock mass as with FEM (Figure 2-33). This results in BEM being easy to prepare and require less computing time as compared to FEM. However, they are not

good for handling complex geometry and excessive variations in rock mass characteristics. One example of BEM used in open pit slope analysis is *BESOL* (Boundary Element Solution) (Scheldt, 2002).

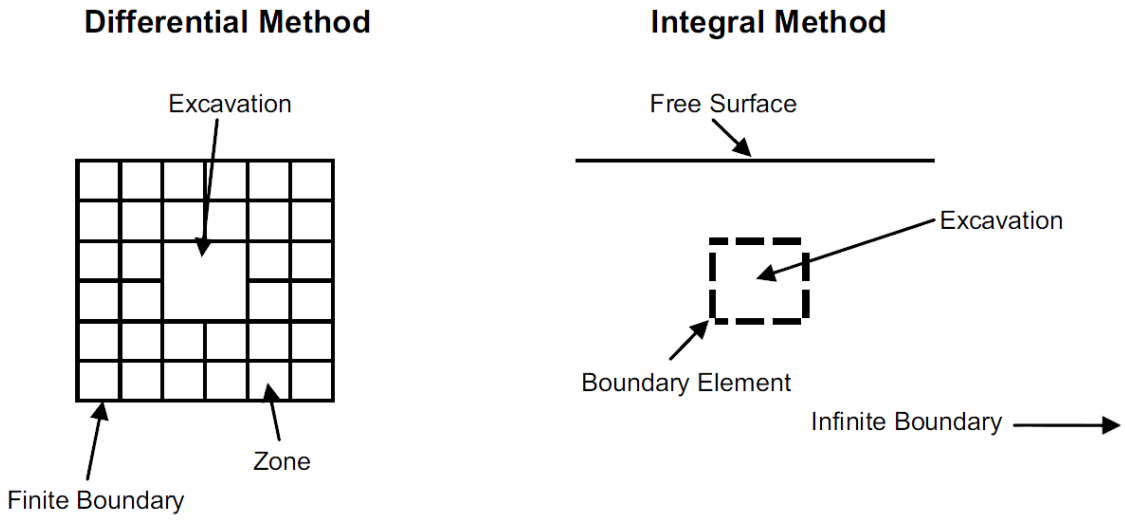


Figure 2-33 Illustration of FEM (Differential Method) and BEM (Integral Method) (Hoek, et al., 1991).

2.9.2 Discontinuum models

Discontinuum models consider the fractures in a rock mass explicitly, and permit sliding of rock blocks along explicitly positioned planes within the model (Wyllie, 2018). Common discontinuum models are (Scheldt, 2002)

- Discrete element method (DEM),
- Discontinuous deformation analysis (DDA)

These methods consider that the rock mass consists of intact rock blocks, separated by a network of fractures or discontinuities and models the rock mass by continuously

detecting the movement of the blocks along the planes of weakness, treating the blocks as rigid or deformable, and modelling them with either FDM or FEM. One common DEM used for open pit slope modelling is *UDEC* (Universal Distinct Element Code).

2.9.3 Comparison between numerical and limit equilibrium analysis techniques

Limit equilibrium techniques considers the rock material to be rigid or perfectly plastic as a result they are not able compute displacements or deformations of the rock mass. On the other hand, numerical techniques are able to compute displacements and deformations as well as taking into consideration various rock material characteristics in a single model (Wyllie, 2018).

With numerical analysis techniques the factor of safety (FOS) is determined using the strength reduction method (SRM) in which the shear strength of the rock mass material is reduced up to a point of failure. The factor of safety is then taken to be the ratio between the rocks actual strength to the reduced shear strength at the point of failure. The advantage of the FOS found by the SRM over the one obtained from the limit equilibrium technique are (Wyllie, 2018):

- The critical failure path is determined automatically and there is no need to predefine the failure path before conducting the analysis as with limit equilibrium analysis. The actual failure paths are more complex as compared to the simple planar or circular paths assumed with limit equilibrium techniques.
- Numerical techniques automatically satisfy the requirements of translational and rotational equilibrium, but not all limit equilibrium techniques fulfil equilibrium

requirements. Table 2-10, below gives a summary of the differences between numerical and limit equilibrium techniques.

Table 2-10 Comparison of numerical and limit equilibrium analysis methods (Wyllie, 2018).

Analysis result	**Numerical solution**	**Limit equilibrium**
Equilibrium	Satisfied everywhere	Satisfied only for certain objects, such as slices.
Stress	Computed everywhere using field equations.	Computed approximately on certain surfaces.
Deformation	Part of the solution	Not considered
Failure	Yield condition satisfied everywhere; slide surfaces develop “automatically” as conditions dictate.	Failure only allowed on pre-defined surfaces; no check on yield condition elsewhere.
Kinematics	The ‘mechanisms’ that develops satisfy kinematic constraints.	A single kinematic condition is specified according to particular geologic conditions.

2.9.4 Benefits of numerical modelling to rock engineering

According to Hoek and Brown (1980) as indicated in (Esterhuizen, 2014) rock samples used in the laboratory are much stronger as compared to large, field-scale rocks, and on the other hand the actual rock mass is much weaker as compared to the laboratory size sample due to the presence of fractures and planes of weakness in the rock mass. As a result, it is very difficult to have a laboratory size sample that can closely model the actual rock mass in the field. Also, the stress magnitudes that are experienced in the mining environment cannot be achieved in a laboratory set up.

However, with numerical modelling it is possible to create a model that can closely resemble the full-size scale of the actual rock mass in the field with its accompanying discontinuities or planes of weakness as well as the actual loads acting on the rock mass. As a result, numerical experiments can be carried out on the full-scale rock mass.

According to (Wyllie, 2018) the following are some of the benefits of numerical techniques:

- Numerical techniques can give reliable results for any conditions whereas empirical techniques are not reliable if the conditions differ from the conditions under which the empirical model was formulated.
- Numerical techniques can take into consideration influential geologic structures like faults and ground water in a more realistic manner than other analysis techniques.
- Numerical techniques can assist in interpreting observed physical slope behaviours.

- With numerical techniques one can analyse a number of options with respect to geological properties, failure modes and design options.

2.10 Open Pit Mine Slope Management

For an economically designed open pit mine slope it is expected that some degree of instability be experienced at different areas of the slope. Good mining practices will be indicated by successful management of such failures. If the pit slope does not experience such instabilities it will be an indication of over-conservative pit slope design and in turn a sign of poor mining practices (Hoek, et al., 2000). For a slope management program (SMP) to be fruitful there is need for mine management and the technical team comprising of the engineering geologist, geotechnical engineers and the mine planners, to work together so as to achieve the SMP objectives, which are (Roux, et al., 2006):

- *To ensure timeous warning of potential slope instability, the primary aim of which is to prevent loss of life,*
- *To allow on-going data collection on actual excavation and stability conditions,*
- *To ensure regular data analysis for confirmation and/or correction of design parameters and assumptions. Meeting this objective furthermore facilitates the use of past experience to anticipate future slope behaviour.*
- *To facilitate access to slope stability expertise.*

2.10.1 Slope stability monitoring

To ensure the above objectives are realized there is need for a slope stability monitoring system to be implemented. Following are some of the slope stability monitoring systems that can be employed in open pit mines (Wyllie, 2018):

- Crack width monitors
- Surveying
- Radar scanning
- Inclinometers
- Borehole/Shear probes

2.10.2 Slope stabilization

The following are some the ways that are used to stabilize open pit mine slopes:

- Dewatering
- Artificial support
- Scaling
- Controlled blasting

2.11 Slope Failure Preparedness

It is a fact that the risk of slope failure cannot be totally eliminated. There will always be some residual risk remaining after all measures have been taken into consideration to control the hazard of slope failure. Therefore, there must be some kind of contingency plan to handle slope failure when it unexpectedly occurs (Hoek, et al., 2000). Following are some of the emergency preparedness plans:

- Pit evacuation procedure
- Installation of catch fences
- Construction of safety berms
- Have an alternative access out of the pit in case one of them is blocked
- Have a way to clean up if there is need to.

2.12 Literature Discussion

As indicated earlier, due to the uniqueness of geological and geotechnical settings in which different open pit mines are constructed, there is need for each mine to be designed and optimized separately considering site specific conditions for each case. Regardless of slope design criteria used, the aim is to achieve the steepest slope possible that will strike a balance between safety and economics. Slope stability analyses are part of the design process regardless of the design approach followed. The outcome of the geotechnical stability analysis carried out for open pit slope design greatly depends upon the amount and quality of geotechnical data collected (Fillion & Hadjigeorgiou, 2016). Due to the cost associated with geotechnical data gathering it is not possible to obtain all the required data during the initial design stages of the project, thus making it a necessity to gather data as the project progresses from the initial stages of exploration through pre-feasibility, feasibility, design and development, exploitation up to closure and reclamation phases. This will enable the geotechnical model and the slope designs to be updated and optimized at each stage of the project. It has been noted that the amount of data used for geotechnical modeling and slope design is very low and of poor quality as compared to that used for classifying resources and reserves as well as orebody modeling (Stacey, 2009). This led to Steffen (1997), as indicated in (Terbrugge, et al., 2006), proposing that

slope designs be grouped into inferred slope angle, probable slope angle and proven slope angle, just as resources are categorized by the Joint Ore Reserves Committee (JORC) and South African Mineral Resource Committee (SAMREC) codes, based on the level of geotechnical knowledge and confidence. Once a recommended slope design has been implemented there is need for a good slope management plan as well as an emergency preparedness plan to handle unexpected failures.

3. METHODOLOGY

3.1 Introduction

The methodology that was followed for this research is discussed in this chapter and consists of the following components:

- Geotechnical data gathering
- Slope stability analysis

3.2 Geotechnical Data Gathering

Geotechnical logging of oriented core samples was done to collect structural data that was required to perform pit slope stability analysis. Data was also gathered from documented previous work that was carried out during the initial stages of the pit slope design. Face mapping of the current pit slopes was also conducted. The data from the core logging and face mapping was used in tandem to provide reliable data for geotechnical models.

3.2.1 Oriented diamond core drilling

A total of eleven boreholes were planned to be drilled around the Peerless (PE03) pit, four on the southern side and seven on the northern side of the pit. Five of the boreholes were planned to serve as both geotechnical and geological diamond drill holes and they were strategically located so that they can achieve this dual purpose. These holes were identified as PE03DDGC8 group of holes. Four of these dual-purpose holes were located on the northern side of the pit since the ore body dips to the north and these drill holes were meant to intersect the ore body at depth. The other six holes identified as

PE03DDGT were planned purely to provide geotechnical data. These geotechnical holes were distributed three on each side of the pit. Figure 3-1 is a contour map of the PE03 pit showing the location of the PE03DDGT geotechnical holes. Figure 3-2 is a plan view of the pit after the pit has extended further in the western direction. Figure 3-3 is a sheet used by the drillers showing the attributes of all the eleven planned holes.

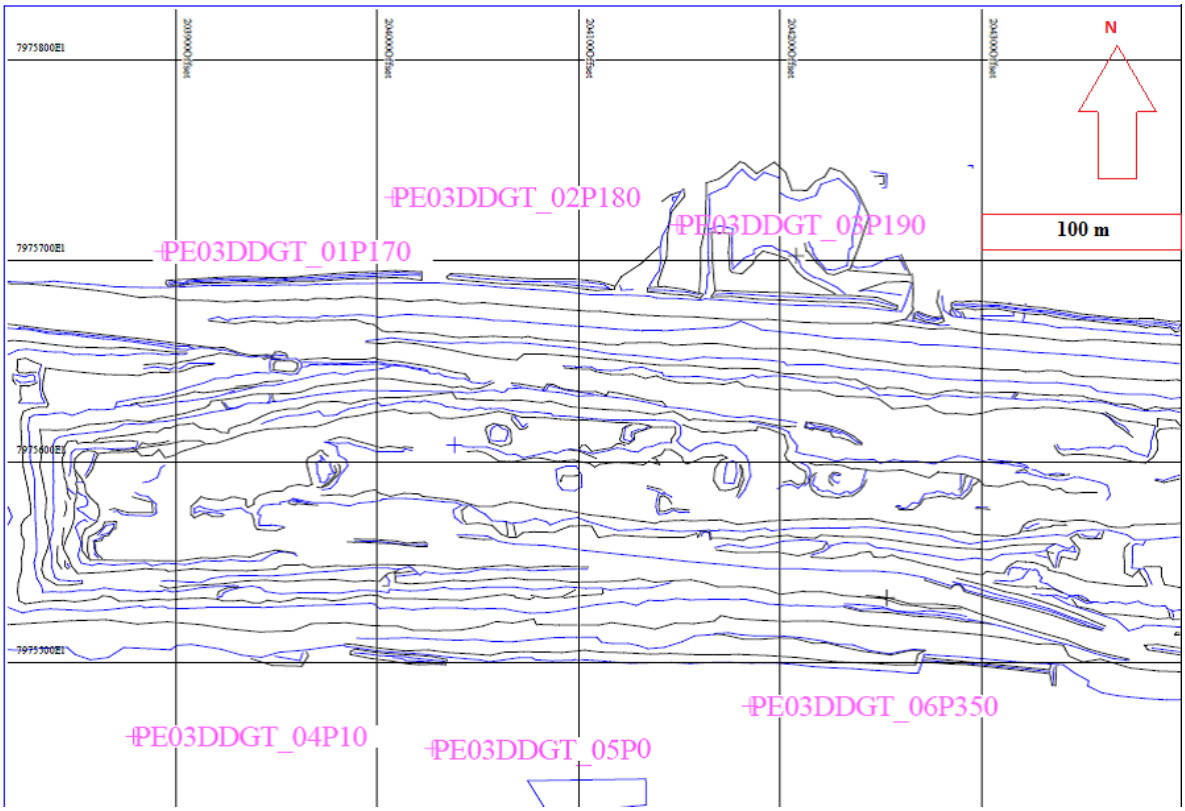


Figure 3-1 Plan view of the PE03 pit showing location of the pure geotechnical holes (PE03DDGT)



Figure 3-2 Satellite image of the PE03 pit. (Google, 2019)

GEOTECHNICAL DIAMOND DRILLING

HoleID	X_Final	Y_Final	Z_Final	Depth	Azimuth	Dip
PE03DDGC8_01P	203990.000	7975701.500	1189.700	224.00	180.00	-63.00
PE03DDGC8_02P	204070.000	7975709.000	1187.200	231.00	180.00	-62.00
PE03DDGC8_03P	204150.000	7975724.500	1190.800	265.00	180.00	-63.00
PE03DDGC8_04P	204230.000	7975507.000	1191.400	184.00	180.00	-60.00
PE03DDGC8_05P	204270.000	7975491.000	1195.000	256.00	0.00	-61.00
PE03DDGT_01P	203950.000	7975704.490	1189.350	205.00	180.00	-60.00
PE03DDGT_04P	204110.000	7975731.000	1190.000	239.00	180.00	-60.00
PE03DDGT_06P	204250.000	7975718.000	1190.000	240.00	180.00	-60.00
PE03DDGT_02P	203880.000	7975463.000	1194.000	240.00	0.00	-59.00
PE03DDGT_03P	204030.000	7975708.600	1189.600	287.00	0.00	-58.00
PE03DDGT_05P	204190.000	7975474.000	1196.000	245.00	0.00	-60.00

Figure 3-3 Total number of planned boreholes as shown on the table that was used by the drillers.

Diamond core drilling was used to gather structural data of the rock mass in which the open pit mine slopes were to be constructed. Orpen (2014) suggested that for data from diamond drilling to be reliably used for geotechnical model creation, there is need to:

- Accurately record the depth of the core so as to accurately locate the position of all the structures collected along the length of the borehole. The depth of the core is the length of the drill string from the borehole collar to the cutting edge of the drill bit.
- Orient the core so as to accurately align the intersection of the geographical vertical plane with the core segments so that the correct orientation, that is the dip and dip direction of the planes of weakness intersected by the borehole can be reliably determined.
- Accurately survey the borehole path from collar to the end-of-hole.

Depth of core

For this project the depth of the core for all the boreholes was measured and recorded at the end of each drill run. The drilling run was taken to be the length of the drill rod that was drilled into the ground prior to recovering the core inner tube. Each depth measurement was recorded on a plastic core block that was then placed at the end of each drill run in the core tray to separate drill runs Figure 3-4.

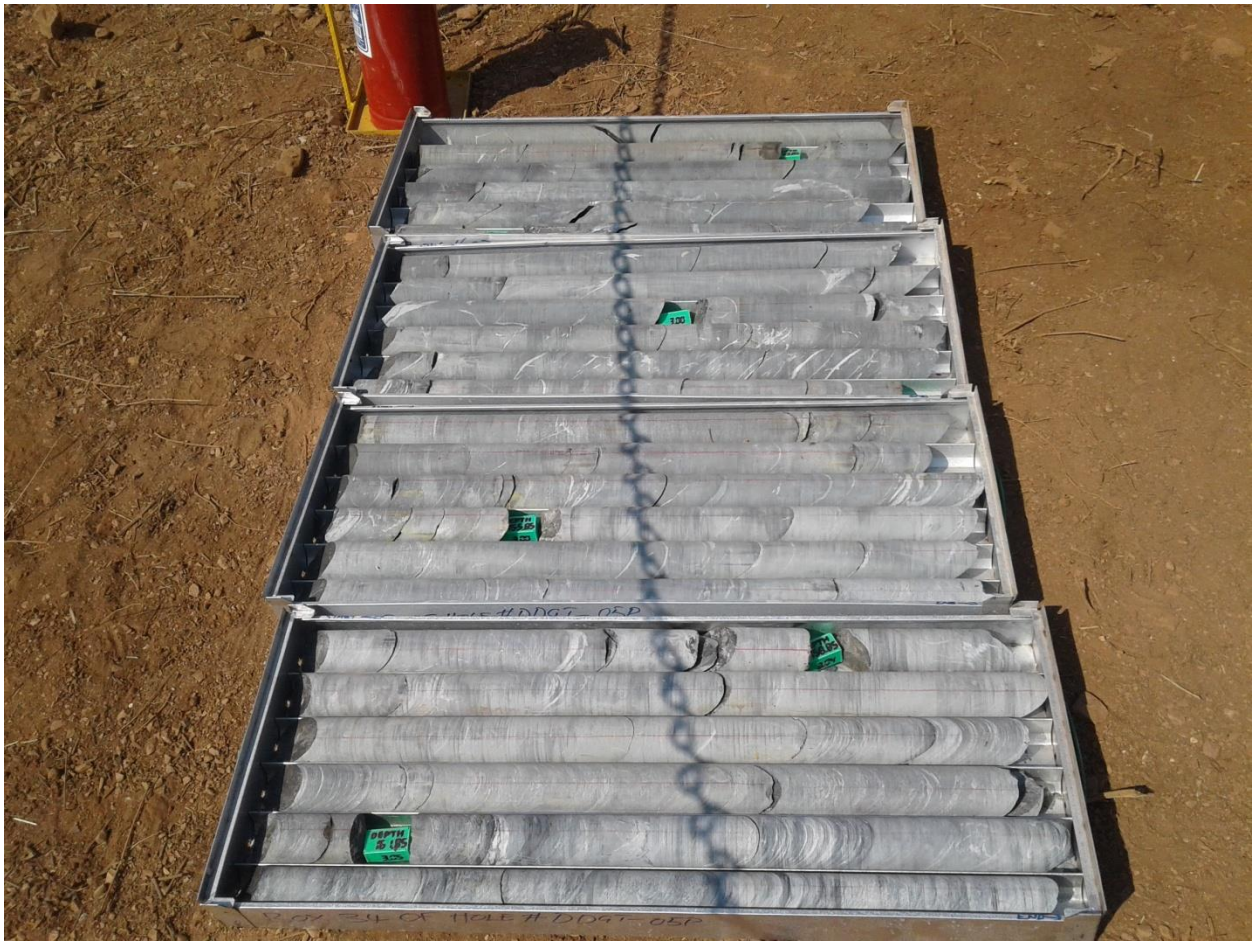


Figure 3-4 Core trays with depth recorded on plastic core blocks separating the drill runs for one of the drilled boreholes (Courtesy of Pickstone-Peerless Mine).

The depth was calculated by taking the difference between the known overall length of the drilling string and the stick-up. The stick-up was taken to be the length of the rod remaining outside the borehole sticking-up above the borehole collar Figure 3-5.

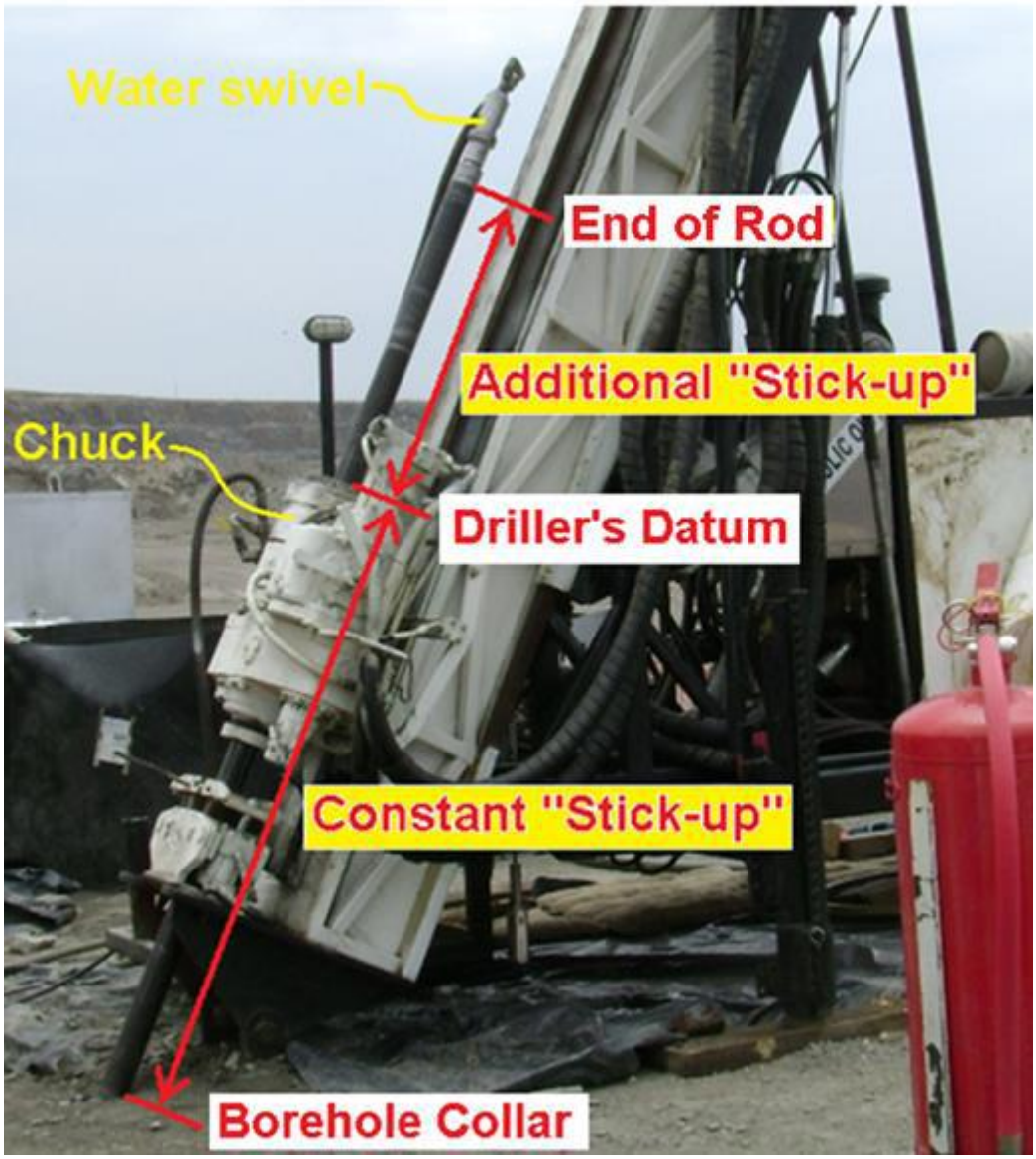


Figure 3-5 Determining the driller's datum against which to measure the stick-up for borehole depth calculation (Orpen, 2014).

Core orientation

All the holes were drilled inclined to the horizontal and a Reflex ACT III tool was used to determine and mark the *in situ* orientation of the core for each run. After drilling each run

the core barrel was retrieved and the core orientation determined, Figure 3-6, and the bottom of core marked before removing the core, Figure 3-7.



Figure 3-6 Determining the in situ core orientation with a Reflex ACT III orientation tool connected to the upper end of the core barrel whilst the core is inside the core barrel (Courtesy of Pickstone-Peerless Mine).



Figure 3-7 Marking the bottom of core with a Reflex marking jig whilst the core is still in the core barrel and the Reflex Orientation tool is still attached on the upper end of the core (Courtesy of Pickstone-Peerless Mine).

The core was then emptied from the core barrel onto a core stand made of angle iron and cleaned, Figure 3-8. Subsequently, the orientation line was drawn from the bottom of core mark extending the entire length of the core with the aid of the straight edge of the angle iron on which the core was placed, Figure 3-9.



Figure 3-8 Drilled core just after removal from the core barrel and cleaned, lying on the angle iron core stand (Courtesy of Pickstone-Peerless Mine).



Figure 3-9 Drawing the orientation line along the entire length of the drill core extending it from the bottom of core mark (Courtesy of Pickstone-Peerless Mine).

When the core orientation procedure was completed the Total Core Recovered (TCR) from the drill run was then measured and recorded, Figure 3-10. The RQD was also determined and recorded for each run. The data recorded at the drill rig was considered as basic core logging. After that the core was carefully placed into the core trays, at the end of each drilling shift the filled core trays were taken to the core shed where they were safely stored waiting for final detailed core logging.



Figure 3-10 Measuring the Total Core Recovery (TRC) for a particular drill run using a steel measuring tape (Courtesy of Pickstone-Peerless Mine).

3.2.2 Oriented core logging

A core logging exercise was then carried out for each of the boreholes. The type of data collected during this logging exercise is shown on the geotechnical log sheet in Table 3-1. The completed data log sheets of logged boreholes are shown in the appendix A (Table A-1 to Table A-7)

Table 3-1 Geotechnical core logging data sheet used for PE03 logging exercise.

GEOTECHNICAL CORE LOGGING DATA SHEET FOR PE03					
LOGGED BY:			**CHECKED BY:**		
NORTHING:			**DIP:**		
EASTING:			**AZIMUTH:**		
ELAVATION:			**HOLE DEPTH:**		
DATE:			**CORE SIZE:**		
DRILLHOLE ID:	**DEPTH INTERVAL**		**STRUCTURAL DATA**		
	From (m)	**To (m)**	**STRUCTURE TYPE**	**BETA**	**ALPHA**

Measuring core orientation parameters

During the logging exercise the alpha and beta angles of the structures intersected by the diamond drill holes were measured and recorded. These measurements were done using a goniometer, Figure 3-11. The description of these angles is given in the following paragraphs.



Figure 3-11 A goniometer for measuring alpha and beta angles (Westernex, 2018)

Any planar structure intersected by a diamond drill hole will create an elliptical outline on the core sample. The longest axis of this ellipse will be in line with the dip direction of the structure. The geometry of the ellipse on the core sample is defined by two angles which are the alpha angle (α) and the beta angle (β). The alpha and beta angles will then be used to determine the true dip and dip direction of the planar structure in the rock mass.

To measure the α and β angles the core sample was inserted into the goniometer with the orientation line on the core sample set directly below the downhole mark on the goniometer. The end of the core sample towards the bottom of the hole was positioned at the arrow head of the mark. According to Orpen (2014), the alpha angle is taken as the acute angle between the core axis and the long axis of the ellipse. The beta angle is the angle measured in a clockwise direction around the core on a plane perpendicular to the core axis. The beta angle was read starting from the zero reading of the instrument located at the downhole mark, in a clockwise direction up to the apical trace of the ellipse. The apical trace used was the one extended down the core from the point of intersection of the ellipse and its long axis, on the down dip side of the ellipse, Figure 3-12.

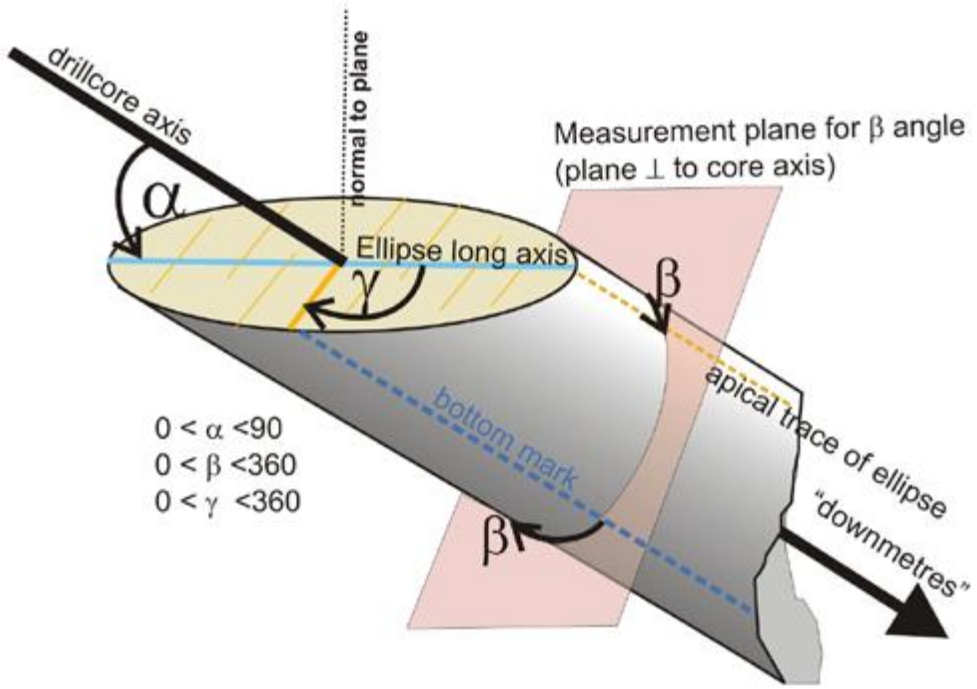


Figure 3-12 Definition of the alpha (α) and the beta (β) angles (HolcombeCoughlinOliver, 2010)

3.2.3 Face mapping

Structural data was also gathered through mapping of exposed slopes of the pit. The orientation of these structures in terms of dip and dip direction was measured and recorded. The orientation measurements were taken using a Brunton geological compass shown in Figure 3-13. Measurements were taken from the northern and southern side of the PE03 pit. The template of the log sheet used for this purpose is shown in Table 3-2. The completed face mapping data log sheets are shown in the appendix B (Table B-1 and Table B-2).



Figure 3-13 Brunton geological compass that was used to measure dip and dip direction during face mapping.

Table 3-2 Face mapping data log sheet used for PE03 mapping exercise.

FACE MAPPING DATA LOG SHEET FOR PE03						
MAPPED BY:				**SURVERYOR:**		
DATE:				**PIT WALL:**		
POINT ID	**POINT COORDINATES**			**STRUCTURAL DATA**		
	X	**Y**	**Z**	**STRUCTURE TYPE**	**DIP**	**DIP DIRECTION**

3.3 Rock Mechanical Properties

Rock mechanical properties used in the analysis were taken from the documented previous work conducted to design the current pit slopes. Results of uniaxial and triaxial strength tests conducted to estimate the intact strength of the rock from previous geotechnical investigations were used. These are shown in Table 3-3 to Table 3-5.

Table 3-3 Uniaxial Compressive Strength test results with elastic constants for fresh rock ((Bosman, 2013).

SPECIMEN PARTICULARS			SPECIMEN DIMENSIONS					SPECIMEN TEST RESULTS								
Rocklab Specimen No 5374-	Sample ID	Rock Type	Diameter mm	Height mm	Ratio of Height to Diameter	Mass g	Density g/cm³	Failure Load kN	Strength (UCS) MPa	Tangent Elastic Modulus @50% UCS GPa	Secant Elastic Modulus @50% UCS GPa	Poisson's Ratio Tangent @50% UCS	Poisson's Ratio Secant @50% UCS	Linear Axial Strain at Failure mm/mm	Failure Code	Note
UCM-06-02	CHDD006-02		47.41	132.7	2.8	642.59	2.74	32.9	18.6	57.0	56.2	0.26	0.22	0.000359	3B	
UCM-07-01	CHDD007-01		63.12	173.3	2.7	1536.97	2.83	27.0	8.6	46.3	38.2	0.18	0.21	0.000204	4B	
UCM-07-04	CHDD007-04		63.24	177.7	2.8	1567.23	2.81	52.2	16.6	26.1	23.3	0.11	0.08	0.000907	4B	
UCM-07-06	CHDD007-06		47.34	114.2	2.4	567.87	2.82	52.2	29.6	47.1	38.9	0.21	0.13	0.000412	3B	
UCM-07-08	CHDD007-08		47.35	119.2	2.5	575.25	2.74	39.8	22.6	40.6	38.0	0.28	0.29	0.000599	6B	

Table 3-4 Results of Triaxial Compressive Strength tests (Bosman, 2013).

SPECIMEN PARTICULARS			SPECIMEN DIMENSIONS					SPECIMEN TEST RESULTS					
Rocklab Specimen No 5374-	Sample No	Rock Type	Diameter mm	Height mm	Ratio of Height to Diameter	Mass g	Density g/cm³	Confining Pressure δ_3 MPa	Failure Load P kN	Strength (TCS) δ_1 MPa	Angle Between Failure Plane with core axis deg.	Failure Mode	Note
TCS-07-05A	CHDD007-05		47.31	94.4	2.0	474.4	2.86	5.0	157.3	89.5	26.6	3B	
TCS-07-05B			47.31	94.8	2.0	481.1	2.89	10.0	145.9	83.0	25.7	3B	
TCS-07-05C			47.36	94.9	2.0	473.6	2.83	15.0	197.8	112.3	26.5	3B	
TCS-07-05D			47.33	91.4	1.9	449.1	2.79	20.0	233.9	133.0	28.9	3B	
TCS-07-05E			47.31	94.6	2.0	464.7	2.80	25.0	195.6	111.3	35.1	4B	
TCS-07-05F			47.31	95.1	2.0	458.7	2.74	30.0	284.8	162.0	33.4	4B	
TCS-06-03D	CHDD006-03		47.43	96.4	2.0	468.50	2.75	5.00	60.55	34.3	26.4	3B	
TCS-07-03B	CHDD007-03		63.16	125.6	2.0	1115.90	2.84	20.00	168.63	53.8	33.5	4B	
TCS-07-06A	CHDD007-06		47.32	81.5	1.7	403.5	2.82	7.5	218.5	124.2	30.7	4B	
TCS-07-06B	CHDD007-06		47.34	82.7	1.7	411.6	2.83	10.0	200.7	114.0	26.0	3B	
TCS-07-06C	CHDD007-06		47.36	81.2	1.7	404.8	2.83	12.5	247.4	140.5	21.9	3B	
TCS-07-07C	CHDD007-07		47.31	80.4	1.7	388.3	2.75	15.0	232.4	132.2	31.8	XA	

Table 3-5 Brazilian Tensile Strength tests (Bosman, 2013)

SPECIMEN PARTICULARS			SPECIMEN DIMENSIONS				SPECIMEN TEST RESULTS		
Rocklab Specimen No 5374-	Sample No.	Rock Type	Diameter mm	Height mm	Mass g	Density g/cm³	Failure Load kN	Tensile Strength MPa	Note
UTB-01a	CHDD007-02		47.75	23.81	121.7	2.85	7.9	4.42	1
UTB-01b			47.75	24.27	122.4	2.82	16.7	9.15	1
UTB-02a	CHDD007-07		47.29	24.39	118.8	2.77	18.0	9.95	
UTB-02b			47.26	24.35	118.1	2.76	20.4	11.29	
UTB-03a	CHDD007-07		47.27	24.46	118.1	2.75	11.5	6.32	
UTB-03b			47.33	24.51	117.3	2.72	15.7	8.63	

It was reported that all the UCS samples failed along pre-existing discontinuities (failure codes are described in Appendix (Figure C-1). The discontinuities were, however, identified as foliation i.e part of rock fabric (Bosman, 2013) . A valuation process ensued, using the Young's Modulus to UCS ratio method (Deere & Miller, 1966). The method requires that the ratio be less than 500 to be acceptable. The lowest Modulus ratio was found to be 1571, making the results unacceptable and they were discarded. As the Young's Modulus values were obtained from the stress strain behaviour, prior to failure, these values were taken to be accurate. The Young's Modulus values were thus used to estimate the UCS values of the samples, and they were found to be about 95 MPa (perpendicular to the foliation). The BTS tests were conducted perpendicularly to the foliation and provided an average strength of about 9 MPa. As it is generally accepted that the tensile strength of rock is about 10% of the UCS, the average UCS could be assumed to be close to 90 MPa which is similar to the estimation using the Modulus Ratio method. Subsequently, the UCS was estimated using a straight-line regression analysis through the TCS results. A similar UCS strength was again shown (Figure 3-14). It was

therefore concluded that the UCS of the rock was between 90 MPa and 95 MPa (perpendicular to the foliation).

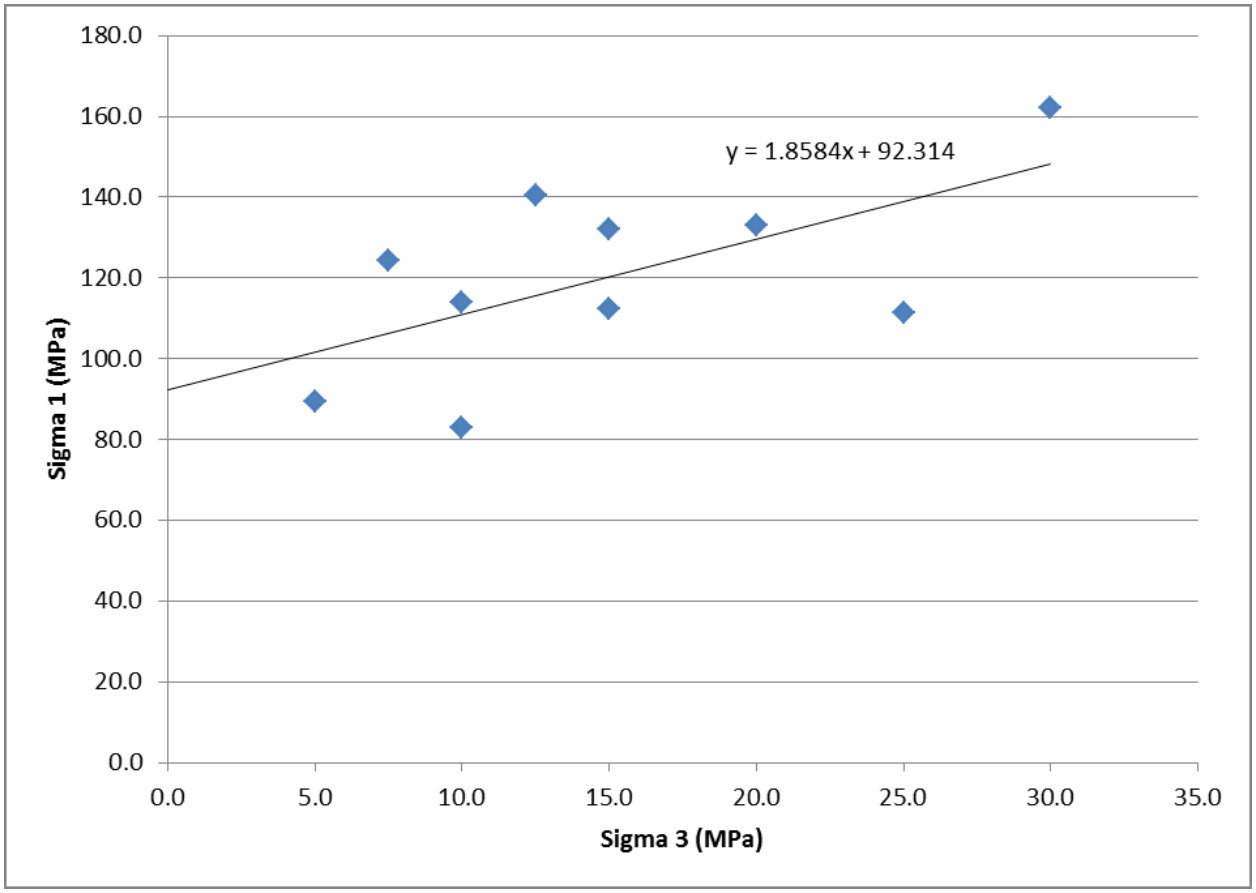


Figure 3-14 Sigma 1 versus Sigma 3 (Bosman, 2013).

The Rock Mass Rating (RMR) was determined using data collected from the diamond drill core samples. Table 3-6 shows the log sheet that was used to record the input data used in the determination of RMR for each diamond drill hole.

Table 3-6 Determination of RMR

Hole ID:							Ratings of RMR parameters					
From (m)	To (m)	Measured length (m)	TCR (%)	Length > 10 cm	RQD (%)	Js (m)	Is	RQD	Js	Jc	Jw	RMR

The RMR value for each hole was taken as the average of the RMR for the drill runs. The RMR value per drill run was determined by adding the ratings of the intact rock strength (Is), RQD, joint spacing (Js), joint condition (Jc) and ground water condition (Jw). The ratings were estimated using Table 3-7.

Table 3-7 Rock Mass Rating System (After Bieniawski, 1989)

A. CLASSIFICATION PARAMETERS AND THEIR RATINGS									
Parameter			Range of values						
1	Strength of intact rock material	Point-load strength index	>10 MPa	4-10 MPa	2-4 MPa	1-2 MPa	For this low range - uniaxial compressive test is preferred		
		Uniaxial comp. strength	>250 MPa	100-250 MPa	50-100 MPa	25-50 MPa	5-25 MPa	1-5 MPa	< 1 MPa
	Rating		15	12	7	4	2	1	0
2	Drill core Quality *RQD*		90%-100%	75%-90%	50%-75%	25%-50%	< 25%		
	Rating		20	17	13	8	3		
3	Spacing of discontinuities		> 2 m	0.6-2 . m	200-600 mm	60-200 mm	< 60 mm		
	Rating		20	15	10	8	5		
4	Condition of discontinuities (See E)		Very rough surfaces Not continuous No separation Unweathered wall rock	Slightly rough surfaces Separation < 1 mm Slightly weathered walls	Slightly rough surfaces Separation < 1 mm Highly weathered walls	Slickensided surfaces or Gouge < 5 mm thick or Separation 1-5 mm Continuous	Soft gouge >5 mm thick or Separation > 5 mm Continuous		
	Rating		30	25	20	10	0		
5	Ground water	Inflow per 10 m tunnel length (l/m)	None	< 10	10-25	25-125	> 125		
		(Joint water press)/ (Major principal σ)	0	< 0.1	0.1-0.2	0.2-0.5	> 0.5		
		General conditions	Completely dry	Damp	Wet	Dripping	Flowing		
	Rating		15	10	7	4	0		

B. RATING ADJUSTMENT FOR DISCONTINUITY ORIENTATIONS (See F)						
Strike and dip orientations		Very favourable	Favourable	Fair	Unfavourable	Very Unfavourable
Ratings	Tunnels & mines	0	-2	-5	-10	-12
	Foundations	0	-2	-7	-15	-25
	Slopes	0	-5	-25	-50	

C. ROCK MASS CLASSES DETERMINED FROM TOTAL RATINGS					
Rating	100 ← 81	80 ← 61	60 ← 41	40 ← 21	< 21
Class number	I	II	III	IV	V
Description	Very good rock	Good rock	Fair rock	Poor rock	Very poor rock

D. MEANING OF ROCK CLASSES					
Class number	I	II	III	IV	V
Average stand-up time	20 yrs for 15 m span	1 year for 10 m span	1 week for 5 m span	10 hrs for 2.5 m span	30 min for 1 m span
Cohesion of rock mass (kPa)	> 400	300-400	200-300	100-200	< 100
Friction angle of rock mass (deg)	> 45	35-45	25-35	15-25	< 15

E. GUIDELINES FOR CLASSIFICATION OF DISCONTINUITY conditions					
Discontinuity length (persistence) Rating	< 1 m 6	1-3 m 4	3-10 m 2	10-20 m 1	> 20 m 0
Separation (aperture) Rating	None 6	< 0.1 mm 5	0.1-1.0 mm 4	1-5 mm 1	> 5 mm 0
Roughness Rating	Very rough 6	Rough 5	Slightly rough 3	Smooth 1	Slickensided 0
Infilling (gouge) Rating	None 6	Hard filling < 5 mm 4	Hard filling > 5 mm 2	Soft filling < 5 mm 2	Soft filling > 5 mm 0
Weathering Ratings	Unweathered 6	Slightly weathered 5	Moderately weathered 3	Highly weathered 1	Decomposed 0

F. EFFECT OF DISCONTINUITY STRIKE AND DIP ORIENTATION IN TUNNELLING**			
Strike perpendicular to tunnel axis		Strike parallel to tunnel axis	
Drive with dip-Dip 45-90°	Drive with dip-Dip 20-45°	Dip 45-90°	Dip 20-45°
Very favourable	Favourable	Very favourable	Fair
Drive against dip-Dip 45-90°	Drive against dip-Dip 20-45°	Dip 0-20-Irrespective of strike°	
Fair	Unfavourable	Fair	

The Mohr Coulomb and the Hoek Brown parameters were estimated using the RocLab Hoek-Brown failure criterion software program (Hoek, et al., 2002). The rock mass quality was determined using the average RMR values shown in Table 3-8.

Table 3-8 Mean RMR values of the core samples used (Bosman, 2013).

Weathered Rock		**Fresh Rock**	
Mean	Standard deviation	Mean	Standard deviation
45.53	11.72	63.86	4.93

RockLab (Hoek, et al., 2002) was used to perform downgrading of intact rock strength values to in-situ strength values. Geological Strength Index (GSI) was determined from RMR value as GSI = (RMR – 5) (Hoek & Brown, 1997). It was therefore assumed that the GSI value for weathered rock was 41 and 59 for fresh rock.

To determine standard deviation of Cohesion (C) and Angle of Friction (Phi), GSI minus one standard deviation and GSI plus one standard deviation was used in RockLab (Hoek, et al., 2002).

For weathered rock:

RMR + standard deviation = 57; GSI = 52

RMR – standard deviation = 34; GSI = 29

For fresh rock:

RMR + standard deviation = 69; GSI = 64

RMR – standard deviation = 59; GSI = 54

The triaxial test data was imported into RocLab (Hoek, et al., 2002) to determine unconfined compressive strength of intact rock (Sigci) Hoek-Brown constant (mi) for the intact rock parameter. The parameter mi is a material constant that influences the strengthening effect of confinement. These intact parameters were downgraded using the GSI values for the respective rock types. The downgraded values, for weathered and fresh rock are shown in Table 3-9 and Table 3-10 respectively. These parameters were used in constructing Figure 3-15 to Figure 3-20, which shows the *insitu* failure envelopes.

.

Table 3-9 Mechanical properties for weathered rock, from surface to 25 m below surface.

Mechanical properties of weathered rock			
GSI	41 (average)	29	52
Hoek Brown Classification			
Sigci (MPa)	21.608	21.608	21.608
GSI	41	29	52
mi	5.599	5.599	5.599
D	0.8	0.8	0.8
Ei	18100	18100	18100
Hoek Brown Criterion			
mb	0.167074	0.0817898	0.321565
s	0.00013112	2.13E-05	0.000694216
a	0.510622	0.523899	0.504991
Failure Envelope Range			
Application	Slopes	Slopes	Slopes
Sig3max (MPa)	1.41581	1.35775	1.4657
Unit Weight (MN/m3)	0.026	0.026	0.026
Mohr-Coulomb Fit			
C (MPa)	0.194614	0.127278	0.278667
phi (degrees)	22.2932	16.9116	27.2614
Rock Mass Parameters			
Sigt (MPa)	-0.016958	-0.00562289	-0.0466488
Sigc (MPa)	0.225016	0.0770873	0.549031
Sigcm (MPa)	1.11444	0.699821	1.63748
Erm (MPa)	973.956	575.554	1878.62

Table 3-10 Mechanical properties for fresh rock, below 25 m from surface.

Mechanical properties of fresh rock			
GSI	59 (average)	64	54
Hoek Brown Classification			
Sigci (MPa)	91.26	91.26	91.26
GSI	59	64	54
mi	2.03	2.03	2.03
D	0.8	0.8	0.8
Ei	43420	43420	43420
Hoek Brown Criterion			
mb	0.176852	0.238158	0.131328
s	0.00200498	0.00427682	0.000939938
a	0.503051	0.502126	0.504342
Failure Envelope Range			
Application	Slopes	Slopes	Slopes
Sig3max (MPa)	1.70008	1.73541	1.66849
Unit Weight (MN/m3)	0.027	0.027	0.027
Mohr-Coulomb Fit			
C (MPa)	1.08642	1.59748	0.754728
phi (degrees)	29.3108	30.1156	28.0959
Rock Mass Parameters			
Sigt (MPa)	-1.03462	-1.63884	-0.653165
Sigc (MPa)	4.00963	5.89936	2.71449
Sigcm (MPa)	5.8111	7.30335	4.71796
Erm (MPa)	6983.47	9355.97	5113.85

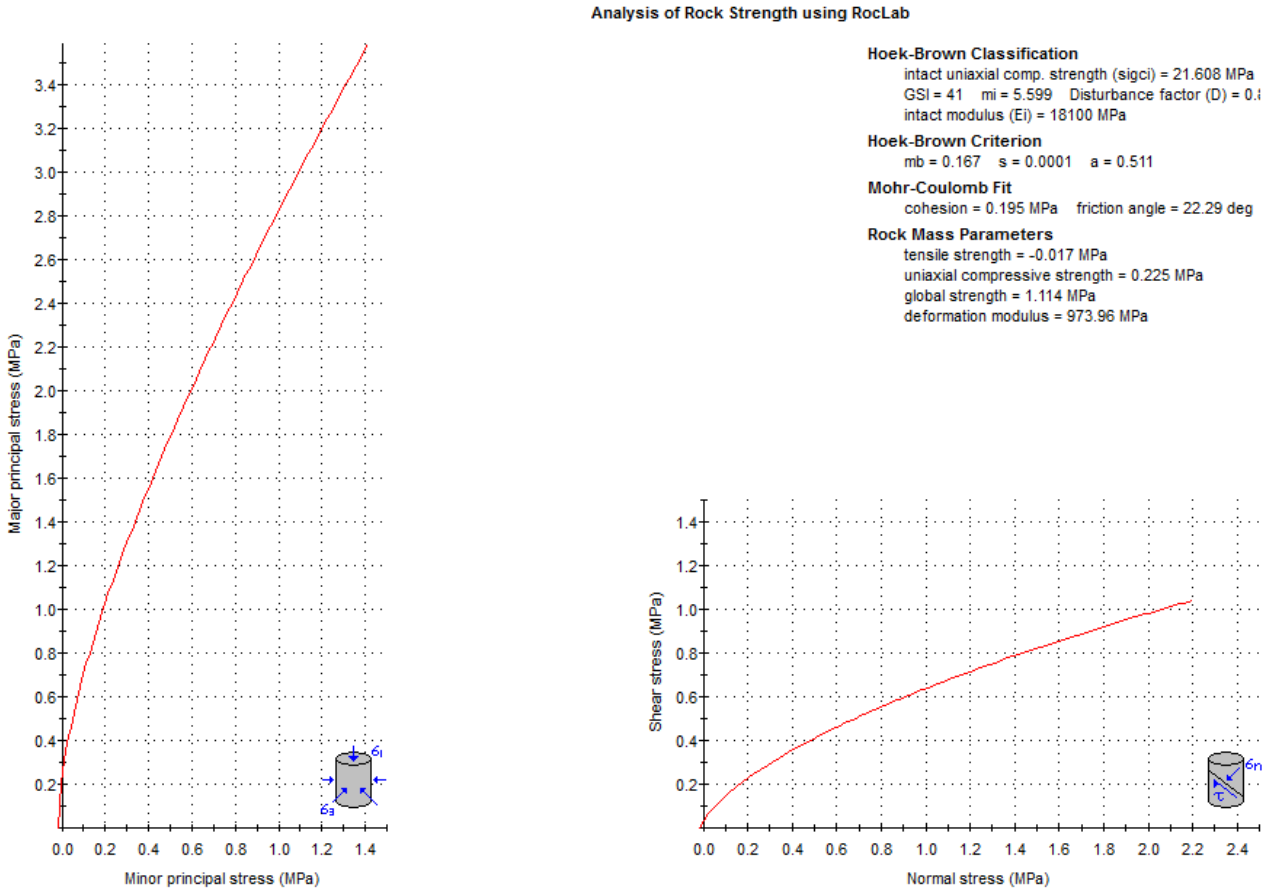


Figure 3-15 Failure envelopes obtained from RockLab software for Weathered Rock, GSI 41 (Bosman, 2013).

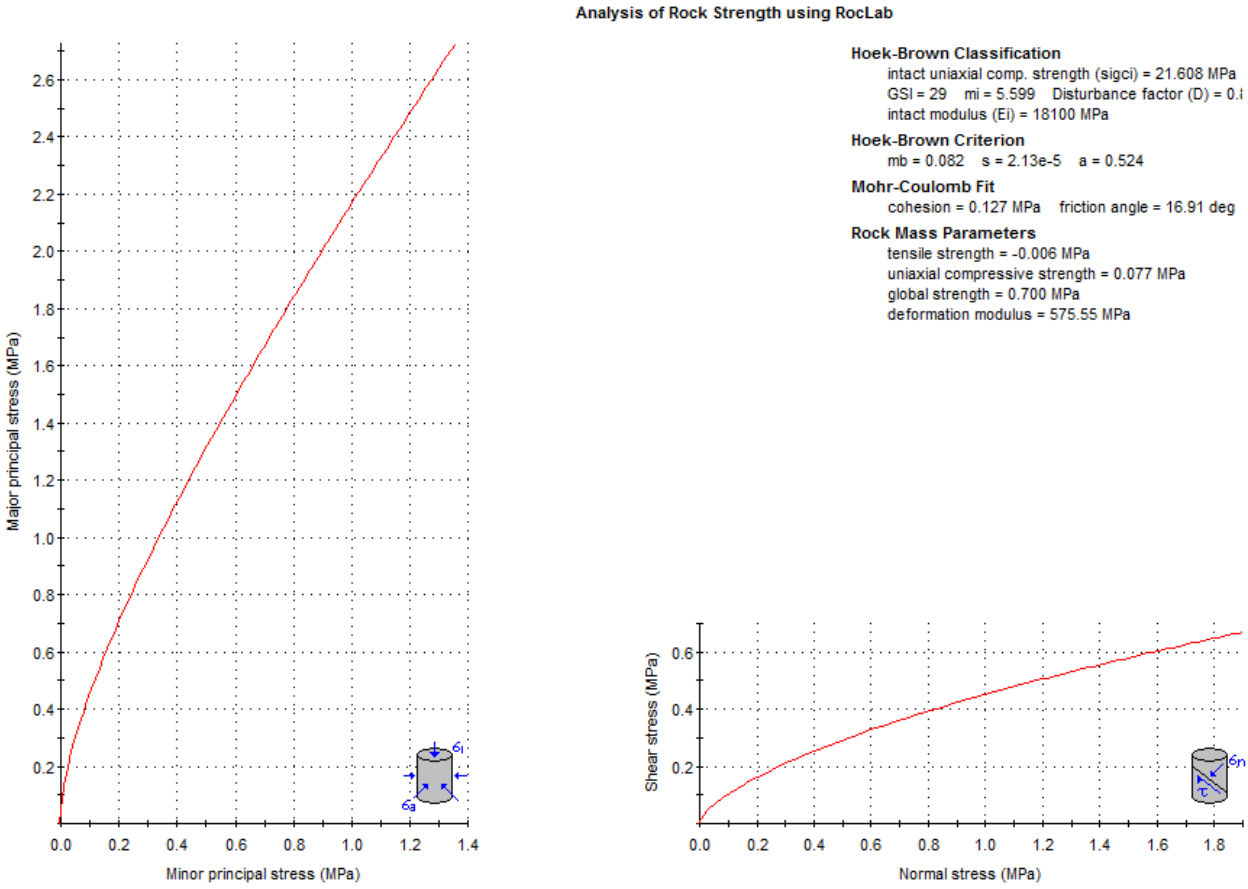


Figure 3-16 Failure envelopes obtained from RockLab software for Weathered Rock, GSI 29 (Bosman, 2013).

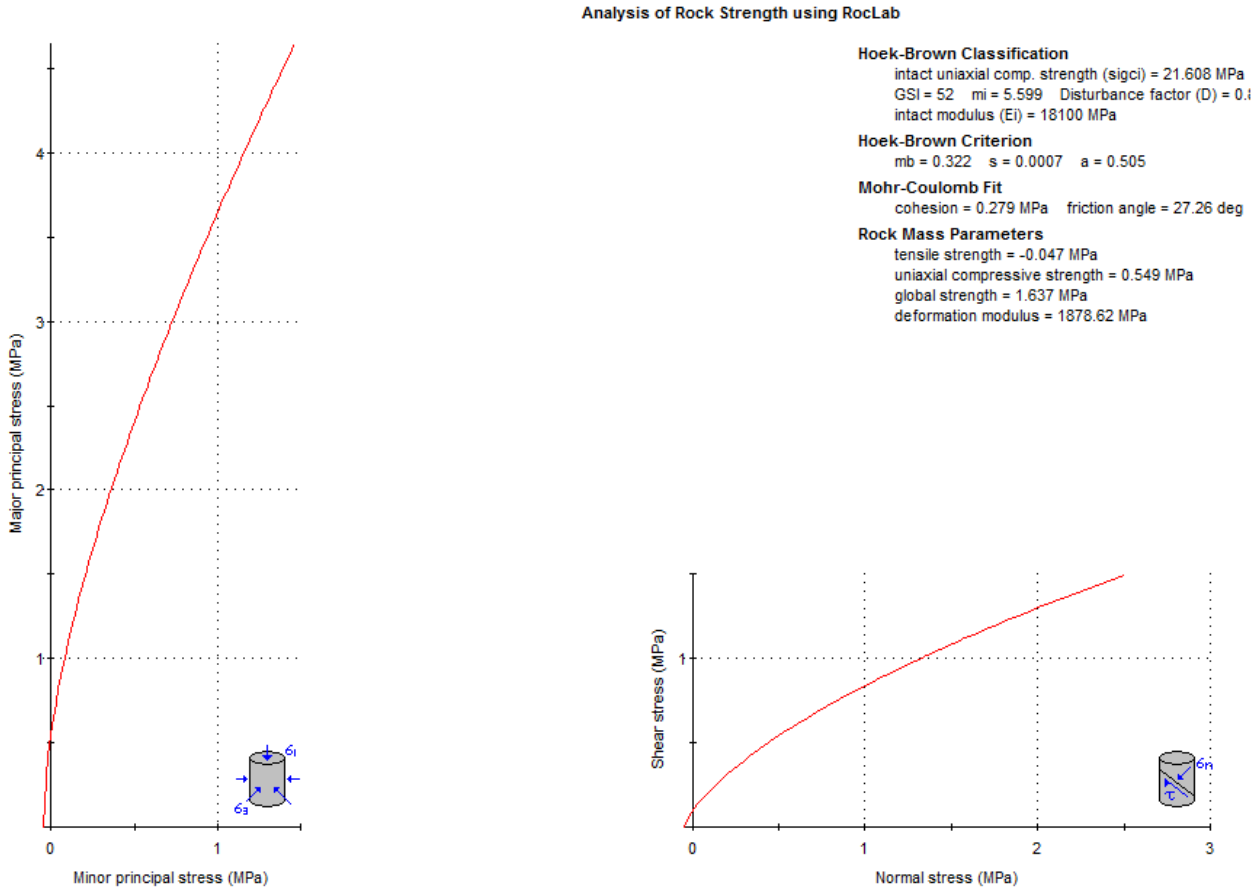


Figure 3-17 Failure envelopes obtained from RockLab software for Weathered Rock, GSI 52 (Bosman, 2013).

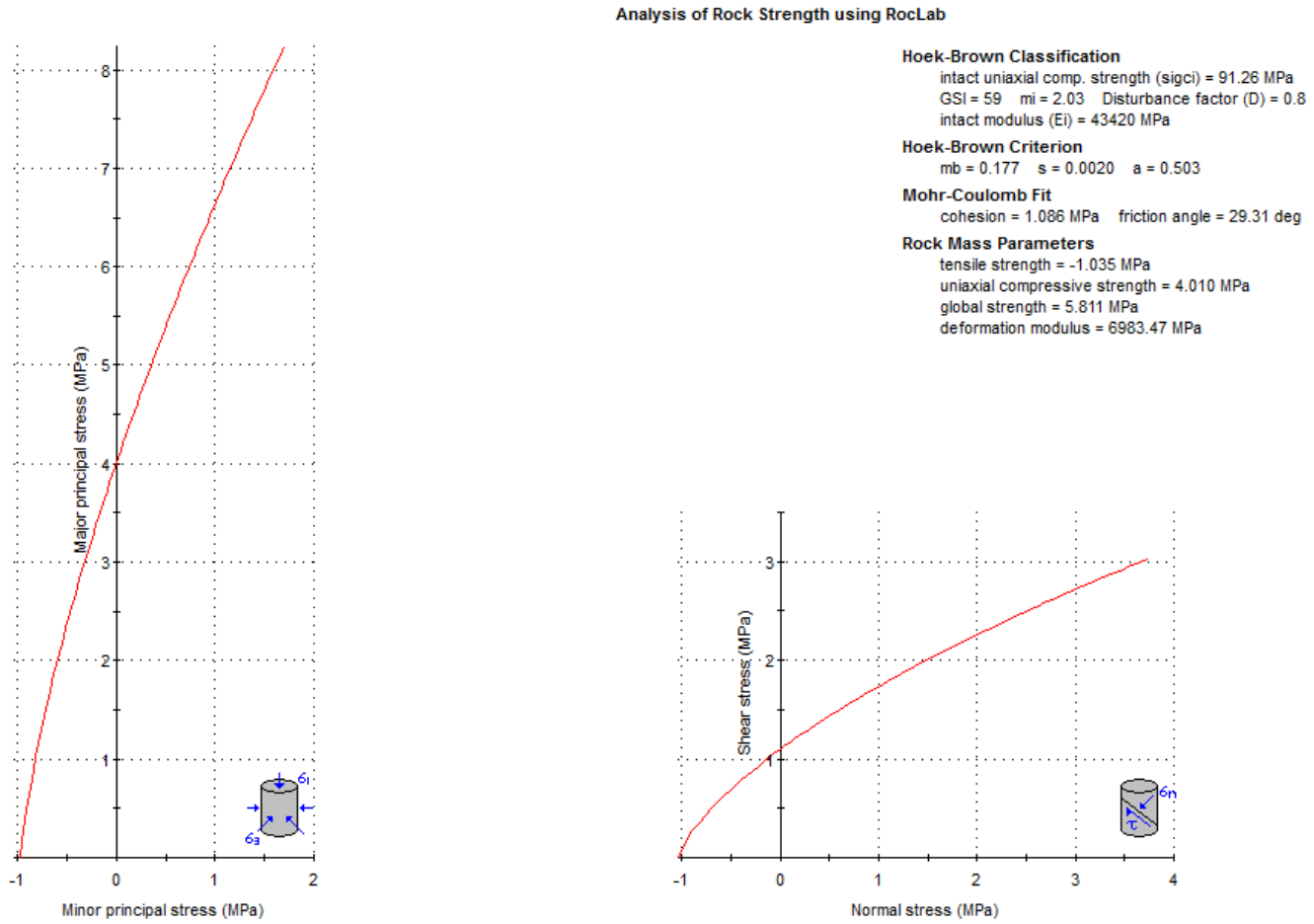


Figure 3-18 Failure envelopes obtained from RockLab software for Fresh Rock, GSI 59 (Bosman, 2013).

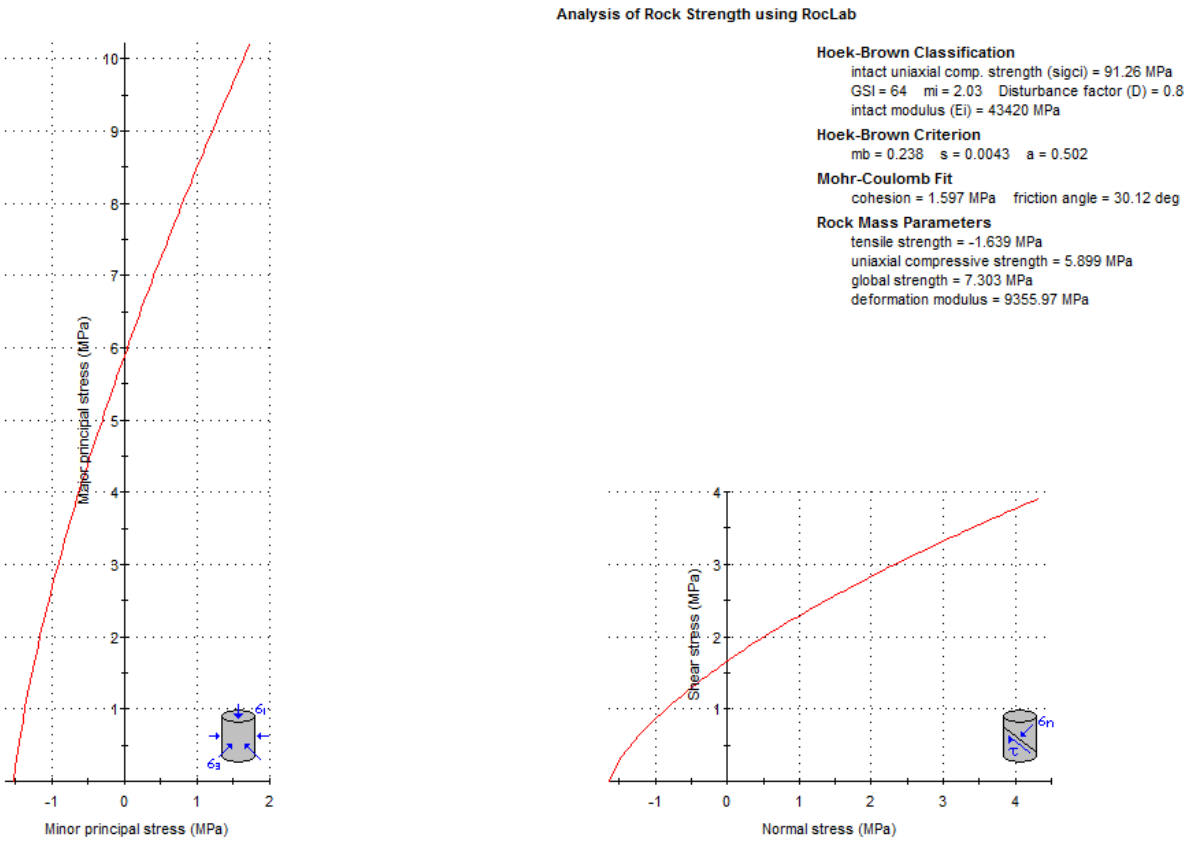


Figure 3-19 Failure envelopes obtained from RockLab software for Fresh Rock, GSI 64 (Bosman, 2013).

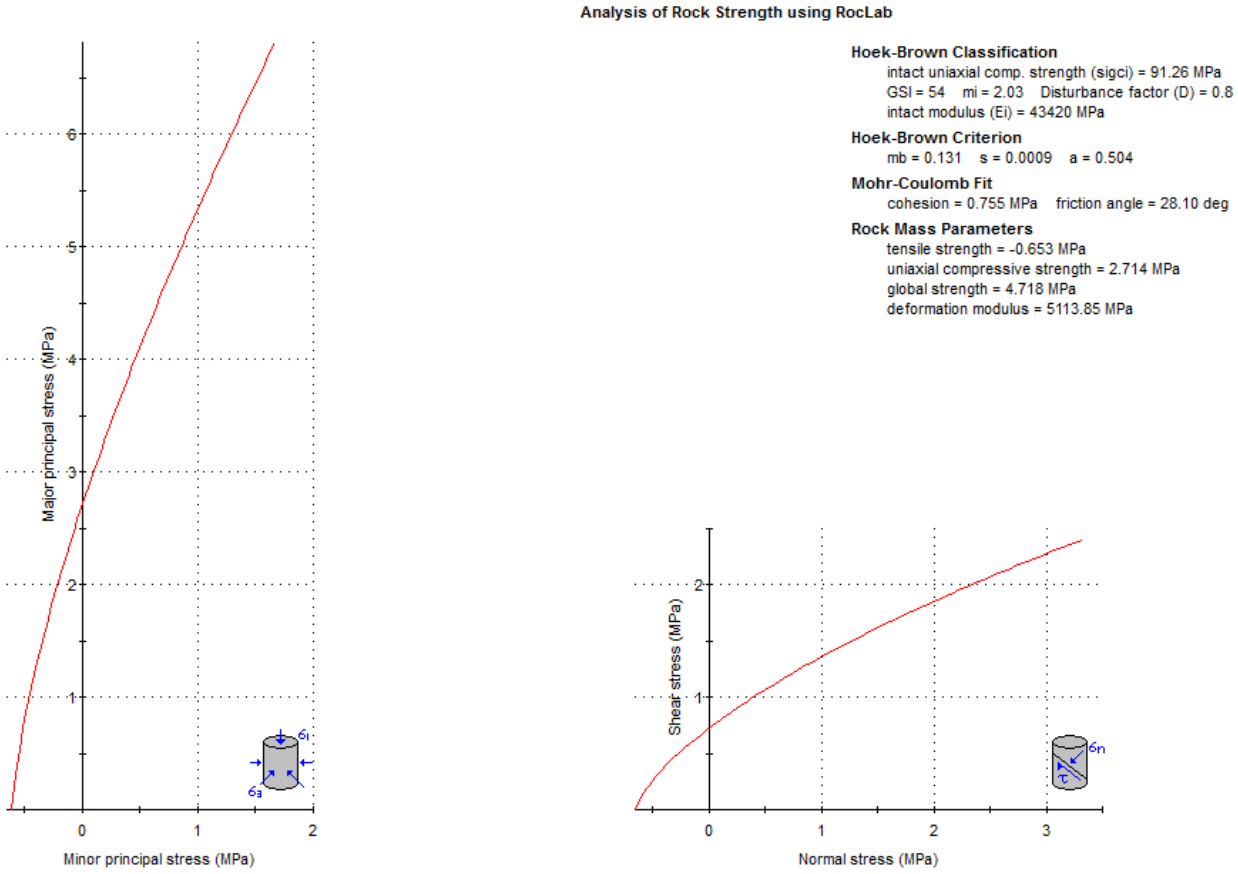


Figure 3-20 Failure envelopes obtained from RockLab software for Fresh Rock, GSI 54 (Bosman, 2013).

The program plots the curves based on the generalized Hoek-Brown criterion and Mohr-Coulomb criterion. The generalized Hoek-Brown criterion equation is as follows:

$$\sigma_1' = \sigma_3' + \sigma_{ci}\left(m_b \frac{\sigma_3'}{\sigma_{ci}} + s\right)^a \qquad \text{Equation 3-1}$$

Where:

σ_1' Major principal stress (MPa)

σ_3' Minor principal stress (Mpa)

σ_{ci} Intact rock strength (UCS) (MPa)

m_b Reduced value of the intact rock parameter m_i

a & s Rock mass constants

Normal (σ_n) and shear (τ) stresses are determined from the principal stresses using the following equations:

$$\sigma_n' = \frac{\sigma_1' + \sigma_3'}{2} - \frac{\sigma_1' - \sigma_3'}{2} \cdot \frac{d\sigma_1'/d\sigma_3' - 1}{d\sigma_1'/d\sigma_3' + 1} \quad \text{Equation 3-2}$$

$$\boldsymbol{\tau = (\sigma_1' - \sigma_3')\frac{\sqrt{d\sigma_1'/d\sigma_3'}}{d\sigma_1'/d\sigma_3' + 1}} \quad \text{Equation 3-3}$$

Where: $\boldsymbol{d\sigma_1'/d\sigma_3'} = 1 + am_b(m_b\sigma_3'/\sigma_{ci}' + s)^{a-1}$ Equation 3-4

The Mohr-Coulomb criterion equation is as follows:

$$\tau = c' + \sigma \tan \phi' \quad \text{Equation 3-5}$$

Where:

c' Cohesion (MPa)

ϕ' Friction angle

Cohesion and friction angle are determined by plotting the best-fit Mohr-Coulomb envelope defined by a stress range selected by user depending on the application

(i.e. tunnelling or slope stability) (Rocscience, 2002). One such envelope is shown in Figure 3-21.

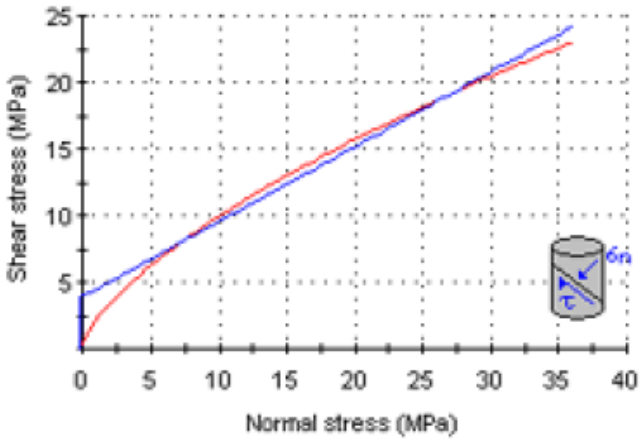


Figure 3-21 The best-fit Mohr-Coulomb envelope (Blue line) on a normal and shear stress plot (Rocscience, 2002).

3.4 Slope Stability Analysis

The data gathered was used as input to slope stability analysis. Stability analysis was carried out on the current design as well as on various optimized design versions. The geometrical parameters of the current and the optimized designs, which were analysed, are shown in Table 3-11. Two of the optimized designs (OD1 and OD2 in Table 3-11) were determined by varying some of the bench geometrical parameters of the current design. One of these optimized designs was further optimized by gradually increasing its overall slope angle in increments of 1^{o} (OD3 to OD5 Table 3-11).

Table 3-11 Geometrical parameters for the current and optimized overall pit slope designs in the unweathered rock, below 25 m.

	CURRENT DESIGN	OPTIMIZED DESIGNS				
		OD1	OD2	OD3	OD4	OD5
Bench slope angle (º)	90º	90º	85º	87º	88º	89º
Bench height (m)	10 m	10 m	10 m	10 m	10 m	10 m
Bench width (m)	10 m & 6 m alternating	10 m & 5 m alternating	7 m & 5 m alternating	7 m & 5 m alternating	7 m & 5 m alternating	7 m & 5 m alternating
Inter-ramp stack height (m)	40 m	40 m	40 m	40 m	40 m	40 m
Ramp width (m)	12 m	12 m	12 m	12 m	12 m	12 m
Inter-ramp slope angle (º)	61.2º	63.4º	62.9º	64º	65º	67º
Overall slope height (m)	170 m	170 m	170 m	170 m	170 m	170 m
Overall slope angle (º)	52º	54º	54º	55º	56º	57º

Optimized designs, OD1 and OD2 were direct variants of the current design whilst the other three, OD3, OD4 and OD5 were derived from OD2. Only three derivatives of OD2 were possible since the last possible increment on the overall slope angle, 57^{o} to 58^{o} resulted in an impractical bench slope angle of 91^{o}. Further attempts to use a bench slope angle of 90^{o} resulted in an overall slope angle of 57^{o} but the minimum bench and ramp width were reduced to 4.84 m and 11.84 m respectively. This was below the minimum requirements for the mine of 5 m and 12 m for the bench and ramp width respectively.

The analysis was done for the two design sectors of the PE03 pit, which are the northern and southern pit slopes. The following techniques were employed during the analysis exercise:

- Empirical slope stability analysis and design
- Kinematic analysis
- Limit equilibrium analysis
- Numerical analysis

The four techniques have different capabilities as indicated in the literature review chapter, thus they were used to complement each other and to compare the results with the aim of providing a reliable design. Among other characteristics the kinematic analysis was said to include the orientation of the planes of weakness relative to that of the excavation face. The results can be used to determine the possible direction of movement of the failing mass but ignored factors like water pressure, weight of sliding mass and *in situ* stresses. Limit equilibrium considers structurally driven instabilities based on FOS taking into account weight of the sliding mass, cohesion and friction angle of sliding planes

as well as forces normal to the sliding planes but does not consider *in situ* stresses. Numerical modelling considers *in situ* stresses, water pressure and/or discontinuities.

3.4.1 Empirical slope stability analysis and design

Standard charts as well as Laubscher's MRMR system were used to analyse the stability of the current and proposed slope designs. This was done to check if there is any agreement with the computer based analysis methods.

Circular failure charts

The circular failure charts (Stacey & Swart, 2001), were designed for soil slopes so the first 25 m of the slope height located in weathered rock were analysed using this technique. The unit weight, (γ), (kN/m^3); friction angle, (ϕ), (degrees) and cohesion, (*c)*, (kPa) are provided in Table 3-9. The values corresponding to a GSI of 29 were used in order to cover the worst case scenario. The ground water conditions were assumed to be partially saturated. This was considered a close estimate since water inflow into the pit from the rock mass was very little almost zero. So this assumption will suffice even during the rainy season. The value of $c/\gamma H.\tan\phi$ was then calculated and found to be 0.64. This value and the chart corresponding to the partially saturated ground water conditions were then used to determine the value of $\tan\phi/F$ from which the factor of safety (F) was determined. An illustration of how the chart was used is shown in Figure 3-22, and the $\tan\phi/F$ value was estimated to be 0.23. The weathered zone overall slope angle of 60.4^o used in the illustration was calculated using optimized design OD2. The corresponding factor of safety was calculated to be 1.32. A summary of results from circular failure charts analysis is presented in Table 4-1, chapter 4.

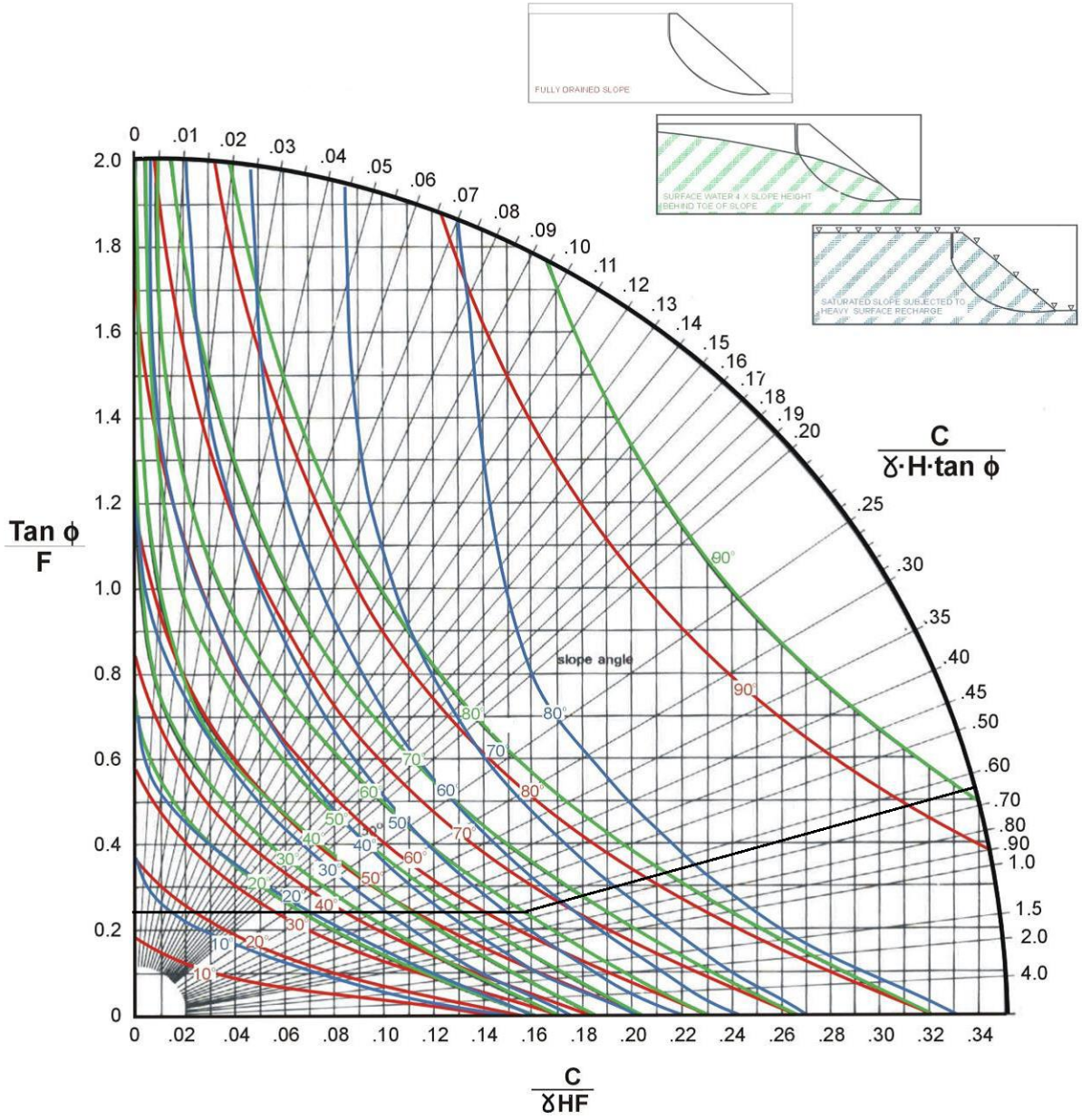


Figure 3-22 Determination of the value of $\tan\phi/F$ for a 60.4 º slope in weathered rock

Mining rock mass rating (MRMR) system

The intact rock strength was taken as 91 MPa for fresh rock as shown in Table 3-10, (Bosman, 2013). The RMR value was adjusted to take into consideration the effects of weathering, joint orientation and blasting to give the MRMR value. Weathering adjustment indicates the extent of weathering of the rock mass over time. The joint orientation adjustment depends on the orientation of the joints with respect to the vertical axis of the block (Stacey & Swart, 2001). The quality of blasting has an influence on the fracturing and loosening of the rock mass. All the above factors were used to adjust the RMR values. The MRMR of the rock mass was taken as the average of all the drill holes provided in Table 3-12. The MRMR value was subsequently plotted on the Haines and Terbrugge slope design chart (Lotheringen, et al., 2016), (Figure 3-23) to determine the overall slope angle that will give a factor of safety equal to 1.5. The red line shows the overall slope angle in the fresh rock to be 54 ^{o} at a FOS of 1.2, and 44 ^{o} for a FOS of 1.5. However, the graph results suggest that additional analysis is needed, which was done using numerical models. A summary of results from MRMR and Haines and Terbrugge charts analysis is presented in Table 4-2, chapter 4.

Table 3-12 Average MRMR value for fresh rock

HOLE ID	RMR	CUMULATIVE ADJUSTMENTS	MRMR
PE03DDGC8_01	71.49	Weathering 96%	51.61
PE03DDGC8_02	71.64		51.72
PE03DDGC8_03	71.83		51.86
PE03DDGC8_04	71.46	Joint orientation 80%	51.59
PE03DDGT_01	71.58		51.68
PE03DDGT_03	72.55		52.38
PE03DDGT_06	71.64	Blasting 94%	51.72
			Average: 51.79

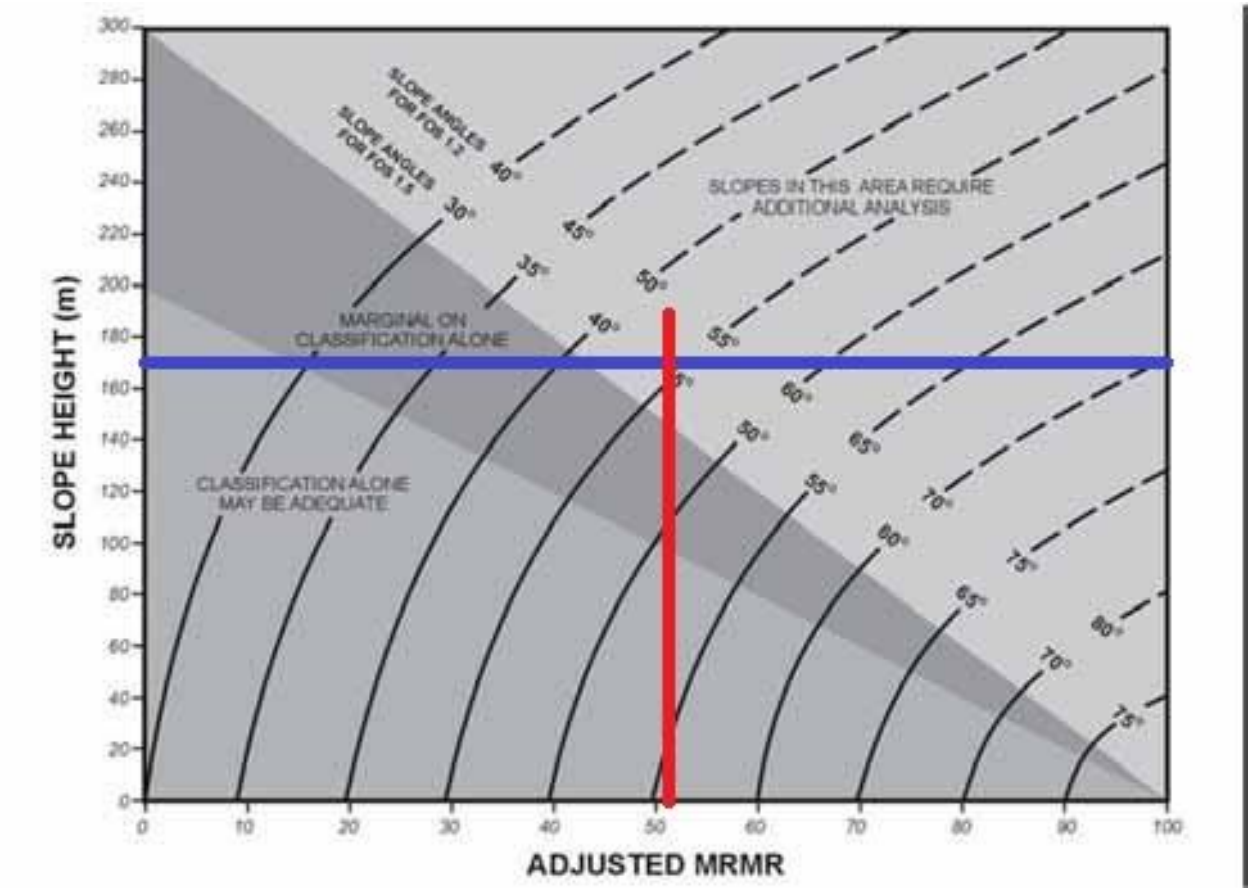


Figure 3-23 Haines and Terbrugge design chart for overall stope angles

3.4.2 Kinematic analysis

Kinematic analysis using stereonet plots was carried out to determine the possibility of structurally driven instabilities which are planar, wedge and toppling failures. Analysis was done at bench, inter-ramp and overall pit slope scales. Based on the fact that the Peerless ore body strikes east-west, the pit slopes were assumed to be predominantly having the same strike orientation as the ore body with the northern slope dipping to the south and the southern slope dipping to the north. No tests were done to determine friction angle; 30 ^{o} was then assumed as it is usually around this value in most cases. Rocscience DIPS software (Rocscience, 2010), was used to perform the kinematic analysis.

The structural data gathered through oriented core logging and face mapping was used to determine the major joint sets for the two design sectors. The data was processed in DIPS using lower hemispherical stereonet projections. Joint sets were defined from Fischer concentration contours of poles. The mean of the defined joint sets for the two design sectors is shown in Figure 3-24 and Figure 3-25 as well as Table 3-13 and Table 3-14 for the southern and northern walls, respectively.

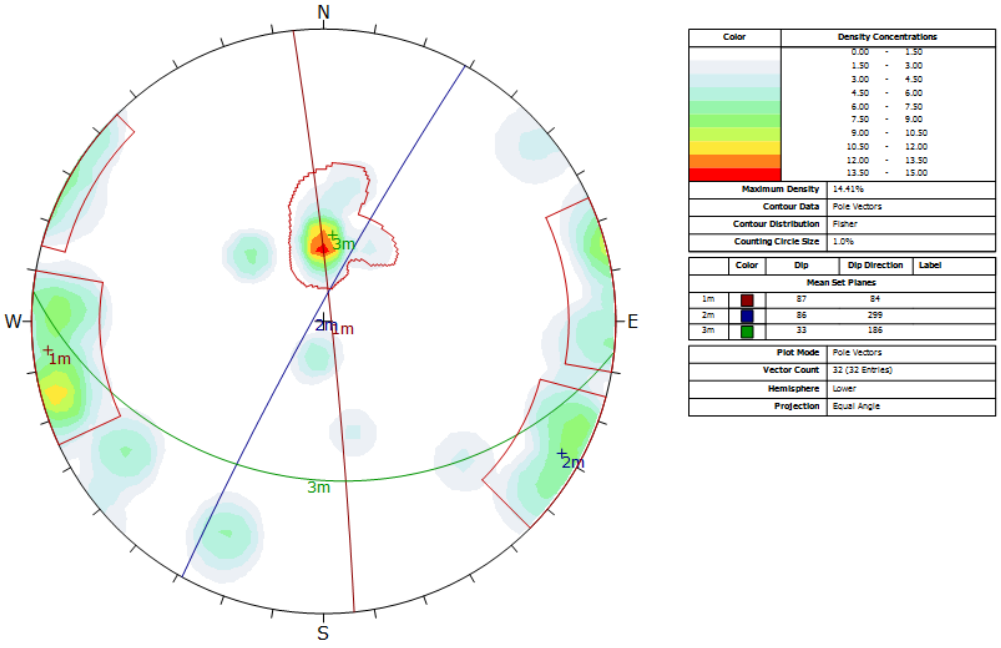


Figure 3-24 Mean joint sets for PE03 southern wall.

Table 3-13 Mean joint sets for PE03 southern wall.

Joint set	Dip	Dip Direction
J1	87	84
J2	86	299
J3	33	186

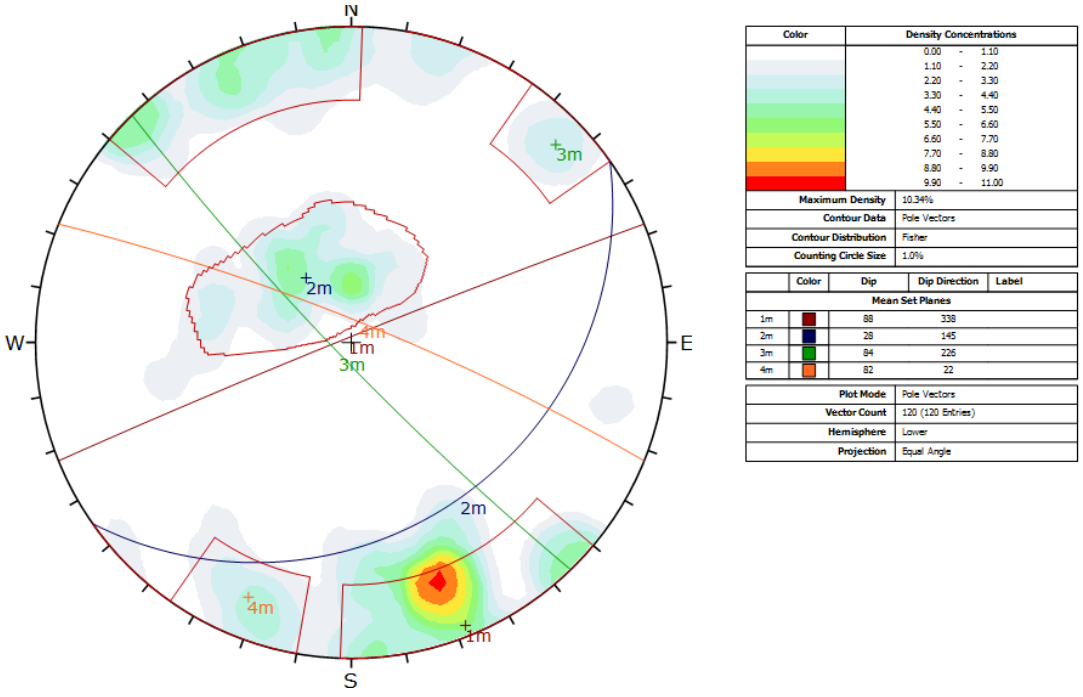


Figure 3-25 Mean joint sets for PE03 northern wall.

Table 3-14 Mean joint sets for PE03 northern wall.

Joint set	Dip	Dip Direction
J1	88	338
J2	28	145
J3	84	226
J4	82	22

3.4.2.1 Planar failure analysis

The analysis for planar failure was conducted using the:

- Daylight envelope
- Pole friction cone, and
- Lateral limits, equal to slope dip direction plus or minus 20^{o}

The stereonet analysis tests the combined effects of frictional and kinematic instabilities of planes. Any block on a plane with its pole located inside the daylight envelope, the lateral limits and outside the pole friction cone is capable of sliding down the slope. The planar failure analysis of the southern wall, at the final pit slope angle of 52 ^{o}, is shown in Figure 3-26. Any block on a plane whose pole falls within the planar failure zone has a potential for failure, if kinematically possible. A summary of results from planar failure analysis is presented in Table 4-3 to Table 4-5, chapter 4.

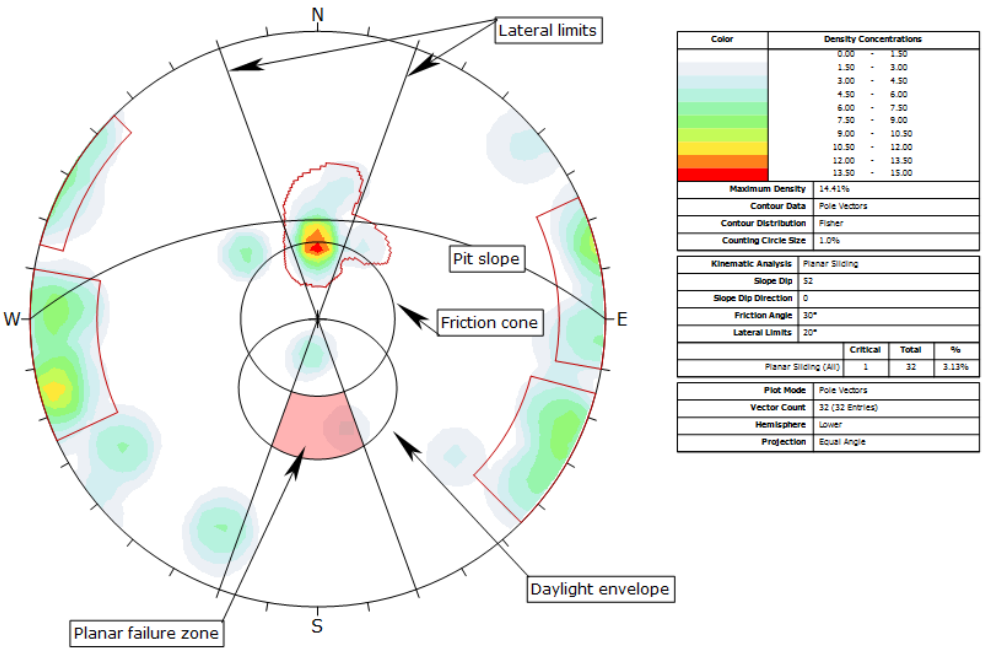


Figure 3-26 Planar failure for PE03 Southern Wall at 52º final pit slope angle.

3.4.3 Wedge failure analysis

Wedge failure analysis was carried out using the:

- Plane friction cone, and
- Slope plane

With the plane friction cone, dip vectors are used and the angle of friction is measured from the circumference of the stereonet. All dip vectors located inside the friction cone represent blocks separated by discontinuities which dip steeper than the friction angle, and these blocks are unstable, if kinematically possible. The arc defined by the intersection between the plane friction cone and the slope plane describes the wedge failure zone (Figure 3-27). The great circles of any two mean joint sets intersecting inside

this zone indicates an unstable wedge which can slide down the slope. Wedge failure analysis of the southern wall (52º) is shown in Figure 3-27. A summary of results from wedge failure analysis is presented in Table 4-3 to Table 4-5, chapter 4.

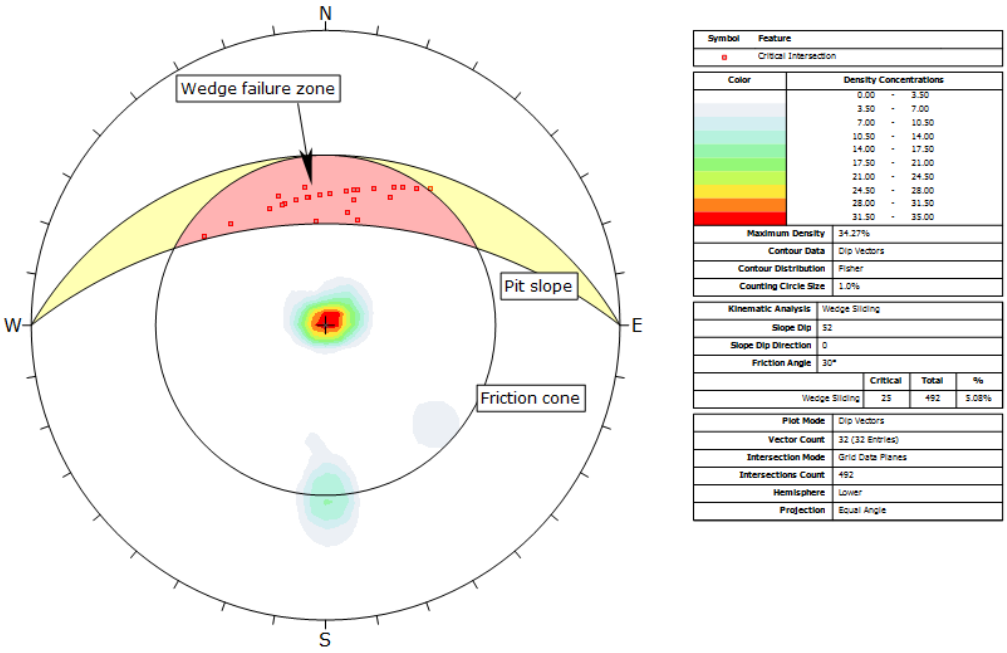


Figure 3-27 Wedge failure for PE03 Southern Wall at 52º final pit slope angle.

3.4.3.1 Toppling failure analysis

The toppling failure analysis was carried out using the:

- Slip limit plane, the dip of this plane was determined by finding the difference between the slope angle and the friction angle and the dip direction was the same as that of the slope.
- Lateral limits, equal to, slope dip direction plus or minus 20º

Any block on a plane with its pole located outside the slip limit plane but inside the lateral limits have the potential of toppling off the slope. Toppling failure analysis of the southern slope is shown in Figure 3-28. A summary of results from toppling failure analysis is presented in Table 4-3 to Table 4-5, chapter 4.

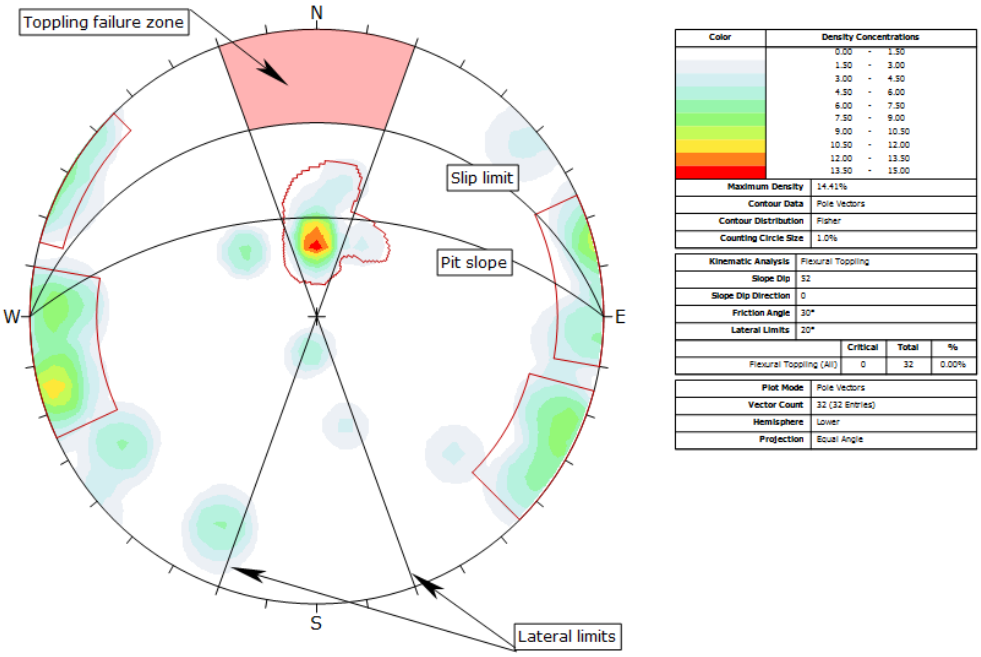


Figure 3-28 Toppling failure for PE03 Southern Wall at 52º final pit slope angle.

The stereonets showing the kinematic analysis of the current design and its optimized derivative designs are provided in the appendices Figure D-1 to Figure D-45.

3.4.4 Limit equilibrium analysis

The analysis was carried out using SLIDE (Rocscience, 2018), geotechnical software which employs Limit Equilibrium approach to analyse slope stability. The software is a 2D program used to determine the factor of safety for both circular and non-circular failure

surfaces in soil and rock slopes (Rocscience, 2018). A simple model was created which represented the geology by two zones, the weathered and the fresh rock zones. The geology was similar around the pit. The length to width ratio of the pit is about 5: 1 as the strike length of the pit is about 1 km with a width of about 210 m. This made the use of a 2D analysis program applicable. The factor of safety for circular failure surfaces were determined for various design scenarios. Only the factor of safety for the critical slip surface, i.e. the failure surface with the lowest factor of safety is documented in this report. A probabilistic analysis was also conducted to determine the Probability of Failure (PoF). The analysis was conducted on the overall slope angle and the critical slip surface was determined using the grid method. When the external boundaries were created slope limits indicated by triangular markers at the top of the vertical edges of the model were automatically calculated. The grid method was used to set a grid of circular slip centres, each slip centre was used to create a number of slip surfaces and for each slip surface to be valid its start and end points had to cut the excavation surface within the slope limits. For each slip centre the minimum and maximum radii was automatically determined based on the minimum and maximum distances from the slip centre to the slope surface. The radius increment was used to determine the number of slip surfaces between the minimum and maximum radii for each slip centre, (Figure 3-29).

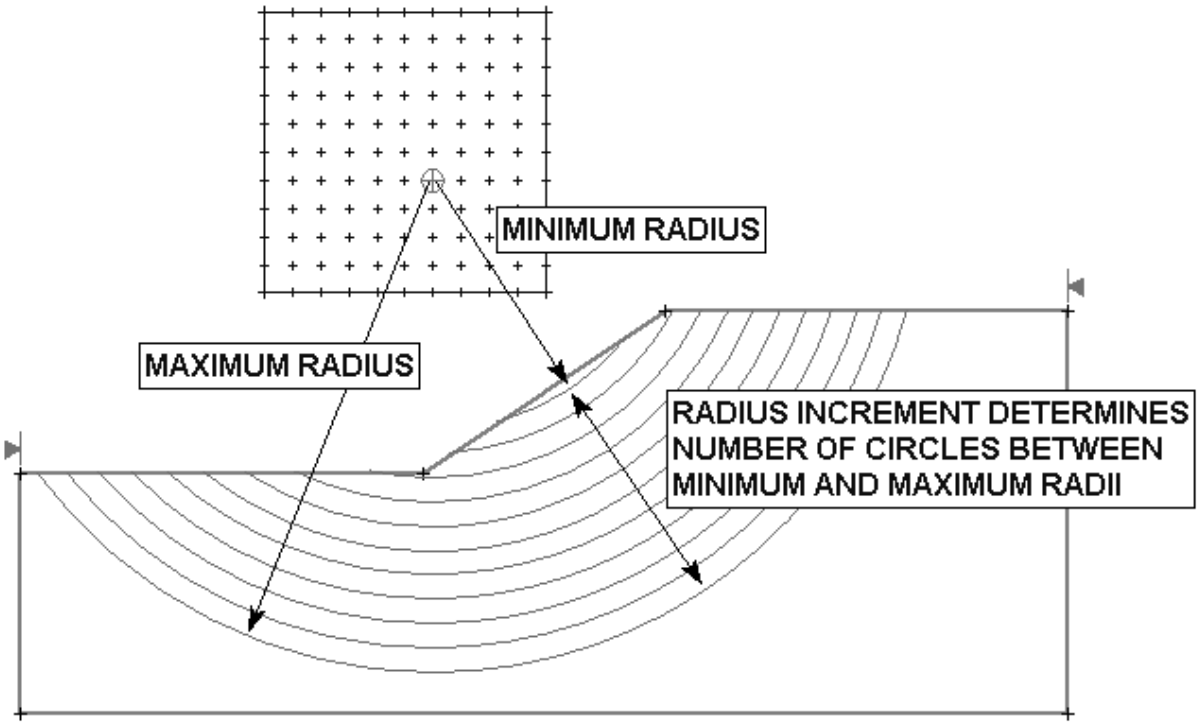


Figure 3-29 Location of the slip surfaces using the grid search method. (Rocscience, 2018)

The slip surface with the minimum Factor of Safety was the critical slip surface. This surface was determined using the Bishop simplified method of slices. The method assumes a circular slide surface and that the side forces are horizontal, the analysis satisfies vertical forces and overall moment equilibrium, (Wyllie & Mah, 2004). Two geotechnical domains were defined during the core logging exercise, i.e. the weathered and fresh rock zones. The water table was found to be 35 m below the ground surface and the contact between weathered and fresh rock was about 25 m. An example of the model geometry used to analyse the different design scenarios is shown in Figure 3-30. A summary of results from Limit Equilibrium analysis is presented in Table 4-6, chapter 4.

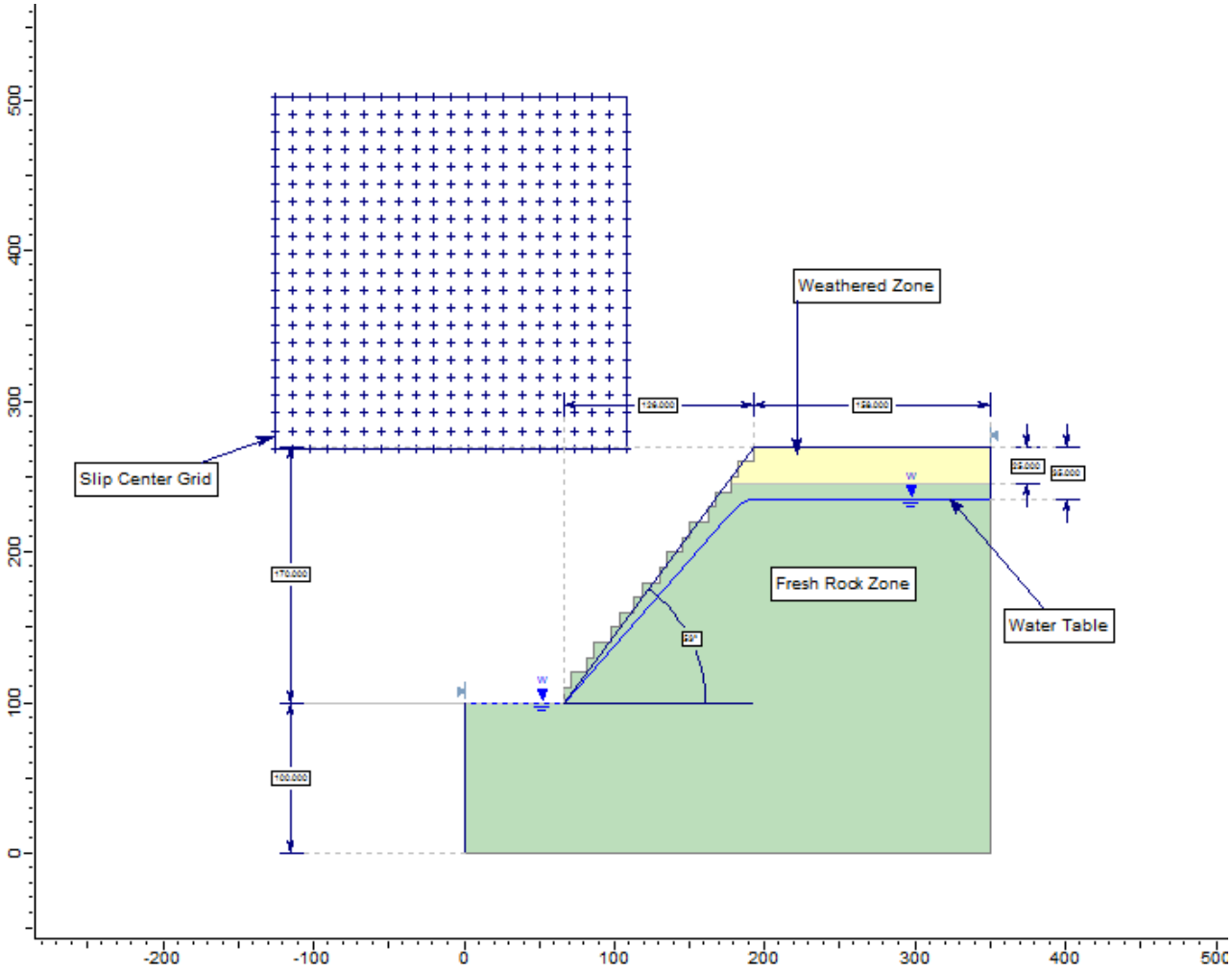


Figure 3-30 Model for overall slope with 90º bench slopes and alternating 10 m and 5 m berms.

3.4.5 Numerical analysis

Phase 2D was used to carry out the slope stability analysis. The computer program is two dimensional, finite element software (Rocscience, 2001). A two dimensional analysis was sufficient for the study as the pit displays a geometry with a long dimension along strike which supports plane strain conditions. Plane strain assumes that the slope face is

infinitely long and strain only occurs in two directions and it is zero in the third direction. Real as well as artificial boundaries were used in creating the model. Real boundaries were those that corresponded to the excavated slope surfaces. The artificial boundaries were used to indicate the vertical edges on the right and left side as well as the base of the model. Artificial boundaries were located as per recommendations by Wyllie & Mah (2004), as shown in Figure 3-31.

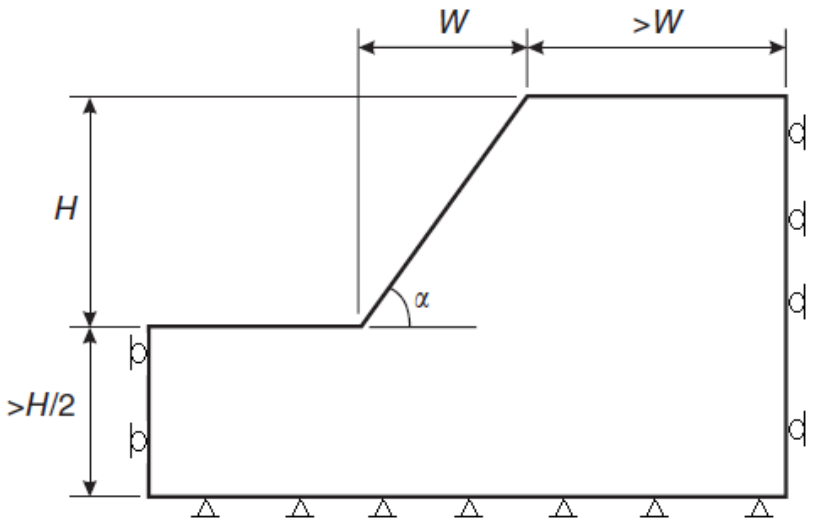


Figure 3-31 Typical recommendations for locations of artificial far-field boundaries in slope stability analyses. (Wyllie & Mah, 2004)

An example of the model geometry and finite element grid is shown in Figure 3-32. The right and the left edges of the model were fixed in the horizontal direction and free to move in the vertical direction, indicated by rollers on the model. The base of the model was fixed in both the horizontal and vertical directions, indicated by fixed points (triangular pin symbols) on the model, to prevent rotation of the model. Models were simulated with the water table located at 35 m below surface and the boundary between the weathered and fresh rock located at 25 m below surface. The overall depth was taken to be 170 m.

The mechanical properties from Table 3-9 and Table 3-10, were used as input parameters, and a summary of relevant parameters is provided in

Table 3-15. The gravity field stress was used for the *in situ* stress conditions. The vertical stress component at any point in the model was calculated from the product of the distance to surface elevation (metres) and the unit weight (MN/m^3) of the overburden. The horizontal stress components were calculated based on the vertical stress component at that point and the *K-ratio* (Horizontal/Vertical stress ratio). At shallow to moderate depth, between 0 m and 1000 m, *K-ratio* is said to range between 0.3 and 3.5 (Wagner, 2019). The value tends to be greater near the surface. The southern African mining industry normally employs a *K-ratio* equal to one or more (Handley, 2013). In this case it was assumed to be unity, the same as the one used by nearby mines. The Mohr Coulomb failure criterion was used; material type was taken as plastic and volume increase of material after shearing (dilation) was considered to be zero. The Factor of Safety was determined using the Shear Strength Reduction Factor method. The method involves the stepwise reduction of the mean shear strength of the material and this is automatically done by the software. Rocscience (2001), indicated that the Factor of Safety is the ratio of the original shear strength to the reduced shear strength, at the point where the model does not reach a state of mathematical equilibrium. A summary of results from numerical analysis is presented in Table 4-7, chapter 4.

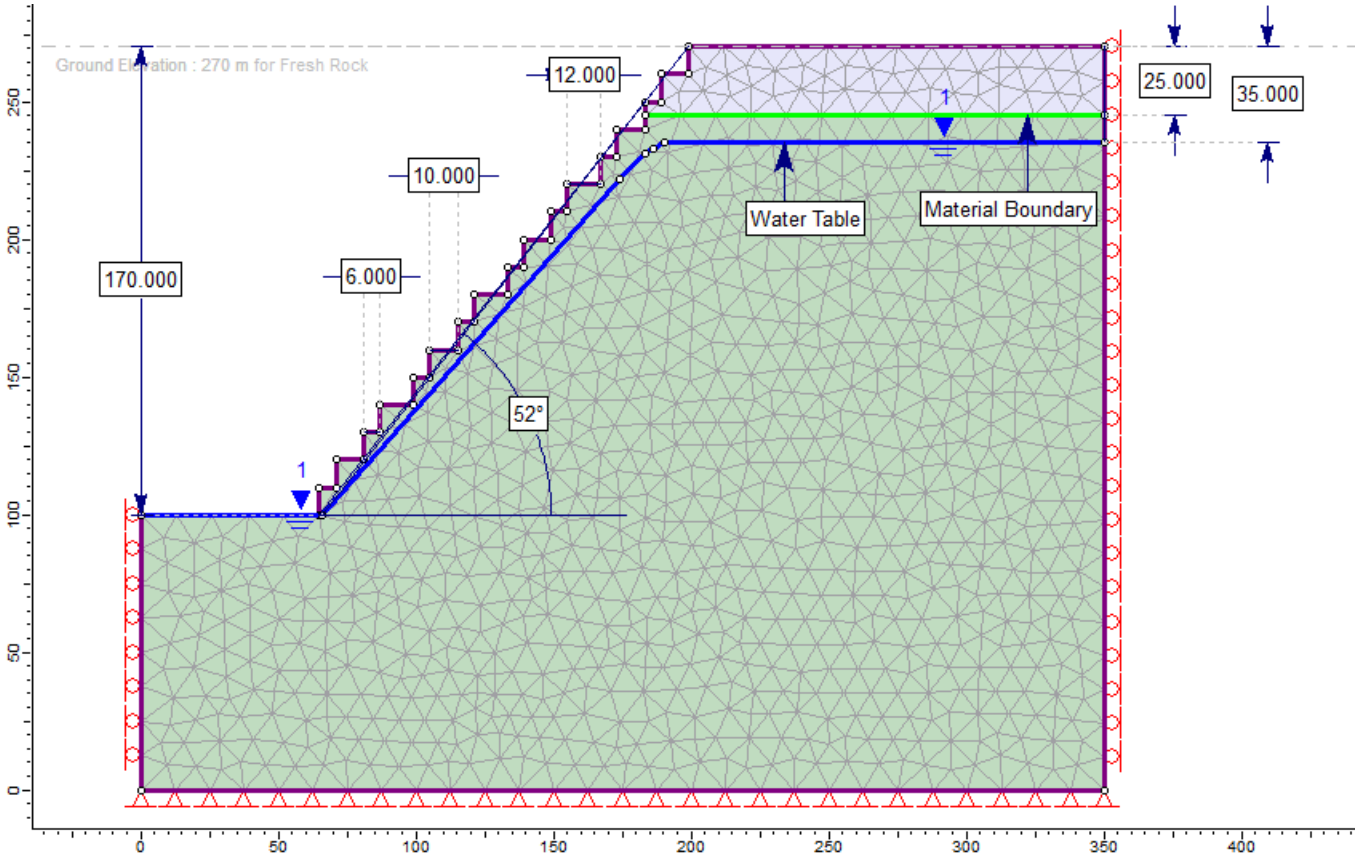


Figure 3-32 Finite element model for a slope with alternating 10 m and 6 m benches at 90º bench slope angle and 51.75º overall slope angle.

Table 3-15 Mechanical properties used as model input parameters.

Material type	**Unit weight (MN/m^3)**	**Young's Modulus (MPa)**	**Poisson's Ratio**	**Tensile strength (MPa)**	**Friction Angle (peak) (deg)**	**Friction Angle (residual) (deg)**	**Cohesion (peak) (MPa)**	**Cohesion (residual) (MPa)**
Weathered Rock	0.026	18100	0.21	0.047	27.26	16.91	0.279	0.127
Fresh Rock	0.027	43420	0.21	1.639	30.12	28.10	1.597	1.086

4. RESULTS AND ANALYSIS

4.1 Introduction

This chapter presents and analyses the results, which were obtained from the methods that were discussed in chapter 3.

4.1.1 Circular charts analysis results

A summary of results from circular charts analysis of slopes in weathered rock are shown in Table 4-1. The results indicated stable conditions for all slope angles analysed.

Table 4-1 circular charts analysis results summary.

Designs	Current	OD1	OD2	OD3	OD4	OD5
$c/\gamma H.\tan\phi$	0.64					
Overall slope angle, weathered portion	47 ^{o}	59 ^{o}	60.4 ^{o}	63 ^{o}	64 ^{o}	65 ^{o}
$\tan\phi/F$	0.20	0.22	0.23	0.24	0.25	0.26
Factor of Safety (F)	1.5	1.38	1.32	1.27	1.22	1.17

4.1.2 Mining rock mass rating (MRMR) system analysis results

A summary of results from MRMR and Haines and Terbrugge design chart analysis are shown in .

Table 4-2.

Table 4-2 MRMR and Haines and Terbrugge design chart analysis results summary

ROCK	MRMR	FACTOR OF SAFETY	OVERALL SLOPE ANGLE
Fresh	51.79	1.2	54 º
Fresh	51.79	1.5	44 º

The Haines and Terbrugge design chart estimated overall slope angle of 54 ° and 44 º for fresh rock for a factor of safety (FoS) of 1.2 and 1.5 respectively.

4.1.3 Kinematic analysis results

A summary of the results from the kinematic analysis is shown in Table 4-3 to Table 4-5. The percentages indicate the probability of experiencing the failure mode in question.

Table 4-3 Kinematic analysis at bench slope scale.

		PE03 Southern Wall					PE03 Northern Wall				
Bench Slope Angle		85^o	87^o	88^o	89^o	90^o	85^o	87^o	88^o	89^o	90^o
Friction Angle	**Failure Mode**										
30^o	**Planar (All)**	3.13%	3.13%	3.13%	3.13%	3.13%	9.17%	10.83%	12.50%	13.33%	14.17%
	Planar (critical Set)	0.00%	0.00%	0.00%	0.00%	0.00%	13.95%	13.95%	13.95%	13.95%	20.59%
	Wedge (All)	26.63%	27.85%	28.25%	28.86%	29.67%	22.18%	24.92%	26.27%	27.49%	28.39%
	Wedge (critical Set)	0.00%	0.00%	0.00%	0.00%	0.00%	0.00%	0.00%	0.00%	0.00%	0.00%
	Toppling (All)	6.25%	6.25%	6.25%	6.25%	15.63%	19.17%	19.17%	19.17%	19.17%	19.17%
	Toppling (critical Set)	25.00%	25.00%	25.00%	25.00%	62.50%	37.50%	37.50%	37.50%	37.50%	37.50%

Table 4-4 Kinematic analysis at Inter-ramp slope scale.

		PE03 Southern Wall					PE03 Northern Wall				
Material Type		**Weathered and Fresh Rock**									
Inter-ramp Slope Angle		61º	63º	64º	65º	67º	61º	63º	64º	65º	67º
Friction Angle	**Failure Mode**										
30º	**Planar (All)**	3.13%	3.13%	3.13%	3.13%	3.13%	5.00%	5.00%	5.00%	5.00%	5.00%
	Planar (critical Set)	0.00%	0.00%	0.00%	0.00%	0.00%	13.95%	13.95%	13.95%	13.95%	13.95%
	Wedge (All)	7.93%	8.33%	8.54%	9.35%	10.37%	10.73%	11.29%	11.67%	11.93%	13.40%
	Wedge (critical Set)	0.00%	0.00%	0.00%	0.00%	0.00%	0.00%	0.00%	0.00%	0.00%	0.00%
	Toppling (All)	0.00%	0.00%	0.00%	0.00%	0.00%	18.33%	19.17%	19.17%	19.17%	19.17%
	Toppling (critical Sets)	0.00%	0.00%	0.00%	0.00%	0.00%	37.50%	37.50%	37.50%	37.50%	37.50%

Table 4-5 Kinematic analysis at Overall Pit slope scale.

		PE03 Southern Wall					PE03 Northern Wall				
Material Type		**Weathered and Fresh Rock**									
Overall pit Slope Angle		52°	54°	55°	56°	57°	52°	54°	55°	56°	57°
Friction Angle	**Failure Mode**										
30°	**Planar (All)**	3.13%	3.13%	3.13%	3.13%	3.13%	5.00%	5.00%	5.00%	5.00%	5.00%
	Planar (critical Set)	0.00%	0.00%	0.00%	0.00%	0.00%	13.95%	13.95%	13.95%	13.95%	13.95%
	Wedge (All)	5.08%	5.69%	6.10%	6.10%	6.71%	8.03%	8.68%	8.93%	9.25%	9.62%
	Wedge (critical Set)	0.00%	0.00%	0.00%	0.00%	0.00%	0.00%	0.00%	0.00%	0.00%	0.00%
	Toppling (All)	0.00%	0.00%	0.00%	0.00%	0.00%	16.67%	18.33%	18.33%	18.33%	18.33%
	Toppling (critical Sets)	0.00%	0.00%	0.00%	0.00%	0.00%	37.50%	37.50%	37.50%	37.50%	37.50%

The results are presented as percentages indicating the proportion of measured discontinuities with the potential of failing. The percentages are calculated for all discontinuities recorded as well as for individual sets. From the kinematic analysis shown in Table 4-5, it was seen that the pit slopes generally have a similar or gently increasing risk for each of the given slope angles in each failure mode. Toppling failures have the highest chances of occurring at 37.50% for joint set 4 on the northern wall, and do not change with slope angle. At bench scale level, where slopes are steeper, the likelihood of wedge and toppling failure was shown to be high (Table 4-3), but generally constant with slope angle increase. However, the risk of failure did gently increase with slope angle in some failure modes, and a few significant increases were also shown. These increases in risk have been highlighted in the table.

4.1.4 Limit equilibrium analysis results

A limit equilibrium model for the current northern and southern walls is shown in Figure 4-1. Similar models were done for two of the optimized designs and are shown in Figure 4-2 and Figure 4-3. The Factor of Safety (FoS) and Probability of Failure (PoF) determined from these models are provided in the figures. The analysis does not consider the discontinuities, but rather the possibilities of circular failure through the rock mass as a result of the overall slope angles.

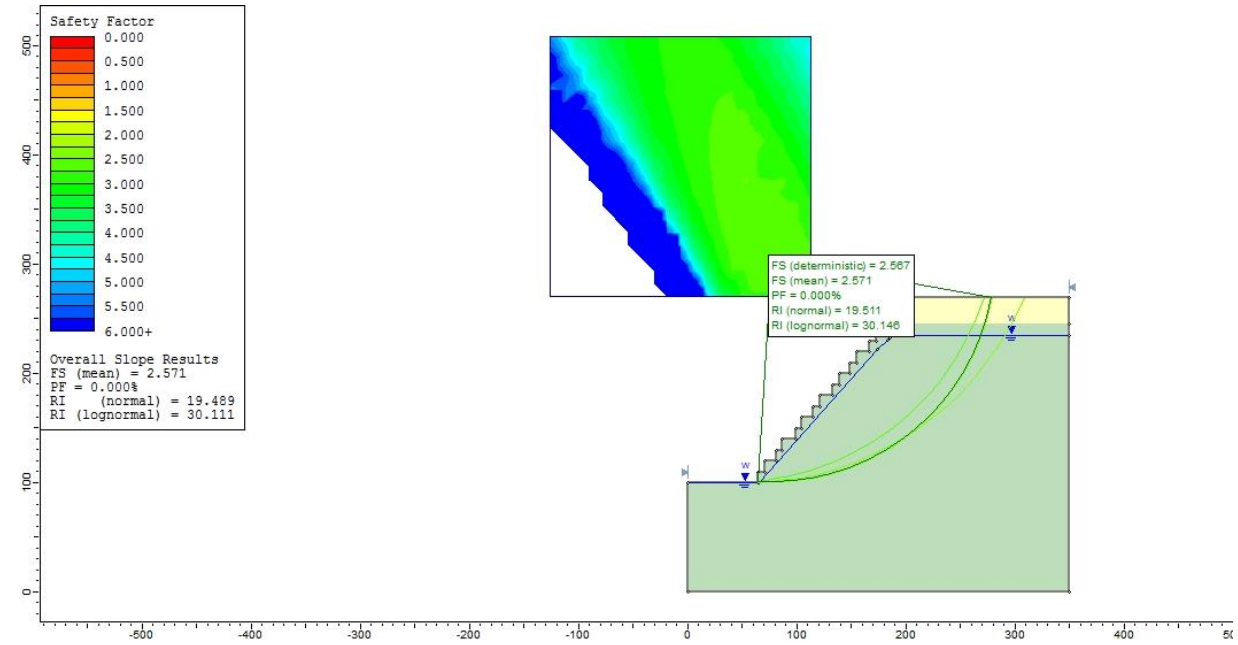


Figure 4-1 Limit equilibrium analysis results for a slope with alternating 10 m and 6 m benches at 90 º bench slope angle and 52 º overall slope angle (Current design).

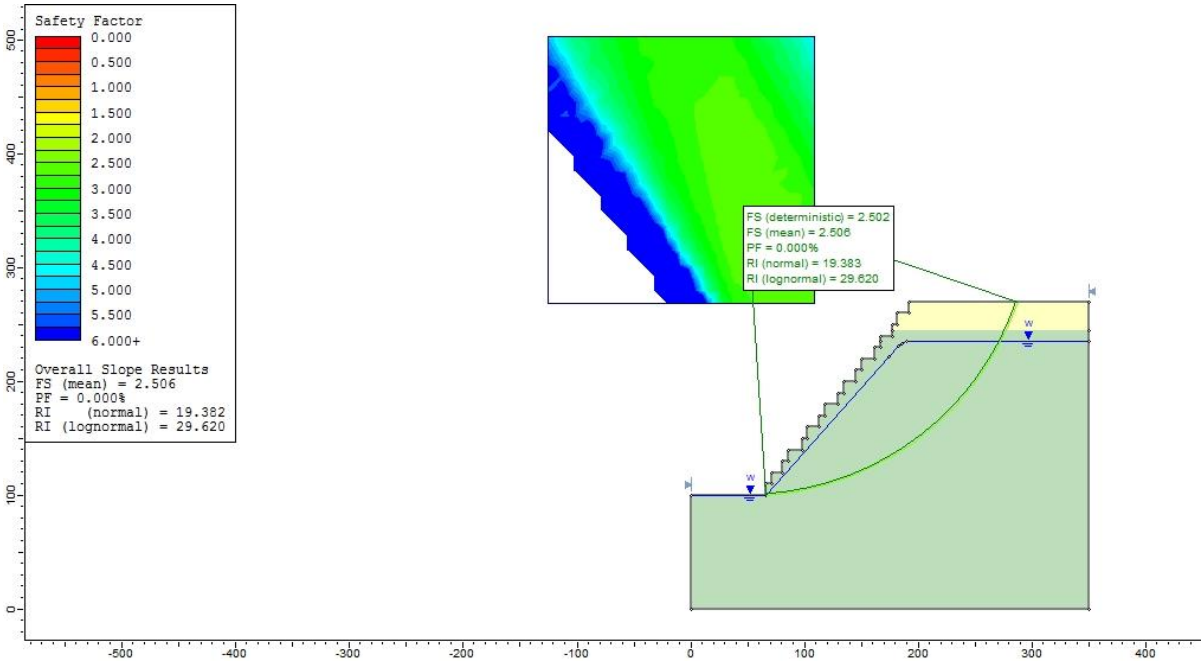


Figure 4-2 Limit equilibrium analysis results for a slope with alternating 10 m and 5 m benches at 90 º bench slope angle and 54 º overall slope angle (OD1).

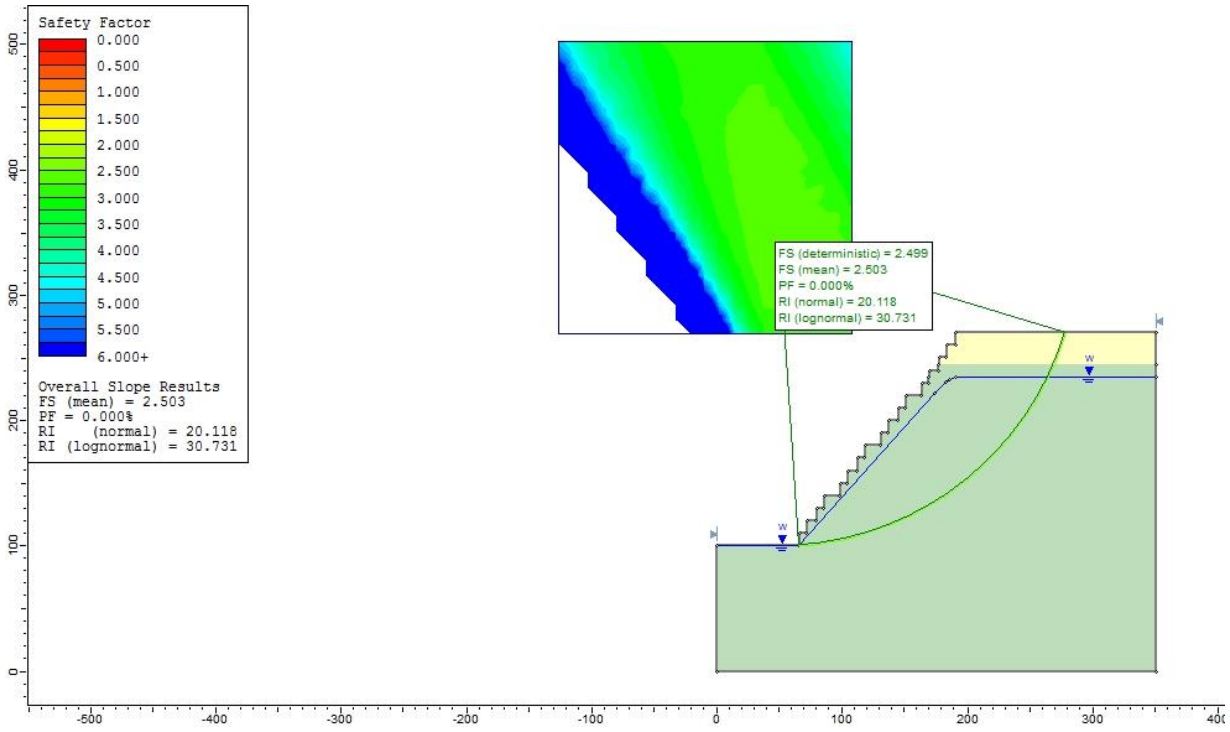


Figure 4-3 Limit equilibrium analysis results for a slope with alternating 7 m and 5 m benches at 85º bench slope angle and 54º overall slope angle (OD5).

The deterministic safety factor is described as the Factor of Safety for the Global Minimum slip surface determined using mean values of the input parameters. The Mean Safety Factor is described as the average of all factors of safety calculated for the overall slope and is determined from the probabilistic analysis (Rocscience, 2018).

A summary of the results from limit equilibrium analysis is shown in Table 4-6. The summary includes the results of the current design and all its derivatives created during the optimization process.

Table 4-6 Limit equilibrium analysis results summary.

Design	Bench Slope Angle	Overall Pit Slope Angle	FoS (mean)	PoF
Current	90º	52º	2.571	0.000%
OD1	90º	54º	2.506	0.000%
OD2	85º	54º	2.503	0.000%
OD3	87º	55º	2.482	0.000%
OD4	88º	56º	2.464	0.000%
OD5	89º	57º	2.431	0.000%

The limit equilibrium analyses for OD4 shows that the design is stable, as the distribution of FOS values (Figure 4-4) is greater than unity. Thus the POF value is equal to zero. Figure 4-4 shows the FoS distribution for OD4. The ratio between the total number of samples with FoS less than unity to the total number of samples used gives the PoF for the slope. The curve indicates that all the samples have Factors of safety above one therefore the probability of failure for this design is zero. The same applies to all the other designs. Therefore, the risk of global or large scale slope failures is very small.

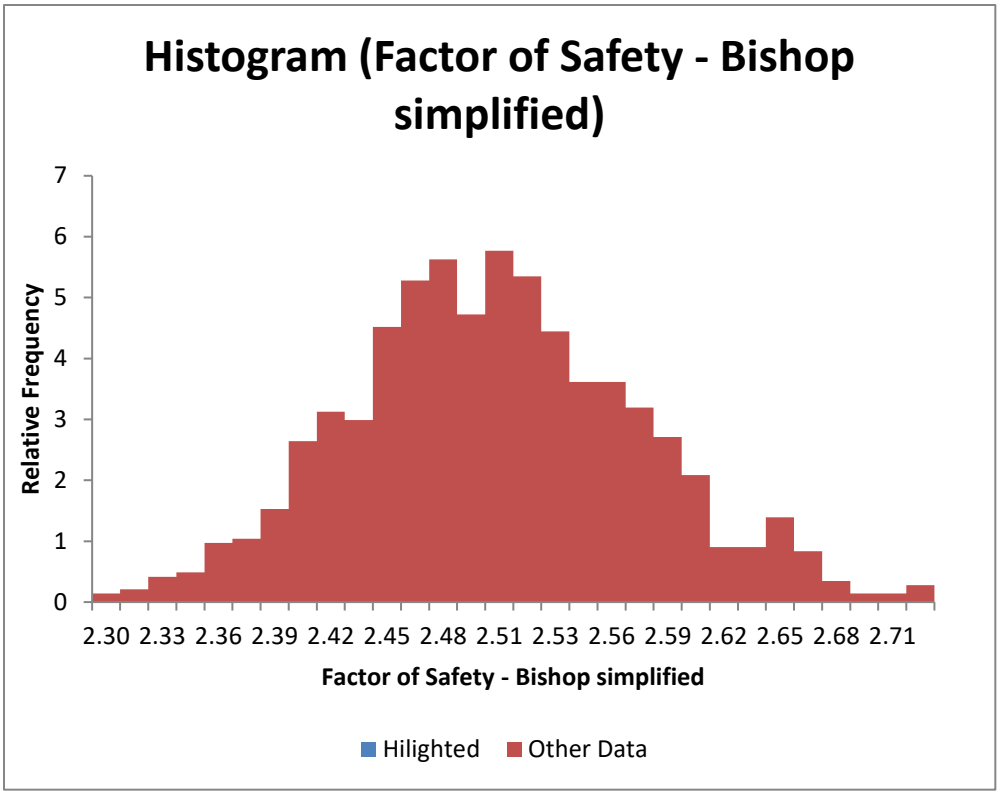


Figure 4-4 Factor of safety (FoS), Relative Frequency curve for OD4.

4.1.5 Numerical analysis results

Finite element models with contours and vectors of displacement for both the northern and southern walls for the current design and two optimized designs are shown in Figure 4-5 to Figure 4-7. The Factor of Shear Strength Reduction Factor or Factor of Safety determined from these models is shown in the Figures.

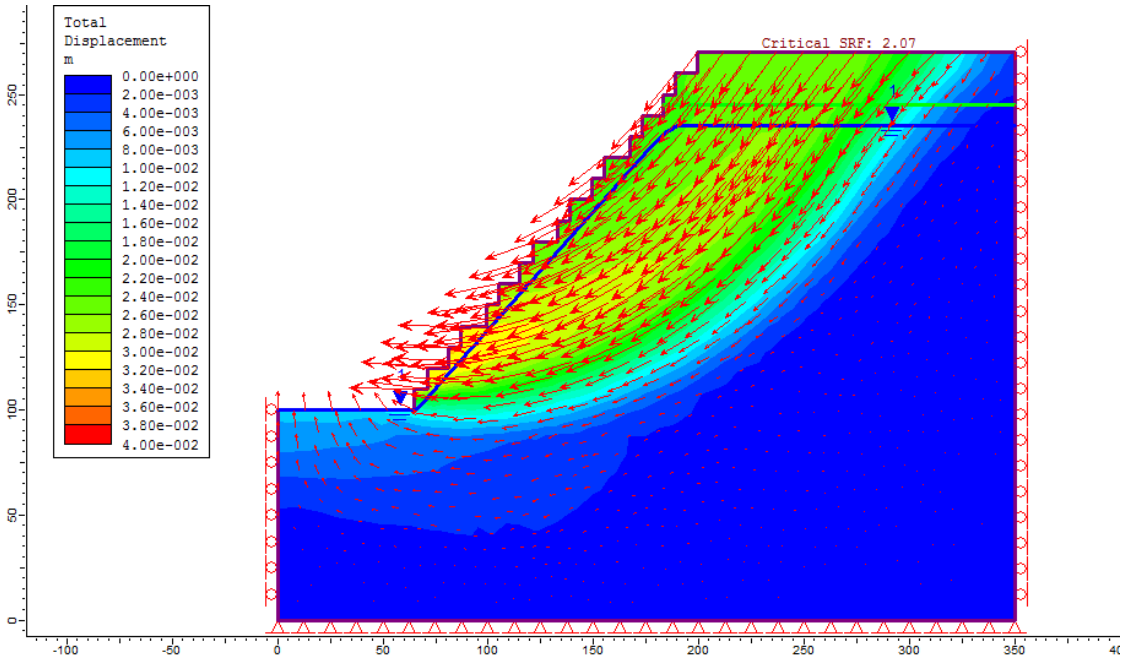


Figure 4-5 Finite element model for a slope with alternating 10 m and 6 m benches at 90 º bench slope angle and 52 º overall slope angle (Current design).

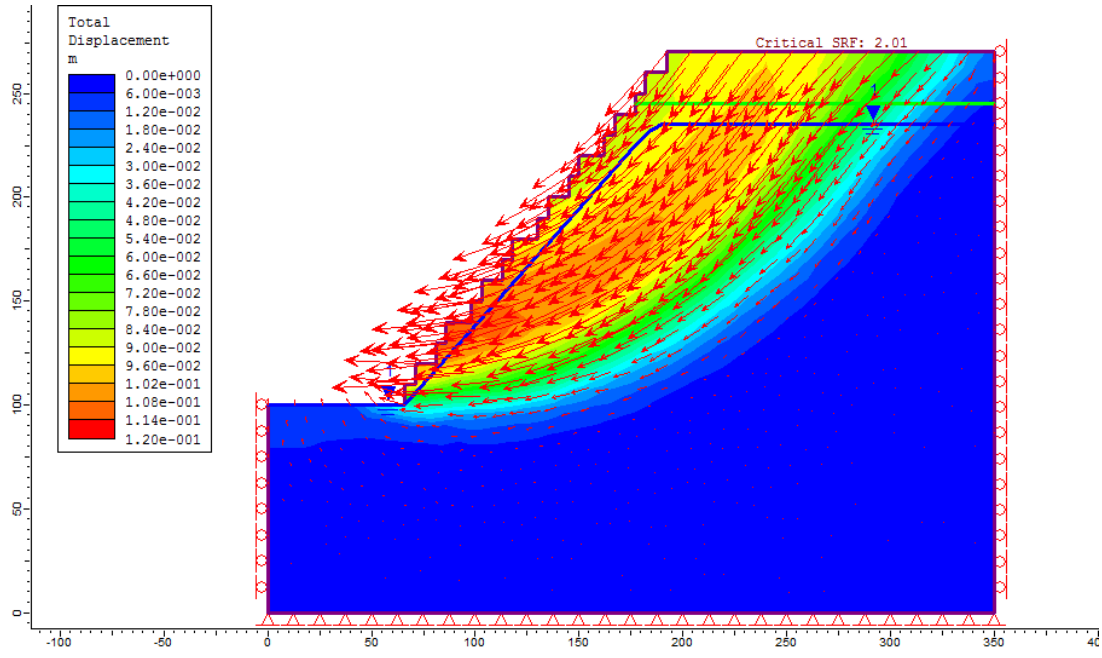


Figure 4-6 Finite element model for a slope with alternating 10 m and 5 m benches at 90 º bench slope angle and 54 º overall slope angle (OD1).

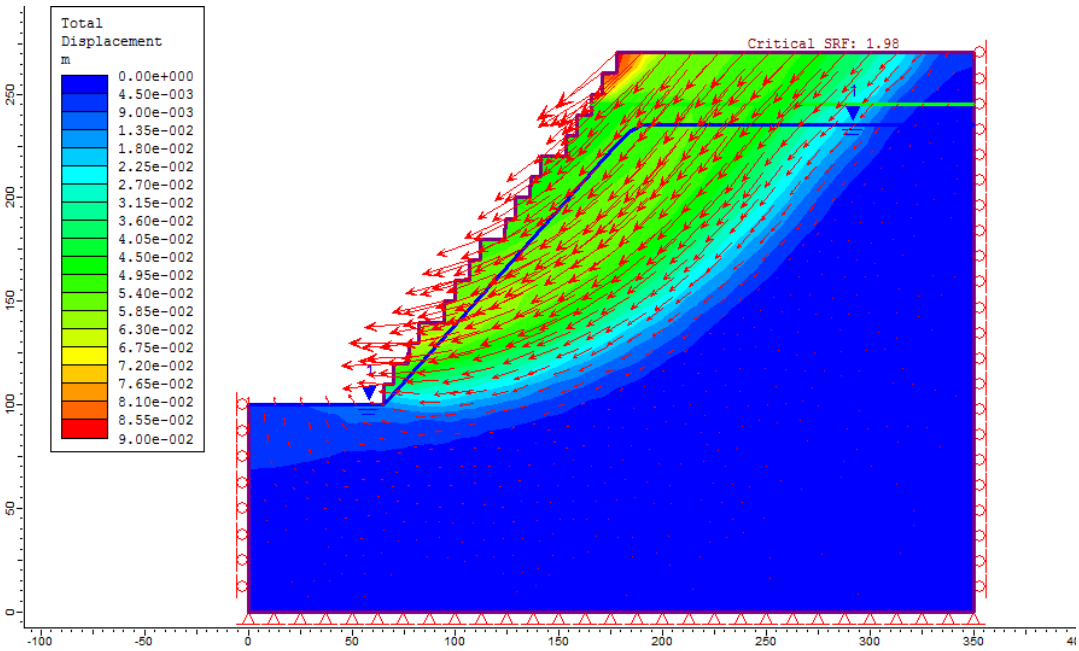


Figure 4-7 Finite element model for a slope with alternating 7 m and 5 m benches at 89 º bench slope angle and 57 º overall slope angle.

A summary of the results from numerical analysis is shown in Table 4-7.

Table 4-7 Finite element modelling results summary.

Design	Bench Slope Angle	Overall Pit Slope Angle	Critical SRF (FoS)
Current	90º	52 º	2.07
OD1	90º	54º	2.01
OD2	85º	54º	2.02
OD3	87º	55º	2.01
OD4	88º	56º	1.99
OD5	89º	57º	1.98

According to numerical analysis the factor of safety of all designs is double the required for stable conditions. The OD5 design is therefore the optimum design according to these analyses. However, in an effort to further improve safety it was decided to use different overall slope angles for the weathered and the fresh rock zones. A shallow overall slope angle was then used for the first three benches which are mainly in the weathered rock zone. The angle was determined by reducing the overall slope angle of 57º in increments of 2º until the SRF (FoS) of the overall pit slope was increased to two or slightly above two. This resulted in an overall pit slope of 53º with an SRF equal to 2.01 at the fifth iteration. The finite element model for this iteration is shown in Figure 4-8.

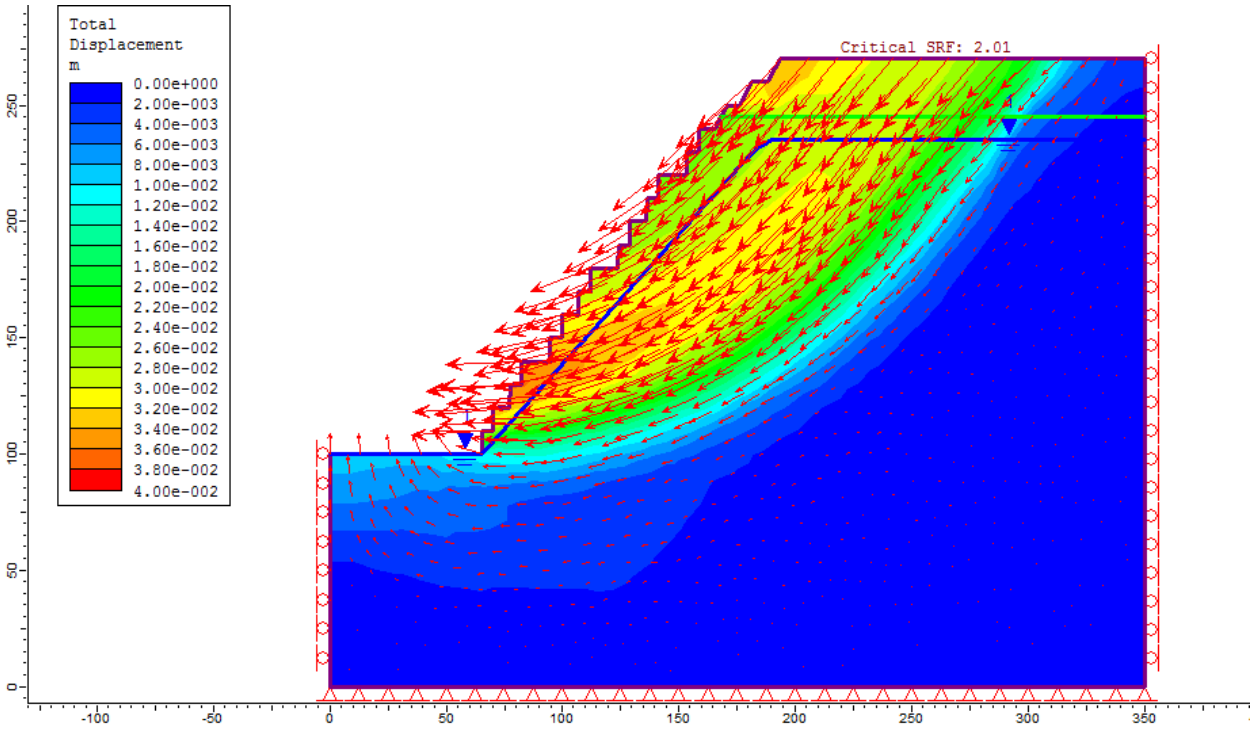


Figure 4-8 Finite element model for a slope with alternating 7 m and 5 m benches with different slope angles in weathered and fresh rock.

The Table 4-8 shows the geometrical parameters of this optimized design.

Table 4-8 Design parameters of the resultant optimum ultimate pit slope.

Design Zone	**Bench height**	**Bench slope angle**	**Bench width**	**Overall slope angle**	**Overall pit slope angle**
Weathered rock	10 m	62º	7 m and 5 m alternating	47º	53º
Fresh rock	10 m	89º	7 m and 5 m alternating	56º	

From kinematic results the 90^{o} bench slope angle of the current design proved to be riskier than the steepest bench slope angle of 89^{o} of the optimum ultimate pit slope. This is indicated by high chances of planar and toppling failure. On the northern side the percentage of discontinuities susceptible to planar failure for a 90^{o} bench slope angle is 20.59% compared with 13.95% for 89^{o} which is 6.64% higher. On the southern side for all discontinuities, the chances of toppling failure for 90^{o} is 15.63% while for 89^{o} it is 6.25% which is 9.38% higher. For the critical set chances of toppling failure for 90^{o} is 62.50% while for 89^{o} it is 25% which is 37.5% higher. Thus the optimum bench slopes are more stable than the current bench slopes. The kinematic analysis results for the inter-ramp and the overall slopes were not much different. The numerical modelling results also indicated stable conditions for the optimum ultimate pit slope. Thus, the 1^{o} steeper overall bench slope is possible with these bench slope requirements as indicated by the stability analyses results The geometry of this optimized overall slope is shown in Figure 4-9.

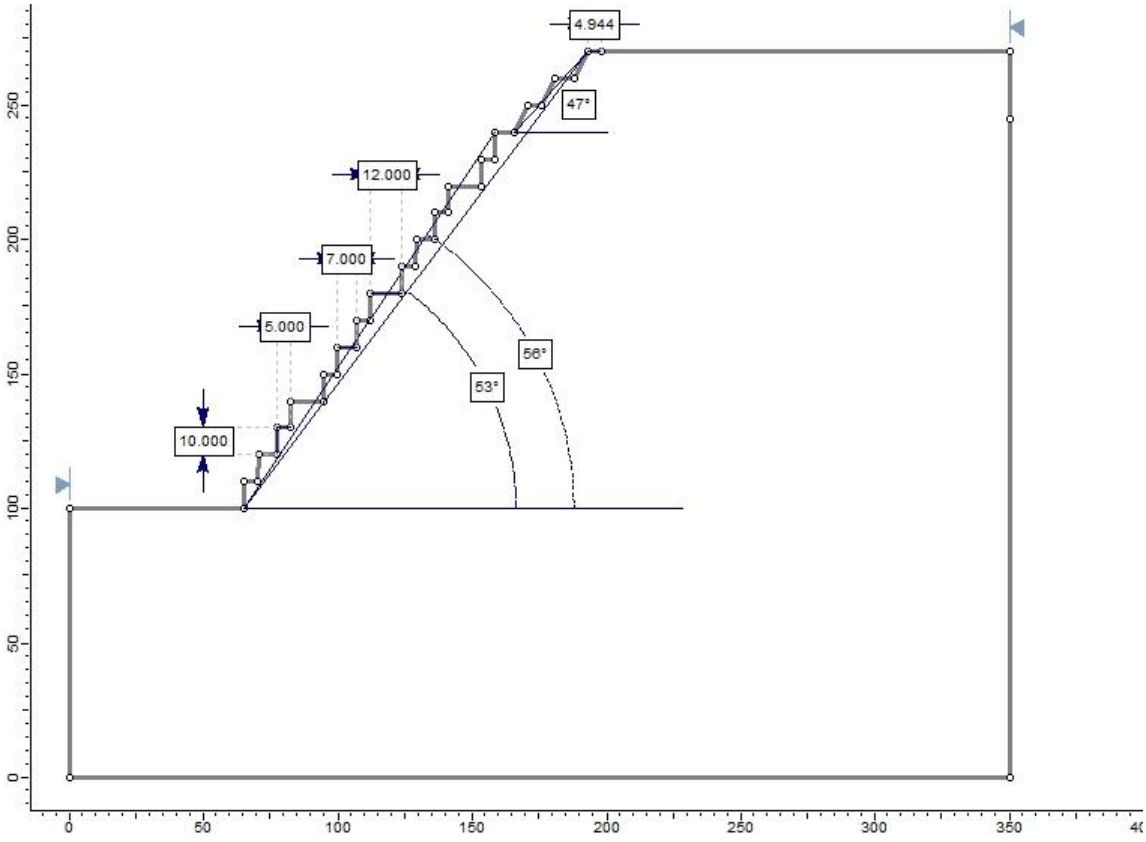


Figure 4-9 Geometry of the optimized final pit slope.

4.2 Comparison Between Existing And Optimized Pit Slopes

The current pit slope angle is compared to the resultant optimum pit slope angle in terms of safety and economics. According to limit equilibrium and numerical analysis results the current and the determined optimum slopes are not much different in terms of safety as they both showed acceptable Safety factors (FoS) and probabilities of failure. However kinematic analysis indicated that toppling and wedge failure are most likely to be experienced especially at bench scale level where slope angles are steeper. Toppling seemed to pose the greatest challenge as its likelihood was almost constant irrespective of the bench slope angle used.

Figure 4-10 shows that for the additional 1^{o}, every linear metre mined along strike length creates an extra 1 340.56 m^{3} of overburden handling (Figure 4-10). The PE03 pit is planned to extend more than 1000 m along strike and this will equate to an excess of 2,681,110 m^{3} of additional overburden material for both the northern and the southern walls. On average it costs the mine $4.50 (USD) to strip a cubic metre of waste. The reduction in waste mined will result in the mine saving more than $12,064,995.00 (USD). Thus the 1^{o} increase in overall pit slope angle will significantly improve the economics of the PE03 open pit operations.

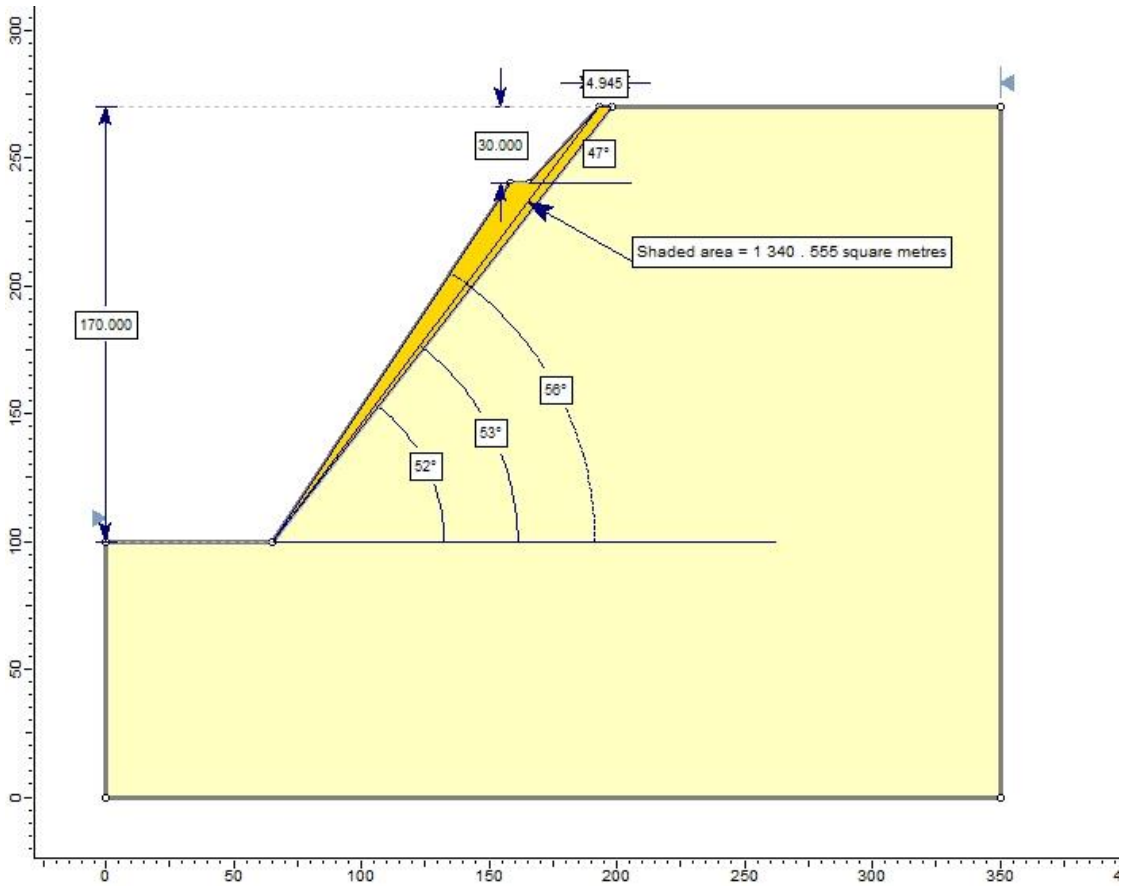


Figure 4-10 Additional overburden material (shaded area) to be mined when using the current design as compared to the optimized design.

5. CONCLUSION AND RECOMMENDATIONS

In this chapter conclusions are made concerning the steepening of the existing pit, savings that could have been made if the optimum slope angle had been used. Recommendations on how to access a further 5 m depth without a cutback are also provided.

5.1 Conclusion

From the stability and economic analysis results it was concluded that the overall pit slope of the PE03 pit can be steepened from the current 52^{o} to 53^{o} without compromising safety as long as proper and adequate slope management measures are taken. The steepening of the slope will result in an improvement of the overall economics of the pit as it will reduce the amount of the overburden material to be mined for the extension of the pit. However, a separate set of boreholes will need to be analysed from the planned extension, to confirm the ground conditions in the area of the extension. The pit depth is also increasing from the planned 165 m to 170 m and this will result in an increase in the amount of open pitable ore reserves. The pit bottom will not be widened as the design will give the same pit base as the one that was going to be produced if the pit was mined at the original slope angle from the crest downwards.

A back analysis of the current pit shows that a 1^{o} increment in the overall pit slope angle was possible and could have saved the mine from handling in excess of 2,681,110 m^{3} of overburden which translates to financial savings of more than $12,064,995.00 (USD).

5.2 Recommendations

1. To determine the depth at which to start steepening the pit slope by superimposing the overall pit slope of the optimised design to the current pit slope. Steepening of the pit to be done starting from the point of intersection of the two slopes downwards.
2. Design parameters of the optimized final pit slope for the southern and the northern walls to be set at:

Bench height	10 m
Bench slope angle	62^o and 89^o for weathered and fresh rock respectively
Bench width	7 m and 5 m alternating
Overall pit slope angle	53^o

3. Geometry of the pit to be as shown in Figure 5-1.

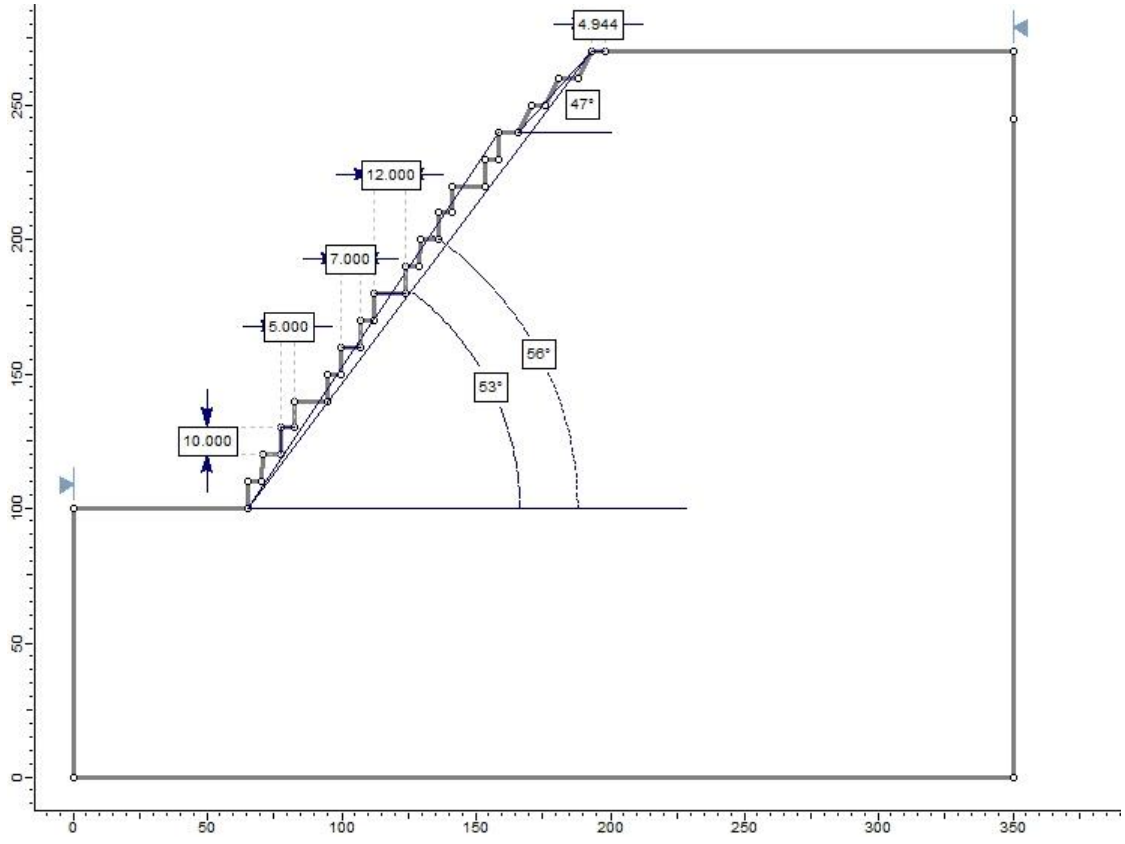


Figure 5-1 Geometry of the optimized final pit slope.

4. From kinematic analysis it was indicated that toppling and wedge failures are likely to occur, with toppling failure presenting the highest risk especially on the northern wall. Thus proper bench face scaling and cleaning of bench floors after scaling is required.
5. To increase catching capacity of safety benches, berms should be constructed along these benches especially in areas where the rock mass is structurally disturbed.
6. To practise pre-split blasting in order to minimize back breaks from production blasting and maintain the integrity of the rock mass forming the pit walls.

7. To regularly carry out visual inspection of the pit walls so as to identify areas that might pose geotechnical risk and correct these before any harm is caused by such hazards.
8. Continuously collect more geotechnical data as mining progresses to refine the designs and make necessary changes.
9. Further geotechnical evaluations should be done on suitably positioned and spaced boreholes in the area of the extension, to verify the stability of steeper slopes in that area.

References

Alegre, D. A. G., Peroni, R. d. L. & Aquino, E. d. R., 2019. The impact of haul road geometric parameters on open pit mine strip ratio. *REM, Int. Eng. J., Special Supplement 1, Ouro Preto, 72(1),,* pp. 25-31.

Atkinson, L. C., 2001. The Role and Mitigation of Groundwater in Slope Stability. In: *Slope Stability in Surface Mining.* Colorado,: Society for Mining, Metallurgy, and Exploration, pp. 89-96.

Azzuhry, Y., 2016. Stability analysis and failure mechanisms of open pit rock slope. *Journal of the Civil Engineering Forum,* pp. 261-269.

Barton, N. B., 1976. The shear strength of rock and rock joints. *Int. J. Mech. Min. Sci. & Geomech.,* pp. Abstr. 13(10), 1-24..

Barton, N. R., 1974. A review of the shear strength of filled discontinuities in rock.. *Norwegian Geotech. Inst..*

Barton, N. R. & Bandis, S. C., 1982. *Effects of block size on the the shear behaviour of jointed rock.* Berkeley, pp. 739-760.

Barton, N. R. & Bandis, S. C., 1990. *Review of predictive capabilites of JRC-JCS model in engineering practice.* Loen, Norway, pp. 603-610.

Barton, N. R. & Choubey, V., 1977. The shear strength of rock joints in theory and practice.. *Rock Mech.,* pp. 10(1-2), 1-54..

Bell, F. G., 1992. *Engineering in rock masses..* Oxford: Butterworth-Heinemann Ltd.

Bieniawski, Z. T., 1984. *Rock mechanics design in mining and tunneling..* Rotterdam: s.n.

Bieniawski, Z. T., 1989. *Engineering Rock Mass Classifications: A Complete Manual for Engineers and Geologist in Mining, Civil and Petroleum Engineering .* New York: Wiley.

Bieniawski, Z. T., 1989. *Rock mass classifications in rock engineering.* Rotterdam., Balkema., pp. 97-106.

Bijmolt, M. J., 2014. *“Implications of dredge mine design on mine optimization and discussing the possible approaches”*: Delft University of Technology and Royal IHC..

Bobet, A., 2010. Numerical methods in geomechanics. *The Arabian Journal for Science and Engineering, Volume 35, Number 1B,* pp. 27-48.

Bosman, J. D., 2013. *Geotechnical design for Pickstone gold mine, Zimbabwe,* s.l.: Open House Management Solutions (Pty) Ltd.

Brady, B. H. G. & Brown, E. T., 2005. *Rock Mechanics for Underground Mining, Third Edition.* Dordrecht: Springer Science + Business Media, Inc.

Brown, E. T. & Hoek, ,. E., 1978. Trends in relationships between measured rock in situ stresses and depth.. *Int. J. Rock Mech. Min. Sci. & Geomech.,* pp. Abstr. 15, pp.211-215..

Chiwaye, H. T. & Stacey, T. R., 2010. A comparison of limit equilibrium and numerical modelling approaches to risk analysis for open pit mining.. *The Journal of the Southern African Institute of Mining and Metallurgy.,* pp. 571-580.

Cilliers, L. & Bosman, J. D., 2016. *Geotechnical investigation for Peerless and Pickstone mine,* Johannesburg, South Africa: Open House Management Solutions (Pty) Ltd.

Coates, R., Bull, G., Glisson, F. J. & Roth, A., 2008. *Highly fl exible catch fences and high performance drape mesh systems for rockfall protection in open pit operations,* Switzerland: Geobrugg AG, Protection Systems.

Contreras, L. F., 2015. An economic risk evaluation approach for pit slope optimization.. *The Journal of the Southern African Institute of Mining and Metallurgy,* pp. 607-622.

Deere, D. U. & Deere, D. W., 1988. *The RQD index in practice.* Philadelphia, ASTM.

Deere, D. U. & Miller, R. P., 1966. *Engineering clasification and index properties of intact rock.Report AFWL-TR-65-116.,* New Mexico: Air Force Weapon Laboratory.

Esterhuizen, G. S., 2014. Extending empirical evidence through numerical modelling in rock engineering design.. *The Journal of The Southern African Institute of Mining and Metallurgy Vol 114,* pp. 755-764.

Fillion, M. H. & Hadjigeorgiou, J., 2016. Implications of collecting additional data for slope design in an open pit operation.. *The Journal of The Southern African Institute of Mining and Metallurgy, Vol 106.,* pp. 357-366.

Fossen, H. & Schultz, R. A., 2008. Terminology for structural discontinuities. *The American Association of Petroleum Geologists. AAPG Bulletin, v. 92, no. 7*, July, p. 853–867.

Golestanifar. M, Ahangari K, Goshtasbi K, Dehkharghani A and Terbrugge P 2018. Governing risk elements through open pit slope optimization.. *The Journal of the Southern African Institute of Mining and Metallurgy.,* pp. 47-55.

Goodman, R. E., 1976. *Methods of Geoogical Engineering in Discontinuous Rocks.*:West Publishing Company.

Goodma, R. E. & Bray, J. W., 1976. *Toppling of Rock Slopes..* Colorado, ASCE.

Google, 2019. *Google Maps.* [Online] Available at: https://www.google.co.zw/maps/place/Pickstone+Peerless+Gold+Mine/@-18.2937298,30.2163009,15z/data=!4m5!3m4!1s0x0:0x4bcda3068cbfd5f1!8m2!3d-18.2937298!4d30.2163009 [Accessed 21 12 2019].

Hack, R., Price, D. & Rengers, N., 2002. A new approach to rock slope stability - a probability classification (SSPC).. *Bulletin of Engineering Geology and the Environment.*, 14 June, pp. Vol. 62: article: DOI 10.1007/s10064-002-0155-4..

Hajdasinski, M. M., 1988. Optimisation of mine size and mine life in a historical perspective. *Mining Science and Technology,* Volume 7, p. 305 310.

Handley, M. F., 2013. Pre-mining stress model for subsurface excavations in southern Africa. *The Journal of The Southern African Institute of Mining and Metallurgy,* pp. 449-471.

Hawley, M., Marisett, S., Beale, G. & Stacey, P., 2009. Performance assessment and monitoring. In: *Guidelines for Open Pit Slope Design*: CRC Press/Balkema, pp. 327-380.

Hoek, ,. E. & Londe, P., 1974. *The Design of Rock Slopes and Foundations.* Denver, International Society for Rock Mechanics, pp. 1-78.

Hoek, E., 1966. Rock Mechanics - an introduction for the practical engineer Parts I, II and III. *Mining Magazine,* pp. 1-66.

Hoek, E., 2006. Practical Rock Engineering.

Hoek, E., 2009. *Fundamentals of slope design.* Santiago, Chile., www.slopestability.cl, pp. 1-26.

Hoek, E. & Brown, E. T., 1997. Practical estimates of rock mass strength. *International Journal of Rock Mechanics and Mining Sciences, Vol 34, No 8,* pp. 1165-1186.

Hoek, E., Carranza-Torres, C. T. & Corkum, B., 2002. *(2002), Hoek-Brown failure criterion – 2002 edition..* Toronto, North American Rock Mechanics Society.

Hoek, E., Carter, T. G. & Diederichs, M. S., 2013. *Quantification of the Geological Strength Index Chart.* San Francisco,, American Rock Mechanics Association, pp. 187-223.

Hoek, E., Grabinsky, M. W. & Diederichs, M. S., 1991. Numerical Modelling For Underground Excavations. *Trans Instn, Min, Metall, (Sect A: Min. industry),100,* pp. A22-A30.

Hoek, E., Hutchinson, J., Kalenchuck, K. & Diederichs, M., 2009. Infuence of in situ stresses on open pit design. In: *Guidelines for Open Pit Slope Design.* s.l.:Csiro Publishing, pp. 437-446.

Hoek, E. & Pentz, D. L., 1968. *The stability of open pit mines, Rock Mechanics Research Report No. 5,* London: Department of Civil Engineering, Geology and Mining and Mineral Technology, Imperial College of Sciece and Technology..

Hoek, E., Read, J., Karzulovic, A. & Chen, Z. Y., 2000. *Rock slopes in Civil and Mining Engineering.* Melbourne., pp. 1-17.

HolcombeCoughlinOliver, 2010. *HolcombeCoughlinOliver.* [Online]
Available at: HTTP://www.holcombecoughlinoliver.com/HCO_downloads [Accessed 8 July 2018].

Hudson, J. A. & Harrison, J. P., 1997. *Engineering rock mechanics an introduction to the principles.*:Published by Elsevier Science Ltd..

Hustrulid, W. & Kuchta, M., 1998. *Open Pit Mine Planning and Design: 2 Volumes"*: A.A.Balkema.

Kennedy, B. A., 1990. *Surface Mining, Second Edition.* US: Society for Mining, Metallurgy and Exploration.

Kim, B. H., Cai, M. & Kaiser, P. K., 2007. *Rock mass strength with non persistent joints..* Vancouver, Canada, ARMA.

Laubscher, D. H., 1990. A geomechanics classification system for the rating of rock mass in mine design. *Journal of the South African Institute of Mining and Metalluagy.,* pp. 257-273.

Lisle, R. J., 2004. Calculation of the daylight envelope for plane failure of rock slopes. *Ge´otechnique 54, No. 4,* p. 279–280.

Lotheringen, J., James , J., Lomberg, K. & Bornman , H., 2016. *Tharisa plc Tharisa Chrome and PGM Mine, South Africa Competent Persons Report ,*: Coffey Mining (SA) Pty Ltd.

Madowe, A., 2016. Design and implementation of steeper slope angles on a kimberlite open pit diamond operation–a practical approach.. *The Journal of the Southern Institute of Mining and Metallurgy Volume 116,* pp. 723-730.

Marinos, P. & Hoek, E., 2000. *GSI – A geologically friendly tool for rock mass strength estimation..* Melbourne, Proceedigs GeoEng2000 Conference.

Mathis, J. I., 2009. *Bench-Inter-ramp-Overall: a guide to statistically designing a rock slope.* Santiago.

Moser, A., Wagner, H. & Schinagl, S., 2017. *Application of rock mass classification systems as a tool for rock mass strength determination.* Perth., Australian Centre for Geomechanics., pp. 569-586.

Nilsen, B. & Ballou, B. J., 2006. *Stability problems and rock support at the Tellnes open pit mine, Norway.* Cape Town, The South African Institute of Mining and Metallurgy, pp. 1-11.

Orpen, J. L., 2014. *Best practice and new technology in core drilling logging and fracture analysis..* Vancouver Canada.

Palmström, A., 1995. *RMi – a rock mass characterization system for rock engineering purposes. PhD thesis,,* Norway,: Oslo University,.

Patton, F. D., 1966. *Multiple modes of shear failure in rock.* Lisbon 1,, Int. Soc. Rock Mech, pp. 509-513.

Piyal, W. P. & Konietzky, H. H., 2016. *Geometrical properties of rock joints and their effects on rock mechanical behaviour..* [Online] Available at: https://tufreiberg.de/fakult3/gt/feme/ebook/13_Geometrical_properties_of_rock_joints_and_their_effects_on_rock_mechanical_behaviour.pdf [Accessed 19 12 2018].

Priest, S. D. & Hudson, J. A., 1981. Estimation of discontinuity spacing and trace length using scanline surveys.. *International Journal of Rock Mechanics and Mining Sciences and Geomechanics ,* Volume 18, pp. 97-183.

Rocscience, 2001. *Phase2 Model Program,* Ontorio, Canada: Rocscience Inc.

Rocscience, 2002. *Rocscience.* [Online] Available at: https://www.rocscience.com/documents/pdfs/rocnews/june2002/RocLab-Overview-Features-FAQs.pdf [Accessed 17 April 2020].

Rocscience, 2010. *DIPS Reference Manual,* Toronto: Rocscience.

Rocscience, 2018. *Slide 2D limit equilibrium analysis of slope stability,* Toronto Canada: Rocscience Inc..

Rocscience, 2019. *Rocscience.* [Online] Available at: https://www.rocscience.com/help/dips/dips/Planar_Sliding.htm [Accessed 14 January 2020].

Roux, R., Terbrugge, P. & Badenhorst, F., 2006. Slope management at Navachab gold mine, Namibia.. *The South African Institute of Mining and Metallurgy,* pp. 579-594.

Runge, I., 2012. *Discover Mongolia 2012 "Mining economics.".* Brisbane Qld Australia, Runge Limited, pp. 1-8.

Ryan, T. M. & Pryor, P. R., 2001. Designing Catch Benches and Interramp Slopes. In: *Slope stability in surface mining.* Littleton, Colorado: Society for Mining, Metallurgy, and Exploration., pp. 27-38.

Sankar, U. S., 2006. *Slope stability and dump stability.*

Scheldt, T., 2002. *Comparison of Continuous and Discontinuous Modelling for Computational Rock Mechanics*: Department of Geology and Mineral Resources Engineering Norwegian University of Science and Technology.

Schultz, R. A. & Fossen, H., 2008. Terminology for structural discontinuities. *The American Association of Petroleum Geologists.,* p. 853–867.

Sheory, P. R., 1994. A theory for in situ stresses in isotropic and transversely isotropic rock. *Int. J. Rock Mech. Min. Sci. & Geomech,* pp. Abstr. 31(1), 23-34..

Singhal, B. B. S. & Gupta, R. P., 2010. *Applied Hydrogeology of Fractured Rocks,* :Springer Science+Business Media.

Sjoberg, J., 1996. *Large scale slope stability in open pit mining - A review.,* Lulea: Lulea University of technology.

Stacey, 2009. Fundamentals of slope design.. In: *Guidelines for Open Pit Slope Design..* Melbourne. CSIRO Publishing, pp. 1-14.

Stacey, T. R., 1968. *Stability of rock slopes in open pit mines.,* Pretoria: National mechanical research institute, CSIR report, MEG 737.

Stacey, T. R. & Swart, A. H., 2001. *Booklet Practical Rock Engineering Practice for Shallow and Opencast Mines (SIMRAC).* Braamfontein South Africa: The Safety in Mines Research Advisory Committee.

Stead, D., Eberhardt, E. & Coggan, J. S., 2006. Developments in the characterization of complex rock slope deformation and failure using numerical modelling techniques. *Engineering Geology 83,* p. 217– 235.

Steffen, O. K., Contreras, L. F., Terbrugge, P. J. & Venter, J., 2008. *A risk evaluation approach for pit slope design..* San Francisco, American Rock Mechanics Association, pp. 1-18.

Sullivan, T. D., 2006. *Pit slope design and risk – A view of the current state of the art.* Johannesburg, The South African Institute of Mining and Metallurgy, pp. 51-78.

Tapia, A., Contreras, L. F., Jefferies, M. G. & Steffen, O., 2007. *Risk evaluation of slope failure at Chuquicamata Mine. Proc. Int. Symp. Rock Slope Stability in Open Pit Mining and Civil Engineering, Perth, Australian Centre for Geomechanics*, ISBN 978 09756756 8 7.

Terbrugge, P. J., Wesseloo, J., Venter, J. & Steffen, O. K., 2006. A risk consequence approach to open pit slope design.. *The Journal of The Southern African Institute of Mining and Metallurgy, Vol 106,* pp. 503-511.

Vast-Resources, 2015. *Zimbabwean Interest: Pickstone-Peerless,*: Vast Resources PLC.

Wagner, H., 2019. Deep Mining: A Rock Engineering Challenge. *Rock Mechanics and Rock Engineering,* Volume 52, p. 1417–1446 .

Wesseloo, J. & Read, J., 2009. Acceptance criteria. In: *Guidelines for open pit slope design.* Australia: CSIRO Publishing, pp. 221-236.

Westernex, 2018. *Westernex.* [Online] Available at: www.westernex.com.au [Accessed 15 August 2018].

Wyllie, D. C., 2018. *Rock Slope Engineering Civil Applications Fifth Edition.* Vancouver: Taylor & Francis Group.

Wyllie, D. C. & Mah, C. W., 2004. *Rock Slope Engineering Civil and mining 4th edition.* London: Spon Press.

Appendix A

Completed geotechnical core logs sheets for the sampled holes.

Geotechnical Core Log Sheets

Table A-1 Geotechnical core logging data sheet for PE03DDGC8_01.

GEOTECHNICAL CORE LOGGING DATA SHEET FOR PE03					
LOGGED BY:	Pardon Nyamande		CHECKED BY:	Martin Mateveke (Mine Geologist)	
NORTHING:	7975709		DIP:	-63^{o}	
EASTING:	203990		AZIMUTH:	180^{o}	
ELAVATION:	1189		HOLE DEPTH:	262 m	
DATE:	03/04/19		CORE SIZE:	HQ	
DRILLHOLE ID:	DEPTH INTERVAL		STRUCTURAL DATA		
	From (m)	To (m)	STRUCTURE TYPE	BETA	ALPHA
PE03DDGC8_01	60.85	70.26	Shear Zone	270	50
PE03DDGC8_01	43.00	43.10	Shear Zone	140	45
PE03DDGC8_01	70.85	71.85	Foliation	0	50
PE03DDGC8_01	90.85	91.00	Foliation	110	40
PE03DDGC8_01	92.65	92.85	Foliation	54	45
PE03DDGC8_01	123.95	124.13	Foliation	160	30
PE03DDGC8_01	131.67	131.85	Foliation	20	30
PE03DDGC8_01	149.73	149.85	Foliation	20	35
PE03DDGC8_01	164.85	165.15	Foliation	30	35
PE03DDGC8_01	167.85	168.18	Foliation/veining	28	30
PE03DDGC8_01	194.00	194.40	Veining	210	50
PE03DDGC8_01	215.85	216.05	Foliation	20	25
PE03DDGC8_01	221.85	222.05	Foliation	340	30
PE03DDGC8_01	227.85	228.10	Foliation	0	35

Table A-2 Geotechnical core logging data sheet for PE03DDGC8_02.

GEOTECHNICAL CORE LOGGING DATA SHEET FOR PE03					
LOGGED BY:	Pardon Nyamande		CHECKED BY:	Martin Mateveke (Mine Geologist)	
NORTHING:	7975711		DIP:	-62^{o}	
EASTING:	204070		AZIMUTH:	180^{o}	
ELAVATION:	1189		HOLE DEPTH:	251.85 m	
DATE:	03/04/19		CORE SIZE:	HQ	
DRILLHOLE ID:	DEPTH INTERVAL		STRUCTURAL DATA		
	From (m)	To (m)	STRUCTURE TYPE	BETA	ALPHA
PE03DDGC8_02	115.45	115.45	Contact	120	30
PE03DDGC8_02	125.85	125.85	Foliation	155	35
PE03DDGC8_02	143.85	143.85	Foliation	170	20
PE03DDGC8_02	161.85	161.85	Foliation	180	20
PE03DDGC8_02	173.85	173.85	Foliation	155	30
PE03DDGC8_02	203.85	203.85	Contact	150	35
PE03DDGC8_02	205.85	205.85	Contact	320	45
PE03DDGC8_02	207	207	Veining	335	45
PE03DDGC8_02	207.85	207.85	Veining	320	50
PE03DDGC8_02	208	208	Contact	350	40
PE03DDGC8_02	209.85	209.85	Foliation	230	15
PE03DDGC8_02	235.25	235.25	Foliation	180	50
PE03DDGC8_02	243.5	243.5	Foliation	175	40

Table A-3 Geotechnical core logging data sheet for PE03DDGC8_03.

GEOTECHNICAL CORE LOGGING DATA SHEET FOR PE03					
LOGGED BY:	Pardon Nyamande		CHECKED BY:	Martin Mateveke (Mine Geologist)	
NORTHING:	7975724		DIP:	-63^{o}	
EASTING:	204150		AZIMUTH:	180^{o}	
ELAVATION:	1188		HOLE DEPTH:	270 m	
DATE:	04/04/19		CORE SIZE:	HQ	
DRILLHOLE ID:	DEPTH INTERVAL		STRUCTURAL DATA		
	From (m)	To (m)	STRUCTURE TYPE	BETA	ALPHA
PE03DDGC8_03	38.85	38.95	Foliation	180	40
PE03DDGC8_03	112.85	112.95	Foliation	110	35
PE03DDGC8_03	118.85	118.95	Foliation	130	30
PE03DDGC8_03	152.85	152.95	Foliation	160	45
PE03DDGC8_03	176.85	176.95	Foliation	150	20
PE03DDGC8_03	188.85	188.95	Foliation	130	25
PE03DDGC8_03	203.85	203.95	Foliation	160	25
PE03DDGC8_03	227.85	227.95	Foliation	120	30
PE03DDGC8_03	236.5	236.6	Foliation	90	30
PE03DDGC8_03	238.3	238.4	Contact	15	20
PE03DDGC8_03	243.85	243.95	Foliation	220	55
PE03DDGC8_03	245.5	245.6	Foliation	140	50
PE03DDGC8_03	246	246.1	Contact	150	30
PE03DDGC8_03	248	248.1	Contact	120	60
PE03DDGC8_03	255.8	255.9	Foliation	190	40
PE03DDGC8_03	2.62	2.72	Foliation	170	30

Table A-4 Geotechnical core logging data sheet for PE03DDGC8_04P.

GEOTECHNICAL CORE LOGGING DATA SHEET FOR PE03					
LOGGED BY:	Pardon Nyamande		CHECKED BY:	Martin Mateveke (Mine Geologist)	
NORTHING:	797550		DIP:	-62^{o}	
EASTING:	204230		AZIMUTH:	180^{o}	
ELAVATION:	1191		HOLE DEPTH:	270 m	
DATE:	04/04/19		CORE SIZE:	HQ	
DRILLHOLE ID:	DEPTH INTERVAL		STRUCTURAL DATA		
	From (m)	To (m)	STRUCTURE TYPE	BETA	ALPHA
PE03DDGC8_04P	171.15	171.45	Contact	178	37
PE03DDGC8_04P	191.15	191.3	Contact	130	35
PE03DDGC8_04P	204.85	205.15	Contact	170	20
PE03DDGC8_04P	218	218.5	Veining	20	60
PE03DDGC8_04P	226.37	226.6	Veining	0	20
PE03DDGC8_04P	226.5	227.05	Veining	0	25
PE03DDGC8_04P	228.15	228.75	Contact	340	45
PE03DDGC8_04P	243.15	243.35	Bedding/Foliation	180	40
PE03DDGC8_04P	250.15	250.25	Bedding/Foliation	178	38
PE03DDGC8_04P	255	258.15	Bedding/Foliation	152	40
PE03DDGC8_04P	268	268.15	Bedding/Foliation	100	30
PE03DDGC8_04P	112.15	112.75	Contact	160	35

Table A-5 Geotechnical core logging data sheet for PE03DDGT_01.

GEOTECHNICAL CORE LOGGING DATA SHEET FOR PE03					
LOGGED BY:	Pardon Nyamande		CHECKED BY:	Martin Mateveke (Mine Geologist)	
NORTHING:	7975704		DIP:	-62º	
EASTING:	203950		AZIMUTH:	180º	
ELAVATION:	1189		HOLE DEPTH:	234 m	
DATE:	04/04/19		CORE SIZE:	HQ	
DRILLHOLE ID:	DEPTH INTERVAL		STRUCTURAL DATA		
	From (m)	To (m)	STRUCTURE TYPE	BETA	ALPHA
PE03DDGT_01	44.8	44.8	Foliation	190	45
PE03DDGT_01	60	60	Foliation	300	30
PE03DDGT_01	95.9	95.9	Foliation	10	40
PE03DDGT_01	132.5	132.5	Foliation	180	30
PE03DDGT_01	173.9	173.9	Foliation	170	40
PE03DDGT_01	197	197	Contact	200	40
PE03DDGT_01	203.2	203.2	Contact	160	30
PE03DDGT_01	224	224	Foliation	160	45

Table A-6 Geotechnical core logging data sheet for PE03DDGT_03.

GEOTECHNICAL CORE LOGGING DATA SHEET FOR PE03					
LOGGED BY:	Pardon Nyamande		CHECKED BY:	Martin Mateveke (Mine Geologist)	
NORTHING:	7975708		DIP:	-58^{o}	
EASTING:	204030		AZIMUTH:	000^{o}	
ELAVATION:	1189		HOLE DEPTH:	307 m	
DATE:	05/04/19		CORE SIZE:	HQ	
DRILLHOLE ID:	DEPTH INTERVAL		STRUCTURAL DATA		
	From (m)	To (m)	STRUCTURE TYPE	BETA	ALPHA
PE03DDGT_03	71.85	72.7	Contact	130	25
PE03DDGT_03	72.7	73.19	Contact	170	30
PE03DDGT_03	149.85	150.18	Contact	170	35
PE03DDGT_03	218.85	218.95	Contact	180	25
PE03DDGT_03	230.6	230.85	Foliation	0	30
PE03DDGT_03	233.85	233.9	Foliation	120	40
PE03DDGT_03	260.85	261	Foliation	170	35
PE03DDGT_03	271.85	272.1	Contact	200	40
PE03DDGT_03	274.7	275.85	Foliation	110	3
PE03DDGT_03	283.9	284.05	Contact	180	35
PE03DDGT_03	288.85	289	Foliation	100	45
PE03DDGT_03	289	289.2	Contact	160	45
PE03DDGT_03	305.6	305.85	Bedding	165	50

Table A-7 Geotechnical core logging data sheet for PE03DDGT_06.

GEOTECHNICAL CORE LOGGING DATA SHEET FOR PE03					
LOGGED BY:	Pardon Nyamande		CHECKED BY:	Martin Mateveke (Mine Geologist)	
NORTHING:	7975718		DIP:	-60^{o}	
EASTING:	204250		AZIMUTH:	180^{o}	
ELAVATION:	1190		HOLE DEPTH:	286 m	
DATE:	05/04/19		CORE SIZE:	HQ	
DRILLHOLE ID:	DEPTH INTERVAL		STRUCTURAL DATA		
	From (m)	To (m)	STRUCTURE TYPE	BETA	ALPHA
PE03DDGT_06	41.95	42.05	Foliation	180	40
PE03DDGT_06	102.95	103.05	Contact	180	35
PE03DDGT_06	197.95	198.05	Foliation	150	30
PE03DDGT_06	218.95	219.05	Foliation	180	30
PE03DDGT_06	224.95	225.05	Foliation	180	30
PE03DDGT_06	242.95	243.05	Foliation	180	30
PE03DDGT_06	240.95	241.05	Foliation	150	30
PE03DDGT_06	246.1	246.2	Foliation	190	10
PE03DDGT_06	248.95	249.05	Foliation/Bedding	180	20
PE03DDGT_06	254.95	255.05	FOL/Bedding	200	30
PE03DDGT_06	258.38	258.48	Contact	160	75
PE03DDGT_06	258.76	258.86	Contact	320	75

Appendix B

Face mapping log sheets for the southern and northern walls.

Table B-1 Northern wall face mapping.

FACE MAPPING DATA SHEET FOR PE03						
MAPPED BY:		Pardon Nyamande		SURVERYOR:	C Ngulube	
DATE:		17/09/2018		PIT WALL:	Northern Wall	
	POINT COORDINATES			STRUCTURAL DATA		
POINT ID	X	Y	Z	STRUCTURE TYPE	DIP	DIP DIRECTION
N1	7975633.384	204244.8	1153.815	Joint	45	138
N2	7975636.674	204219.8	1153.561	Fault	82	150
N3	7975636.838	204200.9	1154.244	Joint	30	210
N4	7975639.966	204174.1	1156.465	Joint	35	193
N5	7975640.88	204158.8	1158.305	Fault	14	210
N6	7975641.935	204142.1	1157.277	Joint	87	231
N7	7975650.24	204130	1162.554	Fault	22	241
N8	7975651.912	204117	1163.12	Joint	34	152
N9	7975654.046	204082.7	1162.841	Fault	83	225
N10	7975653.944	204077.8	1162.247	Joint	80	345
N11	7975653.592	204072.5	1163.158	FAULT	85	223
N12	7975649.049	204241.6	1169.304	Joint	69	332
N13	7975656.447	204213.7	1171.324	Joint	74	334
N14	7975656.343	204206.3	1170.661	Joint	76	340
N15	7975659.427	204199.8	1173.275	Joint	80	340
N16	7975655.766	204187.1	1170.177	Joint	80	340
N17	7975653.333	204182.1	1170.24	Joint	80	340
N18	7975653.890	204177	1170.245	Joint	80	340
N19	7975652.116	204168.5	1170.263	Joint	80	340
N20	7975659.892	204156.3	1172.213	Joint	37	208
N21	7975661.136	204135.9	1173.055	Joint	34	227
N22	7975661.136	204085.9	1173.055	Joint	80	225
N23	7975660.904	204130	1172.479	Joint	70	358
N24	7975658.768	204105.5	1170.485	Joint	68	347
N25	7975661.011	204078.1	1170.819	Joint	73	351
N26	7975662.827	204039.5	1169.422	Joint	60	330
N27	7975662.827	204039.5	1169.422	Joint	80	338
N28	7975670.475	203976	1174.285	Fault	80	335
N29	7975672.851	204026	1177.428	Joint	88	315

Table B-2 Northern wall face mapping (continued)

FACE MAPPING DATA SHEET FOR PE03						
MAPPED BY:		Pardon Nyamande		SURVERYOR:	C Ngulube	
DATE:		17/09/2018		PIT WALL:	Northern Wall	
POINT ID	POINT COORDINATES			STRUCTURAL DATA		
	X	Y	Z	STRUCTURE TYPE	DIP	DIP DIRECTION
N31	7975666.807	204135.9	1179.924	Joint	85	155
N32	7975667.274	204140.3	1179.871	Joint	85	160
N33	7975666.914	204157.6	1180.238	Joint	86	135
N34	7975670.689	204165.6	1180.334	Joint	83	135
N35	7975671.312	204176.3	1180.705	Joint	85	158
N36	7975669.799	204214	1180.571	Joint	85	155
N37	7975669.014	204259.1	1180.909	Joint	78	030
N38	7975670.967	204220.9	1181.904	Joint	80	050
N39	7975668.18	204254.3	1180.212	Joint	75	035
N40	7975658.859	204280.3	1180.658	Joint	46	170
N41	7975658.859	204280.3	1180.658	Joint	40	190

Table B-3 Southern wall face mapping.

FACE MAPPING DATA SHEET FOR PE03						
MAPPED BY:		Pardon nyamande		SURVERYOR:	C Ngulube	
DATE:		18/09/2018		PIT WALL:	Southern Wall	
	POINT COORDINATES			STRUCTURAL DATA		
POINT ID	X	Y	Z	STRUCTURE TYPE	DIP	DIP DIRECTION
S1	7975570.010	204222.632	1143.504	Joint	80	090
S2	7975569.434	204216.739	1143.261	Fault	82	095
S3	7975568.571	204193.128	1143.593	Joint	76	058
S4	7975569.216	204190.025	1143.023	Joint	82	290
S5	7975568.079	204185.408	1143.483	Joint	84	294
S6	7975567.474	204180.343	1143.203	Joint	90	272
S7	7975567.972	204175.024	1143.487	Joint	86	310
S8	7975568.156	204160.197	1143.803	Joint	12	000
S9	7975569.138	204123.868	1143.469	Joint	82	075
S10	7975569.795	204118.755	1142.987	Joint	90	070
S11	7975570.854	204109.874	1142.445	Joint	88	115
S12	7975575.334	204085.948	1142.777	Joint	86	230
S13	7975575.185	204062.893	1143.942	Joint	82	275
S14	7975574.434	204064.261	1144.445	Joint	88	080
S15	7975588.048	203998.117	1141.621	Joint	80	055
S16	7975584.42	203967.921	1142.309	Joint	88	305
S17	7975586.513	203958.593	1141.788	Fault	68	315
S18	7975609.498	203914.629	1141.158	Fault	75	025
S19	7975609.172	203895.646	1142.538	Joint	80	024
S20	7975552.323	203908.189	1146.865	Fault	88	075

Appendix C

Failure codes for compression test of core samples.

CLASSIFICATION OF ROCK SPECIMEN FAILURE MODE INFLUENCED / NOT INFLUENCED BY DISCONTINUITIES DURING COMPRESSION TESTING

FAILURE NOT INFLUENCED BY DISCONTINUITIES (INTACT)

TYPE CODE	DESCRIPTION OF SUB CODES	
	A	B
X	SLIDING SHEAR FAILURE	COMPLETE CONE DEVELOPMENT
Y	SPLITTING	BREAKING INTO A LOT OF PIECES

FAILURE INFLUENCED BY DISCONTINUITIES

TYPE CODE	DESCRIPTION OF SUB CODES	
	A	B
	PARTIAL FAILURE ON DISCONTINUITY	FAILURE COMPLETELY ON DISCONTINUITY
1	AT 0-10° TO AXIS	AT 0-10° TO AXIS
2	AT 11-20° TO AXIS	AT 11-20° TO AXIS
3	AT 21-30° TO AXIS	AT 21-30° TO AXIS
4	AT 31-40° TO AXIS	AT 31-40° TO AXIS
5	AT 41-50° TO AXIS	AT 41-50° TO AXIS
6	AT 51-70° TO AXIS	AT 51-70° TO AXIS
7	AT 71-90° TO AXIS	AT 71-90° TO AXIS
0	Multiple Discontinuities	Multiple Discontinuities

Example: Failure Type3B: Failure completely on a discontinuity with an orientation of between 21° and 30° to the specimen axis.

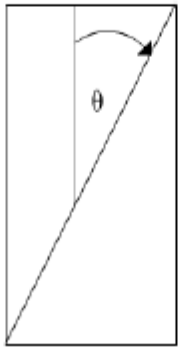
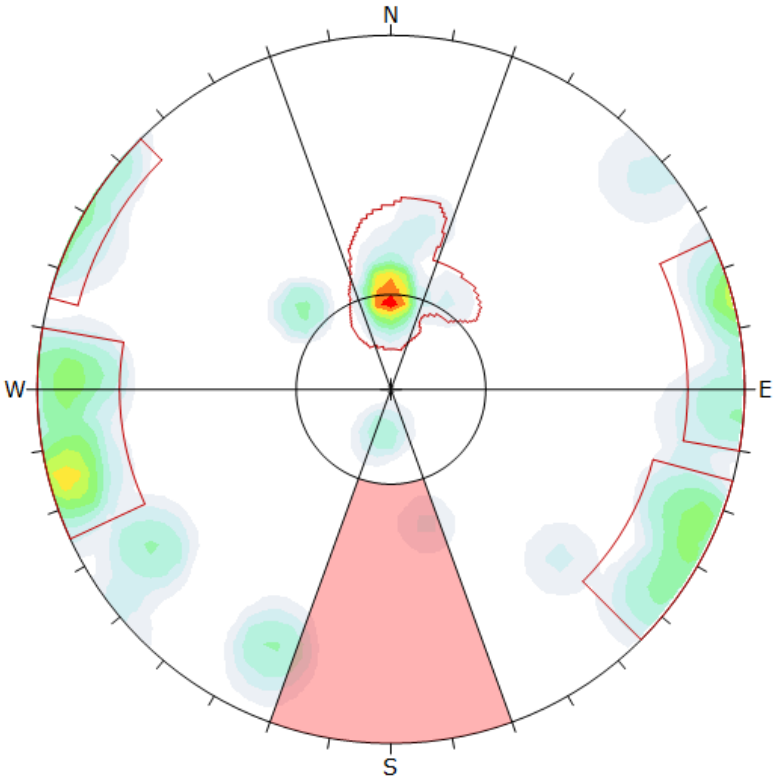


Figure C-1 Failure codes for compression test (Bosman, 2013)

Appendix D

Stereonets for Kinematic Analysis of slopes in weathered and fresh rock for the current and optimized designs (OD1 and OD5).

Kinematic analysis at bench scale level



Color	Density Concentrations
	0.00 - 1.50
	1.50 - 3.00
	3.00 - 4.50
	4.50 - 6.00
	6.00 - 7.50
	7.50 - 9.00
	9.00 - 10.50
	10.50 - 12.00
	12.00 - 13.50
	13.50 - 15.00
Maximum Density	14.41%
Contour Data	Pole Vectors
Contour Distribution	Fisher
Counting Circle Size	1.0%

Kinematic Analysis	Planar Sliding
Slope Dip	90
Slope Dip Direction	0
Friction Angle	30°
Lateral Limits	20°

	Critical	Total	%
Planar Sliding (All)	1	32	3.13%

Plot Mode	Pole Vectors
Vector Count	32 (32 Entries)
Hemisphere	Lower
Projection	Equal Angle

Figure D-1 Planar failure for PE03 Southern Wall at 90º bench slope angle (Current design and OD1).

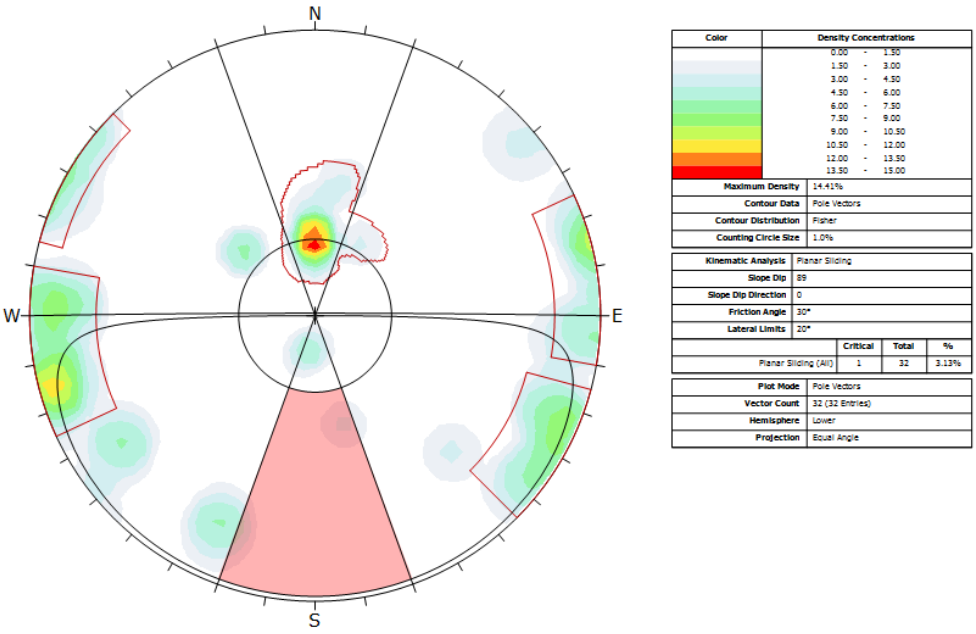


Figure D-2 Planar failure for PE03 Southern Wall at 89º bench slope angle (OD5).

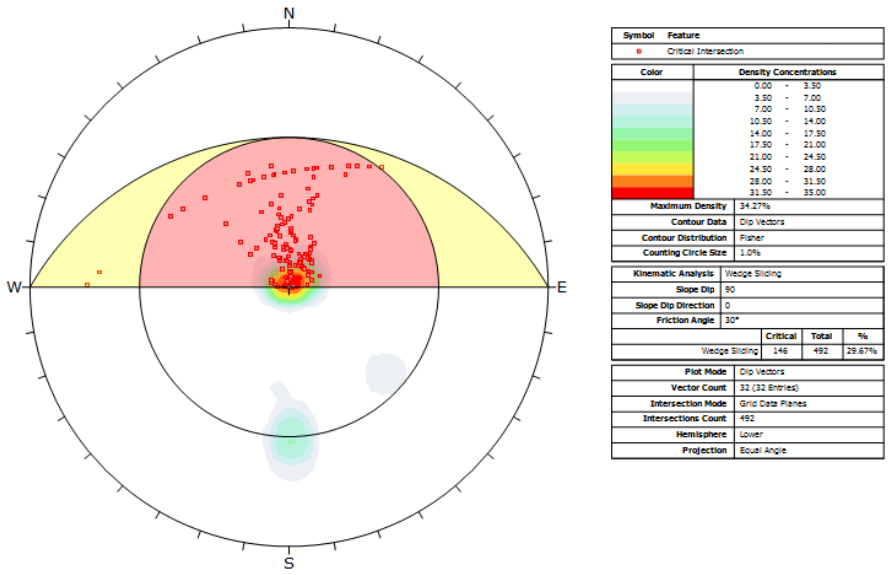


Figure D-3 Wedge failure for PE03 Southern Wall at 90º bench slope angle (Current design and OD1).

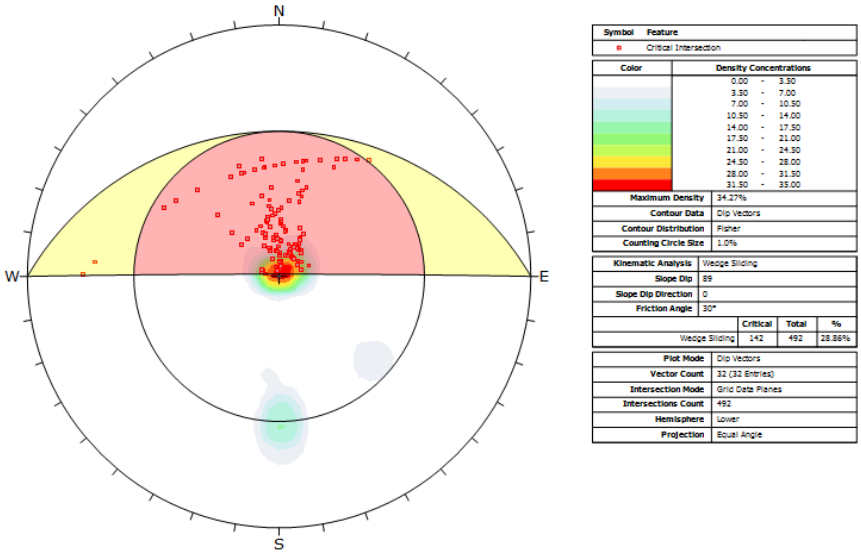


Figure D-4 Wedge failure for PE03 Southern Wall at 89º bench slope angle (OD5).

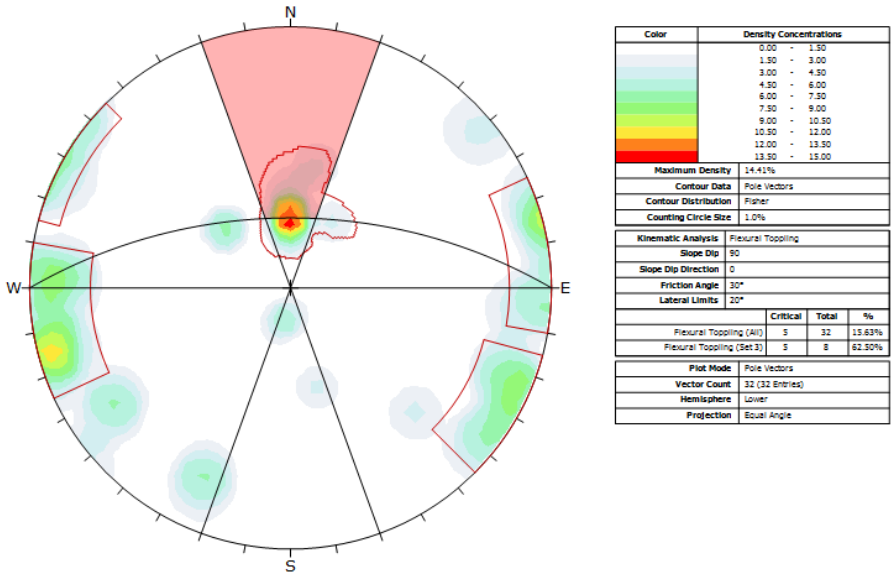


Figure D-5 Toppling failure for PE03 Southern Wall at 90º bench slope angle (Current design and OD1).

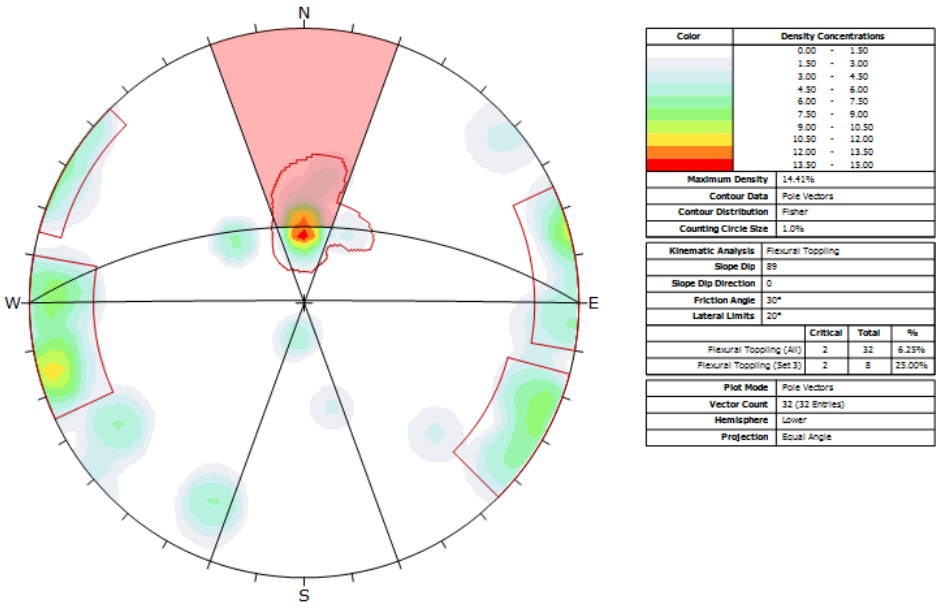


Figure D-6 Toppling failure for PE03 Southern Wall at 89º bench slope angle (OD5).

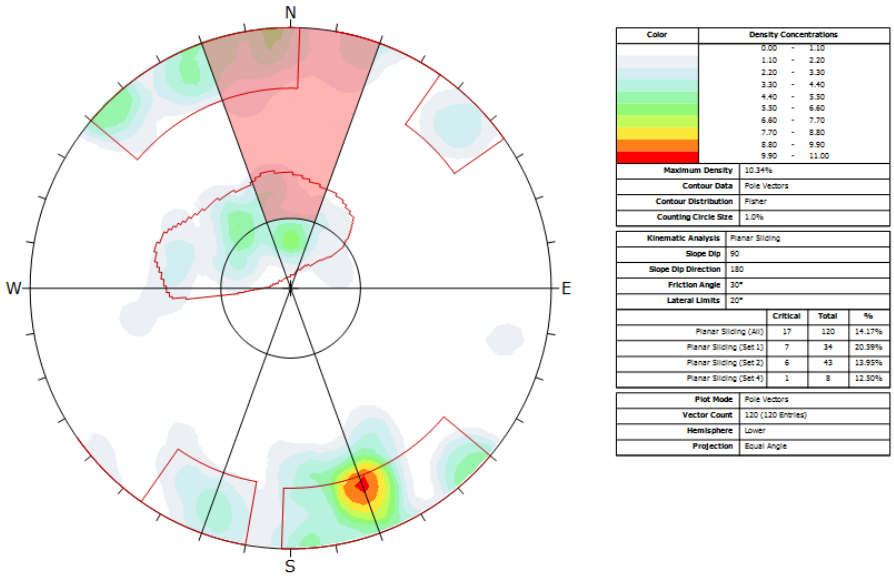


Figure D-7 Planar failure for PE03 Northern Wall at 90º bench slope angle (Current design and OD1).

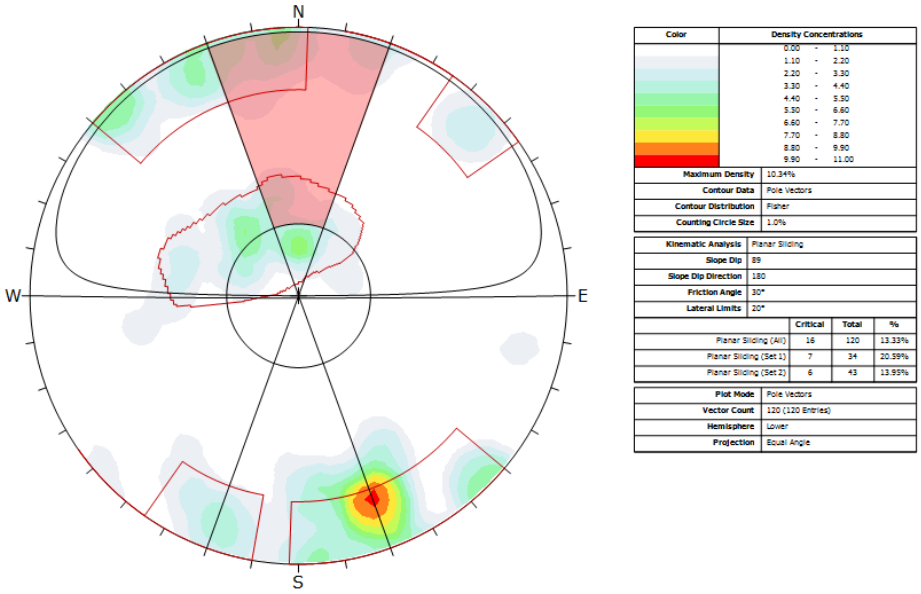


Figure D-8 Planar failure for PE03 Northern Wall at 89º bench slope angle (OD5).

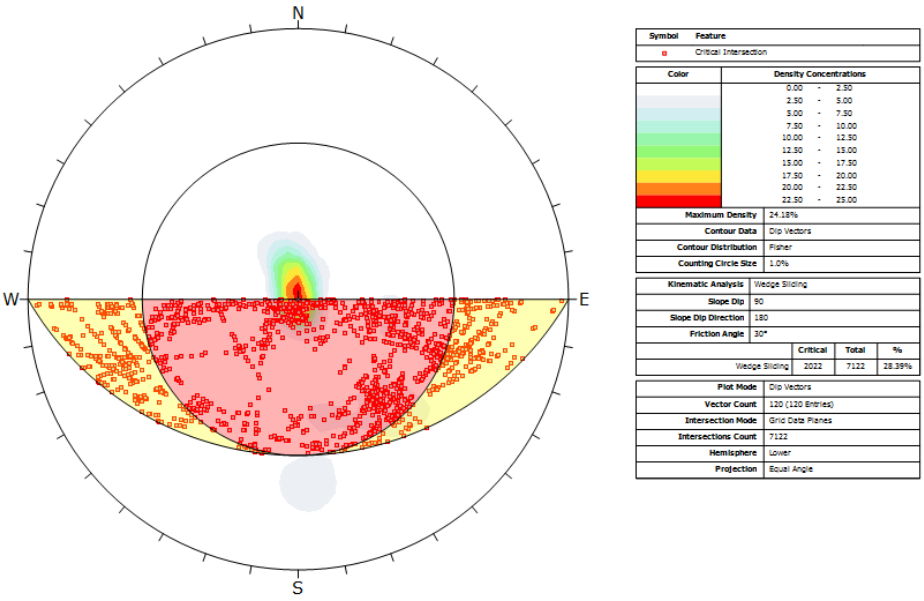


Figure D-9 Wedge failure for PE03 Northern Wall at 90º bench slope angle (Current design and OD1).

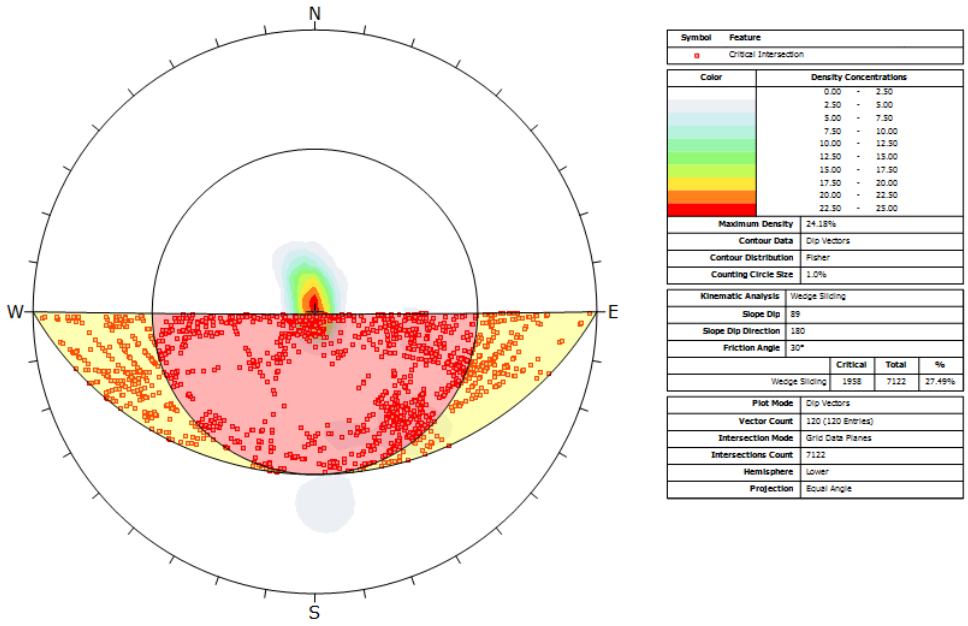


Figure D-10 Wedge failure for PE03 Northern Wall at 89º bench slope angle (OD5).

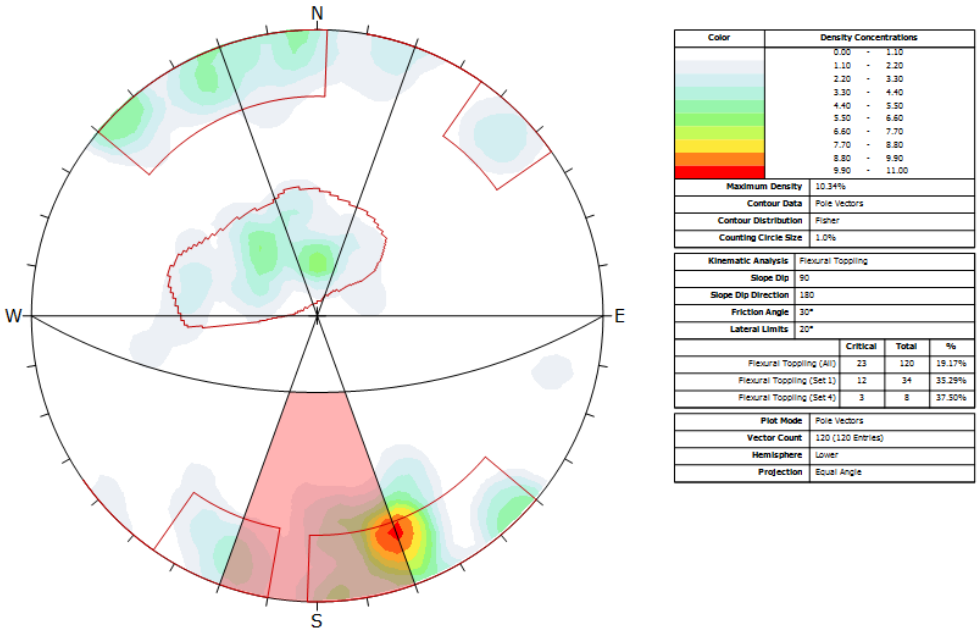


Figure D-11 Toppling failure for PE03 Northern Wall at 90º bench slope angle (Current design and OD1).

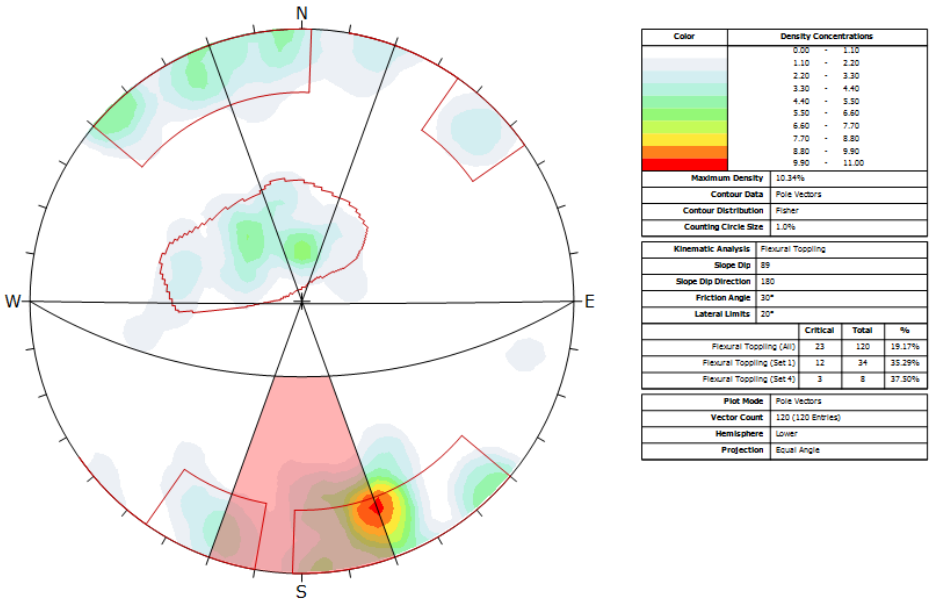


Figure D-12 Toppling failure for PE03 Northern Wall at 89º bench slope angle (OD5).

Kinematic analysis at inter-ramp scale level

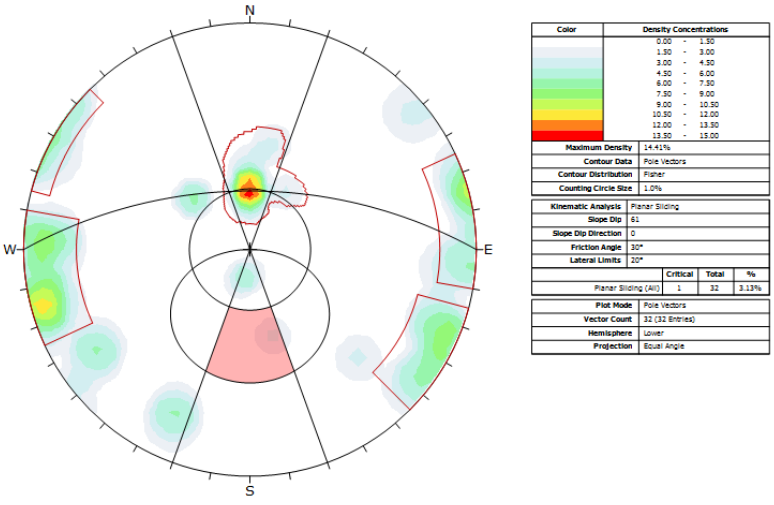


Figure D-13 Planar failure for PE03 Southern Wall at 61º inter-ramp slope angle (Current design).

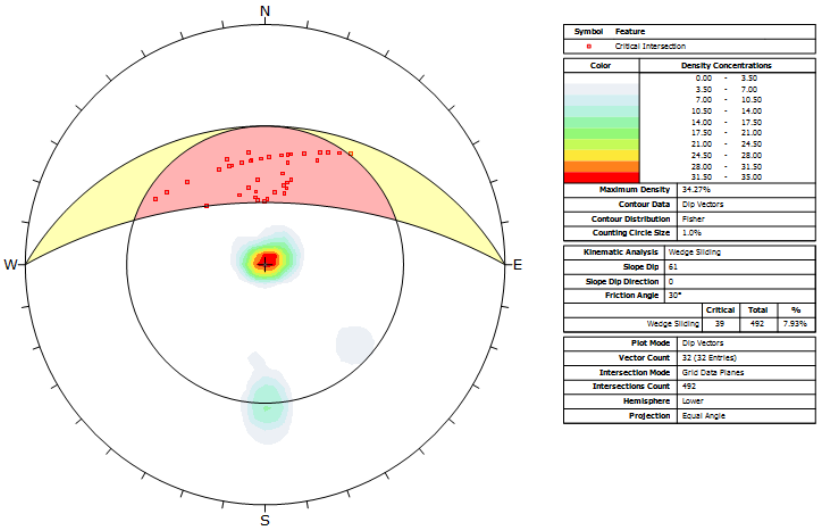


Figure D-14 Wedge failure for PE03 Southern Wall at 61º inter-ramp slope angle (Current design).

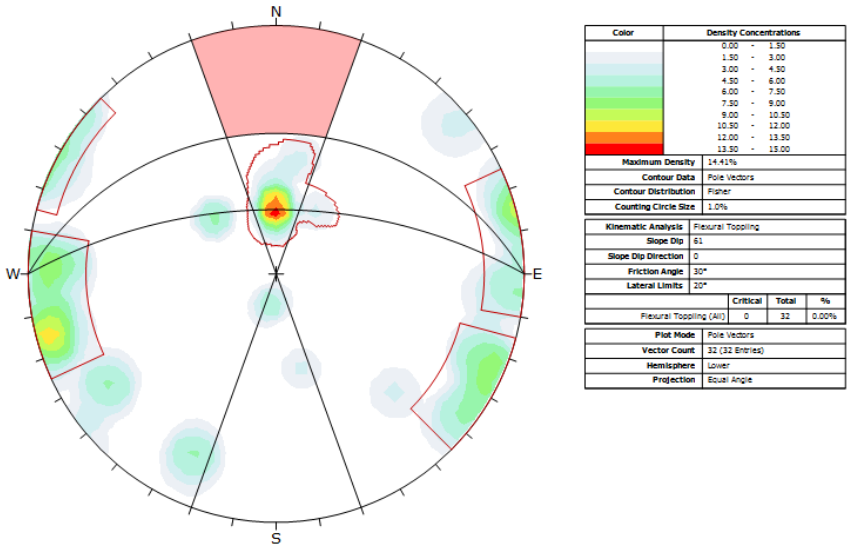


Figure D-15 Toppling failure for PE03 Southern Wall at 61º inter-ramp slope angle (Current design).

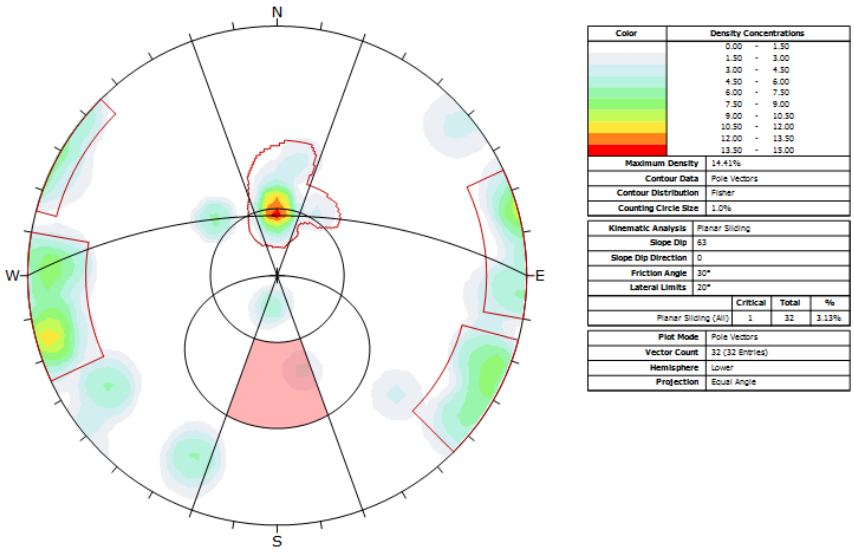


Figure D-16 Planar failure for PE03 Southern Wall at 63º inter-ramp slope angle (OD1).

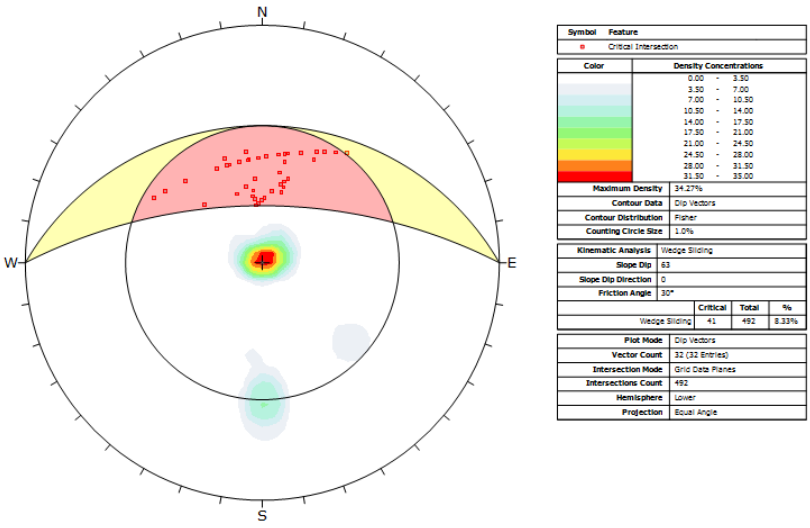


Figure D-17 Wedge failure for PE03 Southern Wall at 63º inter-ramp slope angle (OD1).

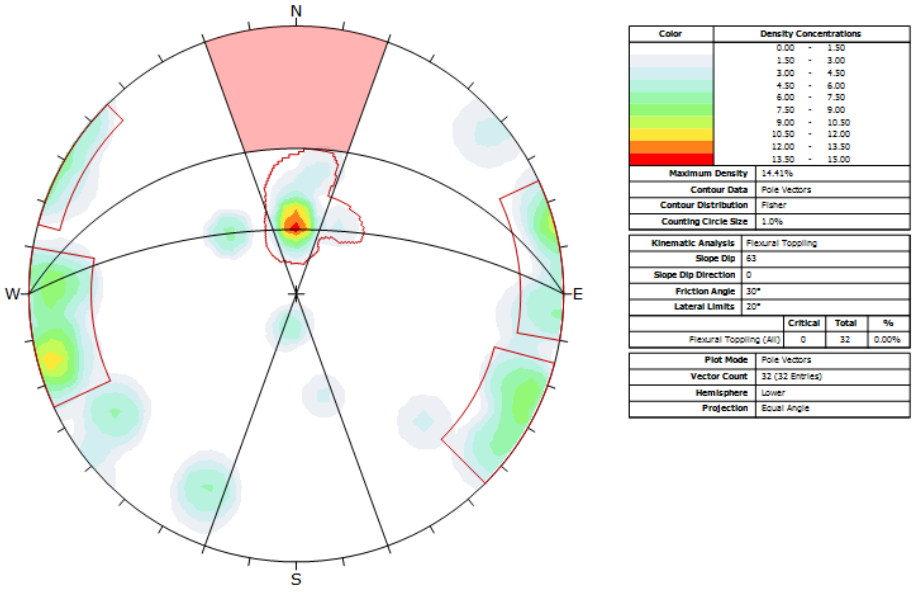


Figure D-18 Toppling failure for PE03 Southern Wall at 63º inter-ramp slope angle (OD1).

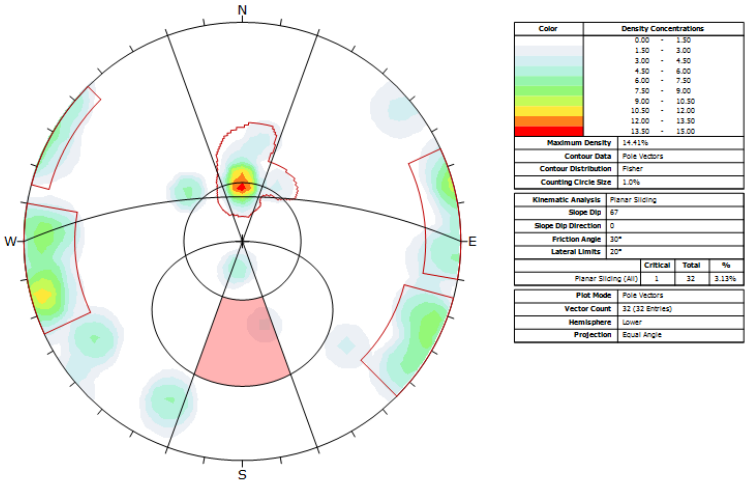


Figure D-19 Planar failure for PE03 Southern Wall at 67º inter-ramp slope angle (OD5).

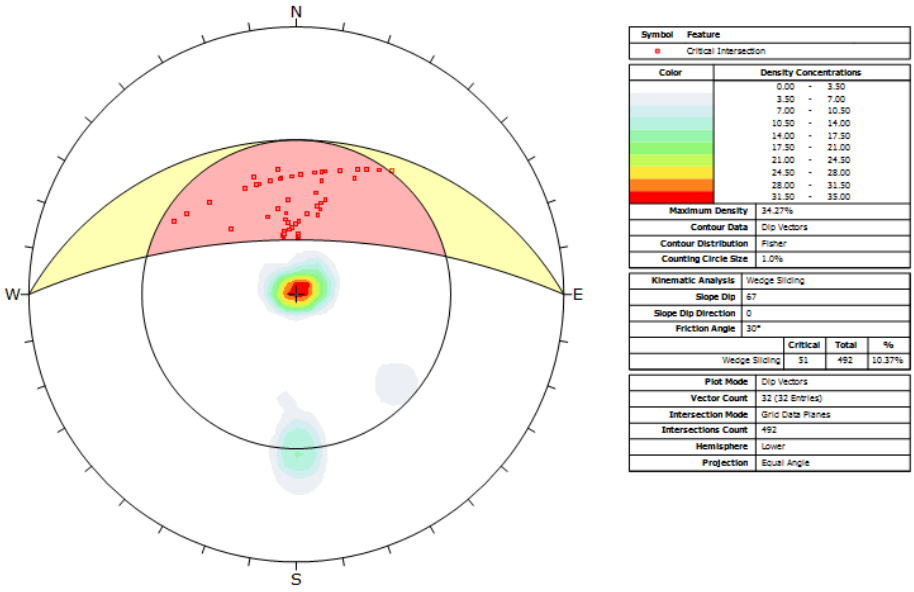


Figure D-20 Wedge failure for PE03 Southern Wall at 67º inter-ramp slope angle (OD5).

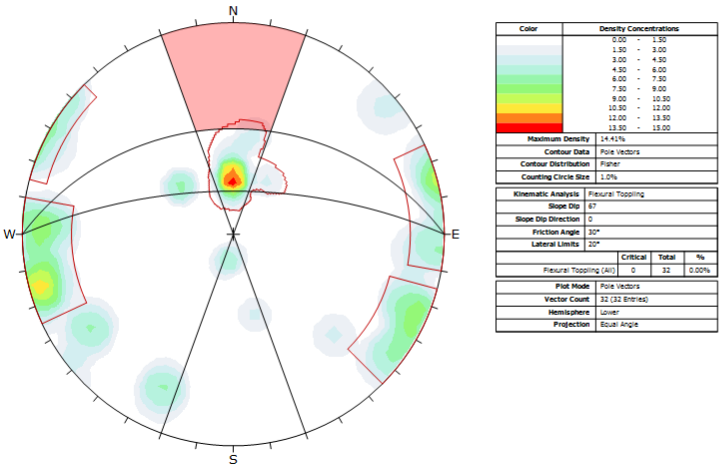


Figure D-21 Toppling failure for PE03 Southern Wall at 67º inter-ramp slope angle (OD5).

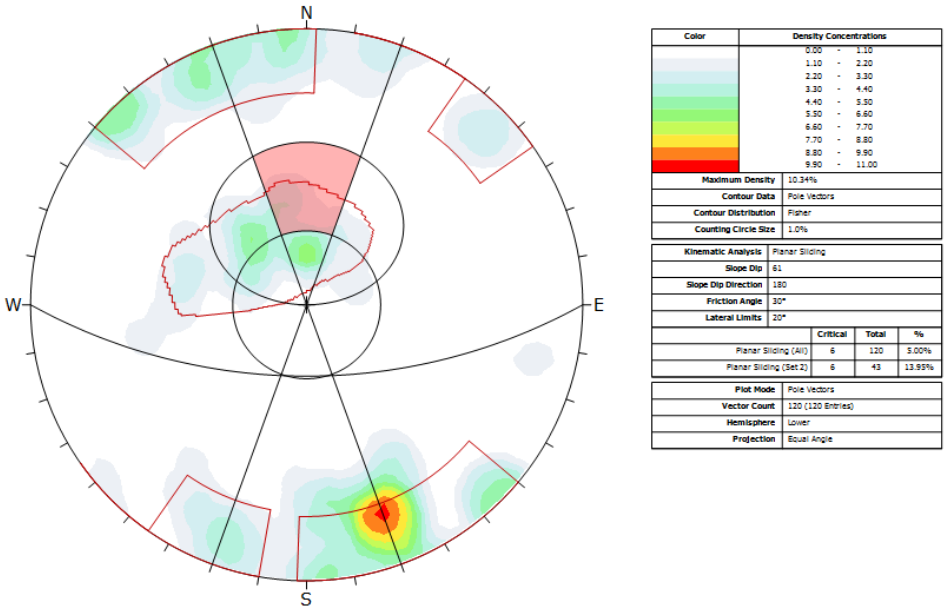


Figure D-22 Planar failure for PE03 Northern Wall at 61º inter-ramp slope angle (Current design).

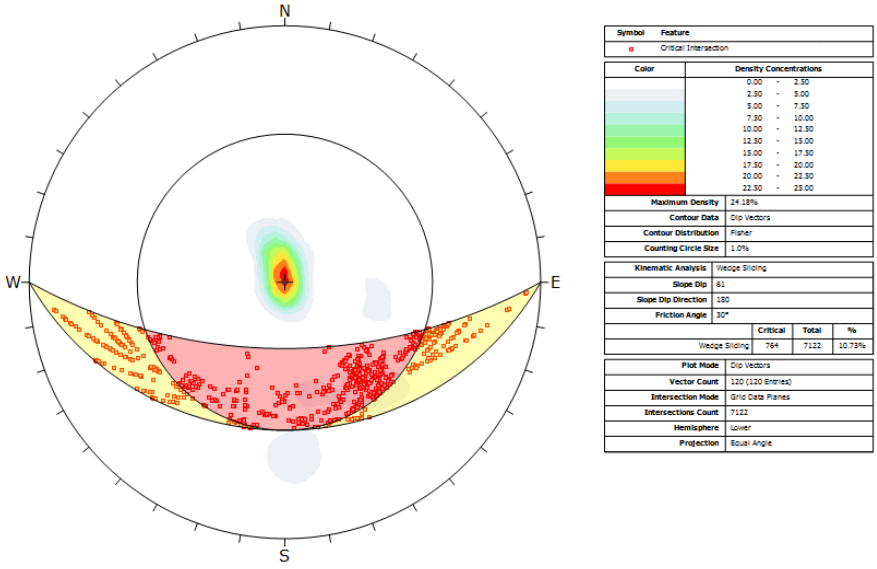


Figure D-23 Wedge failure for PE03 Northern Wall at 61º inter-ramp slope angle (Current design).

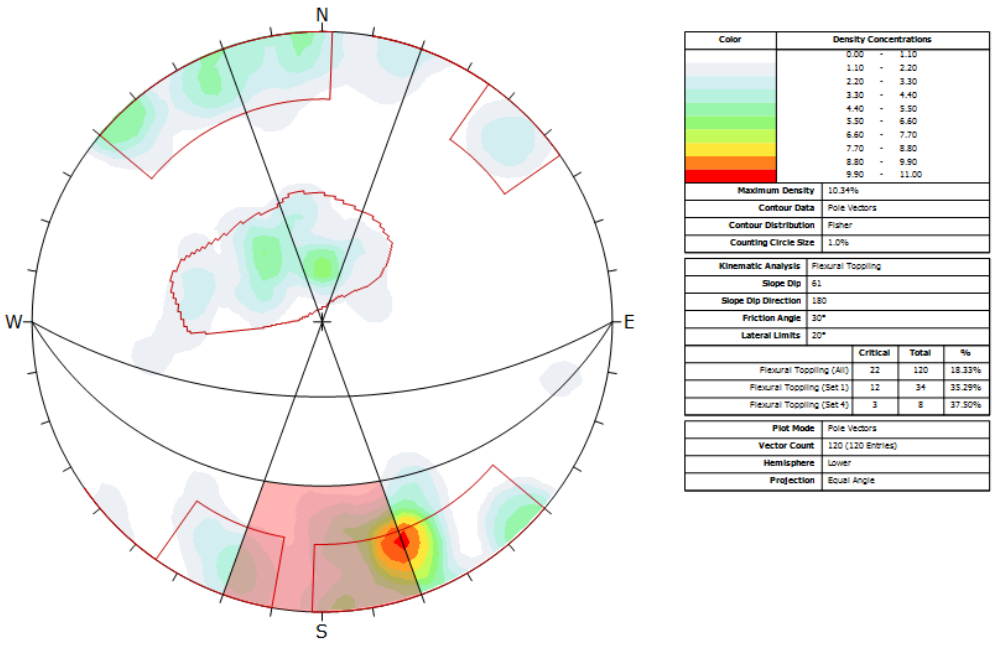


Figure D-24 Toppling failure for PE03 Northern Wall at 61º inter-ramp slope angle (Current design).

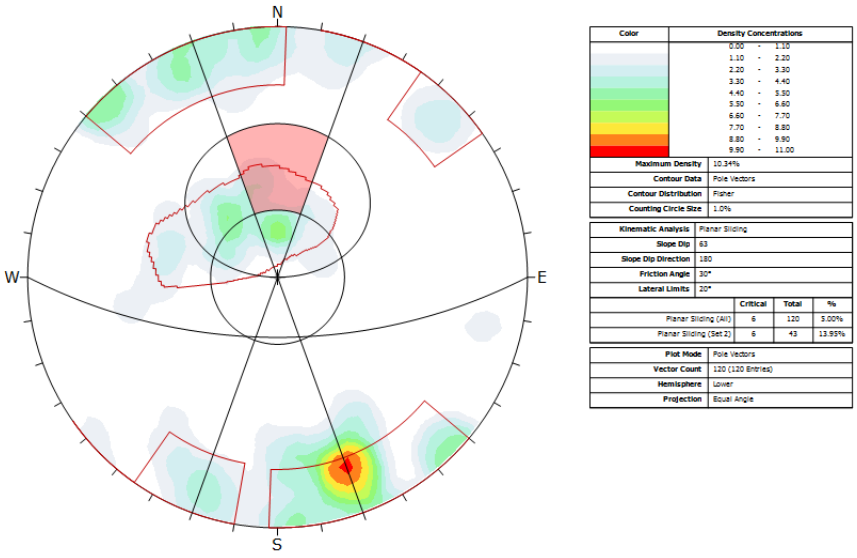


Figure D-25 Planar failure for PE03 Northern Wall at 63º inter-ramp slope angle (OD1).

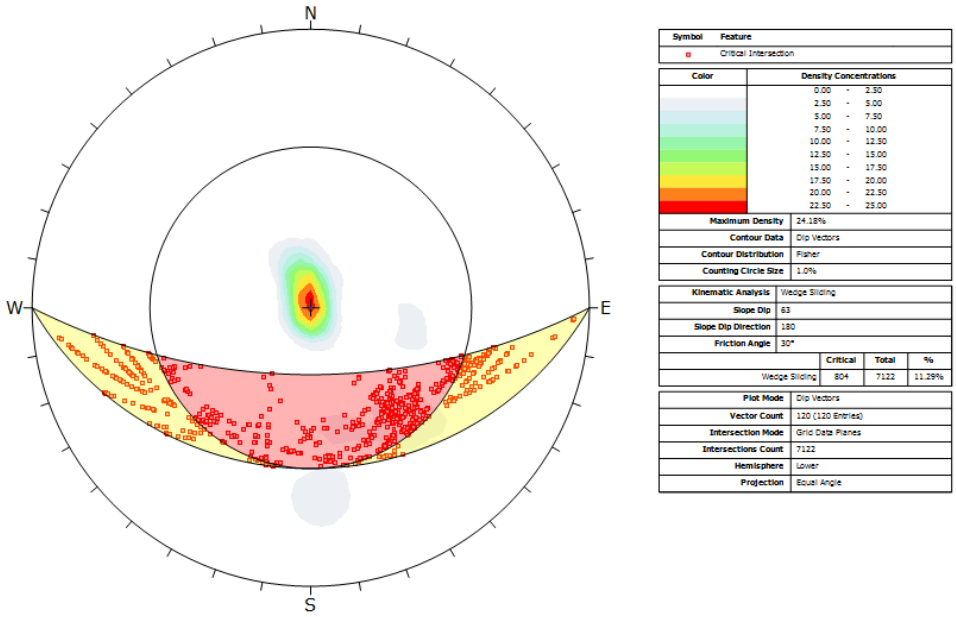


Figure D-26 Wedge failure for PE03 Northern Wall at 63º inter-ramp slope angle (OD1).

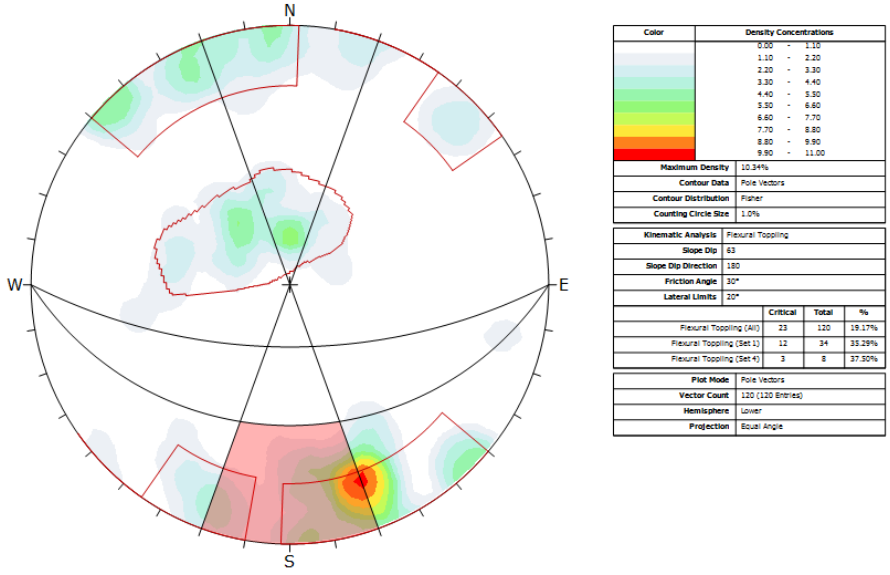


Figure D-27 Toppling failure for PE03 Northern Wall at 63º inter-ramp slope angle (OD1).

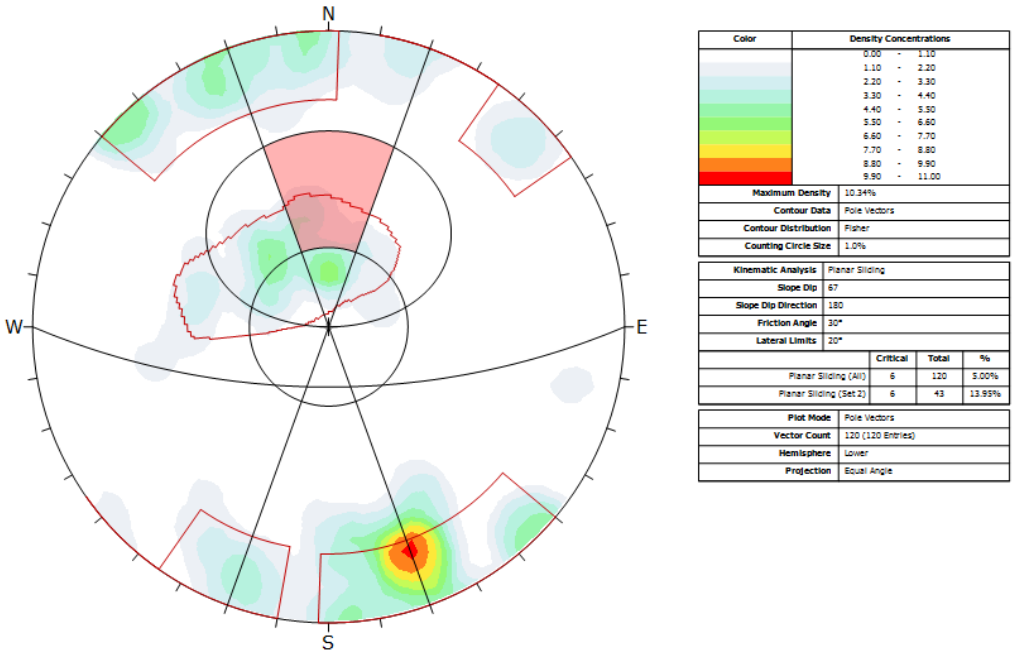


Figure D-28 Planar failure for PE03 Northern Wall at 67º inter-ramp slope angle (OD5).

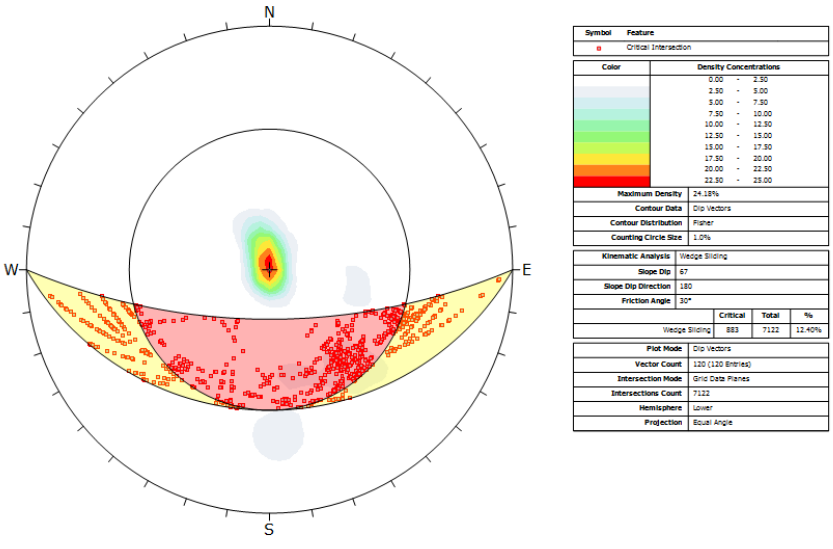


Figure D-29 Wedge failure for PE03 Northern Wall at 67º inter-ramp slope angle (OD5).

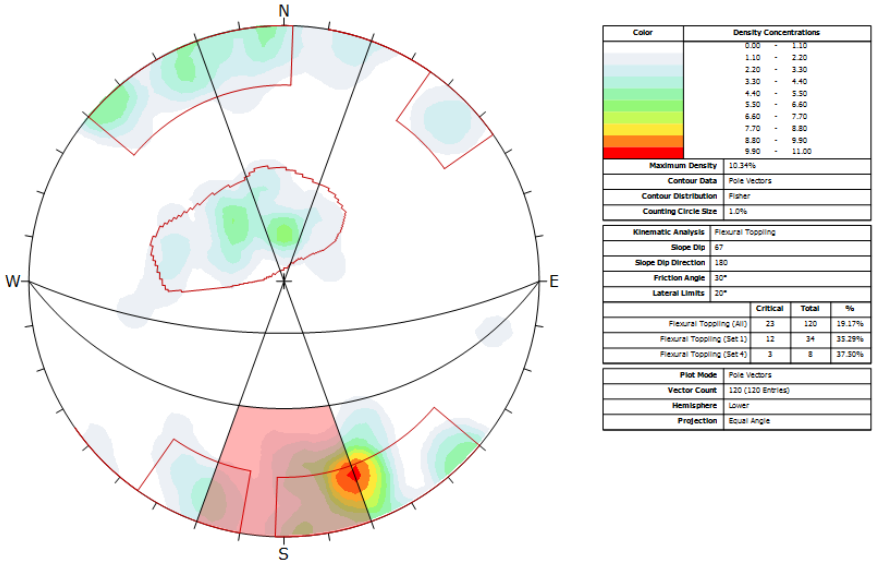


Figure D-30 Toppling failure for PE03 Northern Wall at 67º inter-ramp slope angle (OD5).

Kinematic analysis at overall pit slope scale level

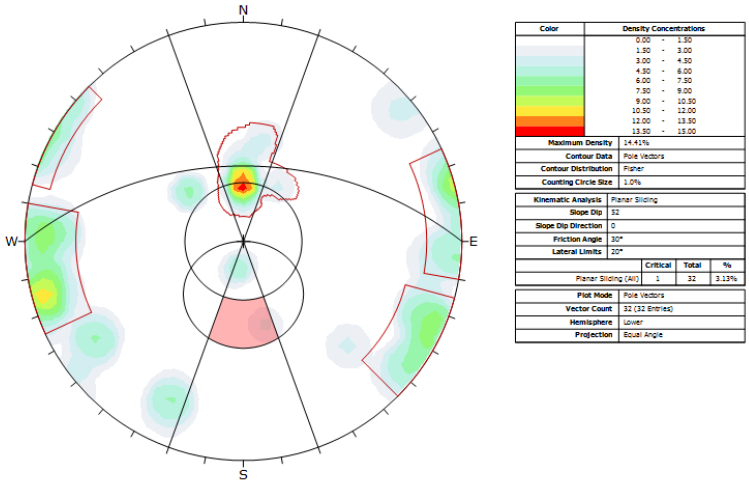


Figure D-31 Planar failure for PE03 Southern Wall at 52º overall slope angle (Current design).

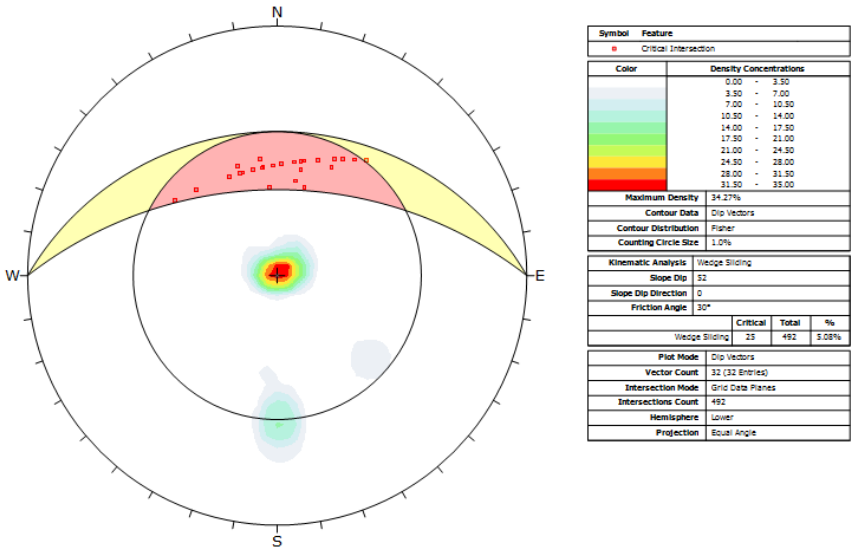


Figure D-32 Wedge failure for PE03 Southern Wall at 52º overall slope angle (Current design).

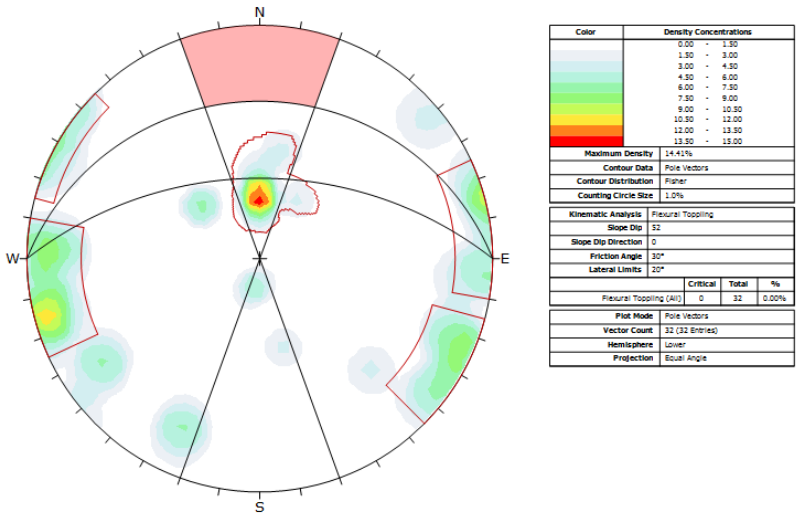
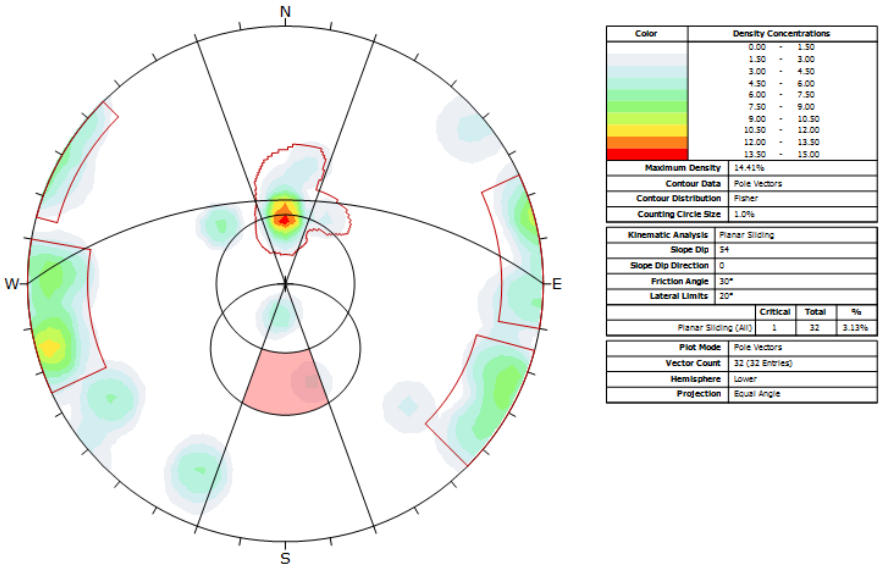


Figure D-33 Toppling failure for PE03 Southern Wall at 52º overall slope angle (Current design).

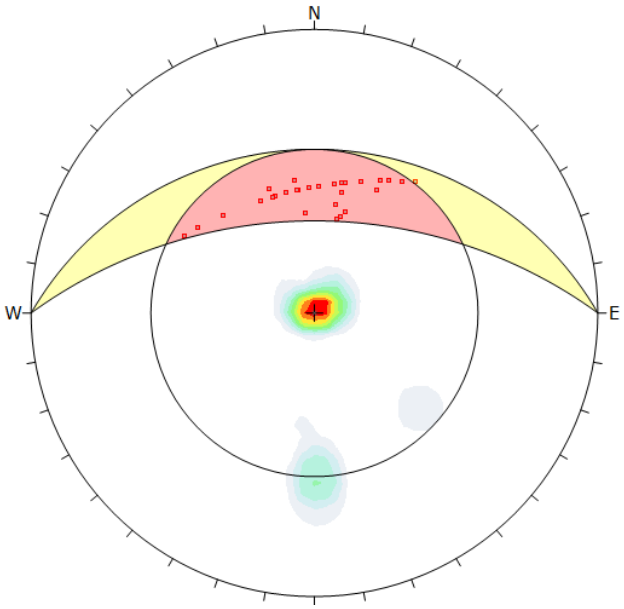


Color	Density Concentrations
	0.00 - 1.50
	1.50 - 3.00
	3.00 - 4.50
	4.50 - 6.00
	6.00 - 7.50
	7.50 - 9.00
	9.00 - 10.50
	10.50 - 12.00
	12.00 - 13.50
	13.50 - 15.00
Maximum Density	14.41%
Contour Data	Pole Vectors
Contour Distribution	Fisher
Counting Circle Size	1.0%

Kinematic Analysis	Planar Sliding		
Slope Dip	54		
Slope Dip Direction	0		
Friction Angle	30°		
Lateral Limits	20°		
	Critical	Total	%
Planar Sliding (All)	1	32	3.13%

Plot Mode	Pole Vectors
Vector Count	32 (32 Entries)
Hemisphere	Lower
Projection	Equal Angle

Figure D-34 Planar failure for PE03 Southern Wall at 54º overall slope angle (OD1).



Symbol	Feature
	Critical Intersection

Color	Density Concentrations
	0.00 - 3.50
	3.50 - 7.00
	7.00 - 10.50
	10.50 - 14.00
	14.00 - 17.50
	17.50 - 21.00
	21.00 - 24.50
	24.50 - 28.00
	28.00 - 31.50
	31.50 - 35.00
Maximum Density	34.27%
Contour Data	Dip Vectors
Contour Distribution	Fisher
Counting Circle Size	1.0%

Kinematic Analysis	Wedge Sliding		
Slope Dip	54		
Slope Dip Direction	0		
Friction Angle	30°		
	Critical	Total	%
Wedge Sliding	28	492	5.69%

Plot Mode	Dip Vectors
Vector Count	32 (32 Entries)
Intersection Mode	Grid Data Planes
Intersections Count	492
Hemisphere	Lower
Projection	Equal Angle

Figure D-35 Wedge failure for PE03 Southern Wall at 54º overall slope angle (OD1).

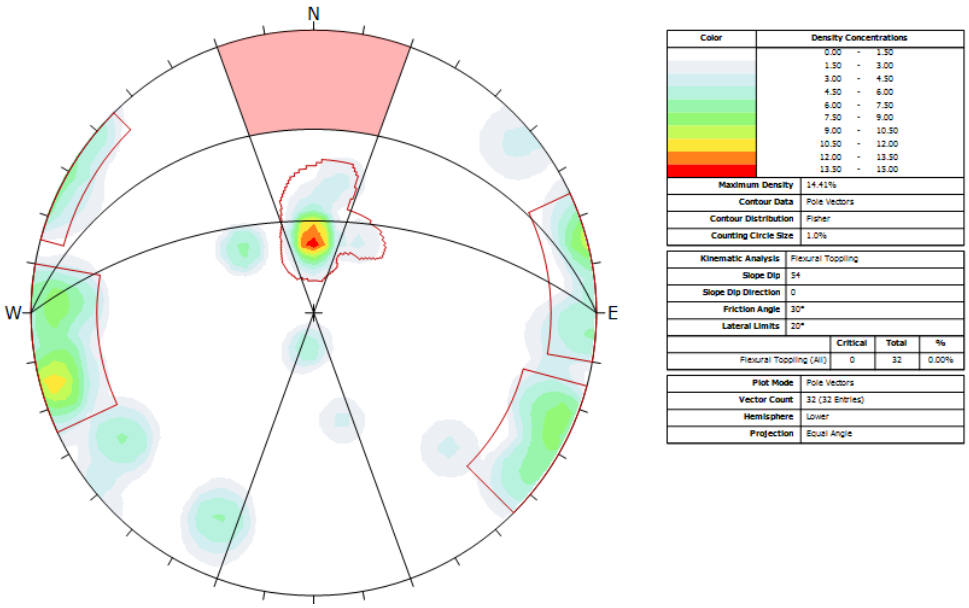


Figure D-36 Toppling failure for PE03 Southern Wall at 54º overall slope angle (OD1).

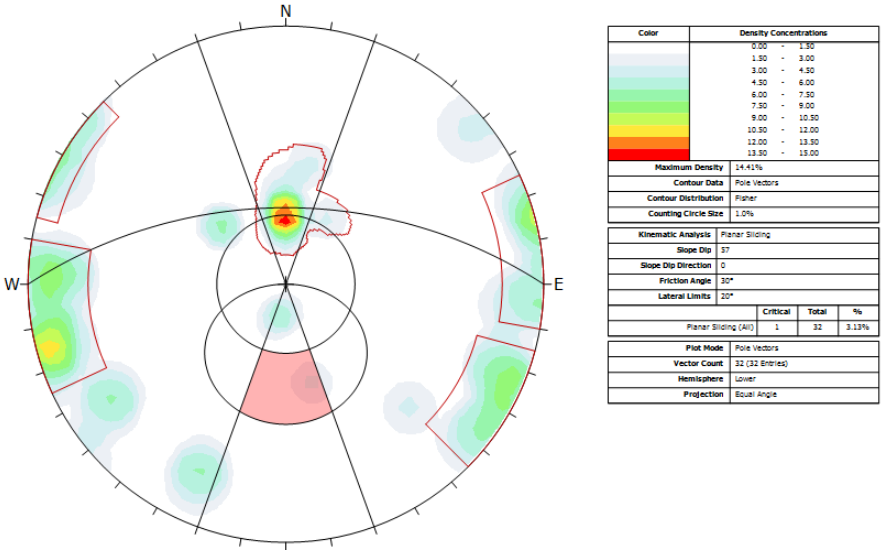
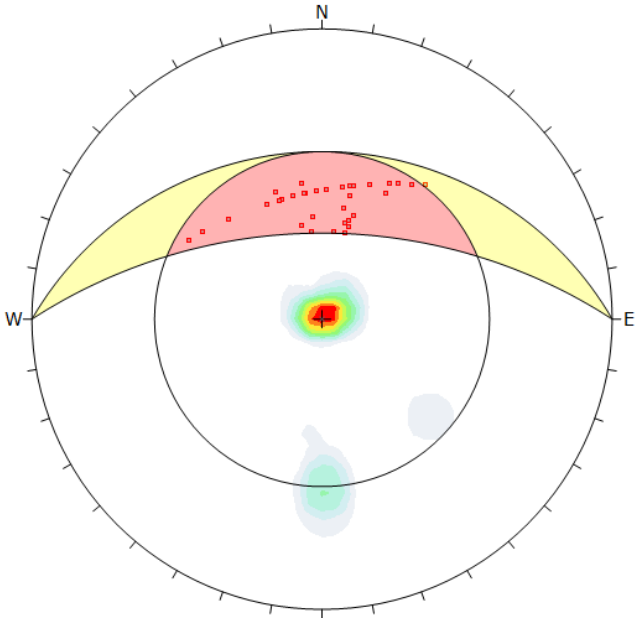


Figure D-37 Planar failure for PE03 Southern Wall at 57º overall slope angle (OD5).



Symbol	Feature
	Critical Intersection

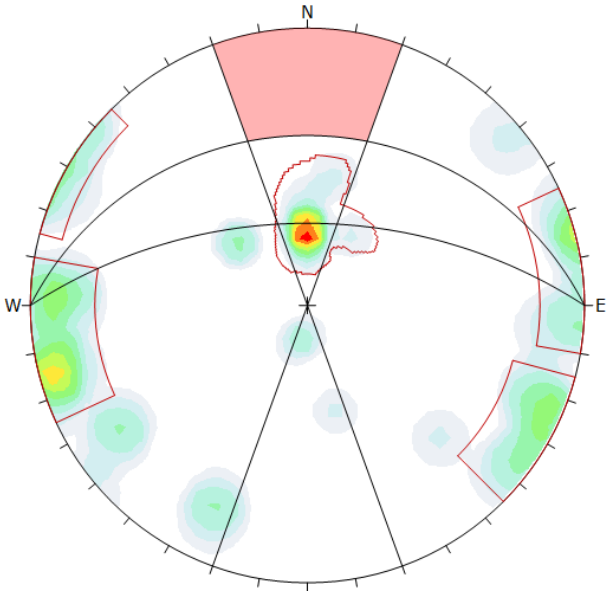
Color	Density Concentrations
	0.00 - 3.50
	3.50 - 7.00
	7.00 - 10.50
	10.50 - 14.00
	14.00 - 17.50
	17.50 - 21.00
	21.00 - 24.50
	24.50 - 28.00
	28.00 - 31.50
	31.50 - 35.00

Maximum Density	34.27%
Contour Data	Dip Vectors
Contour Distribution	Fisher
Counting Circle Size	1.0%

Kinematic Analysis	Wedge Sliding		
Slope Dip	57		
Slope Dip Direction	0		
Friction Angle	30°		
	Critical	Total	%
Wedge Sliding	33	492	6.71%

Plot Mode	Dip Vectors
Vector Count	32 (32 Entries)
Intersection Mode	Grid Data Planes
Intersections Count	492
Hemisphere	Lower
Projection	Equal Angle

Figure D-38 Wedge failure for PE03 Southern Wall at 57º overall slope angle (OD5).



Color	Density Concentrations
	0.00 - 1.50
	1.50 - 3.00
	3.00 - 4.50
	4.50 - 6.00
	6.00 - 7.50
	7.50 - 9.00
	9.00 - 10.50
	10.50 - 12.00
	12.00 - 13.50
	13.50 - 15.00

Maximum Density	14.41%
Contour Data	Pole Vectors
Contour Distribution	Fisher
Counting Circle Size	1.0%

Kinematic Analysis	Flexural Toppling		
Slope Dip	57		
Slope Dip Direction	0		
Friction Angle	30°		
Lateral Limits	20°		
	Critical	Total	%
Flexural Toppling (All)	0	32	0.00%

Plot Mode	Pole Vectors
Vector Count	32 (32 Entries)
Hemisphere	Lower
Projection	Equal Angle

Figure D-39 Toppling failure for PE03 Southern Wall at 57º overall slope angle (OD5).

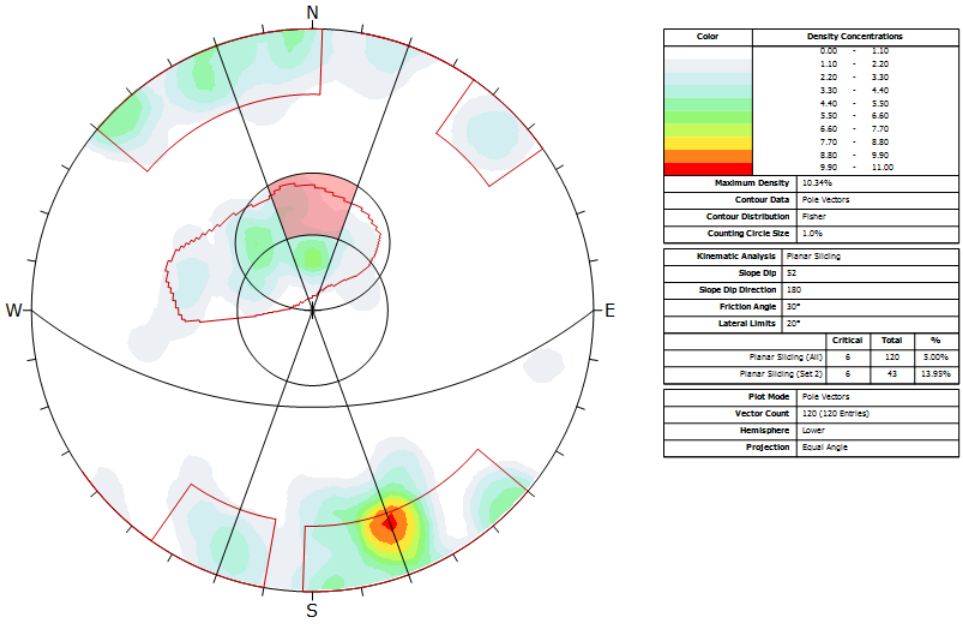


Figure D-40 Planar failure for PE03 Northern Wall at 52º overall slope angle (Current design).

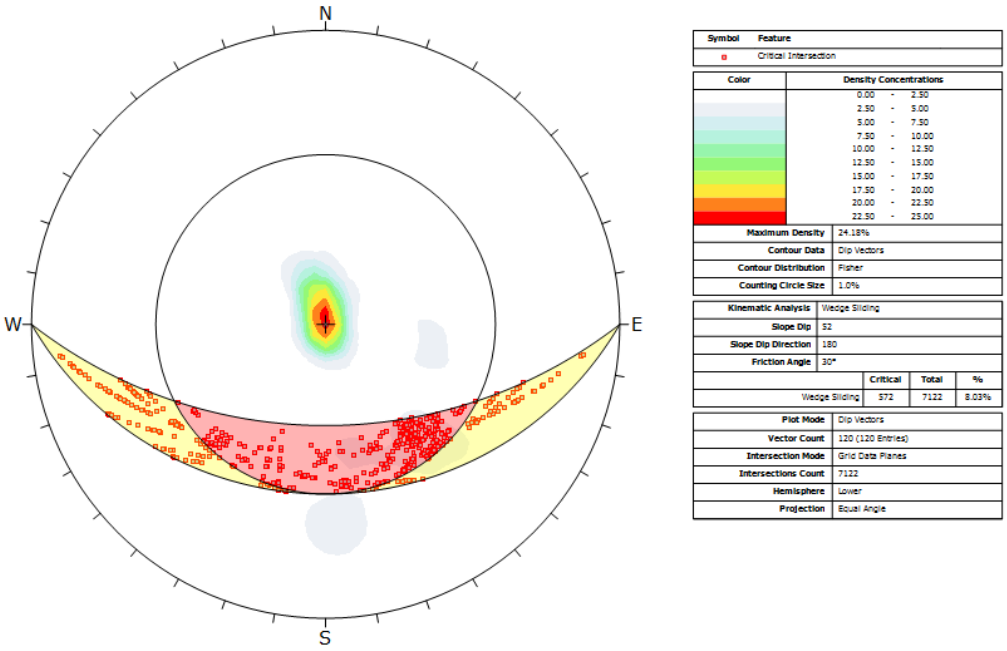


Figure D-41 Wedge failure for PE03 Northern Wall at 52º overall slope angle (Current design).

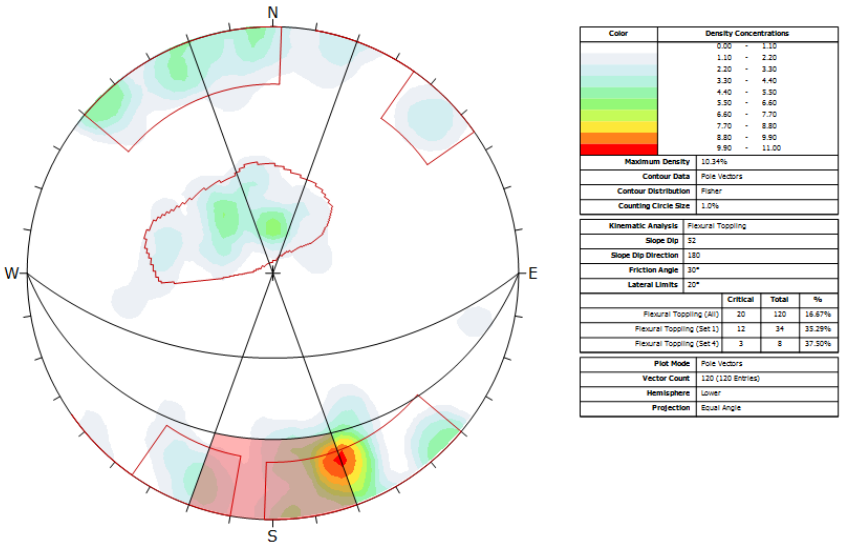
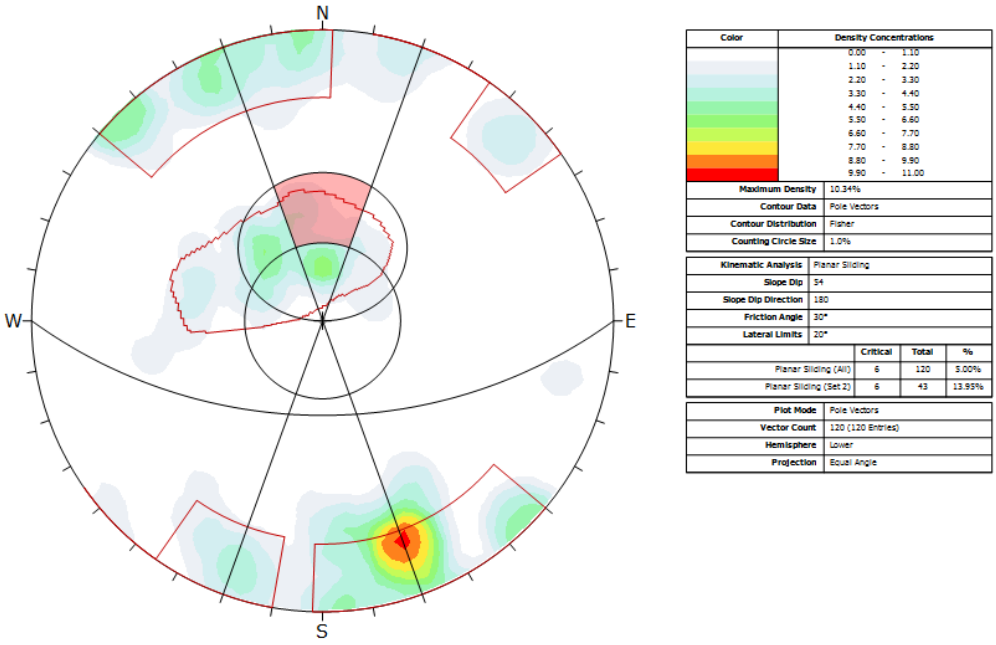


Figure D-42 Toppling failure for PE03 Northern Wall at 52º overall slope angle (Current design).



Color	Density Concentrations
	0.00 - 1.10
	1.10 - 2.20
	2.20 - 3.30
	3.30 - 4.40
	4.40 - 5.50
	5.50 - 6.60
	6.60 - 7.70
	7.70 - 8.80
	8.80 - 9.90
	9.90 - 11.00

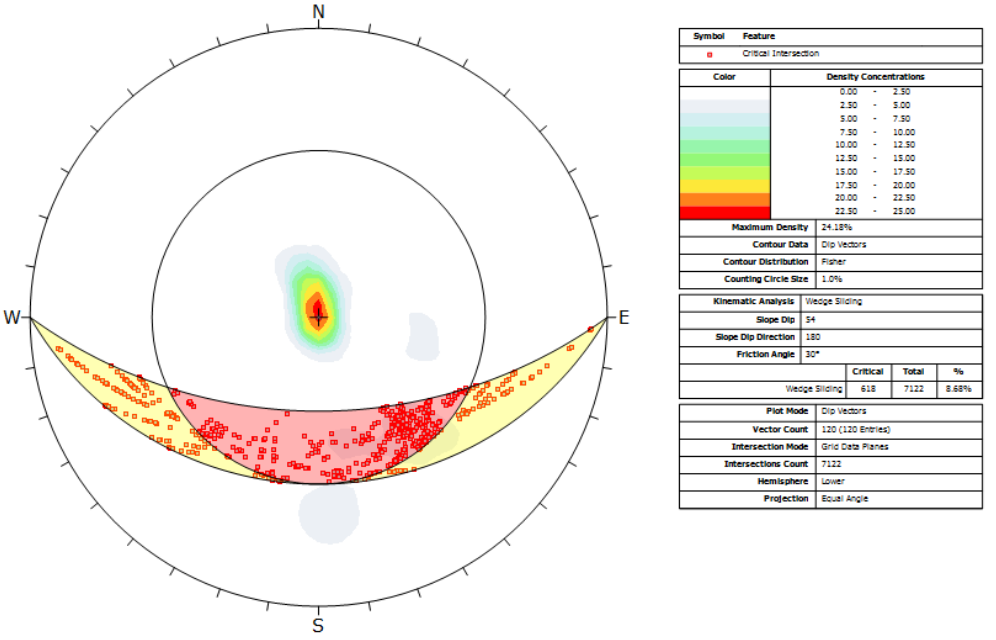
Maximum Density	10.34%
Contour Data	Pole Vectors
Contour Distribution	Fisher
Counting Circle Size	1.0%

Kinematic Analysis	Planar Sliding
Slope Dip	54
Slope Dip Direction	180
Friction Angle	30°
Lateral Limits	20°

	Critical	Total	%
Planar Sliding (All)	6	120	5.00%
Planar Sliding (Set 2)	6	43	13.95%

Plot Mode	Pole Vectors
Vector Count	120 (120 Entries)
Hemisphere	Lower
Projection	Equal Angle

Figure D-43 Planar failure for PE03 Northern Wall at 54º overall slope angle (OD1).



Symbol	Feature
	Critical Intersection

Color	Density Concentrations
	0.00 - 2.50
	2.50 - 5.00
	5.00 - 7.50
	7.50 - 10.00
	10.00 - 12.50
	12.50 - 15.00
	15.00 - 17.50
	17.50 - 20.00
	20.00 - 22.50
	22.50 - 25.00

Maximum Density	24.18%
Contour Data	Dip Vectors
Contour Distribution	Fisher
Counting Circle Size	1.0%

Kinematic Analysis	Wedge Sliding
Slope Dip	54
Slope Dip Direction	180
Friction Angle	30°

	Critical	Total	%
Wedge Sliding	618	7122	8.68%

Plot Mode	Dip Vectors
Vector Count	120 (120 Entries)
Intersection Mode	Grid Data Planes
Intersections Count	7122
Hemisphere	Lower
Projection	Equal Angle

Figure D-44 Wedge failure for PE03 Northern Wall at 54º overall slope angle (OD1).

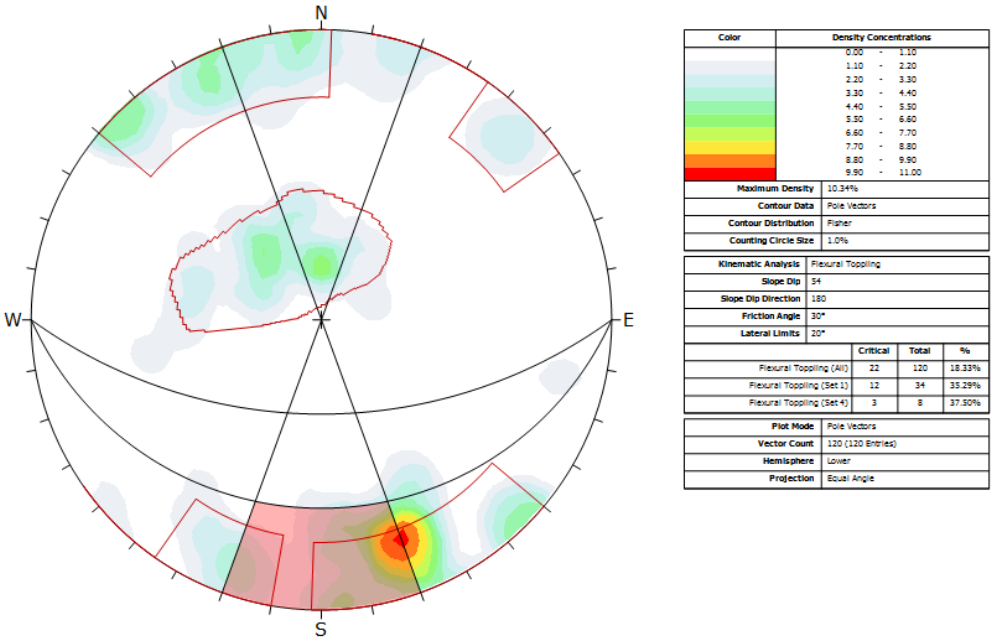


Figure D-45 Toppling failure for PE03 Northern Wall at 54º overall slope angle (OD1).

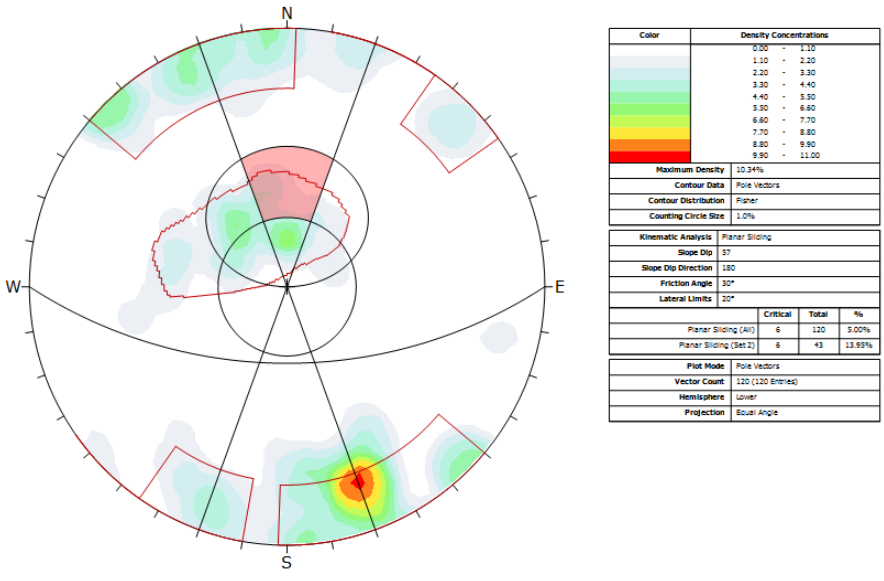


Figure D-46 Planar failure for PE03 Northern Wall at 57º overall slope angle (OD5).

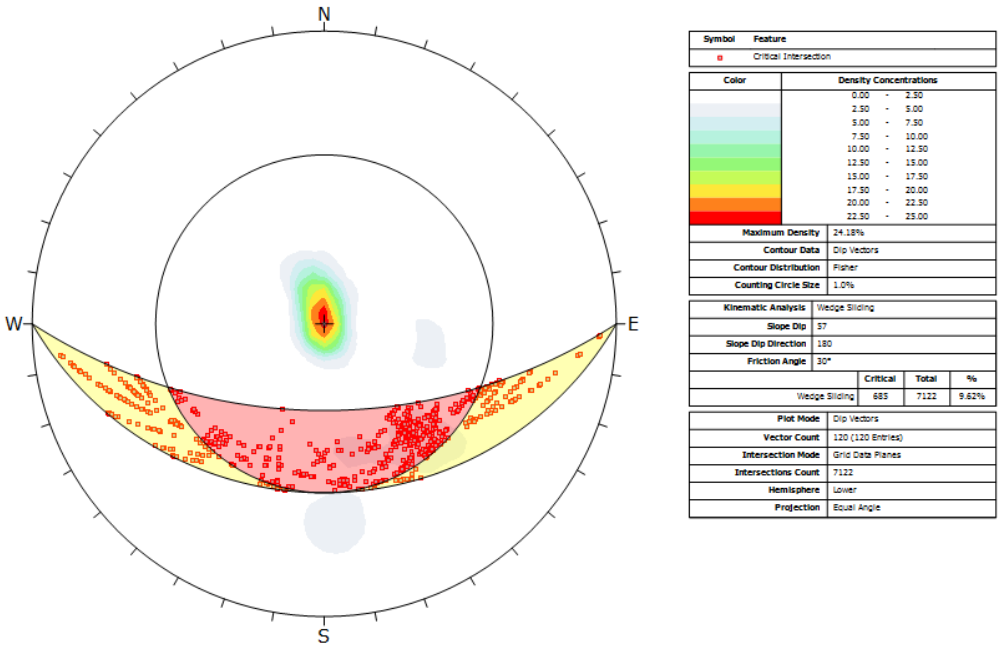


Figure D-47 Wedge failure for PE03 Northern Wall at 57º overall slope angle (OD5).

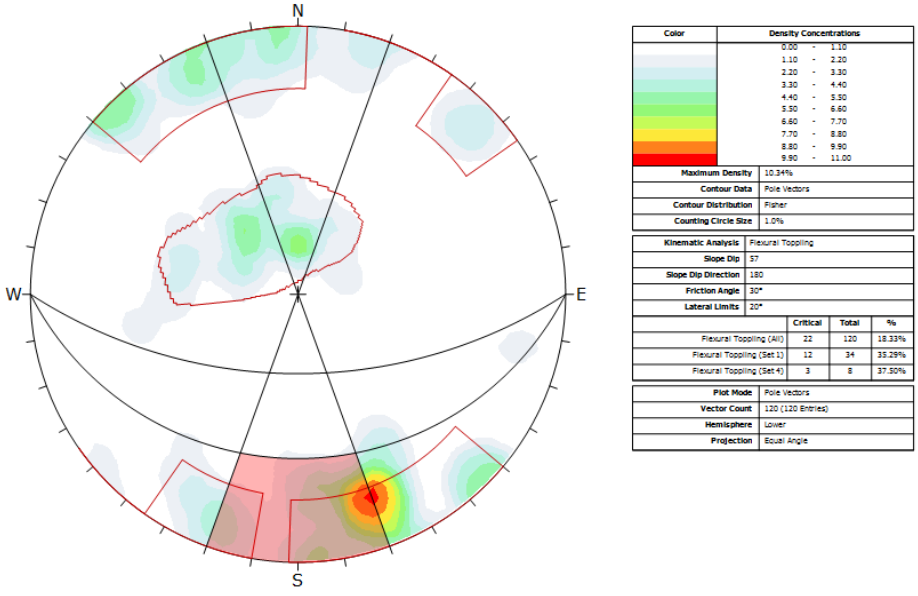


Figure D-48 Toppling failure for PE03 Northern Wall at 57º overall slope angle (OD5).